PUBLIKATIONEN

ALS ARZT HEILE ICH HERZEN.

ALS SPEAKER BEWEGE ICH SIE.

KEYNOTE-SPEAKER DR. MED. NANA-YAW BIMPONG-BUTA

Analysis of human microcirculation in weightlessness: Study protocol and pre-study experiments

Nana-Yaw Bimpong-Buta[a,1], Peter Jirak[b,1], Bernhard Wernly[b], Michael Lichtenauer[b], Maryna Masyuk[a], Johanna Maria Muessig[a], Kristina Braun[a], Sema Kaya[a], Malte Kelm[a] and Christian Jung[a,*]

[a]*Department of Internal Medicine, Division of Cardiology, Pulmonary Diseases, Vascular Medicine, University Hospital Düsseldorf, Düsseldorf, Germany*
[b]*Department of Cardiology, Clinic of Internal Medicine II, Paracelsus Medical University of Salzburg, Austria*

Abstract.

BACKGROUND: In weightlessness, alterations in organ systems have been reported. The microcirculation consists of a network of blood vessels with diameters of a few μm. It is considered the largest part of the circulatory system of the human body and essential for exchange of gas, nutrients and waste products. An investigation of the microcirculation in weightlessness seems warranted but has not yet been performed.

OBJECTIVE: In this paper, we outline a study in which we will investigate the possible interrelations between weightlessness and microcirculation. We will induce weightlessness in the course of parabolic flight maneuvers, which will be conducted during a parabolic flight campaign. In this study protocol also an evaluation of a possible influence of parabolic flight premedication on microcirculation will be described.

METHODS: The microcirculation will be investigated by sublingual intravital measurements applying sidestream darkfield microscopy. Parameters of macrocirculation such as heart rate, blood pressure and blood oxygenation will also be investigated.

RESULTS: In our pre-study experiments, neither dimenhydrinate nor scopolamine altered microcirculation.

CONCLUSIONS: As the application of motion sickness therapy did not alter microcirculation, it will be applied during the parabolic flight maneuvers of the campaign. Our results might deepen the understanding of microcirculation on space missions and on earth.

Keywords: Microcirculation, intravital microscopy, sidestream darkfield-imaging, weightlessness, parabolic flight

1. Introduction

With a formal Mars program established for the 2030 s by national space agencies, the understanding of human physiology in weightlessness is of utmost interest for adequate planning and conduction of such a complex mission of long duration [1, 2]. In weightlessness, adaptive changes in distinct organ systems have been reported, e.g. osteoporosis-like bone changes of the musculoskeletal system as well as muscular atrophy [3, 4]. Furthermore, impairment of lung function and the immune system have been reported [5, 6]. Still, major complications during space missions might mainly be triggered by

---

[1]Both authors contributed equally to this work.

*Corresponding authors: Univ.-Prof. Dr. med. Dr. C. Jung, Department of Internal Medicine, Division of Cardiology, Pulmonary Diseases, Vascular Medicine, University Hospital Düsseldorf, Moorenstrasse 5; 40225 Düsseldorf, Germany. Tel.: +49 211 81 18567; Fax: +49 211 18812; E-mail: christian.jung@med.uni-duesseldorf.de.

unfavorable alterations in the cardiovascular system, leading to life threatening impairment of tissue oxygenation [7–10]. In studies conducted in weightlessness, an increase of cardiac output of up to 41% has been described [11, 12]. In animal experiments with pigs in weightlessness, a change in pulmonary flow was observed and even structural changes of capillaries were documented [6]. Moreover, changes in the baroreceptor reflex and on cerebrovascular auto-regulation have been reported in weightlessness [11–14].

The microcirculation consists of a network of blood vessels of smallest scale, comprising arterioles, venules and capillaries, with diameters ranging from 2 to 100 μm. In terms of surface area, it is considered the largest part of the circulatory system of the human body. The primary role of the microcirculation comprises gas exchange as well as exchange of nutrients and waste products. Accordingly, the microcirculation is accountable for adequate tissue oxygenation and cellular organ perfusion [15–17].

Studies concerning hemodynamic changes of the microcirculatory system in zero-gravity are still lacking, partly because a thorough evaluation of the microcirculation warrants special devices. However, new devices have emerged that allow a direct online visualization of the sublingual microcirculatory blood flow [18]. For instance, intravital microscopy has successfully been applied to estimate clinical outcomes of critically ill patients [19–22]. In our opinion, the measurement of the microcirculation in states of weightlessness in the setting of parabolic flight maneuvers seems feasible.

With regard to long duration space missions, further evaluation of the microcirculation in weightlessness seems indispensable to deeper understand the pathophysiological mechanisms involved and identify possible risks for human beings conducting space missions of long duration. The target of this study is to enhance the understanding of the function and autoregulation of the microcirculation in weightlessness. In the course of participation in the Parabolic Flight Campaign in September 2017, the alterations of the microcirculation under these circumstances will be quantified.

The present paper presents the study protocol for this novel experimental approach as well as two necessary pre-study experiments.

2. Materials and methods

2.1. Pre-study experiments

A common side effect of participation in parabolic flight maneuvers is motion sickness. Therefore, the prophylactic administration of an anti-emetic drug is strongly recommended. In this context, dimenhydrinate and scopolamine remain the most frequently applied drugs. Therefore, in a pre-study, we measured the microcirculation after administration of standard doses of these drugs, to assess possible alterations of the microcirculation.

In this context, we measured the sublingual microcirculation of 8 healthy individuals before and one hour after peroral administration of the standard dose of 50 mg Dimenhydrinate. Furthermore, we assessed the microcirculation of 6 healthy individuals before and after the administration of Scopolamine applied subcutaneously (standard dose for male test subjects: 0,175 mg; standard dose for female test subjects: 0,125 mg; with optional additional doses according to medical history of known motion sickness). For each individual at least 3 repetitive measurements were performed before and after drug administration respectively. After the acquisition of the imagery data, the analysis was done offline, applying the certified Microscan®-Analysis Software (AVA, Version 4.3C). According to consensus for ideal analysis reports in this setting, we documented the perfused vessel density (PVD) and the perfused proportion of vessels (PPV) as well as the total vessel density (TVD) as standard variables. Additionally we assessed the number of vessel crossings.

2.2. Main study protocol

The main study constitutes an observational study. Prior to inclusion into the study, a medical check-up for airworthiness had to be performed by each subject. All subjects gave their informed consent for inclusion before they participated in the study. The study was conducted in accordance with the Declaration of Helsinki (1975, revised in 2008), and the protocol was approved by the German Ethics Committee of the Medical Faculty of the University Hospital Duesseldorf, Germany (Date of approval: August 14th, 2017; Project Identification code: 2017054297) and by the French Ethics Committee (Comite de Protection des Personnes (CPP Nord-Ouest III) of the Medical Faculty of the University of Caen (Date of approval: September 06th, 2017; Project Identification code: 2017-A01185-48)).

2.3. Inclusion and Exclusion criteria

The inclusion criteria were defined as: age >18 years; airworthiness; cardiorespiratory health; spontaneous circulation; accessibility of the sublingual mucosa; signed informed consent.

The exclusion criteria were defined as: history of cardiovascular and respiratory primary diseases or regular intake of medication except oral contraceptives; inaccessible sublingual mucosa e.g. after orofacial trauma or surgery; missing or withdrawal of informed consent; insufficient requirements for airworthiness; positive pregnancy test.

2.4. Parabolic flight

The Parabolic Flight campaign will take place from September 04th to September 16th in Bordeaux, France. The experiment will take place aboard the Airbus A 310 Zero-G of the French company NoveSpace. The A 310 Zero-G is a specially equipped aircraft, meticulously designed for the operation of parabolic flight maneuvers. In order to perform the scheduled flight maneuvers, three jet pilots with profound training simultaneously operate in the cockpit, with each pilot assigned to a different specific task, with respect to different components of the dimensions of the flight maneuver (i.e. speed, vertical movement and horizontal movement). During the parabolic flight maneuver (Fig. 1), from its horizontal
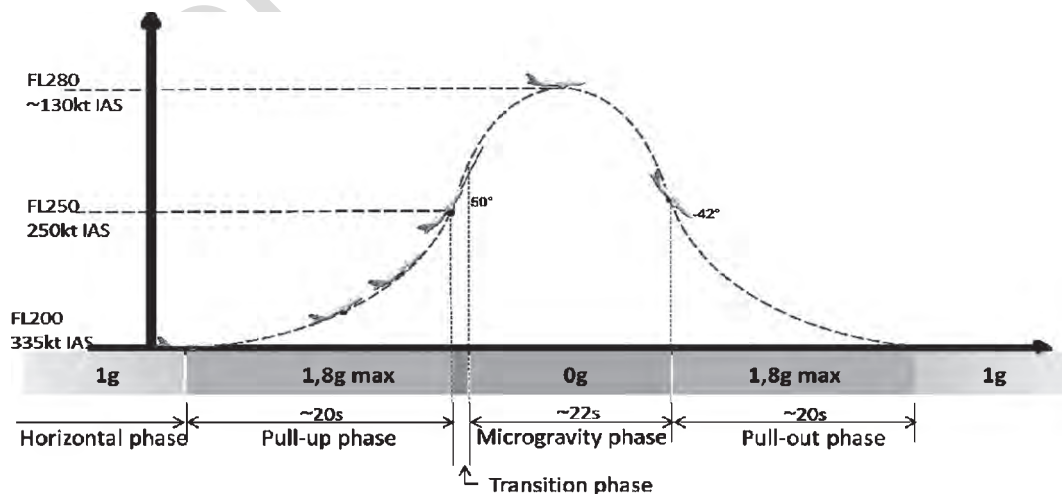

Fig. 1. Profile of a parabolic flight maneuver (copyright by NoveSpace, France).

Table 1
Protocol of measurements of one complete data set, exemplified for 1 test subject

Day I:			
Test subject 1:	Parabola	G-Forces	Measurements per parabola
	1st parabola	1g	1st measurement (1.1)
		0g	2nd measurement (1.2)
		1g	3rd measurement (1.3)
	2nd parabola	1g	1st measurement (2.1)
		0g	2nd measurement (2.2)
		1g	3rd measurement (2.3)
	[...]		
	10th parabola	1g	1st measurement (10.1)
		0g	2nd measurement (10.2)
		1g	3rd measurement (10.3)

flight path, the aircraft climbs steeply upward ("pull-up"), to follow a parabolic trajectory thereafter, as the pilots throttle back the propulsive force of the engines. This results in a free fall, during which the passengers experience nearly zero gravity (0 g) aboard, lasting for about 20 seconds. The phase of microgravity is followed by a "pull-out" phase, during which the pilots steer the aircraft back to its horizontal flight path. The phases of pull-up and pull-out comprise states of hypergravity (up to 1.8 g). As the duration of zero-gravity and hypergravity phases differ slightly between each parabola, a protocol of the exact durations will be kept by the pilots. The protocol will be available to all participants at the end of the flight campaign. A typical parabolic flight day has a total duration of approximately 3 hours and includes 31 parabolic flight maneuvers. In total, 12 experimental setups are mounted in the aircraft. The first parabola on each flight day is a test run for all teams on board. After a successful test run, the individual experimental set-ups are released for their measurement procedures, in accordance with each experimental study protocol. Overall, the Parabolic Flight Campaign will cover 4 flight days within the period of 2 weeks. Our group will participate in all 4 flight days. For each flight day, each one of three test subjects will be assigned to 10 parabolic flight maneuvers. For each of the parabolic flight maneuvers, measurements will be performed in different phases of gravity, as one data set per parabolic flight maneuver (Table 1).

2.5. Measurements

Each data set will comprise measurements of the microcirculation, blood pressure, pulse oxymetry and ECG. Two ECGs will be applied in this study: a standard 12-lead ECG and a Holter-ECG to investigate also changes of autonomic function. Both ECGs will measure heart rate constantly. Additionally, in the Holter-ECG the beginning of each zero-gravity phase will be marked.

Blood pressure, pulse oxymetry and microcirculation will be measured at different time points: Two measurements in normal gravity (1 g), one before and one after the flight of the parabola, and one measurement during zero-gravity (0 g) at the peak of the flight of the parabola (see also Fig. 1).

2.6. Experimental setup

In line with the Experimental Safety Data Package (ESDP) of NoveSpace specifically designed for each experiment, all experiments have been prepared with special emphasis on safety during the

parabolic flight maneuvers. After the final onboard setup of all experiments, a final security check will be conducted by NoveSpace.

In our experimental setup, all ECG-electrodes will be placed on the test subject before take-off. The Holter-ECG (Schiller medilog AR4 plus DARWIN2 Holter-ECG Professional-Package, Schiller AG, Baar, Switzerland) will be mounted completely before take-off and recording will be activated shortly prior to take-off. Recording will be stopped shortly after landing of the aircraft. The 12-lead ECG (Welch Allyn PC-based resting ECG, Skaneateles Falls, New York, USA) will be connected onboard with the test subject in supine position according to the setup for the measurements of the microcirculation. Accordingly, the recording of the 12-lead ECG will only be elicited during the measurements of the microcirculation.

The study subjects will be lying on the back with the feet in flight course, fixed by one strap over the legs and another one over the pelvis, to diminish free floating during the phases of weightlessness. Similarly, the head of the test subject will be fixed in a special mount (Speedblock head immobilizer, by Laerdal, Stavanger, Norway). The cuff of the blood pressure device (Welch Allyn Connex Pro BP 3400 digital blood pressure device, Skaneateles Falls, New York, USA) will be placed on the right upper arm. The study subject will elicit the measurement of the blood pressure at the beginning of each zero-gravity phase. The pulse oxymeter (Pulox PO-300, Nividion GmbH, Cologne, Germany) will be placed on the test subject's left index finger. All investigators will be attached to the grounds of the aeroplane by straps, so that safe and reproducible measurements can be conducted.

Visualization of the sublingual microcirculation will be performed by the application of the sidestream darkfield (SDF) imaging technique. The device used in this context is the Microscan® intravital-microscope (Microvision Medical, Amsterdam, The Netherlands), as implemented in our previous studies on microcirculation [23–25]. This device is a CE-licensed (Conformité Européene-licensed) handheld microscope for high-quality imaging approved for the application in human beings and has already served as diagnostic tool in more than 200 clinical trials. The device's tip carries a microscopic camera that acquires the imagery data of the sublingual capillary network [18]. The measuring process is initialized by placement of the device's tip towards the sublingual mucosa. On the connected tablet (Microsoft Surface Pro 4, Redmond, Washington, USA), the acquired video data are demonstrated as 2-dimensional AVI-videos (Audio Video Interleave – videos). Representative videos will be recorded and saved. The next step of the analysis entails the application of the software (AVA, Version 4.3C) [18, 26]. The main analysis of the recorded intravital blood flow measurements will be done offline.

The operator of the Microscan© device will be placed in supine position, headwards and in square angle to the study subject, with a hereby optimized view and accessibility to the sublingual mucosa, guaranteeing optimized measurements of the microcirculation. Next to the main operator an assistant will be placed who will operate the tablet connected to the Microscan© device. At the feet of the study subject, a second assistant in charge of documentation of the vital signs (blood pressure, heart rate and oxygen saturation) of the test subject will be positioned.

2.7. Schedule and procedures

Each flight day, preparations of the experiments onboard of the aircraft as well as preparations of all participating test subjects start at around 06:00 a.m. From 08:15 a.m., a prophylactic anti-motion sickness therapy is offered on ground, at the NoveSpace medical facility. At 08:45 a.m. the doors of the aircraft are closed. Take-off is scheduled for 09:00 a.m. Each flight day comprises the performance of a total of 31 parabolic flight maneuvers. Between each parabola there is a short break of about 2 minutes. After every set of 5 parabolas, a longer break of 5 minutes will be held. One large break (8 minutes) is scheduled after 15 parabolas.

3. Statistical analysis

Statistical analysis was performed by using a commercially available software (Graph Pad Prism Software, Version 6, Graph Pad Software, San Diego, California, USA). From the repetitive measurements of each subject, for the different experimental settings the mean values were calculated. For detection of differences between groups, not assuming a Gaussian distribution of the obtained parameters, the Wilcoxon matched-pairs signed rank test was used. A 2-tailed *p*-value < 0.05 was considered statistically significant. Data were presented as mean ± SD (Standard Deviation).

4. Results

Administration of standard doses of the anti-motion-sickness therapy regimens, with dimenhydrinate and scopolamine, respectively, did not alter the microcirculation in healthy subjects. Specifically, there was no significant alteration of the microcirculation per se observed one hour after peroral administration of 50 mg Dimenhydrate (Fig. 2) nor after the subcutaneous application of gender-specific doses of scopolamine (Fig. 3).

5. Discussion

Microcirculation is essential for tissue oxygenation, organ perfusion, gas metabolism and exchange of nutrients and waste products [15, 16]. In weightlessness, alterations of the macrocirculation are well known. However, data on the microcirculation is scarce.
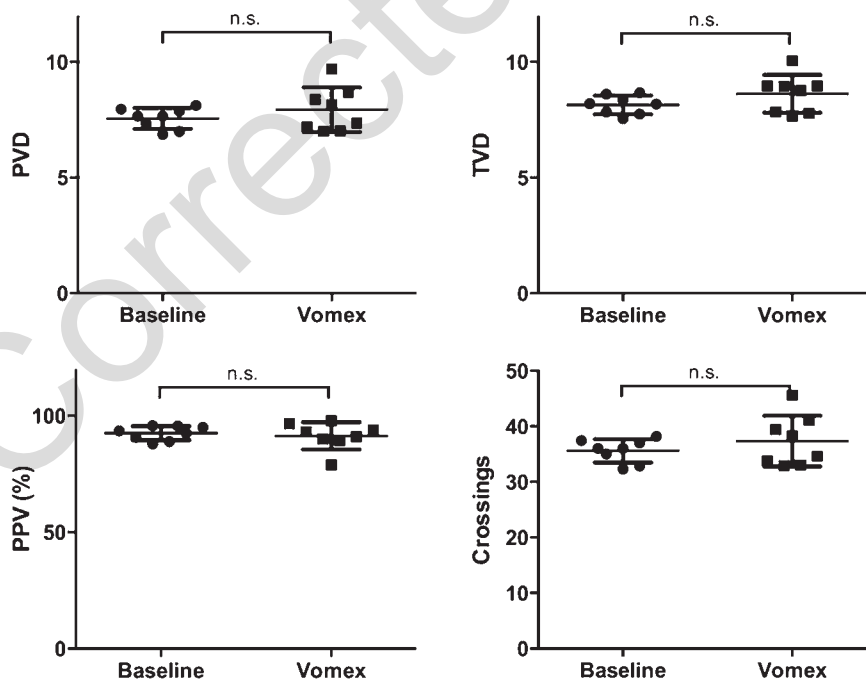

Fig. 2. Results of testing the influence of the administration of the anti-emetic drug Dimenhydrate (Vomex) on the microcirculation, obtained by evaluation of the microcirculation with Sidestream Darkfield (SDF) imaging, for *n* = 8 (PVD: Perfused Vessel Density, PPV (%): Proportion of perfused vessels, TVD: Total Vessel Density, Crossings: number of crossings of vessels recorded).
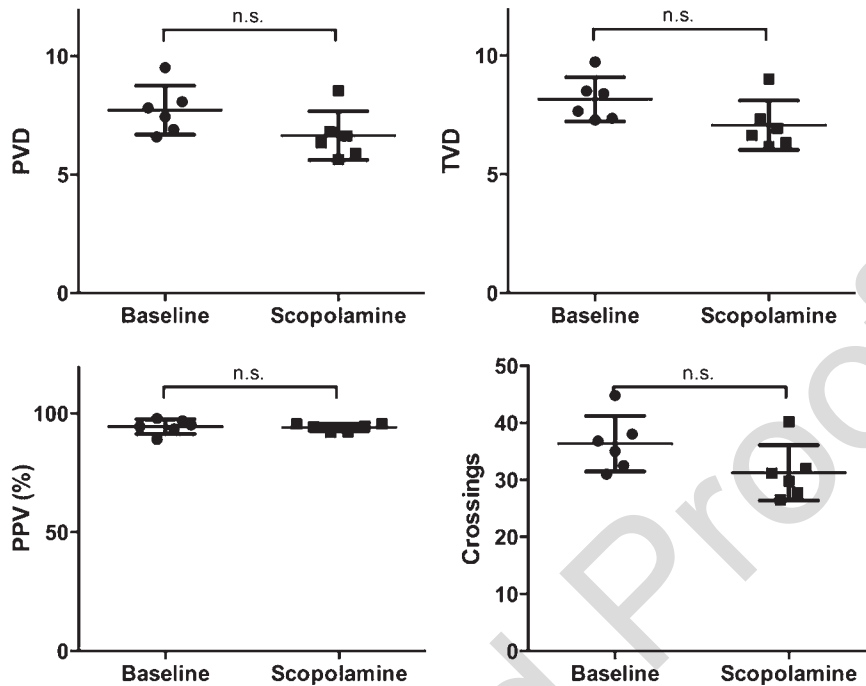
Fig. 3. Results of testing of the influence of the administration of the anti-emetic drug Scopolamine on the microcirculation, obtained by evaluation of the microcirculation with SDF-imaging, for $n = 6$ (PVD: Perfused Vessel Density, PPV (%): Proportion of perfused vessels, TVD: Total Vessel Density, Crossings: number of crossings of vessels recorded).

In our study, we aim at improving the understanding of alterations of the microcirculatory system in weightlessness. Zero-gravity leads to multiple pathophysiological reactions and adaptations in organisms [3, 27]. As a direct consequence of exposure to weightlessness, astronauts experience a number of pathophysiological changes which can lead to serious medical implications [3, 7]. Most immediate and significant is a headward shift of body fluids, as part of the adaptive responses of the cardiovascular system during weightlessness [3, 11]. Furthermore, capillary structural changes have been described in response to weightlessness [6]. As shown with septic patients in previous studies on earth, mortality rates were increased with impaired microcirculation. Interestingly, in this setting, macrohemodynamical variables seemed not to be reliable markers of septic shock recovery. These findings support the assumption that the adequate function of the microcirculation is a prerequisite for adequate organ function. Accordingly, malfunctioning of the microcirculation might cause organ-dysfunctions leading to possible life-threatening dysregulations. With this in mind, the importance of further investigations on the microcirculatory function in weightlessness seems evident, for the prevention of microcirculatory dysfunctions in space missions of long duration [28, 29].

Prior to participation in a parabolic flight, the prophylactic administration of an anti-motion-sickness medication is strongly recommended. In our pre-Campaign-study, we aimed at evaluating potential effects of these drugs on the microcirculation. Our experiments showed no effect of anti-motion sickness therapy on the microcirculation, thereby ruling out a potential influence of the motion sickness therapy on our planned experiments.

The aim of our study during the planned Parabolic Flight Campaign will be to evaluate the microcirculation of healthy subjects *in vivo* and during parabolic flight maneuvers, to deepen the understanding of cardiovascular response mechanisms during weightlessness. The presented study protocol will be applied in the course of the Parabolic Flight Campaign in France in September 2017. The results

observed will certainly enhance health-care on future space missions and might deepen our understanding of microcirculation on earth. Besides, our results might help optimizing both astronauts' and day-to-day patients' outcome.

6. Conclusions

We will thoroughly investigate the interrelations between the microcirculation and weightlessness. Based on our pre-study experiments reported in this paper, the application of motion sickness therapy does not alter the microcirculation and will therefore be applied during the experiments aboard the aircraft, to ensure optimized comfort of our test subjects in the course of the performance of the parabolic flight maneuvers.

The results observed in our investigation of the microcirculation in weightlessness will enhance health-care on future space missions and might deepen the understanding of microcirculation on earth. Our results might therefore optimize both astronauts' and patients' outcomes.

Acknowledgments

References

[1] Limper U, Gauger P, Beck P, Krainski F, May F, Beck LE. Interactions of the human cardiopulmonary, hormonal and body fluid systems in parabolic flight. Eur J Appl Physiol. 2014;114(6):1281-95.

[2] Yaqub F. Space travel: Medicine in extremes. Lancet Respir Med. 2015;3(1):20-1.

[3] Pietsch J, Bauer J, Egli M, Infanger M, Wise P, Ulbrich C, et al. The effects of weightlessness on the human organism and mammalian cells. Curr Mol Med. 2011;11(5):350-64.

[4] Crawford-Young SJ. Effects of microgravity on cell cytoskeleton and embryogenesis. Int J Dev Biol. 2006;50(2-3):183-91.

[5] Kennedy AR, Crucian B, Huff JL, Klein SL, Morens D, Murasko D, et al. Effects of sex and gender on adaptation to space: Immune system. J Womens Health. 2014;23(11):956-8.

[6] Glenny RW, Lamm WJ, Bernard SL, An D, Chornuk M, Pool SL, et al. Selected contribution: Redistribution of pulmonary perfusion during weightlessness and increased gravity. J Appl Physiol. 1985;89(3):1239-48.

[7] Convertino VA. Status of cardiovascular issues related to space flight: Implications for future research directions. Respir Physiol Neurobiol. 2009;169(1):19.

[8] Hughson RL, Shoemaker JK, Blaber AP, Arbeille P, Greaves DK, Pereira-Junior PP, et al. Cardiovascular regulation during long-duration spaceflights to the International Space Station. J Appl Physiol. 1985;112(5):719-27.

[9] Yates BJ, Kerman IA. Post-spaceflight orthostatic intolerance: Possible relationship to microgravity-induced plasticity in the vestibular system. Brain Res Brain Res Rev. 1998;28(1-2):73-82.

[10] Maier JA, Cialdai F, Monici M, Morbidelli L. The impact of microgravity and hypergravity on endothelial cells. Biomed Res Int. 2015;434803(10):13.

[11] Norsk P, Asmar A, Damgaard M, Christensen NJ. Fluid shifts, vasodilatation and ambulatory blood pressure reduction during long duration spaceflight. J Physiol. 2015;593(3):573-84.

[12] Norsk P, Damgaard M, Petersen L, Gybel M, Pump B, Gabrielsen A, et al. Vasorelaxation in space. Hypertension. 2006;47(1):69-73.

[13] Zuj KA, Arbeille P, Shoemaker JK, Blaber AP, Greaves DK, Xu D, et al. Impaired cerebrovascular autoregulation and reduced CO(2) reactivity after long duration spaceflight. Am J Physiol Heart Circ Physiol. 2012;302(12):6.

[14] Blaber AP, Zuj KA, Goswami N. Cerebrovascular autoregulation: Lessons learned from spaceflight research. Eur J Appl Physiol. 2013;113(8):1909-17.

[15] Abularrage CJ, Sidawy AN, Aidinian G, Singh N, Weiswasser JM, Arora S. Evaluation of the microcirculation in vascular disease. J Vasc Surg. 2005;42(3):574-81.

[16] den Uil CA, Klijn E, Lagrand WK, Brugts JJ, Ince C, Spronk PE, et al. The microcirculation in health and critical disease. Prog Cardiovasc Dis. 2008;51(2):161-70.

[17] Colbert JF, Schmidt EP. Endothelial and microcirculatory function and dysfunction in sepsis. Clin Chest Med. 2016;37(2):263-75.

[18] McGarr GW, Hodges GJ, Cheung SS. An adjustable stabilizing device for imaging the cutaneous microcirculation with Sidestream Dark Field imaging. Microvascular Research. 2015;100:1-3.

[19] Jung C, Kelm M. Evaluation of the microcirculation in critically ill patients. Clin Hemorheol Microcirc. 2015;61(2):213-24.

[20] Jung C, Lauten A, Ferrari M. Microcirculation in cardiogenic shock: From scientific bystander to therapy target. Crit Care. 2010;14(5):6.

[21] Jung C, Rodiger C, Fritzenwanger M, Schumm J, Lauten A, Figulla HR, et al. Acute microflow changes after stop and restart of intra-aortic balloon pump in cardiogenic shock. Clinical Research in Cardiology. 2009;98(8):469-75.

[22] Sharawy N, Mahrous R, Whynot S, George R, Lehmann C. Clinical relevance of early sublingual microcirculation monitoring in septic shock patients. Clinical Hemorheology and Microcirculation. 2017. doi: 10.3233/CH-170244

[23] Jung C, Ferrari M, Gradinger R, Fritzenwanger M, Pfeifer R, Schlosser M, et al. Evaluation of the microcirculation during extracorporeal membrane-oxygenation. Clinical Hemorheology and Microcirculation. 2008;40(4):311-4.

[24] Jung C, Ferrari M, Rodiger C, Fritzenwanger M, Goebel B, Lauten A, et al. Evaluation of the sublingual microcirculation in cardiogenic shock. Clin Hemorheol Microcirc. 2009;42(2):141-8.

[25] Jung C, Ferrari M, Roediger C, Fritzenwanger M, Figulla HR. Combined Impella and intra-aortic ballon pump support to improve macro- and microcirculation: A clinical case. Clinical Research in Cardiology. 2008;97(11):849-50.

[26] De Backer D, Hollenberg S, Boerma C, Goedhart P, Buchele G, Ospina-Tascon G, et al. How to evaluate the microcirculation: Report of a round table conference. Crit Care. 2007;11(5).

[27] Lathers CM, Charles JB, Elton KF, Holt TA, Mukai C, Bennett BS, et al. Acute hemodynamic responses to weightlessness in humans. J Clin Pharmacol. 1989;29(7):615-27.

[28] Donati A, Domizi R, Damiani E, Adrario E, Pelaia P, Ince C. From macrohemodynamic to the microcirculation. Crit Care Res Pract. 2013;892710(10):27.

[29] Ince C. Hemodynamic coherence and the rationale for monitoring the microcirculation. Crit Care. 2015;19(3):18.

Frontiers | Frontiers in Cardiovascular Medicine

Assessing physical activity with the wearable cardioverter defibrillator in patients with newly diagnosed heart failure

Konstantinos Iliodromitis[1,2]*, Zsuzsanna Balogh[1],
Filippos Triposkiadis[3], Spyridon Deftereos[4], Dimitrios Vrachatis[4],
Nana-Yaw Bimpong-Buta[1,2], Fabian Schiedat[5†]
and Harilaos Bogossian[1,2†]

[1]Clinic for Cardiology and Electrophysiology, Evangelical Hospital Hagen-Haspe, Hagen, Germany,
[2]School of Medicine, Witten/Herdecke University, Witten, Germany, [3]Department of Cardiology, Larissa
University General Hospital, Larissa, Greece, [4]Medical School, National and Kapodistrian University of
Athens, Athens, Greece, [5]Clinic for Cardiology, Marienhospital Gelsenkirchen Academic Hospital of the
Ruhr University Bochum, Bochum, Germany

Background: The wearable cardioverter defibrillator (WCD), (LifeVest, ZOLL, Pittsburgh, PA, USA) is a medical device designed for the temporary detection and treatment of malignant ventricular tachyarrhythmias. WCD telemonitoring features enable the evaluation of the physical activity (PhA) of the patients. We sought to assess with the WCD the PhA of patients with newly diagnosed heart failure.

Methods: We collected and analyzed the data of all patients treated with the WCD in our clinic. Patients with newly diagnosed ischemic, or non-ischemic cardiomyopathy and severely reduced ejection fraction, who were treated with the WCD for at least 28 consecutive days and had a compliance of at least 18 h the day were included.

Results: Seventy-seven patients were eligible for analysis. Thirty-seven patients suffered from ischemic and 40 from non-ischemic heart disease. The average days the WCD was carried was 77.3 ± 44.6 days and the mean wearing time was 22.8 ± 2.1 h. The patients showed significantly increased PhA measured by daily steps between the first two and the last two weeks (Mean steps in the first 2 weeks: $4,952.6 \pm 3,052.7$ vs. mean steps in the last 2 weeks: $6,119.6 \pm 3,776.2$, p-value: < 0.001). In the end of the surveillance period an increase of the ejection fraction was observed (LVEF-before: $25.8 \pm 6.6\%$ vs. LVEF-after: $37.5 \pm 10.6\%$, $p < 0.001$). Improvement of the EF did not correlate with the improvement of PhA.

Conclusion: The WCD provides useful information regarding patient PhA and may be additionally utilized for early heart failure treatment adjustment.

KEYWORDS

wearable cardioverter defibrillator, life vest, physical activity, ejection fraction, heart failure, sudden cardiac death, remote monitoring

Introduction

Heart failure with reduced ejection fraction (HFrEF) is a clinical condition associated with increased sudden cardiac death (SCD) risk (1–4). In the early phase of newly diagnosed HFrEF, reversible causes such as ongoing myocardial ischemia, tachyarrhythmias, or acute peri-myocarditis must be treated promptly. Furthermore,

despite swift initiation of the evidenced-based medical therapy for heart failure, titration of the of the disease-modifying drugs may be progressively achieved over longer periods (5). During this time frame, the SCD risk may be temporarily high, or cannot be determined. On the other hand, a prophylactic transvenous implantation of a cardioverter-defibrillator (ICD) in patients with severely reduced left ventricular ejection fraction (LVEF) in the early phase after an acute myocardial infarction lacks survival benefit (6, 7).

The wearable cardioverter defibrillator (WCD, LifeVest, ZOLL, Pittsburgh, PA, USA) is a device specifically designed for the temporary detection and treatment of ventricular tachyarrhythmias in patients during a vulnerable period for sudden arrhythmic death. The recently published European Guidelines for the prevention of SCD suggest that the surveillance with the WCD may be prophylactically considered in the early phase after acute myocardial infarction, whereas data on the beneficial effect of the WCD for patients with newly diagnosed non-ischemic cardiomyopathy are sparse (8). The device contains four non-adhesive electrodes positioned orthogonally around the waist (anterior-posterior & right-left), able to produce a two-lead filtered electrocardiogram (ECG) and three self-gelling defibrillation electrodes. This allows an effective and continuous arrhythmia detection from the WCD after combining data from both heart rate and QRS-complex morphology. All detected arrhythmic events are stored in the *LifeVest Network server* (https://lifevestnetwork.zoll.com) and the physician is automatically notified.

Furthermore, WCD has an incorporated accelerometer, which facilitates the counting of the steps, thus providing information about the patients' daily physical activity (PhA). The reliability of the WCD accelerometer as a tool for the assessment of PhA has been already successfully proven compared with the 6-minute-walking test (6MWT) (9).

Registries from Europe and the United States have thoroughly examined the feasibility and safety of the WCD during a vulnerable period for SCD in real world scenarios (10–15). Furthermore, the importance of patient risk stratification over time for SCD after initiation and optimization of heart failure treatment and the reduction of unnecessary ICD implantations has been previously demonstrated (16–18). The VEST-trial examined prospectively a potential benefit of the WCD in patients with reduced LVEF < 35% after AMI (19). The study showed no benefit in this population, however the wearing time with the device was much lower than anticipated (20).

Finally, data selected from the WCD are being stored and can be transmitted to the physician for offline analysis. Available data contain arrhythmic events, heart rate profile and the PhA of the patient in the form of daily steps (**Figure 1**).

In the present single-center, retrospective study we sought to evaluate the PhA of all patients with newly diagnosed severely reduced LVEF of either ischemic, or non-ischemic etiology, being telemonitored with the WCD until the end of the surveillance period. We also sought to identify clinical factors having an impact to the PhA of the patients.

Methods

Study population

A retrospective analysis of all patients treated with the WCD from January 2016 until October 2022 in our clinic was conducted. Inclusion criteria for the study were newly diagnosed non-valvular heart failure, with severely reduced LVEF less than 35% at the day of hospital discharge, of either ischemic, or non-ischemic etiology. Additional inclusion criteria were the duration of the bridging period with the WCD and the compliance to the treatment. Thus, a treatment with the WCD for at least 28 consecutive days and a minimum wearing time of the WCD of at least 18 h daily were prerequisite (**Figure 2**). Patients with primary electrical heart disease, or being bridged with WCD after removal of their implanted cardioverter defibrillator due to device infection were excluded from the study. The study protocol conformed to the ethical guidelines of the 1975 Declaration of Helsinki.

Physical activity estimation

All data for analysis were retrieved from the manufacturer database (LifeVest, ZOLL, Pittsburgh, PA, USA). The detection of either ventricular, or supraventricular episodes was noted. The endpoint of PhA was assessed by calculating the average number of daily steps in the first two weeks and comparing it to the average number of daily steps from the last two weeks prior to termination of the surveillance with the WCD. Additionally, we reported the initiation and/or modifications of all guideline recommended heart failure medications affecting the neurohumoral cycle of heart failure at the day of hospital discharge. Finally, we recorded and compared the change of the LVEF of each patient and correlated it with the PhA estimated with the WCD.

Evaluation of the left ventricular ejection fraction

LVEF evaluation was performed with 2D-transthoracic echocardiography using the modified Simpson's method. Transthoracic echocardiography was performed after reperfusion therapy and/or initiation of medical heart failure treatment (index event) prior to WCD therapy, as well as on scheduled follow-up prior to decision for termination of the WCD therapy.

Statistical analysis

The SPSS 29 (IBM SPSS Statistics) was used for all statistical analyses of this study. Continuous variables are shown as the mean ± standard deviation (SD). Categorical variables are presented as percentages. Pairwise comparisons of continuous variables were performed using the paired t-test. Factors affecting the results were examined with multivariate linear regression

FIGURE 1
Recordings of the trends from wearable cardioverter defibrillator during the entire surveillance period. Highlighted with red color are the first two weeks and the last 14 days of the total wearing period.

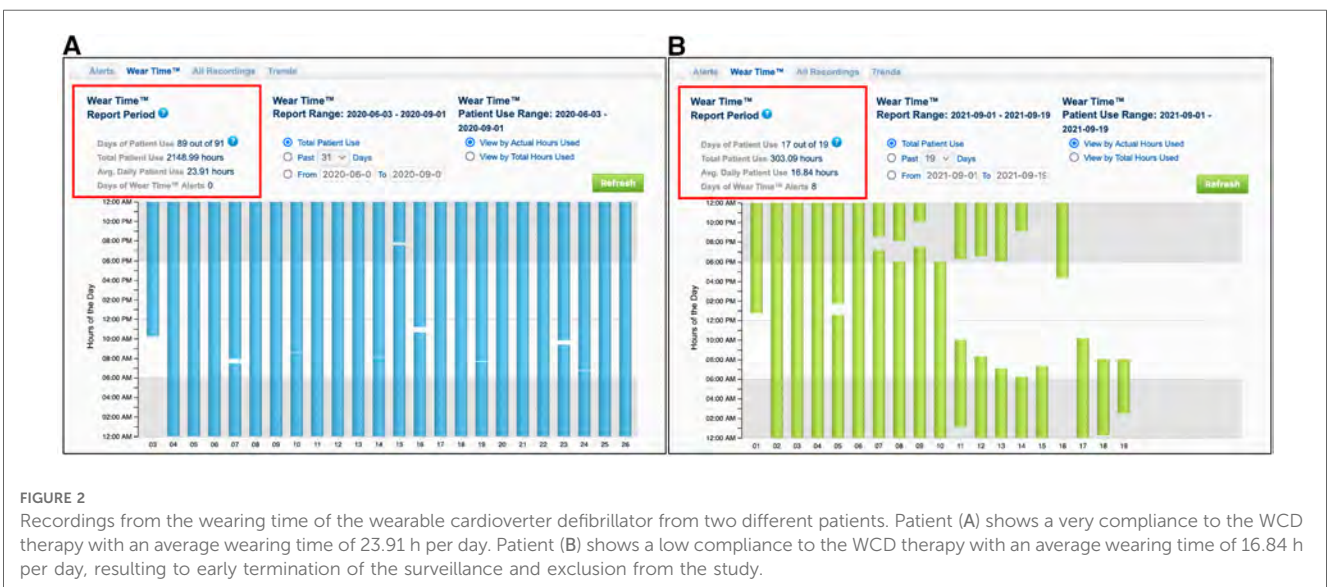FIGURE 2
Recordings from the wearing time of the wearable cardioverter defibrillator from two different patients. Patient (A) shows a very compliance to the WCD therapy with an average wearing time of 23.91 h per day. Patient (B) shows a low compliance to the WCD therapy with an average wearing time of 16.84 h per day, resulting to early termination of the surveillance and exclusion from the study.

analysis. All of the statistical tests were two-sided at a significance level of 0.05.

Results

From January 2016 to October 2022 a total of 136 patients had been treated with the WCD. Inclusion criteria were fulfilled in 77 patients, who were included in the analysis. Fifty-five patients were males (70.5%) and the mean age of the study population was 63.7 ± 11.7 years. WCD therapy without further device implantation was terminated in 50 patients (64.9%). In particular, 44 of the patients showed an improvement of their left ventricular function with a LVEF over 35%, whereas six patients denied a permanent device implantation despite no adequate LVEF improvement under heart failure medication at the end of the follow-up. A transvenous one-chamber cardioverter defibrillator (ICD) was implanted in 18 patients (23.4%) and a biventricular cardioverter defibrillator (CRT-D) in 9 patients (11.7%). Episodes of non-sustained ventricular tachycardia were recorded in four individuals (5.2%), all of whom showed no improvement of their LVEF (Table 1).

The average days that our study population carried the WCD was 77.3 ± 44.6 days and the average daily wearing-time of the WCD was 22.8 ± 2.1 h. An improvement of the LVEF was noted at the end of the surveillance period with the WCD (LVEF-before: $25.8 \pm 6.6\%$ vs. LVEF-after: $37.5 \pm 10.6\%$, $p < 0.001$).

Furthermore, the PhA of the patients increased significantly in the last two weeks of surveillance, compared to the first two weeks (mean steps first two weeks: $4,952.6 \pm 3,052.7$ vs. mean steps last two weeks: $6,116.6 \pm 3,776.2$, $p < 0.001$) (Table 2).

Multivariate regression analysis was used to evaluate the factors affecting the change of the left ventricular ejection fraction (Δ-LVEF). Included factors in the model were the type of cardiomyopathy (ischemic vs. non-ischemic), the wearing time of the WCD in hours, the length of duration the WCD was carried in days and the initiation of each of the guideline recommended heart failure medications (B-Blockers, Angiotensin Converting Enzyme (ACE)-Inhibitors, Angiotensin-1 (AT-1) receptor blockers, Sacubitril/Valsartan, Mineralcorticoid Receptor Antagonists (MRAs) and Sodium-glucose Cotransporter-2 (SGLT2) Inhibitors (Table 3). The only factor that was associated with LVEF improvement was Sacubitril/Valsartan (Table 4).

Additionally, multivariate regression analysis was used to evaluate the factors affecting the change of the physical activity measured in daily steps (Δ-Steps). Included factors in the model were all previously mentioned plus the Δ-LVEF. The only factors associated with improvement in physical activity were wearing

TABLE 1 Demographic data.

Study population ($n = 77$)		n	%
Males		55	71.4
Females		22	28.6
Age (years)		63.7 ± 11.7	
Body mass index (BMI—kg/m²)		28.9 ± 5.7	
Comorbidities		**n**	**%**
Ischemic Cardiomyopathy		37	48.1
Non-ischemic Cardiomyopathy		40	51.9
Atrial Fibrillation		30	39
	Paroxysmal	7	9.1
	Persistent	14	18.2
	Permanent	9	11.7
Coronary Heart Disease		47	61.4
Chronic obstructive pulmonary disease		15	19.5
Diabetes mellitus		22	28.6
Arterial hypertension		57	74
Overweight (BMI >25 kg/m²)		53	68.8
Arrhythmic events and Outcome		**n**	**%**
Non sustained ventricular tachycardia		4	5.2
Sustained ventricular tachycardia		0	0
Ventricular fibrillation		0	0
ICD Implantation		18	23.4
CRT-D Implantation		9	11.7
No device implantation		50	64.9
Improvement of LVEF >35%		44	57,1

LVEF, left ventricular ejection fraction; ICD, implantable cardioverter defibrillator; CRT-D, cardiac resynchronization therapy defibrillator.

TABLE 2 Follow-up Data.

		First two weeks	Last two weeks	P-value
Average daily steps		$4,952.6 \pm 3,052.7$	$6,119.6 \pm 3,776.2$	<0.001
Average heart rate		73.1 ± 11.1	71.4 ± 10.6	ns
		Beginning of follow-up	**End of follow-up**	**P-value**
Left ventricular ejection fraction (%)		25.8 ± 6.6	37.5 ± 10.7	<0.001
Δ-Steps	$1,167.1 \pm 2,455.9$			
Δ-LVEF (%)	11.6 ± 10.6			
Wearing Time (hours)	22.8 ± 2.1			
Days carried	77.3 ± 44.6			

Δ-Steps, Improvement of physical activity measured in daily steps; Δ-LVEF, Improvement of left ventricular ejection fraction.

TABLE 3 Overview of medical treatment for heart failure.

		Prior index event (n)	%	After index event (n)	%
B-Blockers		31	40,3	75	97,4
ACE-Inhibitors		18	23,4	19	24,7
AT-1 Receptor Blockers		15	19,5	8	10,4
Sacubitril/ Valsartan		4	5,2	50	64,9
MRAs		12	15,6	65	84,4
SGLT2-Inhibitors		5	6,5	34	44,2

ACEs, angiotensin converting enzyme; AT-1, angiotensin-1; MRAs, mineralcorticoid receptor antagonists, SGLT2, sodium-glucose cotransporter-2.

TABLE 4 Factors potentially associated with improvement of left ventricular ejection fraction (⊿-LVEF). Results of multivariate regression analysis.

	Unstandardized Coefficients		Standardized Coefficients	t	P Value	95.0% Confidence Interval for B	
	B	Std. Error	Beta			Lower Bound	Upper Bound
(Constant)	−34.706	17.534		−1.979	0.052	−69.704	0.292
Type of heart failure	−2.841	2.369	−0.135	−1.199	0.235	−7.570	1.887
Wearing time (hours)	0.964	0.570	0.189	1.693	0.095	−0.173	2.101
Days carried	0.042	0.026	0.177	1.595	0.115	−0.011	0.095
B-Blockers	8.345	7.406	0.126	1.127	0.264	−6.437	23.127
ACEi	12.080	7.121	0.496	1.697	0.094	−2.132	26.293
ARBs	5.404	8.030	0.157	0.673	0.503	−10.623	21.432
Sacubitril/valsartan	15.323	7.132	0.697	2.148	0.035	1.087	29.559
MRAs	1.905	3.296	0.066	0.578	0.565	−4.673	8.484
SGLT-2i	−1.730	2.457	−0.082	−0.704	0.484	−6.634	3.174

Type of heart failure: ischemic vs. nonischemic; ACEi, angiotensin converting enzyme inhibitors; ARBs, angiotensin receptor blockers; MRAs, mineralocorticoid receptor antagonists; SGLT-2i, sodium-glucose cotransporter-2 inhibitors.

time of the WCD and the length of duration the WCD was carried (**Table 5**).

Discussion

The WCD is a non-invasive option for the treatment of malignant ventricular tachyarrhythmias during a temporary period with increased risk for SCD. Also, the WCD allows daily remote telemonitoring of the patient's PhA during the entire surveillance period.

Currently, the 6*M*WT is a well-established and simple medical tool for the evaluation of functional capacity among patients with heart failure (21, 22). Results from Burch AE. et al. showed that the WCD-guided 6MWT provides similar step counts compared to clinician-guided 6MWT, suggesting the reliability and accuracy of step counts with the WCD (9). However, a limitation of the clinical 6MWT remains its applicability in every-day and out-of-hospital settings, as well as its continuity in real life during the entire day and over longer periods. On the contrary, high adherence during the entire day, which is a prerequisite of an

effective WCD therapy, enables more accurate and representative assessment of PhA in patients with HFrEF.

The high wearing time compliance with an average daily wearing time of the WCD of 22,8 ± 2.1 h per day was aligned with the average wearing time of previous studies (10–13, 23) assuring a careful daily telemonitoring of the patients. Additionally, the average wearing days that our population carried the WCD was 77.3 ± 44.6 days. Tripp C. et al. examined the PhA with the WCD in a large cohort of patients after acute myocardial infarction (24). Results from that study showed a significant increase of the PhA from the beginning of the prescription of WCD to the end of the therapy. Furthermore, they showed a negative relationship between wearing time over 20 h per day and PhA. Our results confirm their first finding, showing a positive correlation between incremental PhA measured by daily steps and wearing days of the WCD. This may be attributed to a general improvement of health condition. On the contrary, we report a positive correlation between prolonged wearing time and increased PhA. We assume that this may be the result of improved familiarization with the WCD and increased confidence of the patient to exercise after the index event, as none of the administered medical substances were

TABLE 5 Factors potentially associated with improvement of physical activity (⊿-steps). Results of multivariable regression analysis.

	Unstandardized Coefficients		Standardized Coefficients	t	P value	95.0% Confidence Interval for B	
	B	Std. Error	Beta			Lower Bound	Upper Bound
(Constant)	−7,403.588	4,378.612		−1.691	0.096	−16,145.770	1,338.594
Type of heart failure	426.845	581.195	0.087	0.734	0.465	−733.548	1,587.239
Change in LVEF	7.474	29.654	0.032	0.252	0.802	−51.731	66.679
Wearing Time (hours)	300.357	141.208	0.253	2.127	0.037	18.427	582.287
Days carried	13.830	6.518	0.251	2.122	0.038	0.816	26.845
B-Blockers	2,756.052	1,814.530	0.180	1.519	0.134	−866.775	6,378.878
ACEi	−2,094.027	1,765.064	−0.370	−1.186	0.240	−5,618.091	1,430.037
ARBs	−1,349.070	1,955.594	−0.169	−0.690	0.493	−5,253.539	2,555.399
Sacubitril/valsartan	−2,022.073	1,789.791	−0.395	−1.130	0.263	−5,595.506	1,551.360
MRAs	−442.009	801.970	−0.066	−0.551	0.583	−2,043.194	1,159.176
SGLT-2i	50.226	598.536	0.010	0.084	0.933	−1,144.789	1,245.241

Type of heart failure: ischemic vs. nonischemic; LVEF, left ventricular ejection fraction; ACEi, angiotensin converting enzyme inhibitors; ARBs, angiotensin receptor blockers; MRAs, Mineralocorticoid receptor antagonists, SGLT-2i, Sodium-glucose cotransporter-2 inhibitors.
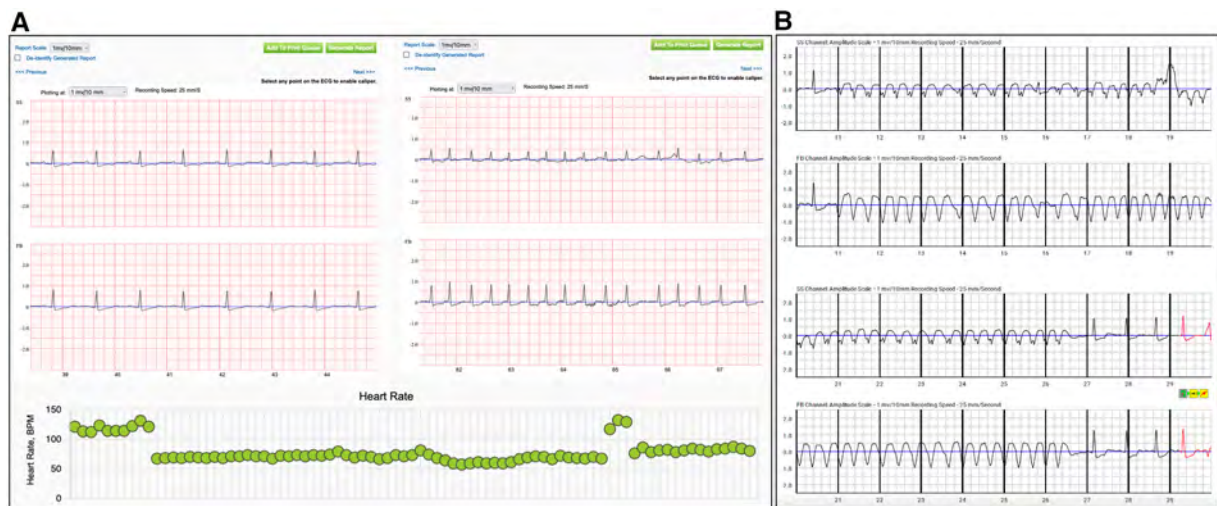
FIGURE 3
Recordings of alerts from the wearable cardioverter defibrillator during the surveillance period. Patient (A) reported worsening of dyspnea, with the electrocardiographic confirmation of atrial fibrillation. In the lower panel are depicted the daily heart rate trends from the same patient, with a sudden increase of the heart rate suggestive for an arrhythmic event. (SS: side-side electrodes, FB: front-back electrodes) Recording from the wearable cardioverter defibrillator of an episode of non-sustained ventricular tachycardia in patient (B) with non-ischemic cardiomyopathy. (SS: side-side electrodes, FB: front-back electrodes).

correlated with the improvement of PhA. Similar results have been published by Hillmann et al., examining the PhA with the WCD in a cohort of patients with both ischemic and non-ischemic cardiomyopathy (25), showing a significant increase of the step count between the first and last week of surveillance.

A novel element from the findings of our study is the lack of correlation between the improvement of the LVEF and the PhA of the patients. During the surveillance period with the WCD, a statistically significant improvement of the LVEF was recorded. The analysis of the applied medication showed, a positive correlation between the sacubitril/valsartan initiation and LVEF improvement. None of the remaining prescribed evidenced-based and recommended heart medication did correlate with the improvement of PhA. Moreover, the improvement of the PhA of the patients did not correlate with the improvement of the LVEF. These results are in accordance with previous studies highlighting the limited value of LVEF as a marker for physiological assessment, as this may vary depending on the loading condition of the patient (preload and afterload) and the myocardial contractility (26–28).

Thus, high adherence to WCD therapy, patient familiarization and education with the device facilitate a high quality daily telemonitoring of PhA. This may lead to early physician interference in cases of patients with good WCD compliance and gradually reduced PhA for the adjustment of the applied medical therapy and avoid unnecessary hospital admissions (Figure 3). None of them showed improvement of their LVEF during the bridging period with the WCD. Although these events may not be enough for conclusions, it highlights the importance of careful interrogation of all available recordings provided from WCD for more accurate, non-invasive risk stratification of the patients.

Limitations

The retrospective design of the current study remains a limitation. Furthermore, the inclusion criteria for the study population may introduce selection bias in the results, however high compliance to the WCD is prerequisite for effective therapy and the extraction of valid results. Finally, alternative ways for the calculation of PhA, such as steps per hour wearing time, might have been more descriptive.

Conclusion

The WCD provides useful information regarding the PhA in patients with heart failure, who are having good compliance.

Data availability statement

The original contributions presented in the study are included in the article, further inquiries can be directed to the corresponding author.

Ethics statement

Ethical review and approval was not required for the study on human participants in accordance with the local legislation and institutional requirements. Written informed consent for participation was not required for this study in

accordance with the national legislation and the institutional requirements.

Author contributions

KI, FT, and HB contributed to conception and design of the study. KI and ZB organized the database. FT performed the statistical analysis. KI wrote the first draft of the manuscript. KI, ZB, FT, SD, DV, FS, NYBB and HB wrote sections of the manuscript. All authors contributed to the article and approved the submitted version.

Funding

Conflict of interest

The authors declare that the research was conducted in the absence of any commercial or financial relationships that could be construed as a potential conflict of interest.

The handling editor DD declared a past co-authorship with the author HB.

Publisher's note

All claims expressed in this article are solely those of the authors and do not necessarily represent those of their affiliated organizations, or those of the publisher, the editors and the reviewers. Any product that may be evaluated in this article, or claim that may be made by its manufacturer, is not guaranteed or endorsed by the publisher.

References

1. Solomon SD, Zelenkofske S, McMurray JJ, Finn PV, Velazquez E, Ertl G, et al. Sudden death in patients with myocardial infarction and left ventricular dysfunction, heart failure, or both. N Engl J Med. (2005) 352(25):2581–8. doi: 10.1056/NEJMoa043938

2. Busk M, Maeng M, Kristensen SD, Thuesen L, Krusell LR, Mortensen LS, et al. Timing, causes, and predictors of death after three years' follow-up in the danish multicenter randomized study of fibrinolysis versus primary angioplasty in acute myocardial infarction (DANAMI-2) trial. Am J Cardiol. (2009) 104(2):210–5. doi: 10.1016/j.amjcard.2009.03.014

3. Beggs SAS, Jhund PS, Jackson CE, McMurray JJV, Gardner RS. Non-ischaemic cardiomyopathy, sudden death and implantable defibrillators: a review and meta-analysis. Heart (British Cardiac Society). (2018) 104(2):144–50. doi: 10.1136/heartjnl-2016-310850

4. Køber L, Thune JJ, Nielsen JC, Haarbo J, Videbæk L, Korup E, et al. Defibrillator implantation in patients with nonischemic systolic heart failure. N Engl J Med. (2016) 375(13):1221–30. doi: 10.1056/NEJMoa1608029

5. McDonagh TA, Metra M, Adamo M, Gardner RS, Baumbach A, Böhm M, et al. 2021 ESC guidelines for the diagnosis and treatment of acute and chronic heart failure. Eur Heart J. (2021) 42(36):3599–726. doi: 10.1093/eurheartj/ehab368

6. Steinbeck G, Andresen D, Seidl K, Brachmann J, Hoffmann E, Wojciechowski D, et al. Defibrillator implantation early after myocardial infarction. N Engl J Med. (2009) 361(15):1427–36. doi: 10.1056/NEJMoa0901889

7. Hohnloser SH, Kuck KH, Dorian P, Roberts RS, Hampton JR, Hatala R, et al. Prophylactic use of an implantable cardioverter-defibrillator after acute myocardial infarction. N Engl J Med. (2004) 351(24):2481–8. doi: 10.1056/NEJMoa041489

8. Zeppenfeld K, Tfelt-Hansen J, de Riva M, Winkel BG, Behr ER, Blom NA, et al. 2022 ESC guidelines for the management of patients with ventricular arrhythmias and the prevention of sudden cardiac death. Eur Heart J. (2022) 43(40):3997–4126. doi: 10.1093/eurheartj/ehac262

9. Burch AE, Scherr D, Rieth A, Griffin J, Bianco NR, Odeneg T, et al. Wearable cardioverter defibrillator-guided 6-min walk test performed at home is accurate and reliable: rESULTS OF THE TRENDS STUDY. J Cardiopulm Rehabil Prev. (2020) 40 (2):E14–e7. doi: 10.1097/HCR.0000000000000441

10. Kutyifa V, Moss AJ, Klein H, Biton Y, McNitt S, MacKecknie B, et al. Use of the wearable cardioverter defibrillator in high-risk cardiac patients: data from the prospective registry of patients using the wearable cardioverter defibrillator (WEARIT-II registry). Circulation. (2015) 132(17):1613–9. doi: 10.1161/CIRCULATIONAHA.115.015677

11. Feldman AM, Klein H, Tchou P, Murali S, Hall WJ, Mancini D, et al. Use of a wearable defibrillator in terminating tachyarrhythmias in patients at high risk for sudden death: results of the WEARIT/BIROAD. Pacing and Clin Electrophysiol: PACE. (2004) 27(1):4–9. doi: 10.1111/j.1540-8159.2004.00378.x

12. Chung MK, Szymkiewicz SJ, Shao M, Zishiri E, Niebauer MJ, Lindsay BD, et al. Aggregate national experience with the wearable cardioverter-defibrillator: event rates, compliance, and survival. J Am Coll Cardiol. (2010) 56(3):194–203. doi: 10.1016/j.jacc.2010.04.016

13. Wäßnig NK, Günther M, Quick S, Pfluecke C, Rottstädt F, Szymkiewicz SJ, et al. Experience with the wearable cardioverter-defibrillator in patients at high risk for sudden cardiac death. Circulation. (2016) 134(9):635–43. doi: 10.1161/CIRCULATIONAHA.115.019124

14. Masri A, Altibi AM, Erqou S, Zmaili MA, Saleh A, Al-Adham R, et al. Wearable cardioverter-defibrillator therapy for the prevention of sudden cardiac death: a systematic review and meta-analysis. JACC Clinical Electrophysiol. (2019) 5 (2):152–61. doi: 10.1016/j.jacep.2018.11.011

15. Garcia R, Combes N, Defaye P, Narayanan K, Guedon-Moreau L, Boveda S, et al. Wearable cardioverter-defibrillator in patients with a transient risk of sudden cardiac death: the WEARIT-France cohort study. Europace. (2021) 23(1):73–81. doi: 10.1093/europace/euaa268

16. Dreher TC, El-Battrawy I, RÖger S, Rosenkaimer SL, Gerhards S, Kuschyk J, et al. Comparison of the outcome of patients protected by the wearable cardioverter defibrillator (WCD) for <90 wear days versus ≥90 wear days. In Vivo. (2020) 34 (6):3601–10. doi: 10.21873/invivo.12205

17. Duncker D, König T, Hohmann S, Bauersachs J, Veltmann C. Avoiding untimely implantable cardioverter/defibrillator implantation by intensified heart failure therapy optimization supported by the wearable cardioverter/defibrillator-the PROLONG study. J Am Heart Assoc. (2017) 6(1). doi: 10.1161/JAHA.116.004512

18. Mueller-Leisse J, Brunn J, Zormpas C, Hohmann S, Hillmann HAK, Eiringhaus J, et al. Extended follow-up after wearable cardioverter-defibrillator period: the PROLONG-II study. ESC Heart Fail. (2021) 8(6):5142–8. doi: 10.1002/ehf2.13586

19. Olgin JE, Pletcher MJ, Vittinghoff E, Wranicz J, Malik R, Morin DP, et al. Wearable cardioverter-defibrillator after myocardial infarction. N Engl J Med. (2018) 379(13):1205–15. doi: 10.1056/NEJMoa1800781

20. Olgin JE, Lee BK, Vittinghoff E, Morin DP, Zweibel S, Rashba E, et al. Impact of wearable cardioverter-defibrillator compliance on outcomes in the VEST trial: as-treated and per-protocol analyses. J Cardiovasc Electrophysiol. (2020) 31(5):1009–18. doi: 10.1111/jce.14404

21. Demers C, McKelvie RS, Negassa A, Yusuf S. Reliability, validity, and responsiveness of the six-minute walk test in patients with heart failure. Am Heart J. (2001) 142(4):698–703. doi: 10.1067/mhj.2001.118468

22. Du H, Wonggom P, Tongpeth J, Clark RA. Six-Minute walk test for assessing physical functional capacity in chronic heart failure. Curr Heart Fail Rep. (2017) 14 (3):158–66. doi: 10.1007/s11897-017-0330-3

23. Blockhaus C, Guelker JE, Feyen L, Bufe A, Seyfarth M, Shin DI. Telemonitoring potential of wearable cardioverter-defibrillators during the follow-up of patients with heart failure. J Cardiovasc Dev Dis. (2022) 9(6):175–85. doi: 10.3390/jcdd9060175

24. Tripp C, Burch AE, Erath JW, Hain A, Sears SF. Physical activity in adults with wearable cardioverter defibrillators in the post-myocardial infarction period. J Cardiopulm Rehabil Prev. (2020) 40(3):164–6. doi: 10.1097/HCR.0000000000000454

25. Hillmann HAK, Hohmann S, Mueller-Leisse J, Zormpas C, Eiringhaus J, Bauersachs, et al. Feasibility and first results of heart failure monitoring using the

wearable cardioverter-defibrillator in newly diagnosed heart failure with reduced ejection fraction. *Sensors (Basel.* (2021) 21(23). doi: 10.3390/s21237798

26. Triposkiadis F, Butler J, Abboud FM, Armstrong PW, Adamopoulos S, Atherton JJ, et al. The continuous heart failure spectrum: moving beyond an ejection fraction classification. *Eur Heart J.* (2019) 40(26):2155–63. doi: 10.1093/eurheartj/ehz158

27. Triposkiadis F, Starling RC. Chronic heart failure: diagnosis and management beyond LVEF classification. *J Clin Med.* (2022) 11(6). doi: 10.3390/jcm11061718

28. Konstam MA, Abboud FM. Ejection fraction: misunderstood and overrated (changing the paradigm in categorizing heart failure). *Circulation.* (2017) 135 (8):717–9. doi: 10.1161/CIRCULATIONAHA.116.025795

Blood parameter analysis after short term exposure to weightlessness in parabolic flight

Nana-Yaw Bimpong-Buta[a], Peter Jirak[b], Bernhard Wernly[b], Michael Lichtenauer[b],
Thorben Knost[a], Thaer Abusamrah[a], Malte Kelm[a] and Christian Jung[a],*

[a]*Division of Cardiology, Pulmonology, and Vascular Medicine, Medical Faculty, University Duesseldorf, Germany*
[b]*Department of Cardiology, Clinic of Internal Medicine II, Paracelsus Medical University of Salzburg, Austria*

Abstract.

BACKGROUND: Parabolic flights offer a unique platform for human experiments in short-term weightlessness. It is generally known that human organ systems react to changes of gravity. Yet, little is known about alterations of blood parameters under these conditions with special emphasis on blood rheology.

OBJECTIVE: We investigated the alterations of distinct blood parameters after exposure to weightlessness.

METHODS: 14 healthy volunteers underwent short-term phases of weightlessness induced by parabolic flight. At different time points (baseline, t2:1 hour after landing, and t3:24 hours after baseline), venous blood was drawn and analyzed.

RESULTS: Analysis of red blood count revealed significant decreases of hemoglobin and hematocrit post flight. While total white blood counts were unaltered, differential subset analysis revealed significant decreases of eosinophil granulocytes and monocytes. Cortisole levels were unchanged and lacked physiologic circadian decrease. Parameters of renal function were found significantly improved (GFR (ml/min/1,73m^2): Baseline: 105 [89;109], t2:117 [98;125], t3:110 [102;119]; $p = 0.0013$. In the sense of mild myocytolysis, levels of myoglobin were significantly elevated post-flight with fast recovery to baseline levels.

CONCLUSIONS: In the current analysis, significant alterations of blood parameters after exposure to weightlessness could be detected. These results contribute to the understanding of physiologic adaptations of the human body to weightlessness.

Keywords: Blood parameter analysis, weightlessness, parabolic flight

Abbreviations

ACTH	Adrenocorticotrope Hormone
BE	Base Excess
BNP	Brain Natriuretic Peptide
CE	Conformité Européenne
CRP	C-reactive Protein
CK	Creatinekinase
DLR	Deutsches Zentrum für Luft- und Raumfahrt (German Aerospace Center)
EPO	Erythropoietine
GFR	Glomerular Filtration Rate

*Corresponding author: Univ.-Prof. Dr. med. Dr. C. Jung, Division of Cardiology, Pulmonology, and Vascular Medicine; Medical Faculty University Duesseldorf, Moorenstrasse 5; 40225 Düsseldorf, Germany. Tel.: +49 211 81 18567; Fax: +49 211 18812; E-mail: christian.jung@med.uni-duesseldorf.de.

IQR   Interquartile Range
LDH   Lactatedehydrogenase
RBC   Red Blood Count
SD   Standard Deviation
WBC   White Blood Count

1. Introduction

With the privatization of space missions and the race to Mars with the first missions expected to launch in the next two decades, space medicine has gained a huge importance over the last years [1, 2]. As a significant increase in short - and long-term missions is expected, the precise evaluation of the physiologic adaptations of the human body in weightlessness represents an indispensable presupposition for the planning of safe and successful space flights [2–4].

Until today, only a few studies regarding physiologic changes in weightlessness have been conducted, most of them focusing on the adaptive response of distinct organ systems to zero gravity. The most important changes with respect to short- and long-term space missions are attributed to the cardiovascular system [5–7]. Above all, an increase in cardiac output as well as changes in pulmonary flow have been reported [4, 6, 8]. Additionally, weightlessness can also influence baroreceptor reflex and cerebrovascular auto-regulation [6, 9]. Other potential influences include osteoporosis-like bone changes, muscular atrophy, and impairment of lung function and the immune system [10–12].

However, the dynamics of blood parameters after exposure to weightlessness have not yet been subject to analysis in detail. Considering the auto regulatory mechanisms and closed-loop systems, which could be easily influenced by zero gravity, the survey of potential changes of blood parameters should be taken into account.

With a predicted increase of manned space missions over the next years, the need for further investigations on the adaptive responses of the human body in weightlessness seems evident, especially pertaining medical safety of all participants under these conditions. With that in mind, the aim of the present study was to analyze selected blood parameters and their dynamics after exposure to weightlessness [13].

2. Materials and methods

2.1. Study protocol, general points

Prior to inclusion into the study, all test subjects gave their written informed consent, for voluntary participation. The study was conducted in accordance with the Declaration of Helsinki (1975, revised in 2008), and the protocol was approved by the German Ethics Committee of the Medical Faculty of the University Hospital Duesseldorf, Germany (Date of approval: August 14th, 2017; Project Identification code: 2017054297) and by the French Ethics Committee (Comité de Protection des Personnes (CPP Nord-Ouest III) of the Medical Faculty of the University of Caen (Date of approval: September 06th, 2017; Project Identification code: 2017-A01185-48).

2.2. Inclusion and exclusion criteria

The inclusion criteria were defined as: age >18 years; airworthiness; cardiorespiratory health; spontaneous circulation; signed informed consent.

The exclusion criteria were defined as: history of cardiovascular and respiratory primary diseases or regular intake of medication with the exception of oral contraceptives, missing or withdrawal of informed consent, insufficient requirements for airworthiness; positive pregnancy test [3].

2.3. Parabolic flight

This study was conducted in the course of the participation in a so-called Parabolic Flight Campaign. A Parabolic Flight Campaign comprises two weeks: one week of preparation of all experiments, and one-week conduction of three to four flight days. The investigated Parabolic Flight Campaign (PFC) took place from February 26th to March 11th, 2018 in Bordeaux, France. Four flight days were scheduled and could be successfully performed.

The aircraft implemented in this campaign was the Airbus A 310 Zero-G of the French company NoveSpace. On each flight day 31 parabolic flight maneuvers were undertaken, as highly-specific flight maneuvers that entail meticulous control of the aircraft by three jet pilots. During a parabolic flight maneuver the aircraft follows the trajectory of a flight path that resembles a parabola. The maneuver leads to altering short phases of gravity: Starting from 1 g (regular gravity) at steady flight, a phase of hypergravity (1,8 g, pull-up-phase, of 20 seconds) follows, leading to the microgravity/zero gravity phase (0 g for 22 seconds) after a short transition phase. Thereafter, another hypergravity-phase (1,8 g, pull-out-phase, of 20 seconds) is needed to resume steady flight (1 g).

Throughout the campaign, all experiments were situated aboard the aircraft, catered for by approximately 40 scientists of 12 teams. The campaign covered four flight days with our group participating in all four flight days.

2.4. Experimental set-up and performed measurements

Venous blood from the cubital vein was collected from 14 healthy test subjects (8 males, aged 31.6 ± 6.0; 6 females, aged 28.2 ± 3.2) in total (according to guidelines for hemorheological laboratory techniques, see [14]. Each test subject participated in one parabolic flight day (comprising 31 parabolas each, with cumulatively 11 min. of weightlessness in total (22 sec. weightlessness per parabola)). The collection of blood was done at 3 different time points with respect to the flight per se, as follows: at baseline (1 hour prior to take off, between 7 a.m. and 8 a.m.), 1 hour after return from the flight (t2) and 24 hours after the first blood sampling (t3). The blood was collected with individual punctures into pre-chilled BD vacutainer tubes (Becton Dickinson, Mountain View, CA), using the following tubes, per single blood sampling: 3 EDTA tubes (Reference # 368861, Tube size: 75×13 mm, Draw volume: 4 ml), 3 SST tubes (Reference # 367957, Tube size: 75×13 mm, Draw volume: 3,5 ml), 1 SST tube (Reference # 367955, Tube size: 100×13 mm, Draw volume: 5 ml), 1 Lithium-Heparin tube (Reference # 368884, Tube size: 75×13 mm, Draw volume: 4 ml), 2 Na-Citrate tubes (Reference # 3683048, Tube size: 75×13 mm, Draw volume: 2,7 ml). Each blood sample underwent the exact same protocol for the analysis of specific parameters, per test subject, as listed in Table 1.

2.5. Statistical analysis

To perform statistical analysis, a commercially available software was used (Graph Pad Prism Software, Version 6, Graph Pad Software, San Diego, California, USA). Due to the small test subject group size, a normal distribution could not be assumed. Data were presented as median with Interquartile Range (IQR). To compare the values at the different time points (repeated measures), for each

Table 1
Overview of analysed blood parameters per blood sample

Entity	SI Unit
Hematology	
Leucocytes	G/l
Neutrophil Granulocytes (Gran.)	%
Eosinophil Gran.	%
Basophile Gran.	%
Lymphocytes	%
Monocytes	%
Hemoglobin	g/dl
Hematocrit	%
Thrombocytes	G/l
Hemostasis	
Fibrinogen	g/l
D-Dimers	ng/ml
Electrolytes	
Sodium	mmol/l
Potassium	mmol/l
Chloride	mmol/l
Calcium	mmol/l
Phosphate	mmol/l
Magnesium	mmol/l
Others	
CRP	mg/l
Base Excess (BE)	mmol/l
Creatinine	μmol/l
GFR	ml/min/1,73m2
LDH	U/l
Lactate	mmol/l
Cardiac parameters	
BNP	pg/ml
CK	U/l
Troponin I	ng/l
Myoglobin	μg/l
Hormones	
Cortisole	nmol/l
ACTH	pmol/l

parameter, the Friedman test was implemented, with Dunn's multiple comparisons test in *post hoc* analysis. A 2-tailed *p*-value < 0.05 was considered statistically significant.

3. Results

3.1. Hematologic and hemostatic parameters

Hemoglobin and hematocrit levels remained without significant changes at t2. However, at t3 a significant decrease in hemoglobin and hematocrit could be observed, in comparison to levels at
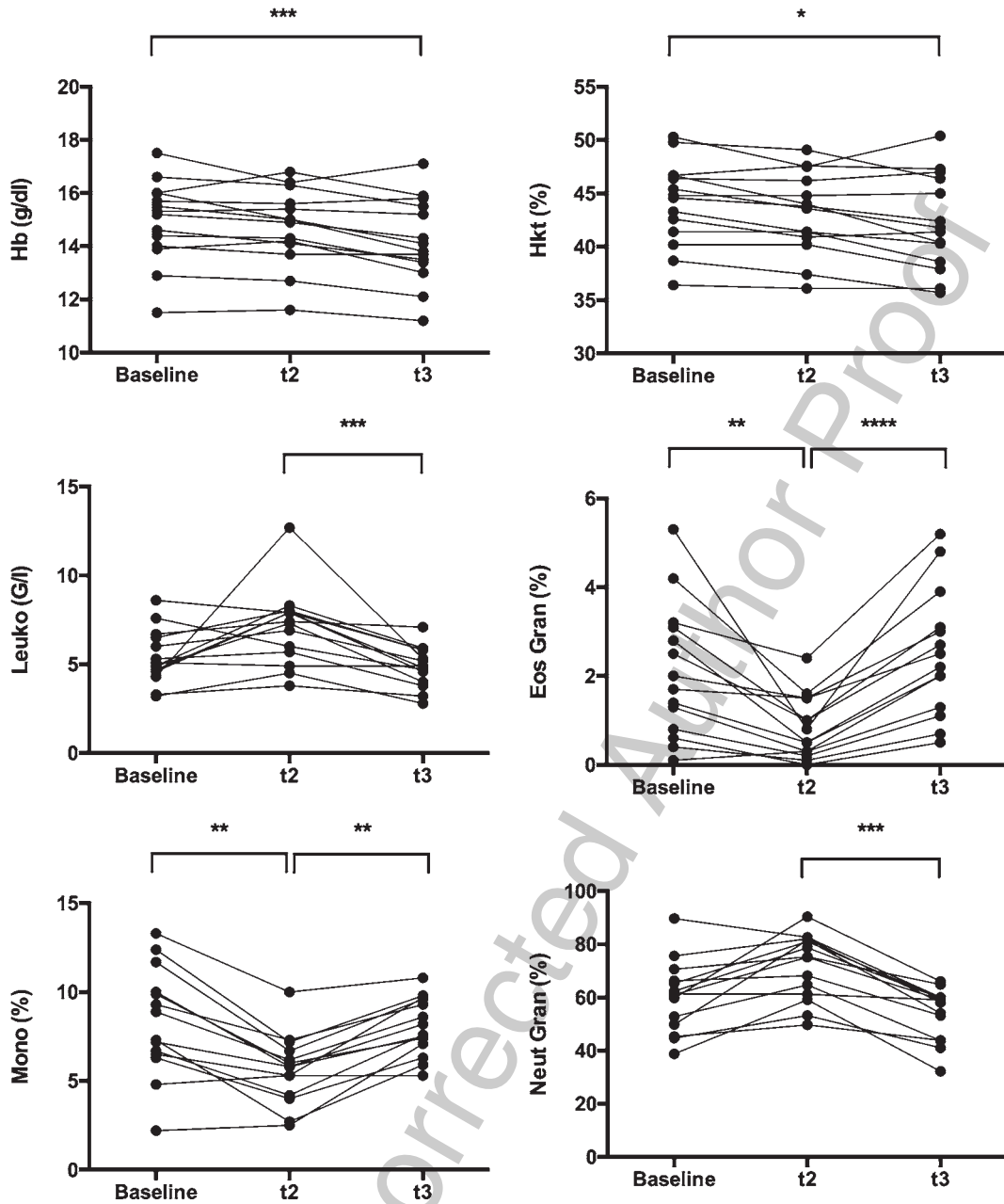
Fig. 1. Comparison of haemoglobin (g/dl) and haematocrit (%) as well as absolute numbers of Leukocytes in total (G/l) and of WBC subsets (eosinophil granulocytes, monocytes and neutrophil granulocytes, each in %) at 3 time points (Baseline; t2:1 hour after landing; t3:24 hours after baseline). The Friedman test was implemented for calculation. A 2-tailed p-value < 0.05 was considered statistically significant. Data were presented as median with Interquartile Range (IQR).

baseline (Fig. 1). For the three time points (baseline, t2 and t3) no significant differences were found in the measurements of thrombocytes (g/dl) [Baseline: Median 191; IQR = 64 [175; 239], t2:192; 91 [162; 253], t3:188; 70 [159; 229]; $p = 0.2231$], fibrinogen (g/l) [Baseline: Median 3,9; IQR = 0,7 [3,7; 4,4], t2:3,9; 0,7 [3,7; 4,4], t3:3,8; 0,5 [3,6; 4,1]; $p = 0.2574$], and D-Dimers (ng/ml) [Baseline: Median 234; IQR = 145 [214; 359], t2:222; 70 [214; 284], t3:214; 133 [214; 347]; $p = 0.5623$].

3.2. Blood count, including white blood count (WBC) differential and C-reactive protein (CRP)

The level of all leukocytes in total was not significantly different at t2 in comparison to baseline level. However, the level at t3 was significantly decreased in comparison to t2 without significant differences to levels at baseline (Fig. 1). In the analysis of WBC subsets, for the eosinophil granulocytes and the monocytes subsets a significant decrease at t2 and a significant increase at t3 was found. After 24 hours, baseline levels were attained (no significant difference between baseline and t3). The neutrophil granulocytes showed no significant differences to the level at baseline whereas the level at t3 was significantly decreased in comparison to the level at t2, yet without significant differences to the level at baseline (Fig. 1). For the lymphocytes and the basophil granulocytes there was no significant difference at t2 in comparison to the baseline level, however a rise to a significant higher level at t3, in comparison levels at t2. The levels at t3 showed no significant differences to levels at baseline.

Serum levels of CRP were concomitantly analyzed. Here, no significant differences could be noted at the reported time points [CRP (mg/l): Baseline: Median 2.0; IQR = 8.5 [1.0; 9.5], t2:1.5; 9.0 [0.99; 10], t3:1; 5 [1; 6]; $p = 0.4317$].

3.3. Adrenocorticotropic hormone (ACTH), cortisole, lactate and base excess

The analyzed levels of ACTH and cortisole remained without significant alterations throughout all performed analyses (data not shown). Lactate levels at t2 were not significantly different from levels at baseline. At t3, a significant drop in concentration could be noted, in comparison to t2, yet without significant difference to the level at baseline [lactate (mmol/l): Baseline: Median 1.6; IQR = 0.9 [1.3; 2.2], t2:1.5; 0.6 [1.1; 1.7], t3:1.9; 0.4 [1.7; 2.1] The Base excess stayed without significant differences at all time points (data not shown).

3.4. Cardiac parameters (Troponin, Brain Natriuretic Peptide (BNP), Lactatdehydrogenase (LDH)), Myoglobin and Creatinekinase (CK)

For myoglobin, there was a significant increase in concentration at t2 with a significant drop at t3, returning to baseline levels (no difference between t3 and baseline), see Fig. 2. For LDH, there were no significant differences for levels at t2, but levels dropped significantly at t3, without significant differences to baseline levels (Fig. 2).

For all time points, there were no detectable significant differences in the concentrations of the cardiac enzymes troponin or brain natriuretic peptide (BNP) nor for levels of creatine kinase (data not shown).

3.5. Markers of renal function (Glomerular Filtration Rate (GFR) and creatinine)

Levels of creatinine were significantly lower at t2 and remained stable at t3, with significant difference to baseline (creatinine (μmol/l): Baseline: Median 72, IQR = 10 [69; 79], t2:65, 11 [60; 71], t3:67,14 [60; 74]; $p = 0.0013$, Fig. 2). Inversely, GFR was significantly higher at t2 and remained high at t3, with significance in comparison to baseline levels (GFR (ml/min/1,73m^2): Baseline: Median 105, IQR = 20 [89; 109], t2:117; 27 [98; 125], t3:110; 17 [102; 119]; $p = 0.0013$), see Fig. 2.
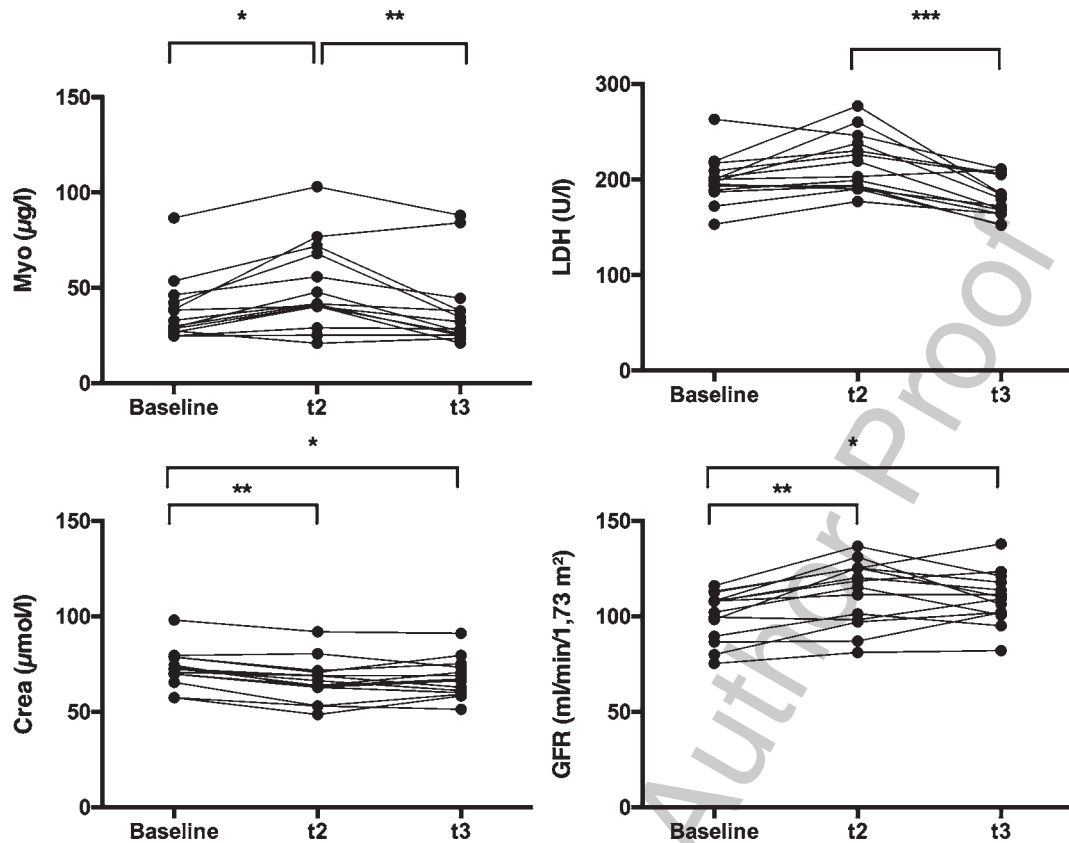
Fig. 2. Comparison of levels of myoglobin (µg/l), LDH (U/l), creatinine (µmol/l) and GFR (ml/min/1,73m^2) at 3 time points (Baseline; t2:1 hour after landing; t3:24 hours after Baseline). The Friedman test was implemented for calculation. A 2-tailed *p*-value < 0.05 was considered statistically significant. Data were presented as median with Interquartile Range (IQR).

4. Discussion

The number of manned space missions in the private as well as in the public sector is expected to rise significantly in the next decades. In this regard, there has been growing interest in future missions to the moon and especially to the mars. Bearing this in mind, the medical safety of humans participating in these missions is of utmost importance which underlines the fervent quest for deeper knowledge about space medicine, with the focus on a precise understanding of physiologic adaptation processes of the human body in weightlessness. Regarding medical safety and success of these missions, deepening knowledge in this field seems indispensable [5]. However, scientific projects regarding the evaluation of distinct blood parameters under these conditions and special focus on blood rheology parameters are lacking. For this reason, in this study the aim was to analyze specific blood parameters and their response to weightlessness and hypergravity by means of participation in parabolic flight maneuvers.

It must be noted, that the time of exposure to phases of weightlessness and hypergravity is limited in the setting of parabolic flights [3]. In a standard parabolic flight day, the total duration of weightlessness and hypergravity is approximately 11 minutes and 22 minutes respectively, interrupted by sequences of regular gravity at steady flight. Thus, the obtained results about alterations of blood parameters under these conditions must be interpreted with care. However, as described above, significant alterations and trends within the inspected laboratory parameters could be detected, even after these comparably short episodes of exposure to weightlessness and hypergravity.

It is well known that the participation in parabolic flights, with induced short-term phases of weightlessness and hypergravity results in alterations of organ functions of the human body. The focus of our experiment was to analyze the concomitantly expected alterations in distinct blood parameters, to detect the extent of the effects by calculating significance in differences.

Regarding red blood count (RBC), a significant post flight decrease in hemoglobin and hematocrit could be noted in our setting. This finding is in line with former studies, that showed decreased RBC counts in the course of exposure to weightlessness [15]. Here, reduced plasma EPO levels were found to be responsible for this finding, as reduced EPO levels result in a shortened survival of red blood cells and increased rates of apoptosis, according to Alfrey et al. [16, 17]. As especially younger red blood cells are affected, this process is also called neocytolysis [18]. These shifts *per se* influence blood rheology following or during weightlessness. Previous studies by Dintenfass et al. showed that erythrocytes of healthy test subjects tended to form swarm-like aggregate structures in space whereas the same blood samples showed rouleaux formation (i.e. cylindrical masses like piles of money) on the ground. In contrary, blood of patients with myocardial infarction, insulin-dependent diabetes, hyperlipidaemia and hypertension showed rouleaux in space at zero gravity, but a clumping pattern on the ground. However, the cellular shape of erythrocytes remained unchanged under zero gravity [19, 20].

Looking at the white blood count (WBC), the present study revealed that total leukocyte counts remained unchanged throughout the experiment with a significant decrease at t3, however without significant differences to baseline levels. To detect leukocyte-inherent reactive differences of subpopulations, analysis of WBC subsets was performed. Here, a significant decrease of eosinophil granulocytes and monocytes at t2 could be noted, with significant increase at t3. It is tempting to speculate that a physiological stress response during conduction of the flight maneuvers occurs possibly being one influential factor. Bearing this in mind, cortisole levels were studied, as cortisole represents one of the profound markers of stress reactions. It is well known, that in the human body peak levels of cortisole usually can be found between 7 a.m. and 8 a.m. [21] (in our experiment equal to the time point for baseline measurements). In physiological states, cortisole levels would show a decrease in the subsequent hours until early afternoon. However, in our experiment cortisole levels remained unchanged throughout the experiment, suggesting that the cortisole levels at t2 could have been increased due to the flight associated stress response.

To deeper investigate the level of inflammation in our setting, analysis of CRP levels and levels of neutrophil granulocytes, as known markers of inflammatory responses was performed. As no significant alterations of CRP levels or of the levels of neutrophil granulocytes throughout the experiment could be documented, one can assume that the overall inflammatory response does not take place or is occult. Overall, it can be stated that in all of our (healthy) participants the recovery was fast, as no significant differences could be noted at t3 in comparison to baseline levels.

As described above, significant alterations in myoglobin- and LDH-concentrations could be found. Taking these facts into account, the results indicate a subclinical deterioration of muscular tissue during parabolic flight, in terms of mild myocytolysis. This becomes evident when considering the fact that in phases of hypergravity body stabilization through intent muscle activation is of utmost importance to maintain solid body postures [22–24].

Looking at the markers of renal function, evidence for improved renal function during parabolic flight could be revealed, possibly as a result of enhanced renal blood circulation due to increased cardiac output [8, 25]. In healthy humans, this mechanism could also explain a somewhat reno-protective effect with respect to imminent muscle deterioration under these conditions, as described.

Intense reactive alterations of the cardiovascular system under conditions of parabolic flights have been well described. For instance, an increase in cardiac output of up to 41 % has been documented in former studies [8, 25]. Bearing this in mind, serum parameter responses of cardiac blood parameters

such as BNP and troponin levels were investigated. Surprisingly, there was no significant difference in BNP and troponin levels at baseline, t2 and t3. In this context, it could be assumed that the comparably short duration of exposure to weightlessness and hypergravity might have not sufficed to trigger significant alterations of cardiac parameters in these healthy volunteers. One of the reasons for this could be that in healthy humans compensatory mechanisms will suffice to impede malfunctions of the cardiovascular system even under short-term weightlessness.

5. Conclusions

The current study shows that even short-term exposure to weightlessness and hypergravity causes blood parameter changes, including RBC and WBC subsets as well as myoglobin, LDH levels and markers of renal function.

This will help to interpret future physiological studies in the context of adaptations of the human body in weightlessness and hypergravity. The current results might help improving safety procedures for medical evaluations of candidates for manned space-missions.

Acknowledgments

References

[1] Kadl A, Huber J, Gruber F, Bochkov VN, Binder BR, Leitinger N. Analysis of inflammatory gene induction by oxidized phospholipids in vivo by quantitative real-time RT-PCR in comparison with effects of LPS. Vascul Pharmacol. 2002;38(4):219-27.

[2] Yaqub F. Space travel: Medicine in extremes. Lancet Respir Med. 2015;3(1):20-1.

[3] Bimpong-Buta NY, Jirak P, Wernly B, Lichtenauer M, Masyuk M, Muessig JM, et al. Analysis of human microcirculation in weightlessness: Study protocol and pre-study experiments. Clin Hemorheol Microcirc. 2018;14(10):CH-170366.

[4] Lathers CM, Charles JB, Elton KF, Holt TA, Mukai C, Bennett BS, et al. Acute hemodynamic responses to weightlessness in humans. J Clin Pharmacol. 1989;29(7):615-27.

[5] Convertino VA. Status of cardiovascular issues related to space flight: Implications for future research directions. Respir Physiol Neurobiol. 2009;169(1):19.

[6] Hughson RL, Shoemaker JK, Blaber AP, Arbeille P, Greaves DK, Pereira-Junior PP, et al. Cardiovascular regulation during long-duration spaceflights to the International Space Station. J Appl Physiol. 1985;112(5):719-27.

[7] Keith Sharp M, Batzel JJ, Montani JP. Space physiology IV: Mathematical modeling of the cardiovascular system in space exploration. Eur J Appl Physiol. 2013;113(8):1919-37.

[8] Norsk P, Asmar A, Damgaard M, Christensen NJ. Fluid shifts, vasodilatation and ambulatory blood pressure reduction during long duration spaceflight. J Physiol. 2015;593(3):573-84.

[9] Blaber AP, Zuj KA, Goswami N. Cerebrovascular autoregulation: Lessons learned from spaceflight research. Eur J Appl Physiol. 2013;113(8):1909-17.

[10] Pietsch J, Bauer J, Egli M, Infanger M, Wise P, Ulbrich C, et al. The effects of weightlessness on the human organism and mammalian cells. Curr Mol Med. 2011;11(5):350-64.

[11] Crawford-Young SJ. Effects of microgravity on cell cytoskeleton and embryogenesis. Int J Dev Biol. 2006;50(2-3):183-91.

[12] Zuj KA, Arbeille P, Shoemaker JK, Blaber AP, Greaves DK, Xu D, et al. Impaired cerebrovascular autoregulation and reduced CO(2) reactivity after long duration spaceflight. Am J Physiol Heart Circ Physiol. 2012;302(12):6.

[13] Shelhamer M. Parabolic flight as a spaceflight analog. J Appl Physiol. 1985;120(12):1442-8.

[14] Baskurt OK, Boynard M, Cokelet GC, Connes P, Cooke BM, Forconi S, et al. New guidelines for hemorheological laboratory techniques. Clin Hemorheol Microcirc. 2009;42(2):75-97.

[15] Schneider S, Brummer V, Carnahan H, Dubrowski A, Askew CD, Struder HK. Stress hormone stability: Processing of blood samples collected during parabolic flight. A pre-flight comparison of different protocols. Clin Biochem. 2007;40(16-17):1332-5.

[16] Alfrey CP, Udden MM, Huntoon CL, Driscoll T. Destruction of newly released red blood cells in space flight. Med Sci Sports Exerc. 1996;28(10 Suppl):S42-4.

[17] Alfrey CP, Udden MM, Leach-Huntoon C, Driscoll T, Pickett MH. Control of red blood cell mass in spaceflight. J Appl Physiol. 1985;81(1):98-104.

[18] Rice L, Alfrey CP. Modulation of red cell mass by neocytolysis in space and on Earth. Pflugers Arch. 2000;441(2-3 Suppl):R91-4.

[19] Dintenfass L. Aggregation of red cells and blood viscosity under near-zero gravity. Biorheology. 1979;16(1-2):29-36.

[20] Dintenfass L, Osman P, Maguire B, Jedrzejczyk H. Experiment on aggregation of red cells under microgravity on STS 51-C. Adv Space Res. 1986;6(5):81-4.

[21] Gamble KL, Berry R, Frank SJ, Young ME. Circadian clock control of endocrine factors. Nat Rev Endocrinol. 2014;10(8):466-75.

[22] Fitts RH, Brimmer CJ, Heywood-Cooksey A, Timmerman RJ. Single muscle fiber enzyme shifts with hindlimb suspension and immobilization. Am J Physiol. 1989;256(5 Pt 1).

[23] Moriya T, Kita K, Sugaya S, Wano C, Suzuki N. Enhanced expression of the LDH-A gene after gravity-changing stress in human RSa cells. Biol Sci Space. 2002;16(1):12-7.

[24] Saiki H, Nakaya M, Sudoh M, Okamoto T, Nakajima J. Changes in enzymes and potassium content of the neuromuscular systems of albino rats during prolonged exposure to simulated hypogravics. Life Sci Space Res. 1979;17:205-11.

[25] Norsk P, Damgaard M, Petersen L, Gybel M, Pump B, Gabrielsen A, et al. Vasorelaxation in space. Hypertension. 2006;47(1):69-73.

Carbondioxide-Aided Angiography Decreases Contrast Volume and Preserves Kidney Function in Peripheral Vascular Interventions

Emilia Stegemann, MD[1], Catharina Tegtmeier, MS[1],
Nana Yaw Bimpong-Buta, MD[1], Roberto Sansone, MD[1],
Mark Uhlenbruch, MS[1], Andreas Richter, MD[2],
Berthold Stegemann, PhD[1], Michael Roden, MD[2,3,4],
Ralf Westenfeld, MD[1], Malte Kelm, MD[1], and Christian Heiss, MD[1]

Abstract

Chronic kidney disease is a common comorbidity in patients with peripheral artery disease. We investigated the safety and efficacy of carbon dioxide (CO_2) as supplemental contrast agent to decrease contrast volume during fluoroscopy-guided peripheral vascular procedures in routine angiological practice. We analyzed 191 consecutive interventions of the lower extremity in claudicants and critical limb ischemia (CLI) that were performed with iodinated contrast media (ICM) alone (n = 154) or with the aided or exclusive use of CO_2 (n = 37). The technical success rate, total irradiation, and intervention time were not significantly different between ICM and CO_2. No severe procedure-related complications occurred. The contrast volume was lower in CO_2 than in ICM. Although kidney function, creatinine, and estimated glomerular filtration rate was lower in CO_2 at baseline, the incidence of contrast-induced nephropathy was lower in CO_2 compared to ICM. These data support CO_2 as an alternative supplemental contrast agent that can be applied safely and efficiently to lower contrast volume during peripheral vascular interventions preventing kidney dysfunction even in patients with disease of the popliteal artery and below the knee and CLI.

Introduction

Atherosclerotic peripheral arterial disease (PAD) is a major public health burden that affects more than 27 million people across Europe and Northern America, equating to 16% of the population older than 55 years.[1] The prevalence of PAD, especially of critical limb ischemia (CLI), is rising worldwide with considerable impact on the health care and socioeconomic systems. In Germany, the number of hospital admissions of individuals with PAD increased between 2005 and 2009 by >20%.[2] In parallel, endovascular revascularization increased by 46%. Chronic renal failure, diabetes, and heart failure are common comorbidities present in almost 37%, 39%, and 15% of patients admitted with PAD, in particular those with CLI.[2]

Current guidelines recommend an "endovascular first" strategy in case of indication for revascularization.[3] The standard approach for endovascular interventions requires conventional radio opaque iodinated contrast media (ICM) for the procedures (acquisition of diagnostic images, wire guidance, and stent placement). Contrast-induced nephropathy (CIN) is a common complication in particular in patients with preexisting chronic renal disease, diabetes, heart failure, and dehydration associated with increased in-hospital and long-term mortality, respectively.[4,5] Approaches to lower the risk of CIN include cessation of concomitant nephrotoxic medication, hydration, statins, and limiting the amount of contrast medium. Besides conventional nephrotoxic contrast medium, carbon

[1] Division of Cardiology, Pulmonology and Vascular Medicine, Medical Faculty, University Duesseldorf, Duesseldorf, Germany
[2] Department of Endocrinology and Diabetology, Medical Faculty, Heinrich-Heine University Duesseldorf, Duesseldorf, Germany
[3] Institute for Clinical Diabetology, German Diabetes Center, Leibniz Institute for Diabetes Research at Heinrich Heine University, Duesseldorf, Germany
[4] German Center for Diabetes Research, Partner Duesseldorf, Germany

Corresponding Author:
Christian Heiss, Division of Cardiology, Pulmonology, and Vascular Medicine, Medical Faculty, University Duesseldorf, Moorenstr. 5, 40225 Duesseldorf, Germany.
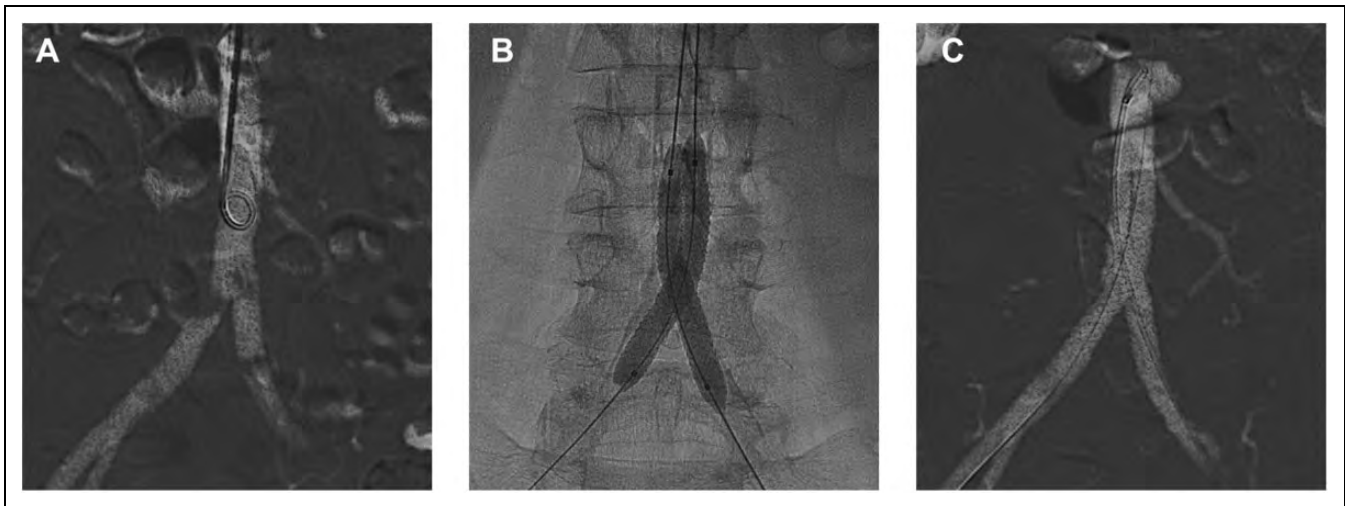Email: christian.heiss@med.uni-duesseldorf.de

Figure 1. Example images of an exclusively CO_2-guided intervention of bilateral common iliac stenosis. A, Baseline CO_2 angiography via pigtail catheter coming from the right brachial artery due to freshly operated right common femoral. B, Treatment of bilateral common iliac stenoses (right: proximal subtotal and left: more distal) with kissing balloon-kissing stent technique using brachial and left common femoral access. C, Postprocedural CO_2 angiography showing excellent primary success.

dioxide (CO_2) gas can be used as an alternative contrast agent, as it is absorbed almost instantaneously as opposed to other gases.[6] The image quality obtained with CO_2 may be limited in particular in small vessels such as below the knee (BTK) or in the pelvic arteries due to bowel gas motion (Figure 1). Despite easy accessibility of manual gas injection, this technique may not permit optimal control of the gas output in all cases.[7] However, interventions can be performed by integrating CO_2 and ICM. In order to optimize image quality when critically necessary, ICM is applied, while CO_2 is used for situations where image accuracy is not critical, aiming at decreasing the total amount of nephrotoxic ICM (CO_2-aided approach). Although CO_2 has been acknowledged for a long time as a safe alternative arterial contrast agent to guide peripheral procedures,[8,9] only a few studies have evaluated its efficacy in daily practice.[10-12]

Therefore, we investigated whether CO_2-aided percutaneous transluminal angioplasty (PTA) is an efficacious and safe method to decrease contrast volume during fluoroscopy-guided peripheral vascular procedures in routine angiological practice.

Materials and Methods

We retrospectively analyzed 191 consecutive patients (November 2012-December 2013) within the *Duesseldorf PTA Registry*, who were admitted for endovascular treatment of lower extremity PAD. The ethics board of Heinrich Heine University Duesseldorf approved the study protocol.

Procedures

Indications for peripheral endovascular treatment of PAD were based on current guidelines.[13] All patients had Doppler ankle–brachial index (ABI) measurements at rest and when possible after treadmill exercise. In patients with suspected or confirmed media sclerosis, segmental oscillography was performed.

Furthermore, all patients received a thorough Duplex ultrasound examination to localize the flow-limiting stenosis and for sizing of later potential stent placement. Angiographic images were obtained via digital subtraction angiography (DSA) on a Philips Alura system with a flat panel detector. All patients with estimated glomerular filtration rate (eGFR) <60 mL/min received saline infusions starting the night before interventions at 1 mL/kg body weight/h for 12-hour preprocedure and 12-hour postprocedure. Metformin treatment was withheld for 48 hours prior to the procedure. All patients with successful peripheral procedures received dual platelet inhibition with acetylsalicylate and clopidogrel for 1 month following the procedure.

Conventional ICM Interventions

Conventional ICM (Visipaque 250, Amersham Buchler GmbH & CoKG, Braunschweig) was injected manually or via an assist pump using standard protocols. Briefly, DSA of the distal aorta and pelvic arteries was performed with a 15 mL bolus injected at 10 mL/s via a pigtail catheter located in the distal abdominal aorta. Images of the femoropopliteal or infrapopliteal (below the knee, BTK) segments were performed with 2 to 10 mL at 3 to 5 mL/s. The standard vascular X-ray protocol options preset by the manufacturer (Alura, Philips, Allura FD20, Philips, Hamburg, Germany) were used for pelvic (24 mAs, 80 kV, 3 frames/s), femoropopliteal (9 mAs, 70 kV, 3 frames/s), and BTK imaging (13 mAs, 65 kV, 1 frames/s).

Carbon dioxide-Aided PTA

Selection criteria for CO_2-aided peripheral interventions included an eGFR of <30 mL/min, with preserved urine excretion, contrast allergy, hyperthyroidism, or patient preference. Exclusion criteria for CO_2-aided peripheral interventions included chronic obstructive pulmonary disease stage Gold IV. In patients with absolute contraindications for ICM, CO_2 was

used as the exclusive contrast agent. These contraindications included hyperthyroidism. Carbon dioxide was injected via the same catheters as used for contrast. Briefly, the gas (Linde, Germany) was passed through a pressure-lowering valve (1.3 atm; Optimed, Ettlingen, Germany) via a 3-way valve into a special 100-mL syringe (Angioset; Optimed, Ettlingen, Germany) in which the piston could be fixed to accommodate a certain volume and hold the supra-atmospheric pressure. Via turning the 3-way valve in a second position, the syringe containing pressurized CO_2 gas was connected to the intra-arterial catheter. This allowed the gas to expand and passively flow through the intra-arterial catheter in the arterial lumen. Images were taken using DSA. In order to minimize bowel motion, patients expected to receive CO_2 angiography of the pelvic arteries received 20 mg butylscopolamine (Boehringer Ingelheim, Ingelheim, Germany) intravenously upon entering the catheterization laboratory. In order to allow better runoff and prevent proximal embolization of CO_2, the legs were elevated by 10° using a pillow placed under the lower part of the legs. The standard "vascular CO_2 Spezial" X-ray protocol options preset by the manufacturer (Alura, Philips) were used for pelvic (30 mAs, 80 kV, 3 frames/s), femoropopliteal, and BTK imaging (35 mAs, 65 kV, 3 frames/s).

Ankle–Brachial Index

The systolic and diastolic blood pressures were obtained automatically (Dynamap Vital Signs Monitor, Dinamap, General Electric Health Care, Solingen, Germany) on both arms. The systolic blood pressure in the distal anterior and posterior tibial arteries of both legs was measured using a nondirectional Doppler flow detector (Schabert Instrumente, Röttenbach, Germany) with a pencil probe (8 MHz). Arm and leg yielding the higher systolic pressure were used to calculate ankle–brachial index.

Assessment of Walking Distance by Treadmill

The walking distance was assessed in all patients before and after PTA. The walking distance was tested by a standardized protocol (slope: 12%, velocity: 3.2 km/h).[13] Relative walking distance was defined as the distance completed until pain started. The investigation was stopped with the onset of ischemic leg pain and the distance covered until was recorded as absolute walking distance.

Evaluation of CIN

We evaluated kidney function by serum creatinine concentrations and eGFR (Modification of Diet in Renal Disease) before and at days 1 and 2 after the intervention. CIN was defined by a rise in serum creatinine of >25% or >0.5 mg/dL.

Statistical Analyses

Results are expressed as mean ± standard deviation (SD). Comparisons between groups were analyzed by analysis of variance (gateway test) and, if significant, consecutive post hoc test (Bonferroni) was performed. Comparisons between 2 groups were performed with independent t test or χ^2 test for frequencies. Linear relationships between continuous variables were expressed as Pearson's r. Statistical significance was assumed at 2-tailed $P \leq .05$. All statistical analyses were performed using PASW Statistics 18.

Results

Study Population

A total of 191 consecutive patients were treated for lower extremity PAD of the aortoiliac, femoral, popliteal as well as BTK disease. Of these, 154 received ICM only and 33 received CO_2 with supplemental ICM. A total of 4 patients received only CO_2 due to overt hyperthyroidism or severe contrast agent allergy. The groups were comparable with regard to all epidemiological characteristics (Table 1) except for kidney function (ICM: 1.1 ± 0.6 mg/dL and 76 ± 28 mL/min, CO_2: 2.1 ± 1.3 mg/dL and 22 ± 34 mL/min, $P < .0001$ each) at admission. All interventions were performed by only 2 interventionalists (CH and ES) either alone or together.

Similar Procedural Success and Irradiation Time Between ICM and CO_2 in Claudicants and Patients With CLI

In general, CO_2 angiography was well tolerated. As we used manual passive injection, and it is very difficult to measure the amount of gas delivered to the patient. Several patients described temporary acute ischemic lower leg pain following both ICM and CO_2 injection once the respective contrast agent had passed the flow-limiting lesion and reached the ischemic lower leg. The pain subsided spontaneously within 20 seconds. One patient experienced acute dyspnea, and 1 patient experienced nausea following CO_2 injection. The latter 2 patients received an oxygen mask and were instructed to remain calm and hyperventilated. All symptoms subsided within 5 minutes.

Primary technical success was achieved in 100% of the CO_2-aided interventions and 148 (96%) of patients with ICM (Table 2; Figure 2). Irradiation (23 ± 16 minutes) and intervention (90 ± 37 minutes) times as well as the dose–area product were not significantly different between ICM and CO_2. A subgroup analysis showed that there was also no difference when evaluating claudicants (irradiation time: ICM 21 ± 16 minutes, CO_2: 24 ± 16 minutes; intervention time: ICM 73 ± 28 minutes, CO_2: 80 ± 33 minutes) and patients with CLI having Fontaine III or IV (irradiation time: ICM 25 ± 16 minutes, CO_2: 22 ± 12 minutes; intervention time: ICM 89 ± 34 minutes, CO_2: 83 ± 33 minutes).

Decreased Contrast Volume and Preserved Kidney Function With CO_2-Aided PTA

The amount of ICM used during interventions was significantly lower with CO_2-aided interventions (34 ± 41 mL) compared to ICM (113 ± 76 mL, $P < .001$; Figure 3). A subgroup analysis

Table 1. Patient Characteristics (*P* Values Refer to *t* Test).

	ICM	CO₂	P
n	154	37	
Age, years	70 ± 10	73 ± 12	.172
Male sex, n (%)	118 (77)	23 (62)	
Body mass index, kg/m²	27 ± 6	27 ± 8	.471
Arterial hypertension, n (%)	136 (88)	30 (81)	
Hypercholesterolemia, n (%)	118 (77)	22 (59)	
Diabetes mellitus, n (%)	78 (51)	19 (51)	
Coronary artery disease, n (%)	110 (71)	24 (65)	
Smoker, n (%)	82 (53)	25 (68)	
Creatinine, mg/dL	1.1 ± 0.6	2.1 ± 1.3	<.001
Estimated glomerular filtration rate, mL/min	76 ± 28	22 ± 34	<.001
Chronic kidney failure, n (%)	55 (36)	31 (84)	
Chronic kidney disease stage, n (1/2/3/4/5)	(45/65/38/4/2)	(2/3/16/13/3)	
Total cholesterol, mg/dL	182 ± 95	158 ± 79	.079
Fasting plasma glucose, mg/dL	122 ± 53	115 ± 33	.486
Hemoglobin_{A1c} (%)	7.1 ± 3.0	7.0 ± 2.3	.792
Acetylsalicylic acid, n (%)	138 (90)	37 (100)	
Clopidogrel, n (%)	135 (88)	32 (86)	
Coumadin, n (%)	23 (15)	10 (27)	
Angiotensin-converting enzyme inhibitor, n (%)	63 (41)	17 (46)	
Angiotensin receptor blocker, n (%)	42 (27)	7 (19)	
Beta-blocker, n (%)	103 (67)	31 (84)	
Statin, n (%)	118 (77)	26 (70)	
Fontaine IIb, n (%)	95 (62)	16 (43)	
Fontaine III, n (%)	13 (8)	3 (8)	
Fontaine IV, n (%)	46 (30)	18 (49)	
Walking distance relative, m	65 ± 42	56 ± 35	.566
Walking distance absolute, m	99 ± 66	82 ± 56	.497
Ankle brachial index rest	0.59 ± 0.24	0.66 ± 0.28	.382
Ankle brachial index after exercise	0.32 ± 0.14	0.32 ± 0.26	.398
		MV ± SD	

Abbreviations: ICM, iodinated contrast medium; CO₂, carbon dioxide; SD, standard deviation.

Table 2. Procedure Related Characteristics and Outcomes.

	ICM	CO₂	P
Iliac arteries, n (%)	57 (37)	8 (22)	
Femoral arteries, n (%)	69 (45)	13 (35)	
Popliteal arteries, n (%)	7 (5)	6 (16)	
Below-the-knee, n (%)	21 (14)	10 (27)	
Plain balloon angioplasty, n (%)	41 (27)	13 (35)	
Stents, n (%)	111 (72)	24 (65)	
Recanalization, n (%)	51 (34)	16 (43)	
Primary technical success, n (%)	148 (96)	37 (100)	
Irradiation time, min	23 ± 17	22 ± 14	.606[a]
Area dose product, cGy × cm²	9359 ± 11 474	8054 ± 12 764	.865[a]
Intervention time, min	79 ± 37	83 ± 32	.747[a]
Contrast medium, mL	112 ± 76	34 ± 41	<.001[a]
Creatinine postprocedural day 1, mg/dL	1.1 ± 0.6	2.0 ± 0.9	<.001[a]
Creatinine postprocedural day 2, mg/dL	1.3 ± 0.6	2.3 ± 0.9	<.001[a]
eGFR postprocedural day 1, mL/min	73 ± 28	37 ± 22	<.001[a]
eGFR postprocedural day 2, mL/min	62 ± 25	30 ± 12	<.001[a]
Contrast induced nephropathy, n (%)	29 (19)	2 (5)	.044[b]
Walking distance relative, postprocedural, m	77 ± 50	76 ± 53	.214[a]
Walking distance absolute, postprocedural, m	119 ± 80	84 ± 38	.016[a]
ABI rest, postprocedural	0.70 ± 0.25	0.89 ± 0.26	.011[a]
ABI after exercise, postprocedural	0.45 ± 0.27	0.59 ± 0.25	.055[a]
		MV ± SD	

Abbreviations: ICM, iodinated contrast medium; CO₂, carbon dioxide; eGFR, estimated glomerular filtration rate; ABI, ankle brachial index; SD, standard deviation.
P value refers to:
[a]*t*-test or
[b]χ^2 test.

showed that this was true in both claudicants (CO₂: 49 ± 53 mL, ICM: 125 ± 79 mL) and patients with CLI (CO₂: 24 ± 23 mL, ICM: 95 ± 65 mL). A different subgroup analysis showed that the contrast volume was significantly lower in CO₂ than in ICM when comparing intervention within individual vessel segments (Table 3). The contrast volume used in the popliteal ICM procedures were significantly lower as compared with interventions of the aortoiliac segment (Table 3). Please note that in both ICM and CO₂ groups 15% and 12% of procedures, respectively, involved additional treatment of the downstream segment to facilitate runoff (data not shown). As shown in Table 1, patients in the CO₂ group exhibited significant lower kidney function at baseline.

In the ICM group, CIN occurred in 29 (19%) patients and in 2 patients in the CO₂ group (5%, *P* = .044). A subgroup analysis showed that within the CO₂ group claudicants did not experience a single CIN, whereas 2 patients with CLI developed CIN. All cases were successfully treated with saline infusion without the need for initiation of hemodialysis and recovered spontaneously within 4 days.

As approximately half of the patients in each group were diabetic, we performed an additional subgroup analysis. This showed that in the ICM group diabetic patients experienced a significantly higher rate of CIN (25%) compared to patients without diabetes (13%) at a similar baseline creatinine of 1.1 ± 0.7 mg/dL and 1.1 ± 0.5 mg/dL, respectively, and similar amounts of contrast medium. Within the CO₂ group, CIN in diabetic patients (5%) and patients without diabetes (6%) did not differ.

Discussion

This study presents real-life data from all patients receiving endovascular treatment for PAD in our institution over
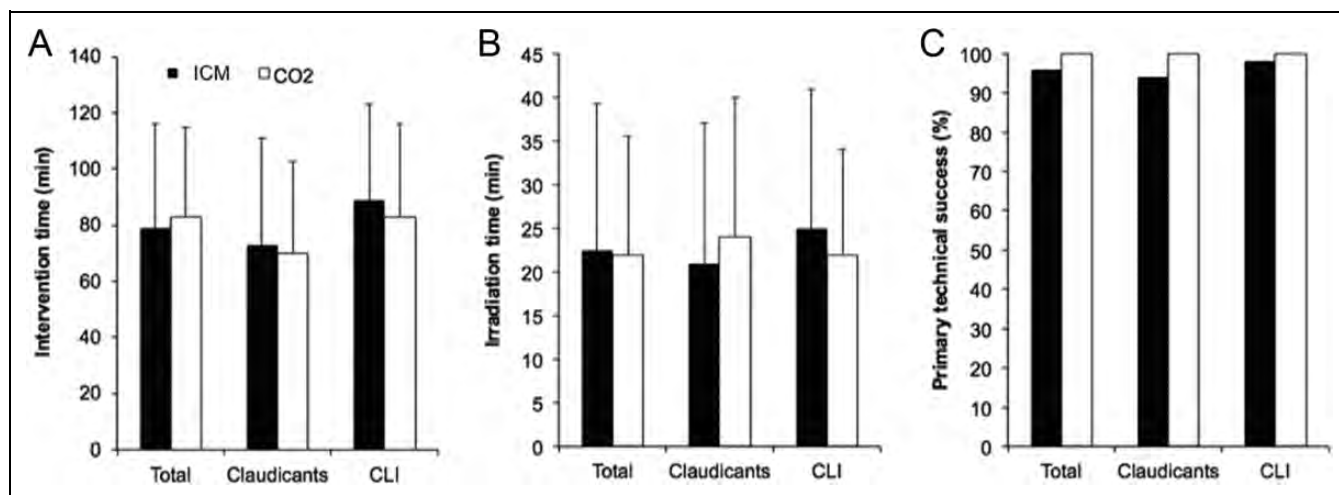
Figure 2. (A) Intervention time, (B) irradiation time, and (C) technical success. Results are comparable between conventional contrast medium (iodinated contrast media [ICM]) and CO_2-aided intervention in overall patients and on subgroup analysis both in claudicants (Fontaine IIb) and in patients with CLI (Fontaine III-IV). No significant differences were found between the groups.
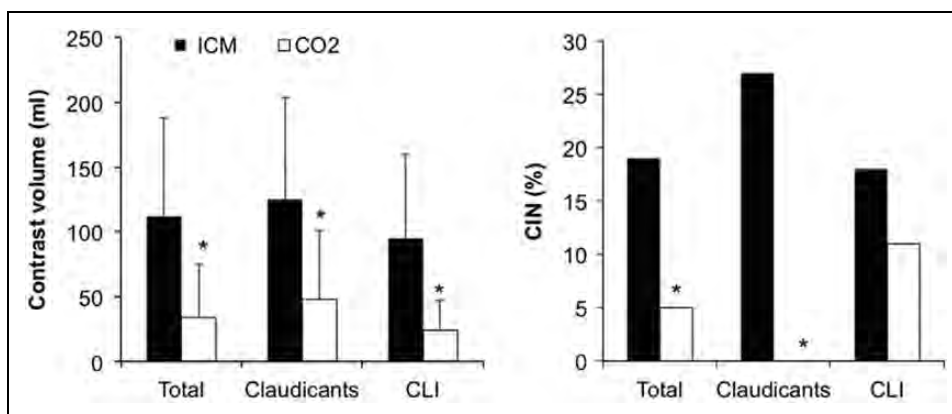

Figure 3. (A) Contrast volume and (B) frequency of contrast-induced nephropathy (CIN) in iodinated contrast media [ICM] and CO_2 group. The necessary contrast volume and incidence of CIN was significantly lower with CO2-aided percutaneous transluminal angioplasty (PTA) in total and in subgroups of both claudicants and patients with critical limb ischemia (CLI). * $P < .05$ vs ICM (A: t test for total and 1-way analysis of variance [ANOVA] for subgroup analysis, B: χ^2 test for individual group comparisons).

Table 3. Amount of Iodinated Contrast Medium (mL) Arranged by Treated Vessel Segment.[a]

	All	ICM[b]	CO_2[c]	P
Iliac, n	109 $\pm$ 58 (65)	118 $\pm$ 54[d] (57)	48 $\pm$ 49 (8)	.001
Femoral, n	92 $\pm$ 58 (82)	104 $\pm$ 53 (69)	26 $\pm$ 26 (13)	<.001
Popliteal, n	50 $\pm$ 33 (13)	72 $\pm$ 20 (7)	25 $\pm$ 28 (6)	.01
BTK, n	73 $\pm$ 71 (31)	93 $\pm$ 77 (21)	31 $\pm$ 21 (10)	.001
			MV $\pm$ SD	

Abbreviations: ANOVA, analysis of variance; ICM, iodinated contrast medium; CO_2, carbon dioxide; SD, standard deviation; LSD, least significant difference; BTK, below the knee.
[a]Overall 1-Way ANOVA $P < .001$; P value ICM vs CO_2.
[b]15% and [c]12% of procedures involved additional treatment of downstream segment.
[d]$P = .048$ vs popliteal ICM, LSD post hoc test.

1 year illustrating that CO_2-aided angiography is an effective method to guide peripheral procedures helping to prevent CIN.

Only few studies have evaluated the efficacy of CO_2-aided angiography in daily practice.[10-12] One recent Japanese registry study has assessed the safety and efficacy of CO_2 angiography-guided endovascular therapy for renal and stable iliofemoral artery disease.[10] They showed in 98 patients with a baseline eGFR of 35 mL/min that CO_2 angiography-guided angioplasty was effective (97.5% primary technical success rate) for preventing CIN. With an average additional dose of ICM of 15 mL, they observed 5% CIN but also 17% CO_2 angiography-related complication. In our current study, we confirm these data with a similar technical success rate (100%), slightly higher overall dose of contrast (35 mL), and similar rates of

CIN (5%) in the CO_2-aided group. However, we only observed minor temporary CO_2 angiography-related side effects (ischemic pain, dyspnea, and nausea), which resolved within minutes. Of note, acute ischemic lower leg pain is a common side effect of both ICM and CO_2 when injected proximal to a severe stenosis. While it can be related to injection pressure, we submit that it was in most of our patients rather due to the temporary displacement of oxygen-saturated blood from the arteries as it did not occur immediately during injection of CO_2 but shortly thereafter when the CO_2 reached the ischemic part of the lower leg. Interestingly, we frequently observe in both ICM and CO_2 that these acute pain symptoms do no longer occur after injection when the revascularization procedure was successful. Taken together, we extend the Japanese data [10] and a more recent study[12] by showing that CO_2 angiography can also be safely and efficaciously used in the treatment of popliteal and BTK interventions and also in patients with CLI (Fontaine III and IV) if individual image quality allows. However, the magnitude of benefit may differ between groups of patients. When evaluating patients with claudication, not a single CIN occurred with CO_2, whereas significantly more CIN was observed after treatment of patients with CLI. As an additional novelty of our present study, we present the CO_2 results as part of an allcomers group side by side with patients receiving only conventional ICM as a control group.

Limitations of using CO_2 as a contrast agent consist of a somewhat lower quality of angiograms compared to DSAs applying conventional ICN and of frequently perceived longer procedure durations.[14] This may be related to the manual injections and to the postprocessing imaging analysis. More adequate opacification of the arteries may be obtained with optimized injection technique including optimized CO_2 pressure and volume injections and X-ray protocols. However, our current data show that these disadvantages can be avoided using a combined approach. Due to potential inaccuracy of CO_2 with regard to diameter quantification,[15,16] sizing of stents was mostly performed by preprocedural ultrasound and by balloon sizing. In many cases, in the absence of absolute contraindications for ICM, we performed focused diagnostic evaluations with conventional contrast agent at the beginning and end of the procedures. Additional runs for wire guidance, setting of road maps, and stent placement were performed with CO_2. Our data demonstrate that the ICM and CO_2-aided approaches can be performed with similar intervention and irradiation times at an almost perfect primary technical success rate. This, however, could only be accomplished by an extensive preinterventional ultrasound examination performed by experienced sonographers. In summary, our CO_2-aided approach combines the advantages of both contrast agents in routine practice achieving optimal interventional results, with short procedural time, while avoiding further injury to predamaged kidneys in the most vulnerable patients by effectively lowering the amount of harmful ICM using CO_2 as supplemental contrast. Nevertheless, it may be argued that CO_2-alone angiography should be used as the initial contrast agent for the evaluation of PAD in patients with renal failure, and CO_2-aided ICM angiography should be considered only if the quality of the images is poor.

Important study limitations apply to the study design including retrospective analysis and lack of blinding and significant differences between the study populations of the ICM and CO_2 groups. Inherently, major limitations of retrospective study design include that there is frequently an absence of data on potential confounding factors, and it may be difficult to identify an appropriate exposed cohort and an appropriate comparison group. However, the fact that the baseline kidney function was significantly lower in the CO_2 group rather strengthens our main message that the CO_2-aided approach can preserve kidney function in the context of peripheral vascular interventions.

Conclusions

The present analysis underscores the value of CO_2 as an alternative contrast agent that can be used routinely to lower contrast volume and prevent CIN during peripheral vascular procedures from the iliac down to BTK even in patients with CLI.

Author Contribution

All authors contributed to (1) conception and design, or acquisition of data or analysis and interpretation of data; (2) drafting the article or revising it critically for important intellectual content; and (3) final approval of the version to be published.

Declaration of Conflicting Interests

The author(s) declared no potential conflicts of interest with respect to the research, authorship, and/or publication of this article.

Funding

References

1. Belch JJ, Topol EJ, Agnelli G, et al. Critical issues in peripheral arterial disease detection and management: a call to action. *Arch Intern Med*. 2003;163(8):884-892.

2. Malyar N, Furstenberg T, Wellmann J, et al. Recent trends in morbidity and in-hospital outcomes of in-patients with peripheral arterial disease: a nationwide population-based analysis. *Eur Heart J*. 2013;34(34):2706-1274.

3. Tendera M, Aboyans V, Bartelink ML, et al. ESC Guidelines on the diagnosis and treatment of peripheral artery diseases: Document covering atherosclerotic disease of extracranial carotid and vertebral, mesenteric, renal, upper and lower extremity arteries: the Task Force on the Diagnosis and Treatment of Peripheral Artery Diseases of the European Society of Cardiology (ESC). *Eur Heart J*. 2011;32(22):2851-2906.

4. Katsiki N, Athyros VG, Karagiannis A, Mikhailidis DP. Contrast-induced Nephropathy: An "All or None" Phenomenon? *Angiology*. 2014;66(6):508-513.

5. Maioli M, Toso A, Leoncini M, Gallopin M, Musilli N, Bellandi F. Persistent renal damage after contrast-induced acute kidney injury: incidence, evolution, risk factors, and prognosis. *Circulation*. 2012;125(25):3099-3107.

6. Moos JM, Ham SW, Han SM, et al. Safety of carbon dioxide digital subtraction angiography. *Arch Surg*. 2011;146(12):1428-1432.

7. Scalise F, Novelli E, Auguadro C, Casali V, Manfredi M, Zannoli R. Automated carbon dioxide digital angiography for lower-limb arterial disease evaluation: safety assessment and comparison with standard iodinated contrast media angiography. *J Invasive Cardiol*. 2015;27(1):20-26.

8. Miller FJ, Mineau DE, Koehler PR, et al. Clinical intra-arterial digital subtraction imaging. Use of small volumes of iodinated contrast material or carbon dioxide. *Radiology*. 1983;148(1):273-278.

9. Krasny R, Hollmann JP, Gunther RW. Initial experiences with CO2 as a gaseous contrast medium in digital subtraction angiography [in German]. *RoFo*. 1987;146(4):450-454.

10. Fujihara M, Kawasaki D, Shintani Y, et al. Endovascular therapy by CO2 angiography to prevent contrast-induced nephropathy in patients with chronic kidney disease: a prospective multicenter trial of CO2 angiography registry. *Catheter Cardiovasc Interv*. 2014;85(5):870-877.

11. Dowling K, Kan H, Siskin G, et al. Safety of limited supplemental iodinated contrast administration in azotemic patients undergoing CO2 angiography. *J Endovasc Ther*. 2003;10(2):312-316.

12. de Almeida Mendes C, de Arruda Martins A, Passos Teivelis M, et al. Carbon dioxide is a cost-effective contrast medium to guide revascularization of TASC A and TASC B femoropopliteal occlusive disease. *Ann Vasc Surg*. 2014;28(6):1473-1478.

13. Perk J, De Backer G, Gohlke H, et al. European Guidelines on cardiovascular disease prevention in clinical practice (version 2012). The Fifth Joint Task Force of the European Society of Cardiology and Other Societies on Cardiovascular Disease Prevention in Clinical Practice (constituted by representatives of nine societies and by invited experts). *Eur Heart J*. 2012;33(13):1635-1701.

14. Lawall H, Diehm C, Balzer K, et al. S3-Leitlinie zur Diagnostik und Therapie der peripheren arteriellen Verschlusskrankheit (PAVK). *VASA*. 2009;38(suppl 75):4-72.

15. Moresco KP, Patel N, Johnson MS, Trobridge D, Bergan KA, Lalka SG. Accuracy of CO2 angiography in vessel diameter assessment: a comparative study of CO2 versus iodinated contrast material in an aortoiliac flow model. *J Vasc Interv Radiol*. 2000;11(4):437-444.

16. Diaz LP, Pabon IP, Garcia JA, de la Cal Lopez MA. Assessment of CO2 arteriography in arterial occlusive disease of the lower extremities. *J Vasc Interv Radiol*. 2000;11(2 pt 1):163-169.

**Characterization of Superoxide-producing
Sites in Isolated Brain Mitochondria**

Alexei P. Kudin, Nana Yaw-B.
Bimpong-Buta, Stefan Vielhaber, Christian E.
Elger and Wolfram S. Kunz

Access the most updated version of this article at doi: 10.1074/jbc.M310341200

Find articles, minireviews, Reflections and Classics on similar topics on the JBC Affinity Sites.

Alerts:

- When this article is cited
- When a correction for this article is posted

Click here to choose from all of JBC's e-mail alerts

This article cites 26 references, 7 of which can be accessed free at
http://www.jbc.org/content/279/6/4127.full.html#ref-list-1

Characterization of Superoxide-producing Sites in Isolated Brain Mitochondria*

Alexei P. Kudin‡§, Nana Yaw-B. Bimpong-Buta§¶, Stefan Vielhaber‡, Christian E. Elger¶, and Wolfram S. Kunz¶‖

From the ¶Department of Epileptology, University Bonn Medical Center, Sigmund-Freud-Str. 25, D-53105 Bonn and the ‡Department of Neurology, University Magdeburg Medical Center, Leipziger Str. 44, D-39120 Magdeburg, Germany

Mitochondrial respiratory chain complexes I and III have been shown to produce superoxide but the exact contribution and localization of individual sites have remained unclear. We approached this question investigating the effects of oxygen, substrates, inhibitors, and of the NAD^+/NADH redox couple on H_2O_2 and superoxide production of isolated mitochondria from rat and human brain. Although rat brain mitochondria in the presence of glutamate+malate alone do generate only small amounts of H_2O_2 (0.04 ± 0.02 nmol H_2O_2/min/mg), a substantial production is observed after the addition of the complex I inhibitor rotenone (0.68 ± 0.25 nmol H_2O_2/min/mg) or in the presence of the respiratory substrate succinate alone (0.80 ± 0.27 nmol H_2O_2/min/mg). The maximal rate of H_2O_2 generation by respiratory chain complex III observed in the presence of antimycin A was considerably lower (0.14 ± 0.07 nmol H_2O_2/min/mg). Similar observations were made for mitochondria isolated from human parahippocampal gyrus. This is an indication that most of the superoxide radicals are produced at complex I and that high rates of production of reactive oxygen species are features of respiratory chain-inhibited mitochondria and of reversed electron flow, respectively. We determined the redox potential of the superoxide production site at complex I to be equal to -295 mV. This and the sensitivity to inhibitors suggest that the site of superoxide generation at complex I is most likely the flavine mononucleotide moiety. Because short-term incubation of rat brain mitochondria with H_2O_2 induced increased H_2O_2 production at this site we propose that reactive oxygen species can activate a self-accelerating vicious cycle causing mitochondrial damage and neuronal cell death.

Superoxide anion, a product of one-electron reduction of oxygen, is the by-product of normal functioning of the mitochondrial respiratory chain (1). It has been reported, that this radical is generated by complexes I and III of the mitochondrial respiratory chain and readily converted to H_2O_2 by mitochondrial Mn-superoxide dismutase (2–6). There is substantial evidence that superoxide and H_2O_2 contribute to the pathogenesis of certain neurodegenerative diseases (7, 8). However, there is considerable disagreement in recent literature concerning generated amounts and sites of superoxide production by isolated mitochondria. In contrast to the well documented production of superoxide at center "o" of antimycin A-inhibited complex III (2, 9, 10), the exact site and the total contribution of reactive oxygen species (ROS)[1] generation in complex I has not been established so far. Although certain investigators (11, 12) suggested low potential iron-sulfur clusters as potential sites, others (6) proposed flavine mononucleotide (FMN) to be the producer of superoxide being responsible for the H_2O_2 generation by brain mitochondria. In addition, there are substantial controversies regarding the exact amounts of ROS production at the different sites of respiratory chain. Although some reports document the highest rates of H_2O_2 production at a site at respiratory chain complex I (5, 12) others point to complex III as the main contributor (6, 10). Therefore, we extensively characterized ROS production at the different generation sites in respect to oxygen consumption of well coupled isolated rat and human brain mitochondria. Our results indicate that most of the superoxide radicals are produced at complex I and that a high production of reactive oxygen species is a feature of respiratory chain-inhibited mitochondria and of reversed electron flow, respectively. Because the redox potential of the superoxide production at complex I was determined to be -295 mV, this suggests that the generation site is most likely the FMN moiety. Moreover, short-term incubation of rat brain mitochondria with H_2O_2 in the lower mM range was observed to induce increased H_2O_2 production at this site, creating a self-accelerating vicious cycle. This mechanism is proposed to be important in brain pathology associated with mitochondrial damage and neuronal cell death.

EXPERIMENTAL PROCEDURES

Materials—Isocitrate dehydrogenase was purchased from Boehringer (Mannhein, Germany); L-adrenaline and bacterial protease (nagarse) from Fluka (Buchs, Switzerland); superoxide dismutase and digitonin from Serva (Heidelberg, Germany); and monochlorobimane from Molecular Probes (Leiden, The Netherlands). All other chemicals were obtained from Sigma-Aldrich.

Solutions—Solutions include the following: MSE solution (225 mM mannitol, 75 mM sucrose, 1 mM EGTA, 5 mM HEPES, 1 mg/ml BSA, pH 7.4); MSE-nagarse solution (0.05% nagarse in MSE solution); MSE-digitonin solution (0.02% digitonin in MSE solution); and MTP medium (10 mM KH_2PO_4, 60 mM KCl, 60 mM Tris-HCl, 110 mM mannitol, 0.5 mM EDTA, pH 7.4).

Isolation of Rat Brain Mitochondria—Mitochondria from one rat brain were isolated according to the protocol described by Rosental *et al.*

---

[1] The abbreviations used are: ROS, reactive oxygen species; FMN, flavine mononucleotide; GSH, reduced glutathione; CMB, *p*-chloromercuriobenzoate; RCR, respiratory control ratio.
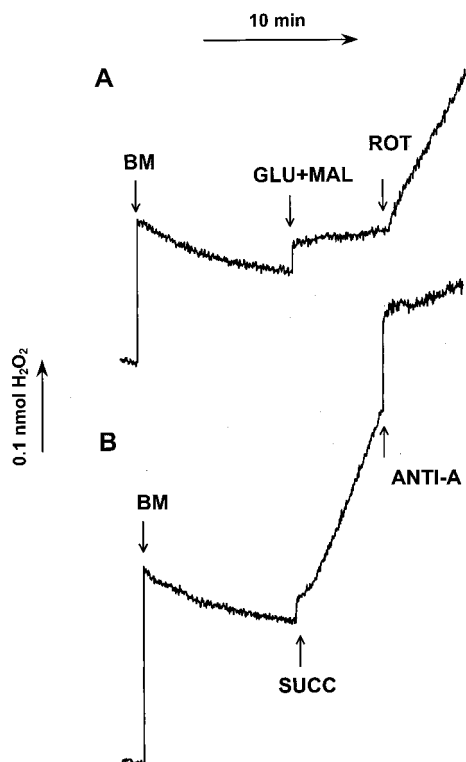
FIG. 1. **Experimental traces of H$_2$O$_2$ generation by isolated rat brain mitochondria in the presence of different mitochondrial substrates.** H$_2$O$_2$ generation was measured fluorimetrically determining the oxidation of *p*-hydroxyphenylacetic acid (200 μM) in oxygen saturated MTP medium in the presence of horseradish peroxidase (20 units/ml). *Vertical arrow*, fluorescence change caused by addition of 0.1 nmol H$_2$O$_2$ to the mitochondrial suspension. For *A*, *BM*, rat brain mitochondria (0.07 mg protein/ml); *GLU+MAL*, glutamate (10 mM) and malate (5 mM); *ROT*, rotenone (6.7 μM). For *B*, *SUCC*, succinate (10 mM); *ANTI-A*, antimycin A (0.5 μM).

(13) with small modification that allowed to obtain mitochondria with much better functional characteristics. In brief, the isolation protocol was the following. Before mitochondrial isolation all solutions were cooled down until the slight appearance of ice. One Wistar rat (60–90 days old) was anesthetized by chloroform and killed by decapitation. Its brain was immediately transferred into the ice-cold MSE solution and shaken to wash out blood. Then we minced the brain, added 10 ml of ice-cold MSE-nagarse solution, and homogenized it at 600 units/s using a potter homogenizer. Thereafter, we added 20 ml of ice-cold MSE solution and centrifuged the homogenate at 2000 × g for 4 min. After centrifugation we passed the supernatant through a cheesecloth and centrifuged it at 12,000 × g for 9 min. To permeabilize synaptosomes we dissolved the resulting pellet with 10 ml of ice-cold MSE-digitonin solution, transferred the solution to a small glass homogenizator, and homogenized it 8–10 times manually to obtain a homogenous suspension. Finally, we centrifuged the suspension at 12,000 × g for 11 min and dissolved the resulting pellet in about 300 μl of MSE solution to obtain about 20 mg protein/ml.

Isolation of Human Brain Mitochondria—Tissue samples from human parahippocampal gyrus were obtained from 9 patients (7 female and 2 male) with therapy-resistant temporal lobe epilepsy, who underwent epileptic surgery. White matter was rapidly removed and the remaining gray matter sample (about 150–200 mg wet weight) was immediately transferred into ice-cold MSE solution. The remaining isolation procedure of mitochondria was identical to the protocol described above. All patients gave written informed consent, and the study was approved by the University of Bonn Ethical Committee.

Preparation of Submitochondrial Particles—Frozen rat brain mitochondria (protein concentration of about 20 mg/ml) were thawed and sonicated three times for 15 s by the ultrasonic processor GEX-600. The further preparation was performed as described in Ref. 14.

Respiration—The oxygen consumption of mitochondria was determined at 30 °C in MTP medium with a PC-supported Oroboros high resolution oxygraph (15).
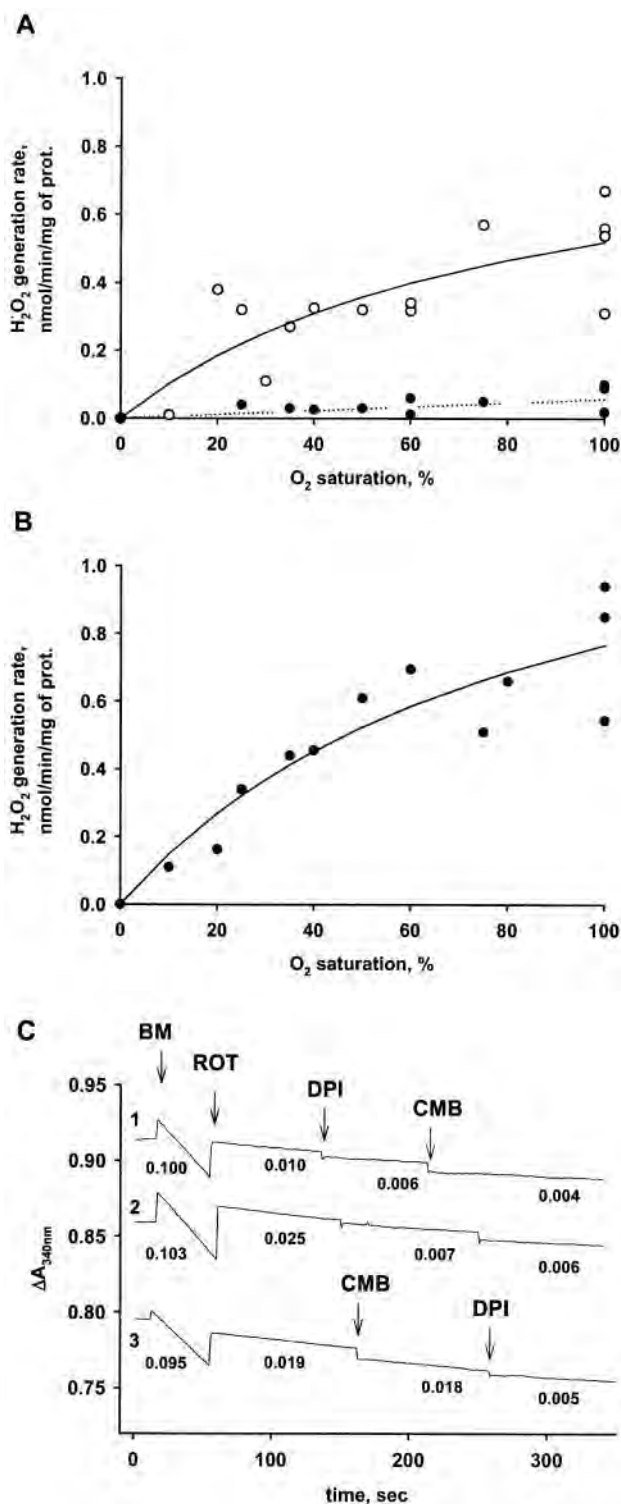

FIG. 2. **O$_2$ dependence of H$_2$O$_2$ generation by rat brain mitochondria.** *A* and *B*, about 0.2 mg protein/ml in the presence of glutamate (10 mM) and malate (5 mM) (*A*, *filled circles*, *dotted curve*) and plus rotenone (6.7 μM) (*A*, *open circles*, *solid curve*) and in the presence of succinate alone (10 mM) (*B*). Different values of O$_2$ saturation were obtained by mixing of MTP medium gassed with pure oxygen (100% saturation) and gassed with argon (0% saturation). The individual data points were obtained in experiments with four independent mitochondrial preparations. *C*, original experimental traces of detection of complex I activity using the NADH absorbance measurement at 340–380 nm. *Trace 1*, MTP medium gassed with air (20% O$_2$); *traces 2* and *3*, MTP medium gassed with 100% O$_2$. Additions: *BM*, brain mitochondria (0.7 mg protein/ml); *ROT*, rotenone (20 μM); *DPI*, 10 μM diphenyleneiodonium; *CMB*, 0.5 μM *p*-chloromercuriobenzoate. The depicted *numerical values* represent the slope of each trace (in ΔA/min).
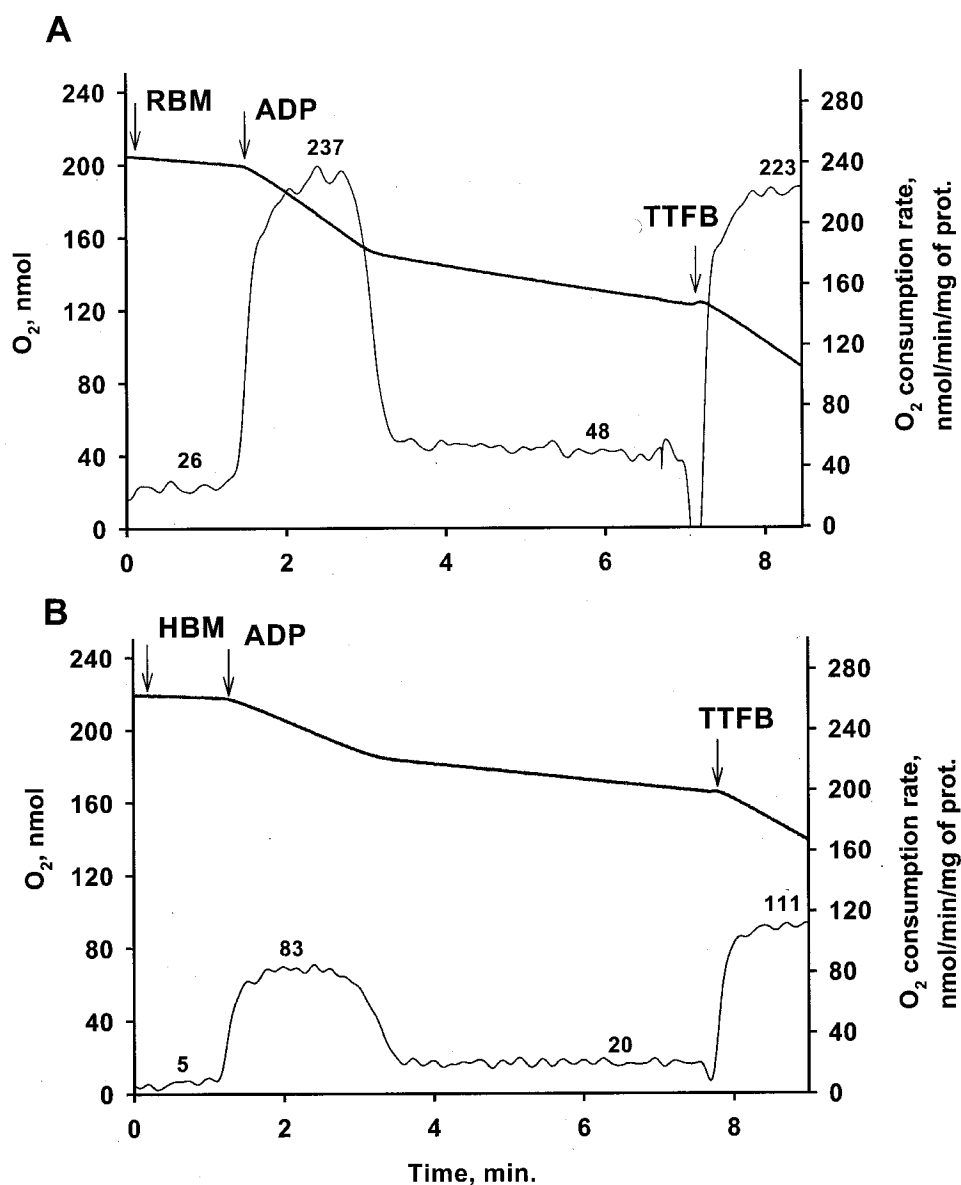
FIG. 3. **Experimental traces of oxygen consumption of brain mitochondria oxidizing glutamate and malate.** Air-equilibrated MTP medium at 30 °C with 10 mM glutamate, 5 mM malate and 3.3 mM MgCl$_2$ was used. *Thick traces*, oxygen content (*left axis*); *thin traces*, rate of respiration (*right axis*). The *numerical values* at the *thin curves* represent averaged respiration rates (in nmol O$_2$/min/mg protein) in the different mitochondrial states. Additions: ADP (250 μM), TTFB (4,5,6,7-tetrachloro-2-trifluoromethylbenzimidazole) (0.4 μM). *A*, rat brain mitochondria (*RBM*, 0.2 mg protein/ml). *B*, human brain mitochondria (*HBM*, 0.32 mg protein/ml).

TABLE I

Maximal rates of H$_2$O$_2$ generation of rat brain and human parahippocampal cortex mitochondria

The rates of H$_2$O$_2$ generation were determined at oxygen saturation. The resting rates of respiration were determined in the absence of nucleotides. Other experimental conditions as described in the legend to Fig. 4. The given values are averages $\pm$ S.D. *n*, number of independent mitochondrial preparations.

	Rat brain mitochondria	Human parahippocampal cortex mitochondria
Resting respiration rate with glutamate+malate (nmol O$_2$/min/mg)	24.4 $\pm$ 7.6 ($n = 21$)	9.6 $\pm$ 5.3 ($n = 9$)
H$_2$O$_2$ generation with glutamate+malate (nmol H$_2$O$_2$/min/mg)	0.04 $\pm$ 0.02 ($n = 9$)	0.03 $\pm$ 0.03 ($n = 8$)
In % of respiration rate	0.19 $\pm$ 0.13%	0.20 $\pm$ 0.15%
H$_2$O$_2$ generation with glutamate+malate+rotenone (nmol H$_2$O$_2$/min/mg)	0.68 $\pm$ 0.25 ($n = 10$)	0.27 $\pm$ 0.1 ($n = 8$)
Resting respiration rate with succinate (nmol O$_2$/min/mg)	48.3 $\pm$ 7.8 ($n = 16$)	16.7 $\pm$ 5.2 ($n = 8$)
H$_2$O$_2$ generation with succinate (nmol H$_2$O$_2$/min/mg)	0.80 $\pm$ 0.27 ($n = 10$)	0.13 $\pm$ 0.08 ($n = 6$)
In % of respiration rate	1.68 $\pm$ 0.56%	1.13 $\pm$ 0.47%
H$_2$O$_2$ generation with succinate+antimycin A (nmol H$_2$O$_2$/min/mg)	0.14 $\pm$ 0.07 ($n = 6$)	0.04 $\pm$ 0.03 ($n = 6$)

A

B

FIG. 4. **Comparison of H$_2$O$_2$ production rate and maximal O$_2$ consumption rate of rat and human brain mitochondria.** *A*, H$_2$O$_2$ production rates: *white bars*, rat brain mitochondria (average protein concentration 0.17 mg protein/ml, $n = 10$); *SUCC*, 10 mM succinate; *GLU+MAL+ROT*, 10 mM glutamate + 5 mM malate + 6.7 μM rotenone; *black bars*, human brain mitochondria (average protein concentration 0.1 mg protein/ml, $n = 8$). The rates were determined at 30 °C in oxygen saturated MTP medium. *B*, O$_2$ consumption rates: *white bars*, rat brain mitochondria (average protein concentration 0.2 mg protein/ml, $n = 16$); *SUCC*, 10 mM succinate + 6.7 μM rotenone; *GLU+MAL*, 10 mM glutamate + 5 mM malate; *black bars*; human brain mitochondria (average protein concentration 0.35 mg protein/ml, $n = 8$). The maximal O$_2$ consumption was induced by addition of 250 μM ADP and measured at 30 °C in MTP medium in the presence of 3.3 mM MgCl$_2$.
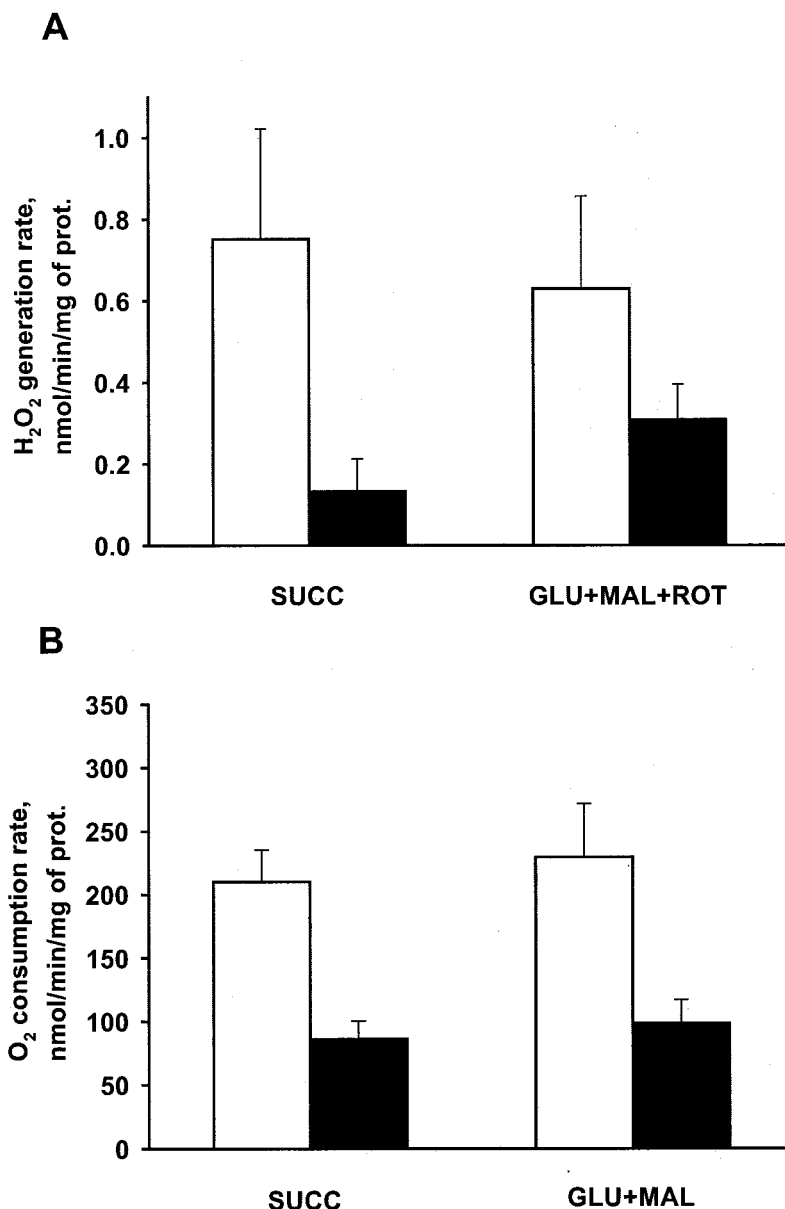
Measurement of H$_2$O$_2$ Production—Mitochondrial H$_2$O$_2$ generation was measured by monitoring the change in fluorescence of 200 μM *p*-hydroxyphenylacetic acid (λ_{ex} = 317 nm, λ_{em} = 414 nm) catalyzed by 20 units/ml horseradish peroxidase (6). Different O$_2$ concentrations were achieved by mixing argon- and oxygen-saturated buffers. Oxygen concentrations were calculated from the O$_2$ solubility in air and oxygen-saturated MSE solution at 30 °C and 101 kPa (0.23 and 1.15 mM, respectively), and from mixing ratios of the argon and oxygen-saturated solutions.

Measurement of Superoxide Production—The O$_2^{\bar{}}$-dependent oxidation of 1 mM epinephrine to adrenochrome in the presence of 7800 units/ml catalase was followed spectrophotometrically at 486–575 nm with a dual wavelength spectrophotometer (Aminco DW 2000, SLM Instruments). In control experiments we monitored the change in fluorescence of *p*-hydroxyphenylacetic acid (λ_{ex} = 317 nm, λ_{em} = 414 nm) catalyzed by horseradish peroxidase (conditions of measurement as described above) in the additional presence of 22 units/ml Cu,Zn-superoxide dismutase.

Determination of Enzymatic Activities—Aconitase activity was measured according to Ref. 16 with small modifications. The mitochondrial suspension was diluted 10 times in a solution, containing 50 mM Tris-Cl and 0.6 mM MnCl$_2$, pH 7.4, just before the activity measurement. Then mitochondria were sonicated for 15 s with the ultrasonic processor GEX-600. Aconitase activity was determined at 30 °C using a dual-wavelength spectrophotometer (Aminco DW 2000, SLM Instruments) following the absorbance change at 340–380 nm (ϵ_{red-ox} = 5.5 mM^{-1} cm^{-1}). The reaction mixture contained 50 mM Tris-Cl, pH 7.4, 5 mM

sodium citrate, 0.6 mM MnCl$_2$, 0.2 mM NADP$^+$, 0.1 mg/ml isocitrate dehydrogenase, 0.2% laurylmaltoside, and 40–70 μg/ml of protein. The activity of citrate synthase was determined by a standard method and the activity of NADH:coenzyme Q$_1$-reductase was measured at 340 nm-380 nm (ϵ_{red-ox} = 5.5 mM^{-1} cm^{-1}); in a buffer containing 50 mM KCl, 10 mM Tris-HCl, and 1 mM EDTA, pH 7.4, in the presence of 150 μM NADH, 100 μM coenzyme Q$_1$, and 2 mM KCN with a dual-wavelength spectrophotometer (Aminco DW 2000, SLM Instruments) (17). The protein content of mitochondria was determined using a protein assay kit based on Peterson's modification of the micro-Lowry method according to the instructions of the manufacturer (Sigma).

Determination of GSH Content—GSH content was determined using the method described in Ref. 18 with small modifications. The mitochondrial suspension was dissolved in MTP medium at a final concentration of ~0.8 mg/ml. After addition of monochlorobimane (100 μM) and glutathione *S*-transferase (1 units/ml) the reaction mixture was sonicated for 15 s with the ultrasonic processor GEX-600. After 30 min development of reaction the mitochondrial suspension was centrifuged at 16,000 × g for 7 min. Thereafter, the fluorescence of each supernatant was measured (λ_{ex} = 380 nm, λ_{em} = 470 nm) using a fluorescence reader (Spectra MAX Gemini, Molecular Devices). As standard we used GSH dissolved in MTP medium in a range of 0 to 100 μM.

Statistics—All data are presented as means ± S.D. and p values smaller than 0.05 (according to two-sided t test) were considered to be statistically significant.

FIG. 5. **Redox titration of mitochondrial superoxide production.** Mitochondrial inner membrane preparations were incubated at about 0.7 mg/ml in oxygen saturated MTP medium in the presence of 6.7 μM rotenone. The $O_2^{\bar{\cdot}}$-dependent oxidation of epinephrine to adrenochrome at different $NADH/NAD^+$ ratios was followed spectrophotometrically at 486–575 nm with a dual wavelength spectrophotometer (*open circles*, conditions of measurement as described under "Experimental Procedures"). In control experiments (*filled circles*) we monitored the change in fluorescence of *p*-hydroxyphenylacetic acid (λ_{ex} = 317 nm, λ_{em} = 414 nm) catalyzed by horseradish peroxidase in the presence of 22 units/ml Cu,Zn-superoxide dismutase. The data were normalized in respect to the $O_2^{\bar{\cdot}}$-generation rate in the presence of 1 mM NADH. For the calculation of redox potentials the midpoint potential of the free $NADH/NAD^+$ couple E_m 7.4 = −310 mV (21) and the Nernst equation were used.
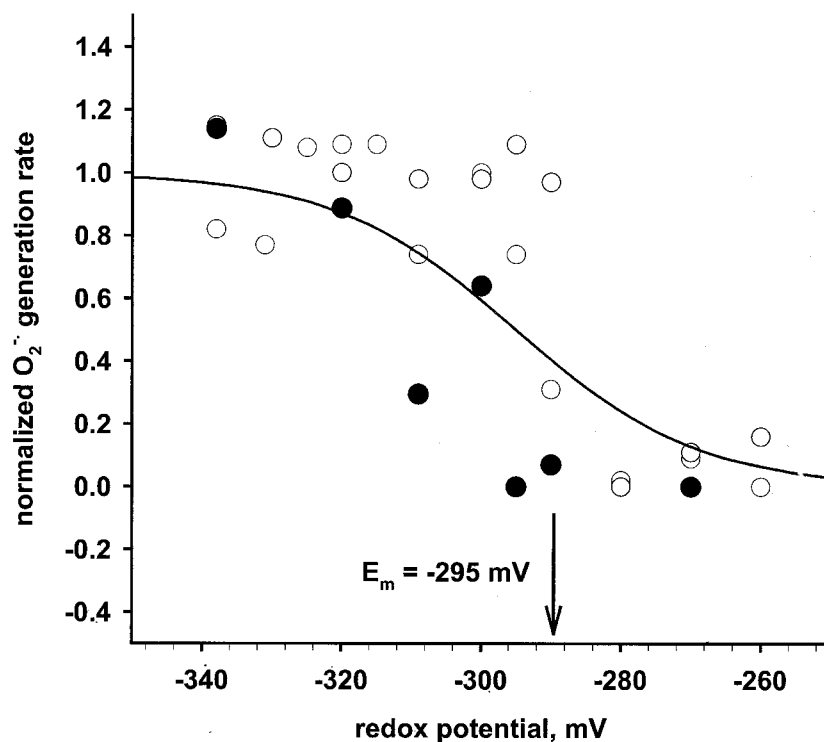
RESULTS

Oxygen Dependence of H_2O_2 Generation by Mitochondria Isolated from Brain Tissue—Fig. 1 shows the measurement of generation of hydrogen peroxide by isolated rat brain mitochondria using the fluorescent probe *p*-hydroxyphenylacetate. Addition of mitochondria (BM) led to transient increase in fluorescence, which returned to a stable stationary level. The addition of the respiratory substrates glutamate+malate resulted in a low rate of fluorescence increase indicating the generation of only small amounts of hydrogen peroxide (*GLU+MAL, upper trace*; 1.6 pmol H_2O_2/min or 0.02 nmol H_2O_2/min/mg protein). An about 20-fold higher slope of the fluorescence trace was observed after the addition of the complex I inhibitor rotenone (*ROT, upper trace*; 37 pmol H_2O_2/min or 0.53 nmol H_2O_2/min/mg protein) or in the presence of the respiratory substrate succinate alone (*SUCC, lower trace*; 46 pmol H_2O_2/min or 0.66 nmol H_2O_2/min/mg protein). The addition of the inhibitor of bc_1 complex antimycin A in the presence of succinate led to an inhibition of H_2O_2 production (*ANTI-A, lower trace*; 7.6 pmol H_2O_2/min or 0.11 nmol H_2O_2/min/mg protein). This is an indication that in rat brain mitochondria most of the superoxide radicals are produced at complex I and that a high production of reactive oxygen species is a feature of respiratory chain-inhibited mitochondria and of reversed electron flow, respectively. Because it is well documented that mitochondrial superoxide production is strongly dependent on oxygen concentration (19, 20) we determined the oxygen concentration dependence of H_2O_2 production of rat brain mitochondria in the presence of the respiratory substrates glutamate+malate (Fig. 2A, *filled circles*), glutamate+malate+rotenone (Fig. 2A, *open circles*), and succinate (Fig. 2B, *filled circles*). We detected hyperbolic concentration dependences from which we calculated a K_m value for oxygen of 0.92 ± 0.01 mM. A similar dependence was also observed for the production of H_2O_2 by complex III determined in the presence of succinate+antimycin A (data not shown).

The existence of a bypass of respiratory chain at the level of complex I in isolated brain mitochondria, leading to superoxide production, can be detected directly when analyzing the rotenone sensitivity of NADH:coenzyme Q_1 oxidoreductase. As shown in Fig. 2C, this enzymatic reaction is much less rotenone sensitive (75–80% inhibition, *traces 2* and *3*) at 100% oxygen saturation than at 20% oxygen tension (about 90% inhibition, *trace 1*), indicating the existence of an oxygen-dependent NADH oxidation pathway bypassing the site of action of rotenone. Very clearly, most of the rotenone-insensitive part of the reaction at oxygen saturation can be inhibited by diphenyleneiodonium, a flavin-modifying agent with certain specificity toward FMN of complex I (trace 2), but not by the thiol reagent *p*-chloromercuriobenzoate, that blocks FeS-clusters at complex I (trace 3). This result is an indication that the site of superoxide production is located upstream of both the rotenone inhibition site and FeS clusters, and therefore presumably the FMN moiety.

The Maximal Rates of H_2O_2 Generation of Mitochondria Isolated from Human and Rat Brain Tissue Depend on Specific Electron Transport Activity—A possible reason for the discrepant results reported about ROS production of isolated brain mitochondria (5, 6, 12) could be variable mitochondria quality. Therefore, we checked the isolated mitochondria in the present investigation with regard to basic characteristics: respiration rates in different functional states and respiratory control values. In Fig. 3, typical oxygraph traces of mitochondria isolated from rat brain (*A*) and human parahippocampal cortex (*B*) are given. Using glutamate and malate as respiratory substrates, active state respiration rates of 231 ± 40 nmol O_2/min/mg protein (n = 21) at an average respiratory control ratio (RCR) = 5.4 ± 0.8 were obtained for rat brain mitochondria and 88 ± 25 nmol O_2/min/mg protein (n = 9) at RCR = 3.2 ± 0.6 for mitochondria of human parahippocampal cortex, respectively. With succinate (+rotenone) as substrate we obtained active state respiration rates of 210 ± 25 nmol O_2/min/mg protein (n = 13) for rat brain mitochondria and 76 ± 22 nmol O_2/min/mg protein (n = 8) for mitochondria of human parahippocampal cortex. These values indicate that both brain mitochondria preparations are tightly coupled, but human parahip-

A

B

C

FIG. 6. **Influence of H_2O_2 treatment on H_2O_2 production (*A* and *B*), O_2 consumption in active state (*C*), reduced glutathione content (*D*), and aconitase activity (*E*) of rat brain mitochondria.** Mitochondria (four independent preparations) were suspended at about 3.5 mg protein/ml in MTP medium and treated with the indicated concentrations of hydrogen peroxide for 10 min. Thereafter, we centrifuged the suspension at $16,000 \times g$ for 5 min. The resulting pellet was dissolved in MSE solution. In control experiments mitochondria were treated with equal quantities of water. *A*, H_2O_2 production (0.17 mg protein/ml) in oxygen saturated MTP medium in the presence of glutamate (10 mM) and malate (5 mM) (*filled circles*, *solid curve*) and succinate (10 mM) (*open circles*, *dashed curve*). *B*, H_2O_2 production in the presence of glutamate (10 mM) and malate (5 mM) and rotenone (6.7 μM). *C*, O_2 consumption rate (0.2 mg protein/ml) in state 3 (after addition of 250 μM ADP) in the presence of glutamate (10 mM) and malate (5 mM) (*filled circles*, *solid curve*) or succinate (10 mM) and rotenone (6.7 μM) (*open circles*, *dashed curve*). *D*, GSH content; *E*, aconitase (*filled circles*, *left ordinate axis*) and citrate synthase (*open circles*, *right ordinate axis*) activities, assay conditions as described under "Experimental Procedures". The total GSH content (100%) of control mitochondria was determined to be 3.5 ± 1.5 nmol/mg protein.
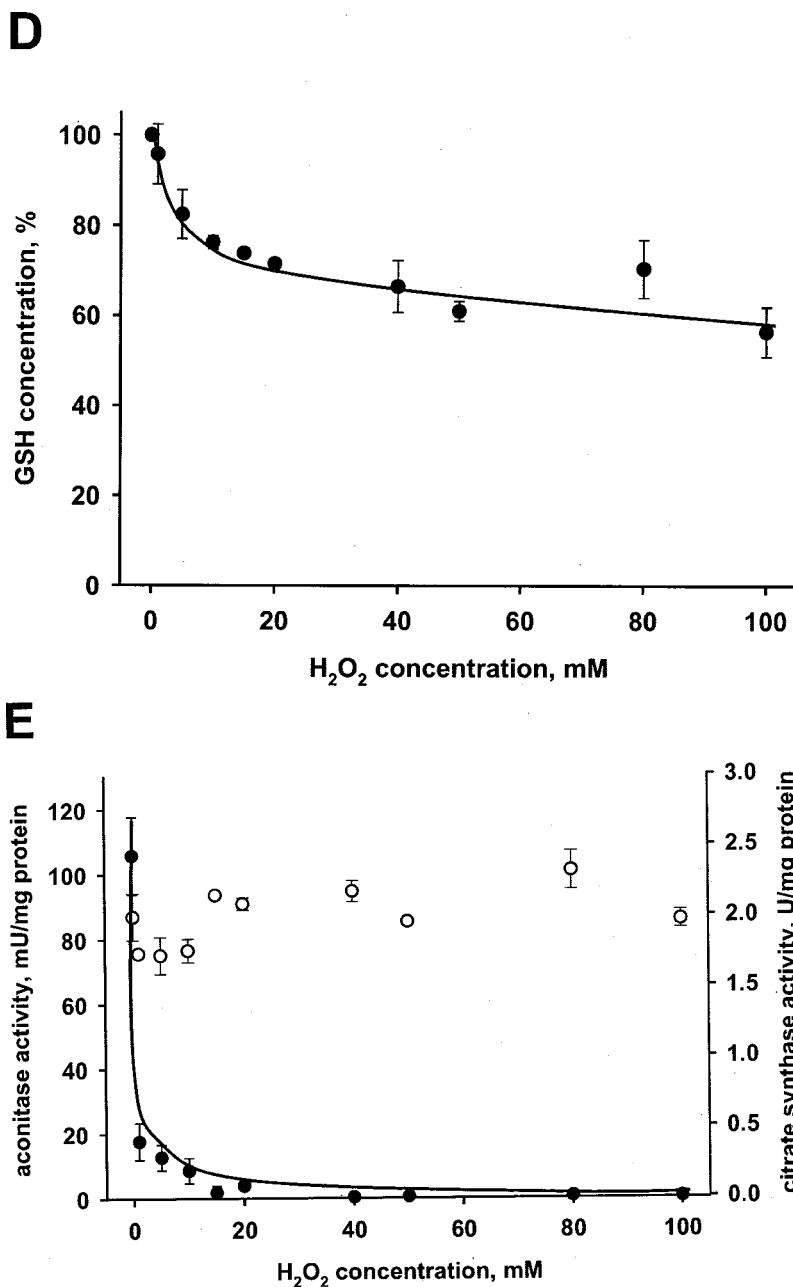
D

FIG. 6—*continued*

E
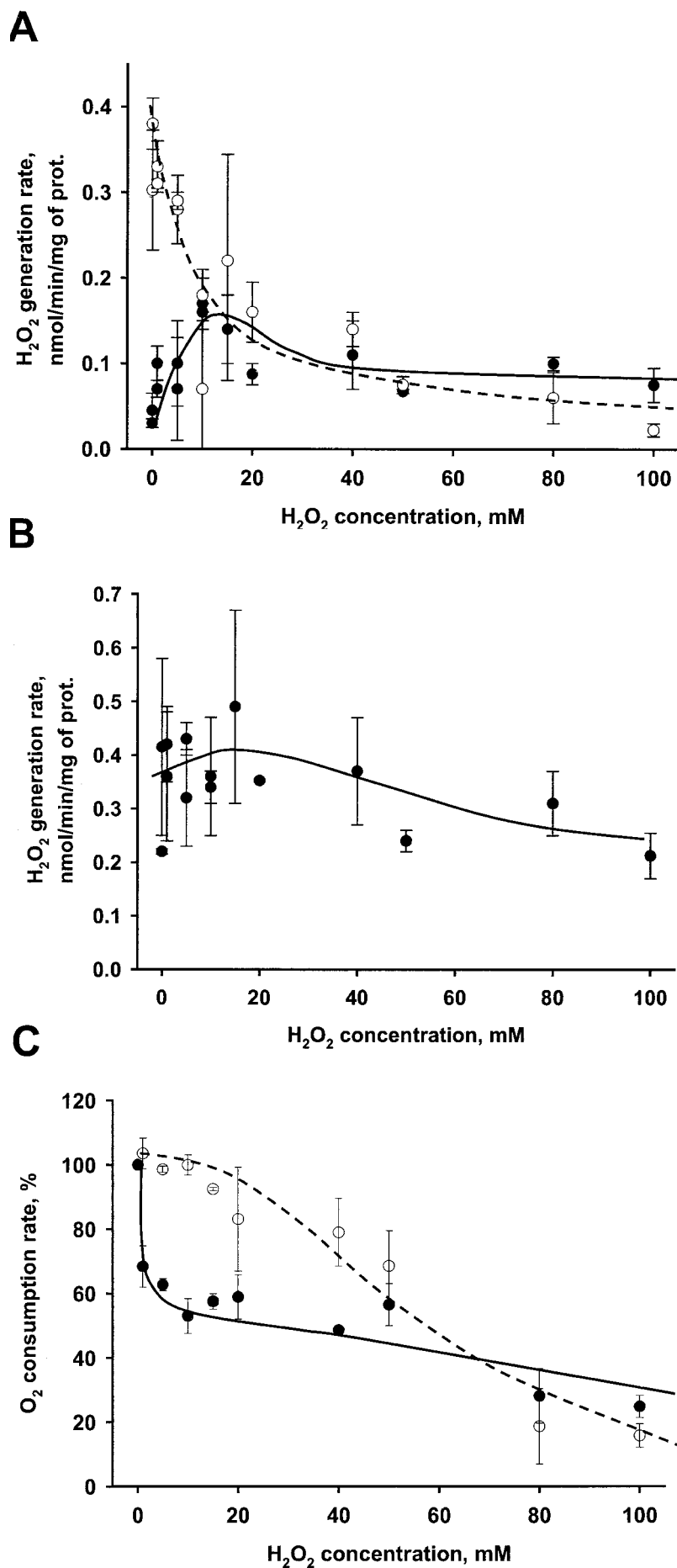
pocampal mitochondria appear to be less pure in respect to respiratory chain activity. Comparing the maximal H_2O_2 production rates (*cf*. Table I and Fig. 4*A*) rat brain mitochondria (Fig. 4*A*, *white bars*) seem to produce much higher quantities of H_2O_2 in the presence of succinate and in the presence of glutamate+malate+rotenone than human parahippocampal mitochondria (*black bars*). An explanation for this phenomenon is the mentioned higher specific electron transport activity of rat brain mitochondria in respect to human parahippocampal mitochondria (Fig. 4*B*). Really, as shown in detail in Table I, the electron transport chain of both types of brain mitochondria produces the by-product H_2O_2 at approximately similar percentage per consumed O_2 (with similar substrates), about 0.2% with glutamate+malate and about 1.5% with succinate.

Midpoint Potential of the Superoxide Producing Site in Complex I—To further characterize the site of superoxide production at complex I we determined the midpoint potential of superoxide production in inner membrane preparations of rat brain mitochondria (submitochondrial particles). For this, we altered the ratio of concentration of added NADH and NAD$^+$

and determined the rate of superoxide production using the oxidation of adrenaline to adrenochrome (Fig. 5, *open circles*) or the oxidation of *p*-hydroxyphenylacetate in the presence of peroxidase and externally added Cu,Zn-superoxide dismutase (Fig. 5, *filled circles*). With both detection methods a midpoint potential of the superoxide producing site of rat brain mitochondria equal to -295 mV was determined (5 independent experiments). The fact that this value of midpoint potential clearly differs from the values reported for FeS clusters (-370mV for N1a; -250mV for N1b and N3-N5; -100mV for N2) but evidently resembles the value reported for FMN,[2] also points to the FMN moiety as potential site of superoxide generation.

Treatment of Rat Brain Mitochondria with H_2O_2 Increases the Rate of H_2O_2 Generation by Direct Electron Flow through Complex I Creating a Vicious Cycle—Because H_2O_2 has been reported to accumulate in the injured brain (22), which has

---

[2] Complex I web site: www.scripps.edu/mem/biochem//CI/index.html.

FIG. 7. **Scheme illustrating the proposed vicious cycle of H_2O_2 effects on complex I of mitochondrial respiratory chain.**
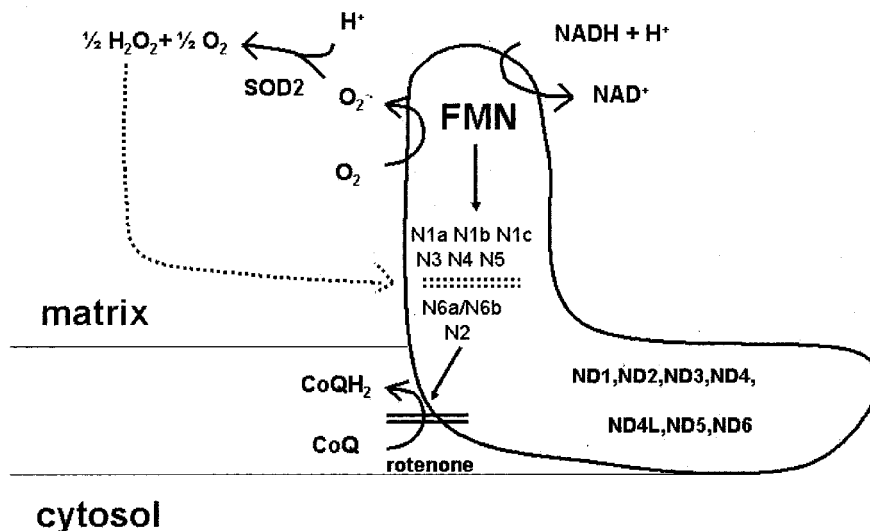
been postulated to cause further injury accompanied by neuronal cell death, we investigated in further experiments how treatment of isolated rat brain mitochondria with H_2O_2 would affect the generation of H_2O_2. In these experiments isolated brain mitochondria were incubated for 10 min with H_2O_2 in a concentration range of 1 to 100 mM. After removal of H_2O_2 by re-sedimentation of mitochondria, we determined the rates of H_2O_2 production in the presence of the respiratory substrates glutamate+malate (Fig. 6A, *filled circles*), succinate (Fig. 6A, *open circles*), and in the presence of glutamate+malate+ rotenone (Fig. 6B, *filled circles*). As shown in Fig. 6A, 10 min incubation of rat brain mitochondria with concentrations of H_2O_2 in the range of 1–10 mM increased the generation of H_2O_2 with glutamate+malate as substrates (*filled circles*) but decreased succinate-dependent H_2O_2 production (*open circles*). The generation of H_2O_2 in the presence of glutamate+malate+ rotenone (Fig. 6B, *filled circles*) remained in this concentration range within experimental error nearly constant. To elucidate the potential cause for the increase of H_2O_2 generation by direct electron flow but the inhibition of H_2O_2 generation by reverse electron flow we determined the maximal oxygen consumption rates of H_2O_2-treated mitochondria in the presence of glutamate+malate (Fig. 6C, *filled circles*) and succinate+ rotenone (Fig. 6C, *open circles*). Very clearly, small amounts of H_2O_2 effectively inhibited maximal respiration with the complex I-dependent substrates glutamate+malate leaving the succinate+rotenone-dependent oxidation rate nearly unaffected. The almost negligible effect of H_2O_2 treatment in the 1–10 mM concentration range on mitochondrial oxidative phosphorylation with succinate (+rotenone) as substrate is further corroborated by the observation that the respiratory control ratio of mitochondria (RCR, defined as ratio between rates in active state (respiration rate in the presence of ADP) and resting state (respiration rate in the presence of ATP)) with this particular substrate changed from 2.7 ± 0.3 (control incubation) to 2.2 ± 0.2 (at 1 mM H_2O_2), to 2.1 ± 0.1 (at 5 mM H_2O_2) and to 2.1 ± 0.3 (at 20 mM H_2O_2). Only the incubation of mitochondria with concentrations of H_2O_2 above 50 mM seriously affected the coupling of mitochondrial oxidative phosphorylation: at 50 mM H_2O_2 the RCR declined to 1.7 ± 0.3, at 80 mM H_2O_2 to 1.2 ± 0.2, and at 100 mM the RCR was equal to 1 (fully uncoupled condition, four independent experiments).

Taken together, the results of our incubation experiments with H_2O_2 concentrations below 20 mM can be only explained assuming a selective partial block of complex I between the

sites of superoxide production and the rotenone-sensitive ubiquinone reduction site. To determine possible targets of H_2O_2 in complex I (sulphydryl-groups, iron-sulfur clusters), we additionally determined the glutathione content (Fig. 6D) and aconitase and citrate synthase activities (Fig. 6E) in H_2O_2-treated rat brain mitochondria. Although the glutathione level was decreased by the short-term H_2O_2-treatment by about 30%, citrate synthase activity remained completely unaffected (Fig. 6E, *open circles*). On the other hand, aconitase activity (Fig. 6E, *filled circles*) was nearly completely lost after incubation of mitochondria with the lowest dose of H_2O_2 (1 mM). Because aconitase activity is inhibited by the oxidation of its ROS-sensitive FeS cluster (23), a similar ROS-sensitive iron-sulfur cluster within complex I could be the direct target of the observed action of H_2O_2.

DISCUSSION

In the present study we have characterized the H_2O_2 generation of mitochondria isolated from rat brain and human parahippocampal cortex. In accordance with several previous reports (5, 12), but in clear contrast to others (6, 10), we observed that the main quantity of H_2O_2 is produced at a site within complex I of the respiratory chain whereas only rather small quantities (10–20% of maximal H_2O_2 generation) are produced at the bc_1 complex in the presence of antimycin A. One potential reason for the discrepant results could be the different quality of mitochondrial preparations (the specific rates of active state respiration of rat brain mitochondria with succinate as substrate reported in Ref. 6 are ~10-fold lower than our rates). In accordance with previous work (19, 20) we detected a clear oxygen dependence of H_2O_2 generation with the rather high K_m value of 0.92 ± 0.01 mM oxygen (equal to ~85% of maximal oxygen saturation at 30 °C) for all conditions studied. In line with these results, at 100% oxygen saturation the superoxide production of brain mitochondria leads to a diminished rotenone sensitivity of NADH/coenzyme Q_1 oxidoreductase. As shown for mitochondria from rat and human brain, under resting state conditions between 0.2% (with glutamate+malate) and 1.5% (with succinate) of respiratory chain electron transport is redirected to superoxide formation. The different total H_2O_2 generation rates observed for isolated rat and human brain mitochondria are most likely related to the different purity of the individual mitochondrial preparations.

Applying two different methods for superoxide detection we determined the redox potential of the superoxide producing site to be -295 mV. This result can explain the strict dependence of

superoxide production on the functional state of mitochondria reported in previous work (5, 6, 12, 24). Conditions leading to high NAD-reduction (resting succinate respiration, inhibition of complex I by rotenone) stimulate superoxide production, whereas conditions that cause rapid oxidation of NADH (active state respiration or uncoupling) lead to very low superoxide production rates. Our result seems to be in contrast to the redox potential of -360 mV given in Ref. 12 for rat heart mitochondria. But for determination of the redox potential, these authors used the β-hydroxybutyrate/acetoacetate redox couple in rat heart mitochondria, which contain only minor amounts of β-hydroxybutyrate dehydrogenase not allowing an efficient substrate couple equilibration.

The following findings point to FMN as the potential site for superoxide generation. (i) The determined redox potential of -295 mV, which is in agreement with the midpoint potential of FMN but not with that of iron sulfur clusters.[2] (ii) The strong diphenyleneiodonium sensitivity (in agreement with Ref. 6) and the rather low *p*-chloromercuriobenzoate sensitivity (in contrast to Ref. 11) of this reaction. It is therefore very likely that the semireduced form of FMN-FMNH$\cdot$ (in close similarity to the bound semiquinone QH$\cdot$ of center i of bc$_1$ complex) is the competent one-electron donor for the one-electron reduction of oxygen to superoxide.

The following experimental problems can explain the controversial quantitative data for H_2O_2 and superoxide production of isolated mitochondria reported so far. (i) The rates of H_2O_2 generation are very low at 20% oxygen saturation used in the previous reports (5, 6, 10, 12, 24), which does not allow accurate determinations. (ii) Some of the fluorescent dyes (especially Amplex Red) tend to show high endogenous fluorescence changes for which considerable corrections have to be made (see discussion in Ref. 24). (iii) And finally, ketoacids, like pyruvate or oxoglutarate, tend to cause artificial fluorescence changes in the presence of *p*-hydroxyphenylacetate or Amplex Red, which can obscure accurate measurement of superoxide and H_2O_2 production. In the present study we therefore avoided the use of ketoacids as mitochondrial substrates and used *p*-hydroxyphenylacetate, which did not show considerable endogenous fluorescence changes as obtained with the more sensitive dye Amplex Red (data not shown). To obtain reliable data for maximal H_2O_2 and superoxide generation rates we also used oxygen saturated media.

Furthermore, we were able to show that incubation of rat brain mitochondria with H_2O_2 can initiate a vicious cycle of H_2O_2 generation, which might be of importance for certain pathological conditions of the brain. *In vivo*, during the ischemia-reperfusion period, the rather stable membrane-permeable H_2O_2 can reach stationary concentrations of about 100 μM (22). In our *in vitro* experiments, we applied a short-term incubation (10 min) of rat brain mitochondria with H_2O_2 in a concentration range of 1–10 mM, which is ~10–100-fold higher than the maximal concentrations observed *in vivo* (however, the *in vivo* challenge of mitochondria with the lower H_2O_2 concentrations might be of much longer duration). We observed increased H_2O_2 generation by direct electron transport and diminished H_2O_2 generation by reversed electron flow. On the other hand, the maximal oxygen consumption of these mitochondria was normal with succinate+rotenone but inhibited

with glutamate+malate to about 50%, pointing to a selective inhibition of complex I activity. The H_2O_2 treatment in this concentration range did not affect the mitochondrial citrate synthase activity and only small alterations of respiratory control ratios with succinate (+rotenone) were observed. These findings exclude a possible unspecific disruption of mitochondrial function by the H_2O_2 treatment. Furthermore, it is improbable that this complex I inhibition is related to the recently reported glutathinylation of complex I (25), because under our conditions, the GSH levels were decreased only by about 30%. However, aconitase, which harbors a highly ROS-sensitive FeS cluster (23), was completely inhibited. Consequently, our findings allow the supposition of the scenario depicted in Fig. 7. H_2O_2 inactivates a ROS-sensitive FeS cluster within complex I localized between the coenzyme Q-reduction site and FMN (*dotted line*). This would initiate a vicious cycle leading to a self-accelerating inhibition of complex I with the result of further elevated H_2O_2 generation. This scenario might explain the following findings relevant to human disease: (i) the rather selective inhibition of complex I in combination with accumulation of markers for oxidative stress which has been reported for Substantia nigra in Parkinson's disease (26), and (ii) the detected inhibition of complex I in the epileptic focus of patients with temporal lobe epilepsy (27).

REFERENCES

1. Chance, B., Sies, H., and Boveris, A., (1979) *Physiol. Rev.* **59,** 527–605
2. Boveris, A., Cadenas, E., and Stoppani, A. O. M. (1976) *Biochem. J.* **156,** 435–444
3. Cadenas, E., Boveris, A., Ragan, C. I., and Stoppani, A. O. (1977) *Arch. Biochem. Biophys.* **180,** 248–257
4. Turrens, J. F., and Boveris, A. (1980) *Biochem. J.* **191,** 421–427
5. Votyakova, T. V., and Reynolds, I. J. (2001) *J. Neurochem.* **79,** 266–277
6. Liu, Y., Fiskum, G., and Schubert, D. (2002) *J. Neurochem.* **80,** 780–787
7. Halliwell, B. (1992) *J. Neurochem.* **59,** 1609–1623
8. Beal, M. F., Howell, N., and Bodis-Wollner, I. (1997) *Mitochondria and Free Radicals in Neurodegenerative Disease*, Wiley-Liss, New York
9. Nohl, H., and Jordan, W. (1986) *Biochem. Biophys. Res. Commun.* **138,** 533–539
10. Chen, Q., Vazquez, E. J., Moghaddas, S., Hoppel, C. L., and Lesnefsky, E. J. (2003) *J. Biol. Chem.* **278,** 36027–36031
11. Genova, M. L., Ventura, B., Giuliano, G., Bovina, C., Formiggini, G., Castelli, G. P., and Lenaz, G. (2001) *FEBS Lett.* **505,** 364–368
12. Kushnareva, Y., Murphy, A. N., and Andreyev, A. (2002) *Biochem. J.* **368,** 545–553
13. Rosental, R. E., Hamud, F., Fiskum, G., Varghese, P. J., and Sharpe, S. (1987) *J. Cereb. Blood Flow Metab.* **7,** 752–758
14. Cino, M., and Del Maestro, R. F. (1989) *Arch. Biochem. Biophys.* **269,** 623–638
15. Kunz, W. S., Kudin, A., Vielhaber, S., Elger, C. E., Attardi, G., and Villani, G. (2000) *J. Biol. Chem.* **275,** 27741–27745
16. Gardner, P. R., Nguyen, D.-D. H., and White, C. W. (1994) *Proc. Natl. Acad. Sci. U. S. A.* **91,** 12248–12252
17. Wiedemann, F. R., Vielhaber, S., Schröder, R., Elger, C. E., and Kunz, W. S. (2000) *Anal. Biochem.* **279,** 55–60
18. Kamencic, H., Lyon, A., Paterson, P. G., and Juurlink, B. H. J. (2000) *Anal. Biochem.* **286,** 35–37
19. Boveris, A., and Chance, B. (1973) *Biochem. J.* **134,** 707–716
20. Alvarez, S., Valdez, L. B., Zaobornyj, T., and Boveris, A. (2003) *Biochem. Biophys. Res. Commun.* **305,** 771–775
21. Jensen, M. A., and Elving, P. J. (1984) *Biochim. Biophys. Acta* **764,** 310–315
22. Hyslop, P. A., Zhang, Z., Pearson, D. V., and Phebus, L. A. (1995) *Brain Res.*, **671,** 181–186
23. Flint, D. H., Tuminello, J. F., and Emptage, M. H. (1993) *J. Biol. Chem.* **268,** 22369–22376
24. St-Pierre, J., Buckingham, J. A., Roebuck, S. J., and Brand, M. D. (2002) *J. Biol. Chem.* **277,** 44784–44790
25. Taylor, E. R., Hurrell, F., Shannon, R. J., Lin, T.-K., Hirst, J., and Murphy, M. P. (2003) *J. Biol. Chem.*, **278,** 19603–19610
26. Beal, M. F. (1996) *Curr. Opin. Neurobiol.* **6,** 661–666
27. Kunz, W. S., Kudin, A. P., Vielhaber, S., Blümcke, I., Zuschratter, W., Schramm, J., Beck, H., and Elger, C. E. (2000) *Ann. Neurol.*, **48,** 766–773

Comprehensive Analysis of Macrocirculation and Microcirculation in Microgravity During Parabolic Flights

Nana-Yaw Bimpong-Buta[1†], Johanna M. Muessig[1†], Thorben Knost[1], Maryna Masyuk[1], Stephan Binneboessel[1], Amir M. Nia[1], Malte Kelm[1,2] and Christian Jung[1]*

[1] *Medical Faculty, Division of Cardiology, Pulmonology, and Vascular Medicine, University Hospital Düsseldorf, Heinrich-Heine-University, Düsseldorf, Germany,* [2] *CARID, Cardiovascular Research Institute Düsseldorf, Düsseldorf, Germany*

Background: Profound knowledge about cardiovascular physiology in the setting of microgravity can help in the course of preparations for human space missions. So far, influences of microgravity on the cardiovascular system have been demonstrated, particularly pertaining to venous fluid shifts. Yet, little is known about the mechanisms of these adaptations on continuous macrocirculatory level and regarding the microcirculation.

Methods: Twelve healthy volunteers were subjected to alternating microgravity and hypergravity in the course of parabolic flight maneuvers. Under these conditions, as well as in normal gravity, the sublingual microcirculation was assessed by intravital sidestream dark field microscopy. Furthermore, hemodynamic parameters such as heart rate, blood pressure, and cardiac output were recorded by beat-to-beat analysis. In these settings, data acquisition was performed in seated and in supine postures.

Results: Systolic [median 116 mmHg (102; 129) interquartile range (IQR) vs. 125 mmHg (109; 136) IQR, $p = 0.01$] as well as diastolic [median 72 mmHg (61; 79) IQR vs. 80 mmHg (69; 89) IQR, $p = 0.003$] blood pressure was reduced, and cardiac output [median 6.9 l/min (6.5; 8.8) IQR vs. 6.8 l/min (6.2; 8.5) IQR, $p = 0.0002$] increased in weightlessness compared to normal gravitation phases in the seated but not in the supine posture. However, microcirculation represented by perfused proportion of vessels and by total vessel density was unaffected in acute weightlessness.

Conclusion: Profound changes of the macrocirculation were found in seated postures, but not in supine postures. However, microcirculation remained stable in all postures.

Keywords: weightlessness, microcirculation, parabolic flight, microgravity, hemodynamic changes

INTRODUCTION

Over the past decades, spaceflight has been a thriving field of scientific interest (Buckey, 1999; Mairesse et al., 2019). In the meantime, hundreds of astronauts have spent months in space, challenged by the circumstances of microgravity. However, striving to space is not without perils looking at in-flight and postflight health risks (Buckey et al., 1996; Lawley et al., 2017). As commercial flights to space will become accessible in the near future, even more humans with different health states will be exposed to microgravity. Even though putative health risks do not seem permanent, understanding more about physiological processes of the human body under these conditions is of great interest (Hubbard and Hargens, 1989; Demontis et al., 2017; Garrett-Bakelman et al., 2019) as good human health is a prerequisite for the success of any space mission (Hubbard and Hargens, 1989; Demontis et al., 2017).

It is evident that there are only a few platforms that harbor the possibility of fruitful experiments in space or else can mimic conditions of space here on earth. In this regard, spaceflight analogs, such as bed rest, head-down tilt at a moderate angle, or water immersion, have been implemented, particularly in scientific settings (Hargens and Vico, 2016). Even so, since a few decades, parabolic flights have equally proven a promising spaceflight analog (Caiani et al., 2009; Petersen et al., 2011; Norsk, 2014; Shelhamer, 2016; Klein et al., 2019).

It is well known that gravitational changes have significant effects on the cardiovascular system, constantly challenging the cardiovascular system in diminishing venous blood return to the heart and therewith altering cardiac outputs, particularly in seated, and upright postures (Norsk et al., 2006). Here, cardiopulmonary and arterial baroreflexes compensate for gravity-induced dropping of blood pressure by induction of vasoconstriction (Norsk et al., 2006). Prior studies have revealed that in microgravity, the effects on the cardiovascular system are somewhat even more prominent (Aratow et al., 1991; Baisch et al., 2000). In microgravity in particular, headward venous fluid shifts have been reported as hydrostatic gradients are abolished and tissue pressures change (Buckey et al., 1993). In this regard, prominent clinical features of microgravity are puffy faces, nasal congestion, headaches, and bird legs due to dehydration of the lower legs (Hargens et al., 1983; Hargens and Richardson, 2009). Buckey et al. (1993) stressed that, in particular, central venous pressure is altered. It has also been described that in the course of acute loss of gravity in weightlessness, substantial fluid shifts are induced, leading to central volume expansion (Fritsch-Yelle et al., 1996; Norsk et al., 2006, 2015). Hargens et al. (1983) documented the acute effects of these fluid shifts with transition into microgravity (Breit et al., 1993; Hargens and Richardson, 2009) as well as in simulated models of weightlessness. Looking at these facts, one has to bear in mind that understanding the mechanism of fluid shifts under these conditions remains complex, particularly as overall fluid response mechanisms may have significant medical implications (Nicogossian et al., 1991; Simanonok and Charles, 1994). As stated above, one of the primary fluid shift mechanisms upon entrance into microgravity is the relocation of vascular fluids to

cephalad compartments (White and Blomqvist, 1998; Drummer et al., 2000; Hawkey, 2003). However, it should be mentioned that overall fluid distribution also entails fluid allocations into other locations such as extravascular and extracellular compartments (Leach et al., 1996; Drummer et al., 2000), for instance, in the course of transcapillary fluid shifts (Hargens and Richardson, 2009). Furthermore, shifts of interstitial fluids have been reported in former studies as potentially underlying causes of complex systemic adaptations of the human body to weightlessness (Kirsch and Von Ameln, 1981; Blomqvist, 1983). Another noteworthy aspect of fluid distributions under these conditions is its timescale: previous studies have revealed the importance of characterizing short-term, mid-term, and long-term fluid shift alterations in this setting (Norsk et al., 2015; Gerber et al., 2018; Norsk, 2020), even with respect to postflight readaptations (Moore and Thornton, 1987).

Furthermore, details about general physiologic adaptations during spaceflights have been addressed (Tipton and Hargens, 1996). These changes occur immediately upon entering microgravity and last for at least several days or even weeks (Norsk et al., 2006, 2015). As an excellent health status is a prerequisite of any astronaut, candidates for space missions undergo profound prior medical testing proving excellent health states. Thus, most astronauts recover from postflight health deficits in a timely fashion of a few weeks, and permanent health deficiencies have remained scarce. However, postflight cardiovascular deconditioning, as in orthostatic intolerance, is an important issue. Buckey et al. (1996) and Lee et al. (2015) have investigated about its clinical relevance and implications (Buckey et al., 1996; Lee et al., 2015).

So far, scientific works have been focusing on macrocirculatory parameters such as blood pressure, cardiac output, and heart rate during human space missions as well as with spaceflight analogs (Mukai et al., 1991; Fritsch-Yelle et al., 1996; Schlegel et al., 1998; Norsk et al., 2006, 2015; Caiani et al., 2009; Coupé et al., 2009). However, in-flight measurements of these cardiovascular parameters are diÿcult to obtain, and results have been inconsistent (Fritsch-Yelle et al., 1996; Norsk et al., 2006; Verheyden et al., 2009; Petersen et al., 2011; Klein et al., 2019).

With respect to the known data about cardiovascular adaptations in space, alterations of the microcirculation under these conditions seem likely, but the impact of acute weightlessness on the microcirculation has not yet been addressed. The microcirculation is regarded the largest part of the circulation. It entails a large network of arterioles and venules that facilitates gas and nutrient exchange on tissue and endothelial levels (Coupé et al., 2009), with an estimated surface area of 350 m^2. In this regard, the microcirculation plays a crucial role in blood flow regulations, ensuring adequate organ function (Jung et al., 2016a). The evaluation of the microcirculation has become more and more clinically relevant, in particular, in the setting of critically ill patients (De Backer et al., 2014; Jung et al., 2016b). In these scenarios, the microcirculation has been identified as one of the key predictors of mortality. The timely evaluation of the microcirculation has been esteemed one of the tools for improvement of therapeutic strategies. Former studies demonstrated that in challenging scenarios with profound

alterations of the cardiovascular system, macrocirculation, and microcirculation might differ substantially in responses (Jung et al., 2010; Jung et al., 2016b). Therefore, in our setting, one of the aims was to investigate about differences of macrocirculation and microcirculation as substantial effects on the cardiovascular system are generally known. Handheld video microscopes, as the one we implemented in our setting, have been classified helpful in the assessment of microcirculatory flow (Massey and Shapiro, 2016; Ince et al., 2018).

There were two aims of this study: (1) to test the feasibility of measurements of the sublingual microcirculation during parabolic flight maneuvers as a novel approach on a spaceflight-mimicking platform and (2) to assess alterations of hemodynamic cardiovascular parameters of the macrocirculation and the microcirculation during microgravity and to evaluate the effect of supine and seated body postures on these variables.

MATERIALS AND METHODS

Study Population

Twelve healthy volunteers (seven male, median age of the whole group 29 years) were recruited for this study. Airworthiness (proven by medical certificate) was attested prior to participation in this study. The study was conducted in accordance with the Declaration of Helsinki (1975, revised in 2008), and the protocol was approved by the German Ethics Committee of the Medical Faculty of the University Hospital Duesseldorf, Germany (Date of approval: August 14, 2017; Project Identification number: 2017054297), and by the French Ethics Committee [Comité de Protection des Personnes (CPP) Nord-Ouest III] of the Medical Faculty of the University of Caen (Date of approval: September 6, 2017; Project Identification number: 2017-A01185-48). Written informed consent was voluntarily provided by all participants of the study.

Parabolic Flight

The study was conducted within a participation in a so-called parabolic flight campaign by the German space agency [Deutsches Zentrum für Luft-und Raumfahrt (DLR)] as described previously (Bimpong-Buta et al., 2018a). The location of this campaign was in Bordeaux (France) with flight over the Mediterranean Sea and the Atlantic Ocean. On-site in Bordeaux, the French company NoveSpace (headquarter in Mérignac, France) was in charge of regulations of adequate aviation procedures. On each flight day, 31 parabolic flight maneuvers were performed. The aircraft implemented in this flight campaign was an Airbus 310. To obtain best parabolic flight trajectories, the aircraft was aviated by well-trained jet pilots. In the course of each parabolic flight path, alternating states of gravity can be experienced aboard. These gravity states range from earthly gravity (1 G) to begin with ("steady flight") followed by a state of hypergravity ("1.8 G pull-up") followed by a state of microgravity (0 G) for the duration of 22 s. Hereafter, *via* a second phase of hypergravity ("1.8 G pull-out"), regular gravity (1G) is resumed at the end of each parabolic flight maneuver. Details about the flight

maneuver have been published before (Schlegel et al., 1998; Shelhamer, 2016).

One of the primary concerns in the course of preparation of the flight campaign was the possible occurrence of motion sickness due to the anticipated abrupt gravitational changes inherent to the scheduled flight maneuvers. In worst-case scenarios, health issues of the crew or participants might have led to cancelation of a flight day. With respect to the extensive efforts of preparation of each experiment prior to the campaign, one aim prior to takeoff was to minimize possible interferences or interruptions of the flight maneuvers, especially as this physiologic reaction has proven foreseeable. On the basis of experiences from former flight campaigns, the intentional application of antiemetic medications prior to takeoff has helped alleviate this issue. Thus, in order to prevent motion sickness during the parabolic flight maneuvers, the antiemetic drug scopolamine was administered subcutaneously around 2 h prior to takeoff on a voluntary basis. In one of our previous studies, we could demonstrate that scopolamine does not affect our measurements of the sublingual microcirculation (Bimpong-Buta et al., 2018b). Nonetheless, one has to bear in mind that the application of scopolamine in this setting might have unknowingly modified the results of the performed measurements in other ways (see also limitations).

Experimental Setup

In our experimental setup, for each flight day, three test subjects were scheduled. As 31 parabolas were flown per flight day, each test subject was examined in the course of 10 consecutive parabolas, with five parabolas in the supine posture and five parabolas in the seated posture. Each data set comprised the measurements of parameters of microcirculation and parameters of macrocirculation, respectively.

Macrocirculation

The macrocirculation was investigated using a device for continuous and non-invasive beat-to-beat measurement of hemodynamic blood flow (CNAP® Monitor 500 HD, CNSystems Medizintechnik GmbH, Graz, Austria). In short, the analysis includes blood pressure wave form documentation and provides derived parameters. The device has been validated in clinical trials indicating an excellent comparability with invasive measurements (Smolle et al., 2015; Wagner et al., 2015; Rogge et al., 2017). In the course of preparations of the project, a specially trained CNAP® instructor was invited from Austria for hands-on training sessions with our team of operators. With respect to the planned rotations of the test subjects aboard and therewith indicated changes of postures, this training focused on optimization of procedures of (re-) calibrations of the device to ensure correct measurements throughout the experiment. For correct measurements, the calibration entailed positioning the left hand on the chest. Aboard, all beat-to-beat data were stored with defined markers for later analysis. For quick setup, the monitor was connected to each test subject *via* a single-line finger sensor placed on the right index finger.

Before each set of measurements, notably after the change of postures, the monitor was calibrated and checked to ensure proper function in all its particulars. In this manner in our setup, for each parabola, the following parameters were obtained: blood pressure (BP), heart rate (HR), stroke volume (SV), cardiac output [(CO) = HR × SV], cardiac index [(CI) = CO/body surface area (BSA)], and systemic vascular resistance {(SVR) = [80 × (mean arterial pressure − mean right pressure)]/CO}.

Microcirculation

The microcirculation was assessed by implementation of the sidestream dark field microscopy (MicroScan® device, Microvision Medical, Amsterdam, Netherlands) as described before (Ince, 2005; De Backer et al., 2007; Bimpong-Buta et al., 2018b). This intravital microscope is designed for real-time measurement of the human sublingual microcirculation. In more than 200 clinical studies, it has been proven to serve as a valid diagnostic tool for high-quality imaging of the sublingual capillary network. With a highly sensitive camera at the tip of the device, real-time recordings of the sublingual capillary network can be performed and visualized on a tablet screen to be saved for later analysis. In this regard, in our setting, the device was mounted on the side of the tongue of each participant with application of gentle pressure to ensure just sufficient contact of the tip of the device with the sublingual surface. As part of the visualization software, the monitor offered a real-time feedback about the quality of the intended recording. Thus, high-quality visualization of the microcirculatory network could be ensured.

The tablet we utilized in this setting is the Microsoft Surface Pro 4 (Redmond, Washington, United States). After acquisition of the imagery data, a device-specific software (AVA, Version 4.3 C) is implemented for data analysis. For the evaluation of the microcirculation, for each parabola, the following parameters were measured: Proportion of perfused vessels [(PPV) = 100 × (total number of perfused vessels/total number of vessels)], perfused vessel density [(PVD) = total length of perfused vessels divided by the analyzed area], total vessel density [(TVD) = total number of vessel crossings], number of crossings [(NC) = number of vessel intersections the lines in a grid of 3 equidistant horizontal and vertical lines], and the perfused number of crossings [(PNC) = number of vessel crossings with continuous flow].

Statistical Analysis

Statistical analysis was performed applying a commercially available software (GraphPad Prism Software, Version 6, GraphPad Software, San Diego, CA, United States). As the size of the group of test subjects was rather small, we did not assume a Gaussian distribution in this setting. The data are presented as median in the course of repeated measures. In this regard, the statistical tests applied were the Mann–Whitney test and the Friedman test, respectively. In the course of post hoc analysis, the Dunn's multiple comparisons test was implemented. A two-tailed p-value < 0.05 was considered statistically significant.

RESULTS

The baseline characteristics of the study population are shown in **Table 1**. Throughout the course of each parabola in seated postures, significant changes of hemodynamic parameters reflecting the macrocirculation could be observed. Thus, systolic as well as diastolic blood pressure decreased in weightlessness. Blood pressures reached a median of 116 mmHg (102; 129) interquartile range (IQR) vs. 125 mmHg (109; 136) IQR, $p = 0.01$, e.g., a median of 72 mmHg (61; 79) IQR vs. 80 mmHg (69; 89) IQR, $p = 0.003$, respectively, after 20 s of microgravity in the seated posture (**Figure 1**). Furthermore, in the seated posture, cardiac output increased in 0 G as well as in hypergravity compared to steady flight values with a median of 6.9 l/min (6.5; 8.8) IQR vs. 6.8 l/min (6.2; 8.5) IQR, $p = 0.0002$, upon 20 s of weightlessness and of 7.3 l/min (6.5; 8.9) IQR, $p < 0.0001$ after 10 s of 1.8 G in the pull-out phase of the parabola, as shown in **Figure 1**. Interestingly, heart rate increased during phases of hypergravity up to median values of 87 bpm (74; 97) IQR after 15 s of hypergravity in the pull-up phase compared to steady flight values with a median of 73 bpm (63; 85) IQR, $p < 0.0001$, whereas heart rate returned to baseline levels with median values of 73 bpm (64; 84) IQR after 20 s of microgravity (**Figure 1**). Stroke volume decreased in microgravity, whereas systemic vascular resistance was unchanged in weightlessness in seated as well as in supine postures (data not shown).
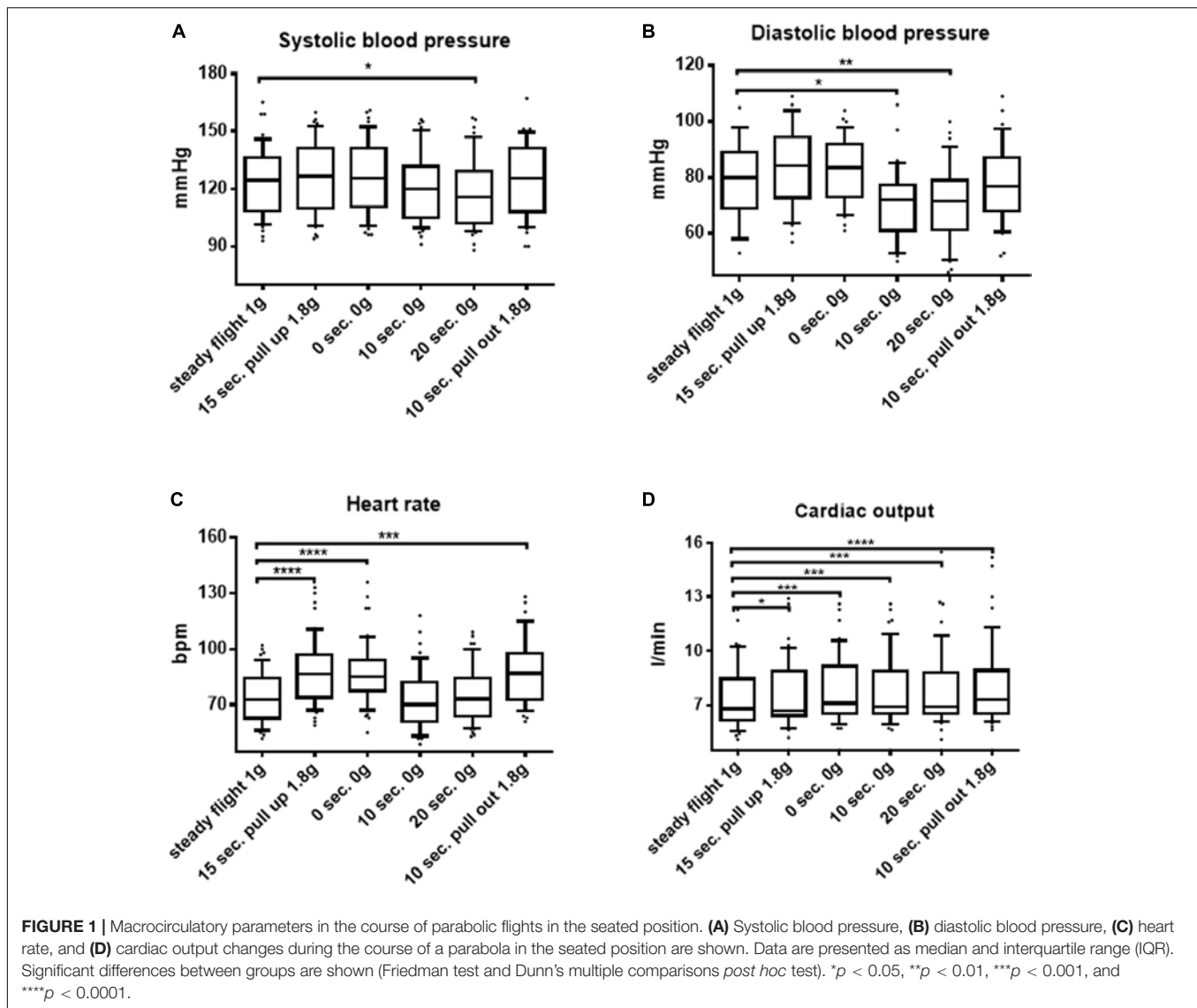
In contrast to the macrocirculatory changes observed in seated postures throughout the course of each parabola, in supine postures, no significant alterations regarding blood pressure, heart rate, or cardiac output could be observed, as shown in **Figure 2**.

Visualization and recording of high-quality imaging of the sublingual capillary network with a highly sensitive intravital sidestream dark field microscope connected to a tablet screen were feasible in microgravity and during steady flight phases. Despite the observed impact of parabolic flight maneuvers on the macrocirculation, on the level of microcirculation, no significant alterations could be detected in parabolic flight maneuvers in supine and seated postures, as shown in **Figure 3A**: PPV (%): 1 G

TABLE 1 | Baseline characteristics of the study population. Data are presented in counts or as median and IQR.

n	12
Sex	7 male, 5 female
Age (years)	29 [23–31]
Height (m)	1.77 [1.71–1.90]
Weight (kg)	80 [62–90]
BMI (kg/m^2)	24.5 [20–25]
BSA (m^2)	2 [1.72–2.13]
BP sys (mmHg)	110 [106–127]
BP mean (mmHg)	92 [87–94]
BP dia (mmHg)	78 [69–81]
HR (bpm)	79 [61–95]

BMI, body mass index; BSA, body surface area; BP, blood pressure, HR, heart rate; and IQR, interquartile range.
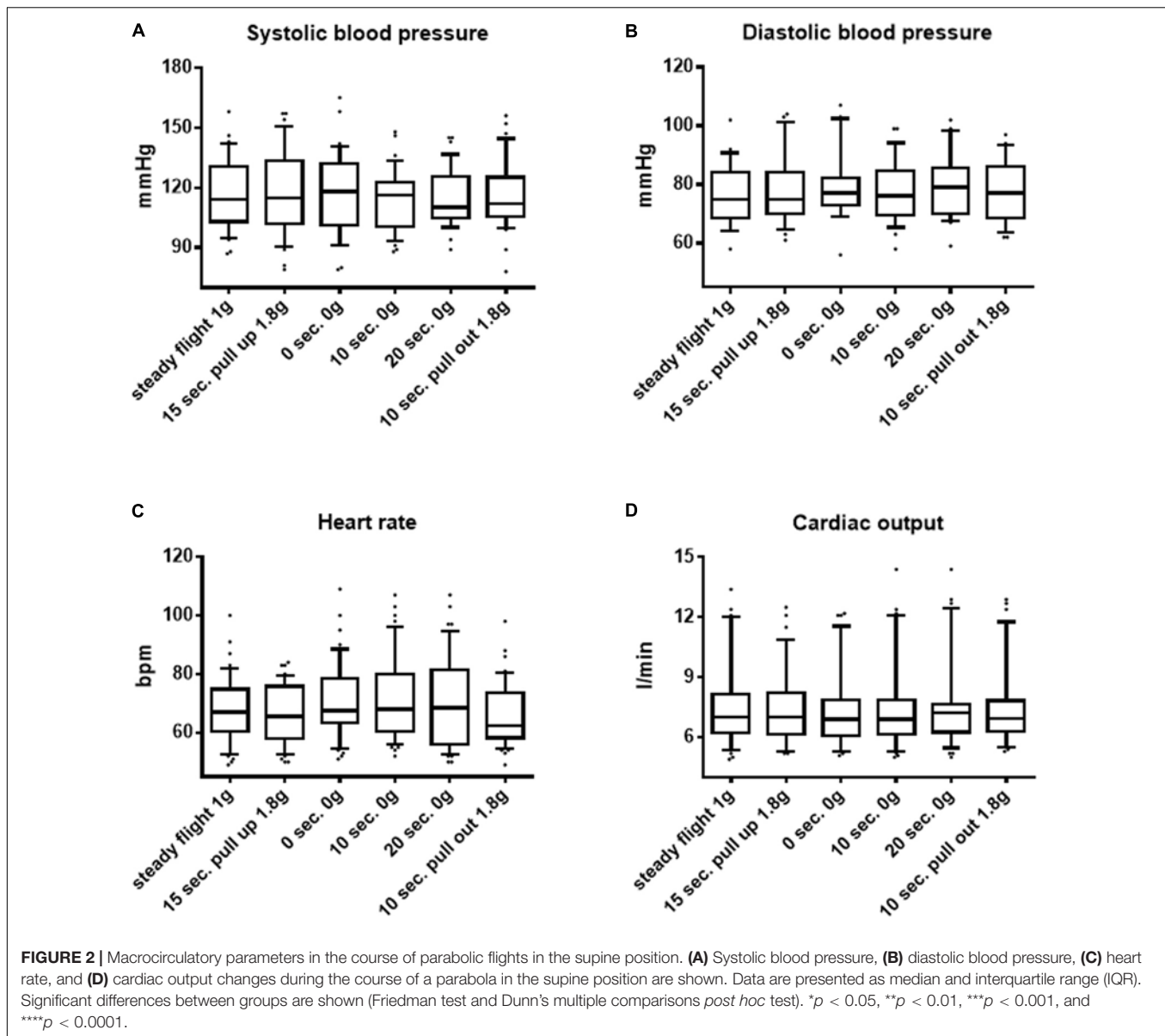
FIGURE 1 | Macrocirculatory parameters in the course of parabolic flights in the seated position. (A) Systolic blood pressure, (B) diastolic blood pressure, (C) heart rate, and (D) cardiac output changes during the course of a parabola in the seated position are shown. Data are presented as median and interquartile range (IQR). Significant differences between groups are shown (Friedman test and Dunn's multiple comparisons *post hoc* test). *$p < 0.05$, **$p < 0.01$, ***$p < 0.001$, and ****$p < 0.0001$.

supine [median of 93 (90; 97) IQR] vs. 0 G supine [96 (94; 100) IQR], $p = 0.07$; **Figure 3B**: PPV (%): 1 G seated [96 (92; 100) IQR] vs. 0 G seated [95 (90.5; 99.5) IQR], $p = 0.57$; **Figure 3C**: TVD: 1 G supine [7 (6; 9) IQR] vs. 0 G supine [7 (6; 10) IQR], $p = 0.92$; and **Figure 3D**: TVD: 1 G seated [8.1 (7; 9.35) IQR] vs. 0 G seated [8.2 (6.9; 8.7) IQR], $p = 0.63$.

DISCUSSION

The aims of the presented study were to investigate the impact of acute weightlessness as well as of acute hypergravity on macro-hemodynamic parameters and on the sublingual microcirculation in the setting of parabolic flight maneuvers as an established spaceflight analog (Shelhamer, 2016). Moreover, we were interested in learning more about responses of the cardiovascular system in seated postures in comparison to supine postures under these conditions. So far, gravitational loads have

had the most prominent effects on the cardiovascular system in upright postures. This is evident as in upright postures that the weight of the blood column is more prominent than in supine postures. Thus, upon microgravity exposure with abrupt loss of the effect of the blood column, more intense alterations are expected in upright postures due to abrupt loss of the weight of the blood column. On the other hand, for supine postures, with primarily abolished vertical weight of the blood column, even upon entrance into microgravity, effects would be anticipated to remain low. Bearing these thoughts in mind, we did not expect high alterations of cardiovascular parameters in supine postures.

As a novel approach, we implemented continuous beat-to-beat-analysis and visualization of the microcirculation with a handheld video microscope to monitor the sublingual microcirculation under these conditions. Prior works in the setting of septic and cardiogenic shock underlined the fact that, particularly in these life-threatening states with high
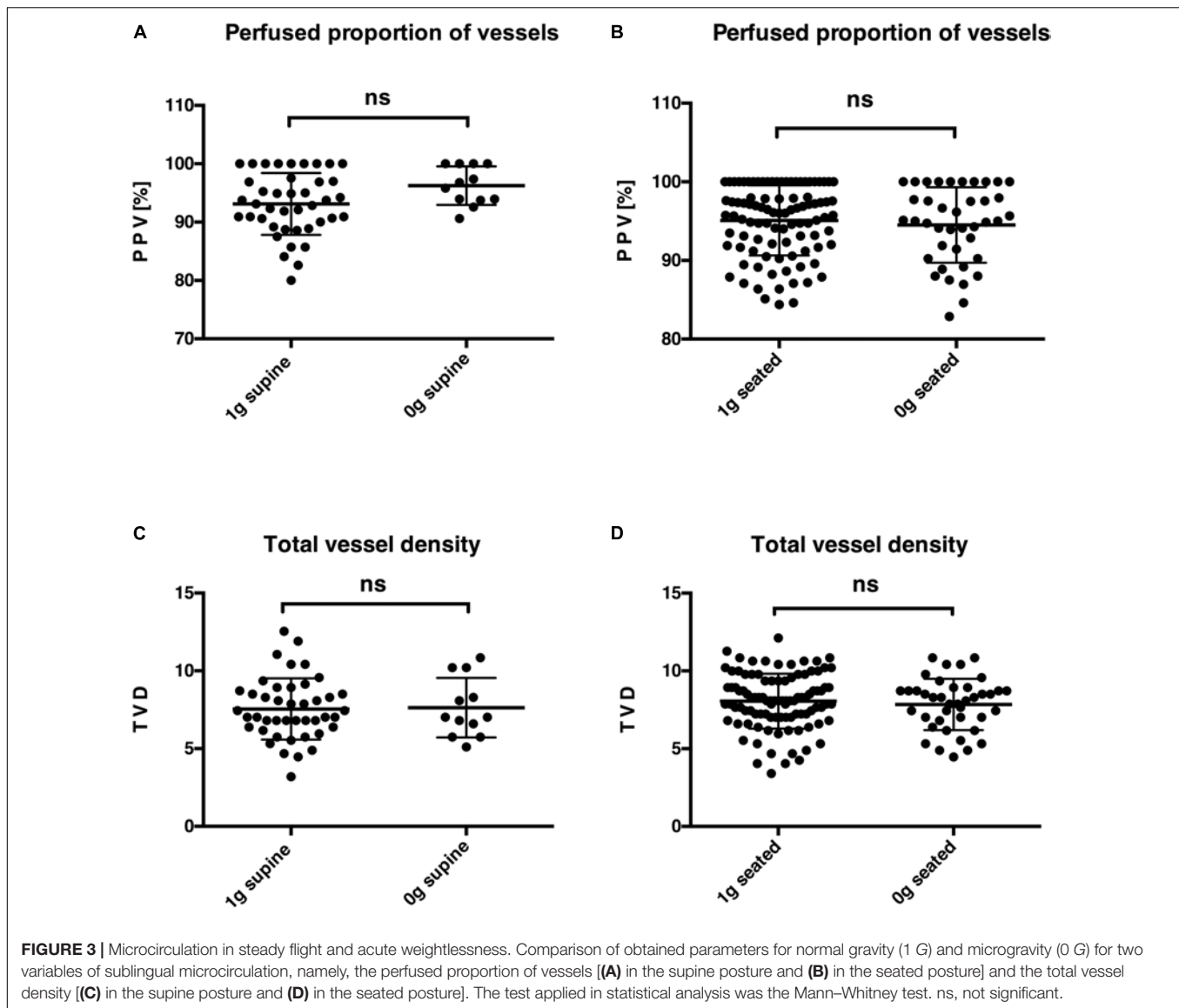
FIGURE 2 | Macrocirculatory parameters in the course of parabolic flights in the supine position. **(A)** Systolic blood pressure, **(B)** diastolic blood pressure, **(C)** heart rate, and **(D)** cardiac output changes during the course of a parabola in the supine position are shown. Data are presented as median and interquartile range (IQR). Significant differences between groups are shown (Friedman test and Dunn's multiple comparisons *post hoc* test). $*p < 0.05$, $**p < 0.01$, $***p < 0.001$, and $****p < 0.0001$.

mortality rates, assessment of the cardiovascular status can be challenging as tracked macrocirculatory parameters may seem stable enshrouding deleterious microcirculatory disorders causative for organ dysfunctions (Jung et al., 2016a; Jung, 2019; Legrand et al., 2019). The evaluation of microcirculation at the bedside has been esteemed highly important (Kara et al., 2016). In particular in these settings, the assessment of the sublingual microcirculation with handheld videos microscopes has proven feasible and reliable (De Backer and Dubois, 2001; Ince et al., 2018).

In our current experiment, we demonstrated that measurement of sublingual microcirculation using intravital sidestream dark field microscopy is feasible in microgravity. In line with prior studies, our work demonstrates that acute weightlessness significantly affects the cardiovascular system.

In our setting, significant alterations of macrocirculatory parameters such as blood pressure and cardiac output were evident in seated but not in supine postures, as anticipated. Interestingly, the microcirculation remained unchanged in the course of the parabolic flight maneuvers regardless of body posture.

For the acute setting, previous studies conducted during human space missions and spaceflight analogs on earth have reported inconsistent data regarding the changes of cardiovascular parameters under these conditions (Fritsch-Yelle et al., 1996; Petersen et al., 2011; Norsk, 2014; Klein et al., 2019). For instance, Klein et al. (2019) documented decreases of mean arterial pressures, whereas Norsk et al. (2006) constituted no changes of mean arterial pressures in the same setting. These discrepancies might be caused by the

FIGURE 3 | Microcirculation in steady flight and acute weightlessness. Comparison of obtained parameters for normal gravity (1 *G*) and microgravity (0 *G*) for two variables of sublingual microcirculation, namely, the perfused proportion of vessels [**(A)** in the supine posture and **(B)** in the seated posture] and the total vessel density [**(C)** in the supine posture and **(D)** in the seated posture]. The test applied in statistical analysis was the Mann–Whitney test. ns, not significant.

fact that blood pressure evaluation under baseline conditions in some studies was done in the standing or seated posture, whereas in other studies, blood pressure was measured in the supine posture. This might have affected on account of differing references. In our setting, baseline parameters for all variables were documented under normal gravity (1 G) and for both tested body positions (seated and supine) to ensure correct correlations to baseline references. Another reason for differing results for macrocirculatory parameters among diverse studies pertaining to short-term microgravity during parabolic flight maneuvers might be different techniques for blood pressure measurements. In our setting, hemodynamic variables were obtained by beat-to-beat analysis closely linked to a defined time line. Thus, great time resolutions could be provided. Our findings confirmed those of Verheyden et al. (2009) with decrease of blood pressures during space missions with more prominent effects for upright postures in

comparison to the effects measured in supine postures. However, these results contrast the findings of Norsk et al. in other studies that showed that blood pressure was unchanged in parabolic flight maneuvers (Norsk et al., 2006) but reduced during space missions (Norsk et al., 2015), even though Norsk (2020) performed their baseline measurements in supine postures as we did.

Another cardiovascular parameter we looked at is the heart rate. Here, we found an increase in heart rate during phases of hypergravity in seated but not in supine postures, whereas heart rate remained unchanged during phases of microgravity compared to baseline values. However, previous studies reported a decrease in heart rate in weightlessness (Fritsch-Yelle et al., 1996; Hughson, 2009). In our setting, these decreased heart rates might have been overridden on account of the rapid changes between hypergravity and microgravity in the course of repeated parabolic flight maneuvers. On the

other hand, the increase of heart rate we documented might have been reactive to diminution of peripheral resistance upon entrance into microgravity, accounting for the increase of cardiac output. Thus, heart rate might have primarily fueled the compensatory mechanism to counteract fluid shifts and blood pressure alterations. These findings are in line with findings of previous studies (Norsk et al., 2006, 2015) as we found an increase in cardiac output in acute weightlessness in seated postures compared to measurements performed in normal gravity. This increase in cardiac output is furthermore caused by increased central blood volume (Norsk et al., 2006, 2015) as previous echocardiographic studies showed a distension of the heart chambers in this process (Videbaek and Norsk, 1996; Pump et al., 1999; Caiani et al., 2009). Again, in supine postures, we could not detect any significant differences in cardiac output when comparing normal gravity, microgravity, and hypergravity.

In acute settings, possible discrepancies of macrocirculatory and microcirculatory measurements are known (Jung et al., 2009). Accordingly, in our study, despite observed significant consequences of altering gravitational loads on the parameters of macrocirculation, the sublingual microcirculation remained unchanged, regardless of body posture, or gravitational state. This investigation of the sublingual microcirculation is a novel approach as, to our knowledge, there are no data thereabout to date. However, previous studies looked at other circulatory networks of the human body. In the assessment of putative health risks for astronauts, visual impairment has been documented (Zhang and Hargens, 2014; Zhang and Hargens, 2018). Lawley et al. (2017) constituted that in prolonged stays in microgravity, slightly elevated intracranial pressures might be causative for remodeling of the eye but intracranial pressures were reduced in acute microgravity. Other studies about cerebral autoregulation showed that cerebral autoregulation and perfusion are not altered in weightlessness or head-down bed rest (Arbeille et al., 2001; Iwasaki et al., 2007). Thus, it is tempting to speculate that the human organism somewhat harbors safety mechanisms to counteract hemodynamically challenging scenarios such as weightlessness aiming at preserving steady organ perfusion to ensure nutrient and gas exchange. In this regard, localized vascular adaptations of the sublingual vascular beds might explain the stability of sublingual flow, even in microgravity. Possibly, pre-capillary sphincters and myogenic responses could contribute to this process. As previous studies have demonstrated, vasoactive hormones such as elevated aldosterone levels (Limper et al., 2014) might additionally contribute to vasoconstriction of arterioles. In contrast to our finding of unaltered microcirculation in the setting of acute weightlessness, a previous study by Coupé et al. (2009) indicated a microvascular dysfunction upon 56 days of head-down bed rest, as another spaceflight analog. In that study, as a marker of microcirculatory function, the endothelial dysfunction was measured, whereas our approach entailed direct visualization of the sublingual microcirculation with subsequent software-based calculation of microvasculatory parameters. Taking these differences into account, these studies might not be adequately comparable.

Certain limitations of our study have to be addressed: Parabolic flights have been known as established spaceflight analog for emulation of acute states of microgravity. However, as with other spaceflight analogs, there might be differences to prolonged states of microgravity during human space missions. In this regard, measurements of cardiovascular parameters over longer periods might differ from our measurements of acute alternating gravitational loads with rather short periods of weightlessness of a little more than 20 s per aviated parabola.

As motion sickness during the parabolic flight maneuvers has been a common side effect in former flight campaigns, application of scopolamine remains a strong recommendation for all flight participants. Frankly, there was no strong scientific justification for its use. On the other hand, in our pre-study experiment prior to the campaign, we could show that use of scopolamine does not interfere with our measurements of sublingual microcirculation (Bimpong-Buta et al., 2018b). However, one has to admit that other known effects of scopolamine, in particular on the cardiovascular system, might have altered our results. On the other hand, scopolamine has an elimination half-life of approximately 2 h (Stetina et al., 2005), which might have mitigated its subsequent effects on our measurements, as scopolamine was administered around 2 h prior to takeoff.

Another point is that one has to bear in mind that the sublingual microcirculation harbors tissue-specific responsiveness that does not necessarily represent all microcirculation of the human body, so that findings in this particular vascular bed cannot necessarily be transferred to all other vascular beds. However, as described earlier, in former studies, the microcirculation could serve as a reliable predictor of mortality outcomes and may gain further importance in future studies as a tool of improvement of therapeutic strategies, particularly for critically ill patients.

Finally, it should be noted that the CNAP monitor was calibrated multiple times in the course of our data acquisition, as mentioned above. Reasonable accuracy of its measurements has been proven (Wagner et al., 2015; Rogge et al., 2017). The intention of repeated calibrations was to ensure correct measurements throughout the experiment. However, possible impacts of macrocirculatory and microcirculatory changes on the accuracy of the instrument cannot be fully excluded.

CONCLUSION

In summary of our works, as a novel approach, we could demonstrate that the measurement of the sublingual microcirculation in microgravity induced by parabolic flight maneuvers is feasible. Our results underline the fact that profound alterations of the macrocirculatory hemodynamic parameters occur under these circumstances. In our setting, these alterations were most prominent in seated postures but not evident in supine postures, as could be anticipated with regard to known abolished weight of blood columns in supine postures. However, microcirculation remained stable in

acute weightlessness regardless of body posture, suggesting that localized and tissue-specific reactions in this vascular bed might be causative. For instance, it would be interesting to examine standing participants with a similar setting to investigate about possible effects of a more prominent blood column in standing postures. Here, we would expect more prominent results of the documented differences as the weight of the blood column in standing humans is again more than for seated postures.

Future studies on cardiovascular parameters seem warranted to learn more about physiologic circulatory response mechanisms under these conditions. This could be helpful for establishments of health safety strategies, as the good health of humans in space will remain a primary concern for upcoming commercial and scientific endeavors.

DATA AVAILABILITY STATEMENT

All datasets generated for this study are included in the article/**Supplementary Material**.

ETHICS STATEMENT

The studies involving human participants were reviewed and approved by Heinrich-Heine-University. The patients/ participants provided their written informed consent to participate in this study.

AUTHOR CONTRIBUTIONS

All authors listed have made a substantial, direct and intellectual contribution to the work, and approved it for publication.

FUNDING

ACKNOWLEDGMENTS

SUPPLEMENTARY MATERIAL

The Supplementary Material for this article can be found online at: https://www.frontiersin.org/articles/10.3389/fphys. 2020.00960/full#supplementary-material

FIGURE S1 | Macrocirculatory parameters in the course of parabolic flights: seated and supine positions in comparison. **(A)** Systolic blood pressure, **(B)** Diastolic blood pressure, **(C)** Heart Rate, and **(D)** Cardiac Output. As an overview here, the **Figures 1**, **2** have been combined, for easier apprehension of the outcomes of differing postures.

REFERENCES

Aratow, M., Hargens, A. R., Meyer, J. U., and Arnaud, S. B. (1991). Postural responses of head and foot cutaneous microvascular flow and their sensitivity to bed rest. *Aviat. Space Environ. Med.* 62, 246–251.

Arbeille, P., Fomina, G., Roumy, J., Alferova, I., Tobal, N., and Herault, S. (2001). Adaptation of the left heart, cerebral and femoral arteries, and jugular and femoral veins during short- and long-term head-down tilt and spaceflights. *Eur. J. Appl. Physiol.* 86, 157–168. doi: 10.1007/s004210100473

Baisch, J. F., Wolfram, G., Beck, L., Drummer, C., Stormer, I., Buckey, J., et al. (2000). Orthostatic stress is necessary to maintain the dynamic range of cardiovascular control in space. *Pflugers Arch.* 441, R52–R61.

Bimpong-Buta, N. Y., Jirak, P., Wernly, B., Lichtenauer, M., Knost, T., Abusamrah, T., et al. (2018a). Blood parameter analysis after short term exposure to weightlessness in parabolic flight. *Clin. Hemorheol. Microcirc* 70, 477–486. doi: 10.3233/ch-189314

Bimpong-Buta, N. Y., Jirak, P., Wernly, B., Lichtenauer, M., Masyuk, M., Muessig, J. M., et al. (2018b). Analysis of human microcirculation in weightlessness: study protocol and pre-study experiments. *Clin. Hemorheol. Microcirc.* 70, 119–127. doi: 10.3233/ch-170366

Blomqvist, C. G. (1983). Cardiovascular adaptation to weightlessness. *Med. Sci. Sports Exerc.* 15, 428–431.

Breit, G. A., Watenpaugh, D. E., Ballard, R. E., Murthy, G., and Hargens, A. R. (1993). Regional cutaneous microvascular flow responses during gravitational and LBNP stresses. *Physiologist* 36, S110–S111.

Buckey, J. C. Jr. (1999). Preparing for Mars: the physiologic and medical challenges. *Eur. J. Med. Res.* 4, 353–356.

Buckey, J. C. Jr., Lane, L. D., Levine, B. D., Watenpaugh, D. E., Wright, S. J., Moore, W. E., et al. (1996). Orthostatic intolerance after spaceflight. *J. Appl. Physiol.* 81, 7–18.

Buckey, J. C., Gaffney, F. A., Lane, L. D., Levine, B. D., Watenpaugh, D. E., and Blomqvist, C. G. (1993). Central venous pressure in space. *N. Engl. J. Med.* 328, 1853–1854.

Caiani, E. G., Weinert, L., Lang, R. M., and Vaida, P. (2009). The role of echocardiography in the assessment of cardiac function in weightlessness-Our experience during parabolic flights. *Respir. Physiol. Neurobiol.* 169(Suppl. 1), S6–S9.

Coupé, M., Fortrat, J. O., Larina, I., Gauquelin-Koch, G., Gharib, C., and Custaud, M. A. (2009). Cardiovascular deconditioning: from autonomic nervous system to microvascular dysfunctions. *Respir. Physiol. Neurobiol.* 169(Suppl. 1), S10–S12.

De Backer, D., and Dubois, M. J. (2001). Assessment of the microcirculatory flow in patients in the intensive care unit. *Curr. Opin. Crit. Care* 7, 200–203. doi: 10.1097/00075198-200106000-00010

De Backer, D., Hollenberg, S., Boerma, C., Goedhart, P., Buchele, G., Ospina-Tascon, G., et al. (2007). How to evaluate the microcirculation: report of a round table conference. *Critical Care* 11:R101.

De Backer, D., Orbegozo Cortes, D., Donadello, K., and Vincent, J. L. (2014). Pathophysiology of microcirculatory dysfunction and the pathogenesis of septic shock. *Virulence* 5, 73–79. doi: 10.4161/viru.26482

Demontis, G. C., Germani, M. M., Caiani, E. G., Barravecchia, I., Passino, C., and Angeloni, D. (2017). Human pathophysiological adaptations to the space environment. *Front. Physiol.* 8:547. doi: 10.3389/fphys.2017. 00547

Drummer, C., Gerzer, R., Baisch, F., and Heer, M. (2000). Body fluid regulation in micro-gravity differs from that on Earth: an overview. *Pflugers Arch.* 441, R66–R72.

Fritsch-Yelle, J. M., Charles, J. B., Jones, M. M., and Wood, M. L. (1996). Microgravity decreases heart rate and arterial pressure in humans. *J. Appl. Physiol.* 80, 910–914. doi: 10.1152/jappl.1996.80.3.910

Garrett-Bakelman, F. E., Darshi, M., Green, S. J., Gur, R. C., Lin, L., Macias, B. R., et al. (2019). The NASA twins study: a multidimensional analysis of a year-long human spaceflight. *Science* 364:eaau8650.

Gerber, B., Singh, J. L., Zhang, Y., and Liou, W. (2018). A computer simulation of short-term adaptations of cardiovascular hemodynamics in microgravity. *Comput. Biol. Med.* 102, 86–94. doi: 10.1016/j.compbiomed.2018.09.014

Hargens, A. R., and Richardson, S. (2009). Cardiovascular adaptations, fluid shifts, and countermeasures related to space flight. *Respir. Physiol. Neurobiol.* 169(Suppl. 1), S30–S33.

Hargens, A. R., Tipton, C. M., Gollnick, P. D., Mubarak, S. J., Tucker, B. J., and Akeson, W. H. (1983). Fluid shifts and muscle function in humans during acute simulated weightlessness. *J. Appl. Physiol. Respir. Environ. Exerc. Physiol.* 54, 1003–1009. doi: 10.1152/jappl.1983.54.4.1003

Hargens, A. R., and Vico, L. (2016). Long-duration bed rest as an analog to microgravity. *J. Appl. Physiol.* 120, 891–903. doi: 10.1152/japplphysiol.00935.2015

Hawkey, A. (2003). The physical price of a ticket into space. *J. Br. Interplanet. Soc.* 56, 152–159.

Hubbard, G. S., and Hargens, A. R. (1989). Sustaining humans in space. *Mech. Eng.* 111, 40–44.

Hughson, R. L. (2009). Recent findings in cardiovascular physiology with space travel. *Respir. Physiol. Neurobiol.* 169(Suppl. 1), S38–S41.

Ince, C. (2005). The microcirculation is the motor of sepsis. *Crit. Care* 9(Suppl. 4), S13–S19.

Ince, C., Boerma, E. C., Cecconi, M., De Backer, D., Shapiro, N. I., Duranteau, J., et al. (2018). Dynamics Section of the, Second consensus on the assessment of sublingual microcirculation in critically ill patients: results from a task force of the European Society of Intensive Care Medicine. *Intensive Care Med.* 44, 281–299. doi: 10.1007/s00134-018-5070-7

Iwasaki, K., Levine, B. D., Zhang, R., Zuckerman, J. H., Pawelczyk, J. A., Diedrich, A., et al. (2007). Human cerebral autoregulation before, during and after spaceflight. *J. Physiol.* 579, 799–810. doi: 10.1113/jphysiol.2006.119636

Jung, C. (2019). Assessment of microcirculation in cardiogenic shock. *Curr. Opin. Crit. Care* 25, 410–416. doi: 10.1097/mcc.0000000000000630

Jung, C., Ferrari, M., Rodiger, C., Fritzenwanger, M., Goebel, B., Lauten, A., et al. (2009). Evaluation of the sublingual microcirculation in cardiogenic shock. *Clin. Hemorheol. Microcirc.* 42, 141–148. doi: 10.3233/ch-2009-1194

Jung, C., Fritzenwanger, M., Lauten, A., Figulla, H. R., and Ferrari, M. (2010). [Evaluation of microcirculation in cardiogenic shock]. *Deutsche Medizinische Wochenschrift* 135, 80–83.

Jung, C., Jung, F., and Kelm, M. (2016a). The microcirculation in hypoxia: the center of the battlefield for oxygen. *Clin. Hemorheol. Microcirc.* 63, 169–172. doi: 10.3233/ch-1663301

Jung, C., Kelm, M., and Ferrari, M. (2016b). [Assessment of microcirculation in critically ill patients]. *Med. Klin. Intensivmed. Notfmed.* 111, 605–609.

Kara, A., Akin, S., and Ince, C. (2016). Monitoring microcirculation in critical illness. *Curr. Opin. Crit. Care* 22, 444–452. doi: 10.1097/mcc.0000000000000335

Kirsch, K. A., and Von Ameln, H. (1981). Current views and future programs in cardiovascular physiology in space. *Acta Astronaut.* 8, 939–950. doi: 10.1016/0094-5765(81)90064-3

Klein, T., Wollseiffen, P., Sanders, M., Claassen, J., Carnahan, H., Abeln, V., et al. (2019). The influence of microgravity on cerebral blood flow and electrocortical activity. *Exp. Brain Res.* 237, 1057–1062. doi: 10.1007/s00221-019-05490-6

Lawley, J. S., Petersen, L. G., Howden, E. J., Sarma, S., Cornwell, W. K., Zhang, R., et al. (2017). Effect of gravity and microgravity on intracranial pressure. *J. Physiol.* 595, 2115–2127. doi: 10.1113/jp273557

Leach, C. S., Alfrey, C. P., Suki, W. N., Leonard, J. I., Rambaut, P. C., Inners, L. D., et al. (1996). Regulation of body fluid compartments during short-term spaceflight. *J. Appl. Physiol.* 81, 105–116. doi: 10.1152/jappl.1996.81.1.105

Lee, S. M. C., Feiveson, A. H., Stein, S., Stenger, M. B., and Platts, S. H. (2015). Orthostatic intolerance after ISS and space shuttle missions. *Aerosp. Med. Hum. Perform.* 86, A54–A67.

Legrand, M., De Backer, D., Depret, F., and Ait-Oufella, H. (2019). Recruiting the microcirculation in septic shock. *Ann. Intensive Care* 9:102.

Limper, U., Gauger, P., Beck, P., Krainski, F., May, F., and Beck, L. E. (2014). Interactions of the human cardiopulmonary, hormonal and body fluid systems in parabolic flight. *Eur. J. Appl. Physiol.* 114, 1281–1295. doi: 10.1007/s00421-014-2856-3

Mairesse, O., MacDonald-Nethercott, E., Neu, D., Tellez, H. F., Dessy, E., Neyt, X., et al. (2019). Preparing for Mars: human sleep and performance during a 13 month stay in Antarctica. *Sleep* 42:zsy206.

Massey, M. J., and Shapiro, N. I. (2016). A guide to human in vivo microcirculatory flow image analysis. *Crit. Care* 20:35.

Moore, T. P., and Thornton, W. E. (1987). Space shuttle inflight and postflight fluid shifts measured by leg volume changes. *Aviat. Space Environ. Med.* 58, A91–A96.

Mukai, C. N., Lathers, C. M., Charles, J. B., Bennett, B. S., Igarashi, M., and Patel, S. (1991). Acute hemodynamic responses to weightlessness during parabolic flight. *J. Clin. Pharmacol.* 31, 993–1000. doi: 10.1002/j.1552-4604.1991.tb03662.x

Nicogossian, A. E., Charles, J. B., Bungo, M. W., Leach-Huntoon, C. S., and Nicgossian, A. E. (1991). Cardiovascular function in space flight. *Acta Astronaut.* 24, 323–328. doi: 10.1016/0094-5765(91)90181-4

Norsk, P. (2014). Blood pressure regulation IV: adaptive responses to weightlessness. *Eur. J. Appl. Physiol.* 114, 481–497. doi: 10.1007/s00421-013-2797-2

Norsk, P. (2020). Adaptation of the cardiovascular system to weightlessness: surprises, paradoxes and implications for deep space missions. *Acta Physiol.* 228:e13434. doi: 10.1111/apha.13434

Norsk, P., Asmar, A., Damgaard, M., and Christensen, N. J. (2015). Fluid shifts, vasodilatation and ambulatory blood pressure reduction during long duration spaceflight. *J. Physiol.* 593, 573–584. doi: 10.1113/jphysiol.2014.284869

Norsk, P., Damgaard, M., Petersen, L., Gybel, M., Pump, B., Gabrielsen, A., et al. (2006). Vasorelaxation in space. *Hypertension* 47, 69–73. doi: 10.1161/01.hyp.0000194332.98674.57

Petersen, L. G., Damgaard, M., Petersen, J. C., and Norsk, P. (2011). Mechanisms of increase in cardiac output during acute weightlessness in humans. *J. Appl. Physiol.* 111, 407–411. doi: 10.1152/japplphysiol.01188.2010

Pump, B., Videbaek, R., Gabrielsen, A., and Norsk, P. (1999). Arterial pressure in humans during weightlessness induced by parabolic flights. *J. Appl. Physiol.* 87, 928–932. doi: 10.1152/jappl.1999.87.3.928

Rogge, D. E., Nicklas, J. Y., Haas, S. A., Reuter, D. A., and Saugel, B. (2017). Continuous noninvasive arterial pressure monitoring using the vascular unloading technique p system) in obese patients during laparoscopic bariatric operations. *Anesth. Analg.* 126, 454–463. doi: 10.1213/ane.0000000000002660

Schlegel, T. T., Benavides, E. W., Barker, D. C., Brown, T. E., Harm, D. L., DeSilva, S. J., et al. (1998). Cardiovascular and Valsalva responses during parabolic flight. *J. Appl. Physiol.* 85, 1957–1965. doi: 10.1152/jappl.1998.85.5.1957

Shelhamer, M. (2016). Parabolic flight as a spaceflight analog. *J. Appl. Physiol.* 120, 1442–1448. doi: 10.1152/japplphysiol.01046.2015

Simanonok, K. E., and Charles, J. B. (1994). Space sickness and fluid shifts: a hypothesis. *J. Clin. Pharmacol.* 34, 652–663. doi: 10.1002/j.1552-4604.1994.tb02020.x

Smolle, K. H., Schmid, M., Prettenthaler, H., and Weger, C. (2015). The accuracy of the CNAP(R) device compared with invasive radial artery measurements for providing continuous noninvasive arterial blood pressure readings at a medical intensive care unit: a method-comparison Study. *Anesth. Analg.* 121, 1508–1516. doi: 10.1213/ane.0000000000000965

Stetina, P. M., Madai, B., Kulemann, V., Kirch, W., and Joukhadar, C. (2005). Pharmacokinetics of scopolamine in serum and subcutaneous adipose tissue in healthy volunteers. *Int. J. Clin. Pharmacol. Ther.* 43, 134–139. doi: 10.5414/cpp43134

Tipton, C. M., and Hargens, A. (1996). Physiological adaptations and countermeasures associated with long-duration spaceflights. *Med. Sci. Sports Exerc.* 28, 974–976. doi: 10.1097/00005768-199608000-00006

Verheyden, B., Liu, J., Beckers, F., and Aubert, A. E. (2009). Adaptation of heart rate and blood pressure to short and long duration space missions. *Respir. Physiol. Neurobiol.* 169(Suppl. 1), S13–S16.

Videbaek, R., and Norsk, P. (1996). Atrial distension in humans during weightlessness induced by parabolic flights. *J. Gravitational Physiol.* 3, 48–49.

Wagner, J. Y., Negulescu, I., Schofthaler, M., Hapfelmeier, A., Meidert, A. S., Huber, W., et al. (2015). Continuous noninvasive arterial pressure measurement using the volume clamp method: an evaluation of the CNAP device in intensive care

unit patients. *J. Clin. Monit. Comput.* 29, 807–813. doi: 10.1007/s10877-015-9670-2

White, R. J., and Blomqvist, C. G. (1998). Central venous pressure and cardiac function during spaceflight. *J. Appl. Physiol.* 85, 738–746. doi: 10.1152/jappl.1998.85.2.738

Zhang, L. F., and Hargens, A. R. (2014). Intraocular/Intracranial pressure mismatch hypothesis for visual impairment syndrome in space. *Aviat. Space Environ. Med.* 85, 78–80. doi: 10.3357/asem.3789.2014

Zhang, L. F., and Hargens, A. R. (2018). Spaceflight-induced intracranial hypertension and visual impairment: pathophysiology and countermeasures. *Physiol. Rev.* 98, 59–87. doi: 10.1152/physrev.00017.2016

Check for updates

Differential pacing: a traditional electrophysiological maneuver in a modern era

Konstantinos Iliodromitis[1] · Sebastian Robl[1] · Nana-Yaw Bimpong-Buta[1] · Harilaos Bogossian[1,2]

[1] Klinik für Kardiologie und Rhythmologie, Ev. Krankenhaus Hagen, Hagen, Germany

[2] Universität Witten/Herdecke, Witten, Germany

Case presentation

An 81-year old lady was referred to the authors' clinic for the interventional treatment of medically intractable, symptomatic persistent atrial fibrillation. A procedure with radiofrequency catheter ablation was scheduled. The three-dimensional (3D) electroanatomic system Rhythmia™ (Boston Scientific, Marlborough, MA, USA) was implemented and high-density electroanatomic voltage mapping of the left atrium (LA) was acquired.

The voltage map of the LA showed at index procedure extended scarring both in the anterior and posterior wall with severe fractionated potentials. Bilateral wide antral circumferential ablation (WACA) of the pulmonary vein (PV) antra followed. After first pass ablation, a diagnostic multipolar basket catheter (Orion™, Boston Scientific) was positioned inside each PV and control for bidirectional electrical block was performed. Three of four PVs were effectively electrically isolated. After positioning the mapping catheter inside the left superior pulmonary vein (LSPV) and the ablation catheter inside the left atrial appendage (LAA), the intracardiac electrograms of ◘ **Fig. 1** were acquired.

Question

Which of following statements is correct:
1. The LSPV is electrically isolated. The EP tracings show far field signals from the LAA.
2. The LSPV is not electrically isolated. The EP tracings show only PV signal on the mapping catheter.
3. The LSPV is not electrically isolated. The EP tracings show both far field and PV signals on the mapping catheter.

Scan QR code & read article online
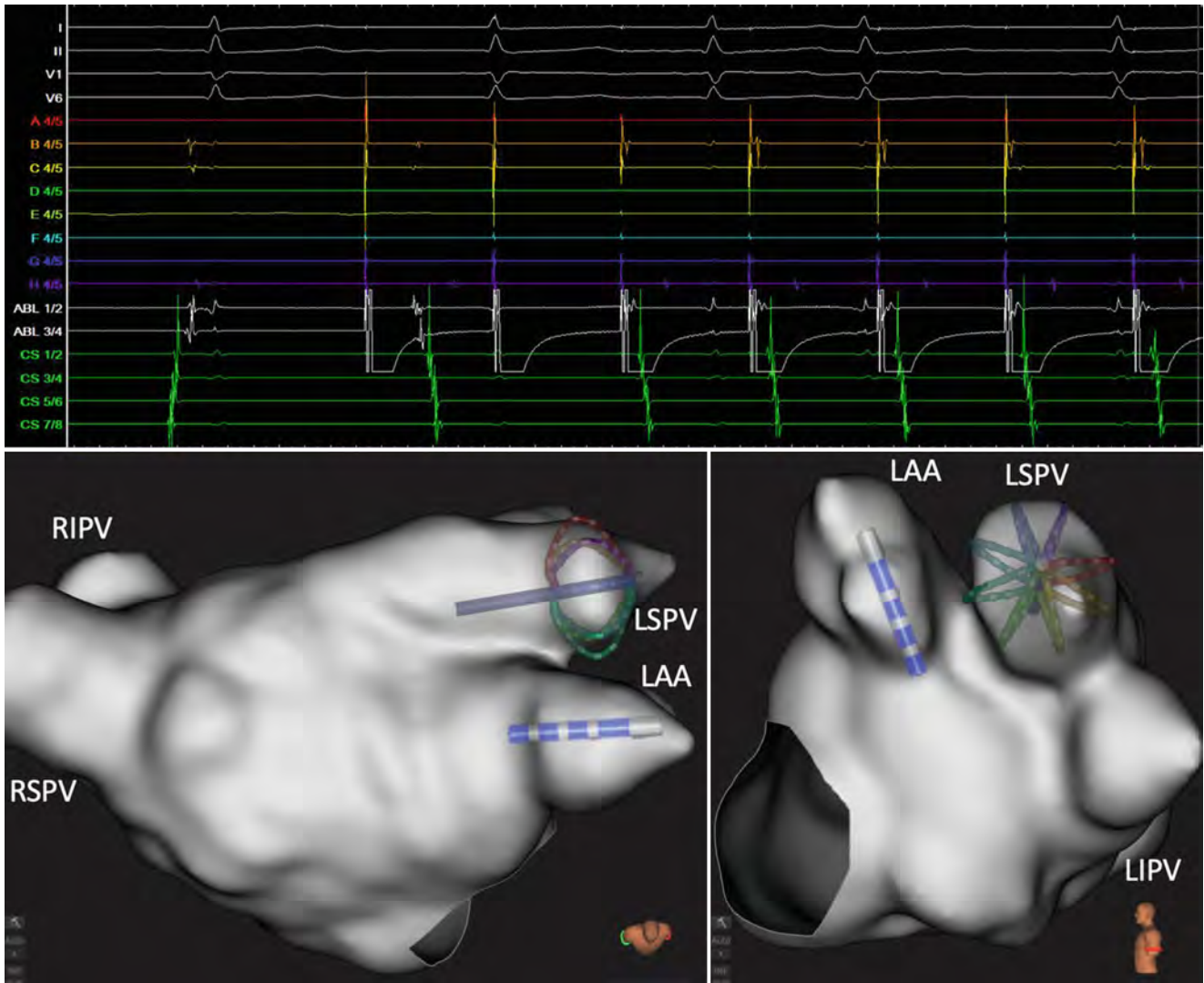
Fig. 1 ▲ *Upper panel*: Recordings from the surface electrocardiogram and intracardiac recordings from the Orion™ multipolar mapping catheter ($A^{4/5}$–$H^{4/5}$), the ablation catheter ($ABL^{1/2}$–$ABL^{3/4}$) and the coronary sinus catheter ($CS^{1/2}$–$CS^{9/10}$). *Lower panel*: Three-dimensional electroanatomical mapping of the left atrium (LA) from the superior and left lateral view and schematic presentation of intracardiac signals (*ABL* ablation catheter, *CS* coronary sinus, *LA* left atrium)
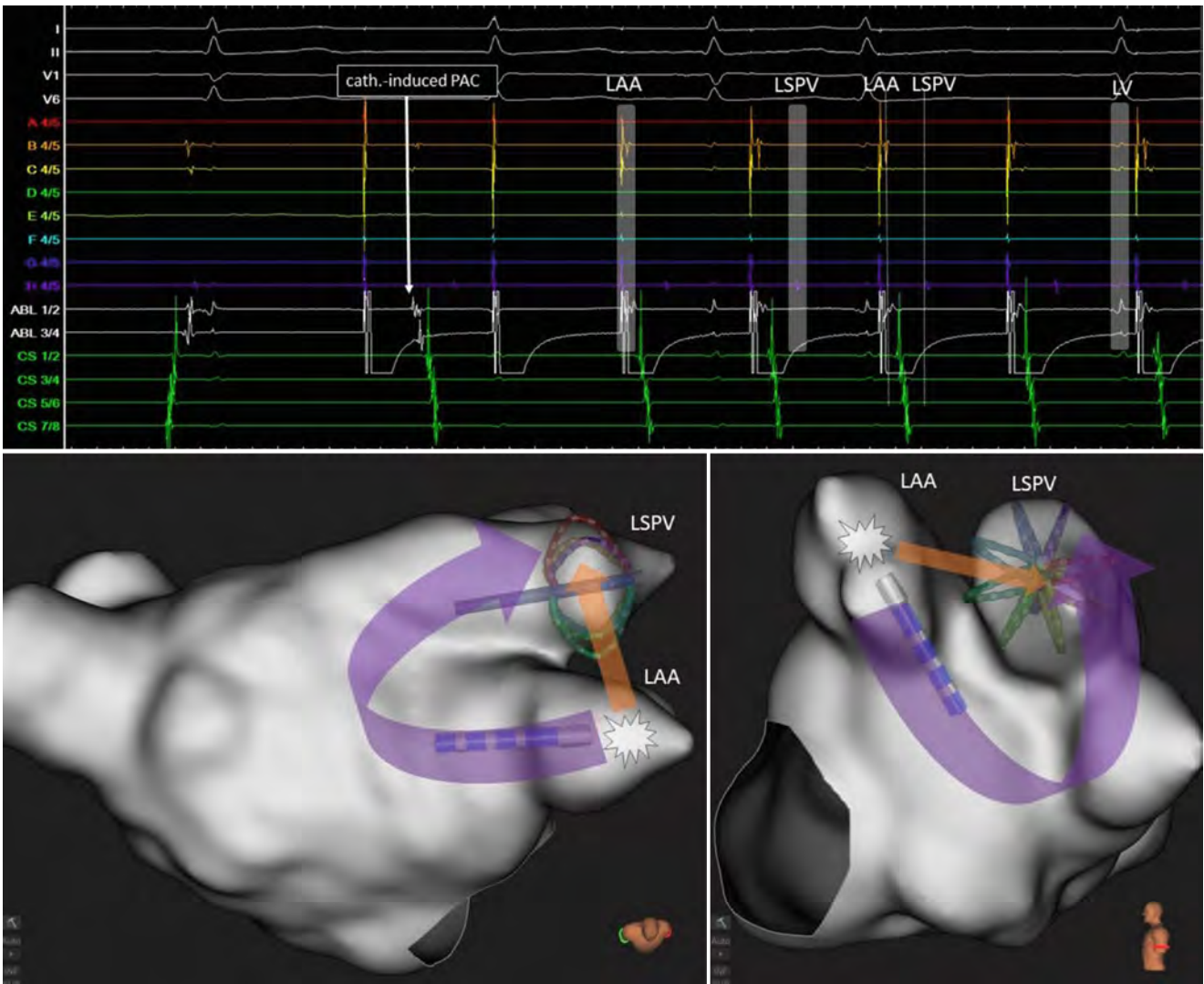
Fig. 2 ▲ *Upper panel*: Recordings from the surface electrocardiogram and intracardiac recordings from the Orion™ multipolar mapping catheter ($A^{4/5}$–$H^{4/5}$), the ablation catheter ($ABL^{1/2}$–$ABL^{3/4}$) and the coronary sinus catheter ($CS^{1/2}$–$CS^{9/10}$). *Lower panel*: Three-dimensional electroanatomical mapping of the left atrium (LA) from the superior and left lateral view and schematic presentation of intracardiac signals (*ABL* ablation catheter, *CS* coronary sinus, *LA* left atrium)

Correct answer: 3

Discussion

Differential pacing is a "traditional" electrophysiological maneuver, offering valuable information for understanding and differentiating the origin of recorded electrical intracardiac signals during an electrophysiological study. It is also a very useful tool for confirming durable electrical conduction block in the ablated areas of any heart chamber [1, 2]. Despite the currently available high density mapping systems with sophisticated signal filters and algorithms, differentiation between far field signals and true local signals often remains challenging. Such cases require additional confirmation from "traditional" electrophysiology, proving that "old" maneuvers are still necessary in the modern era.

In the present case, stimulation from the LAA was performed and three signals with different timings were recorded on the Orion™ catheter. The first electrical potential (LAA) is indeed the stimulation far field signal from the LAA sensed from the positioned mapping catheter in the LSPV. The second electrical potential (LSPV) that is clearly recorded on the $H^{4/5}$ pole of the Orion™ catheter is the local PV potential of a non-isolated LSPV. Note the significant timing difference between the LAA and LSPV potentials recorded on the splines of the Orion™ catheter (◻ **Fig. 2**). The third potential (LV) is indeed the far field signal from the left ventricle (LV), as the recorded timings are isochronal with LV far field signals of the catheter in the coronary sinus (CS) and the QRS complex of the surface ECG.

Additional radiofrequency lesions on the roof of the left atrium—upper WACA area—resulted in successful isolation of the LSPV.

Conclusion

Differential pacing from the PVs and the LAA is a very useful classical electrophysiological maneuver and is helpful for the confirmation of successful pulmonary vein isolation.

Corresponding address

PD Dr. Harilaos Bogossian
Klinik für Kardiologie und Rhythmologie, Ev. Krankenhaus Hagen
Brusebrinkstraße 20, 58135 Hagen, Germany
bogossian@evk-haspe.de

Declarations

References

1. Macle L, Weerasooriya R, Scavee C, Jais P (2009) Pulmonary vein recordings. A practical guide to the mapping and ablation of atrial fibrillation, 2nd edn. Cardiotext, Minneapolis
2. Huang SKS, Miller JM (2014) Catheter ablation of cardiac arrhythmias, 3rd edn. Saunders, Philadelphia

Article

Dynamic Changes of Heart Failure Biomarkers in Response to Parabolic Flight

Peter Jirak [1], **Bernhard Wernly** [1], **Michael Lichtenauer** [1], **Vera Paar** [1], **Marcus Franz** [2],
Thorben Knost [3], **Thaer Abusamrah** [3], **Malte Kelm** [3], **Johanna M. Muessig** [3],
Nana-Yaw Bimpong-Buta [4] **and Christian Jung** [3,*]

[1]   Department of Internal Medicine II, Division of Cardiology, Paracelsus Medical University of Salzburg,
      5020 Salzburg, Austria; p.jirak@salk.at (P.J.); b.wernly@salk.at (B.W.); m.lichtenauer@salk.at (M.L.);
      v.paar@salk.at (V.P.)
[2]   Department of Internal Medicine I, Jena University Hospital, Friedrich Schiller University Jena,
      07743 Jena, Germany; Marcus.Franz@med.uni-jena.de
[3]   Division of Cardiology, Pulmonology, and Vascular Medicine, Medical Faculty, University Duesseldorf,
      40225 Duesseldorf, Germany; Thorben.Knost@med.uni-duesseldorf.de (T.K.);
      Thaer.Abusamrah@med.uni-duesseldorf.de (T.A.); Malte.Kelm@med.uni-duesseldorf.de (M.K.);
      Johanna.Muessig@med.uni-duesseldorf.de (J.M.M.)
[4]   Division of Cardiology and Rhythmology, Evangelical Hospital Hagen-Haspe, 58135 Hagen, Germany;
      nanaybbb@yahoo.com
*   Correspondence: Christian.Jung@med.uni-duesseldorf.de; Tel.: +49-211-81-18800

check for
updates

Abstract: Background: we aimed at investigating the influence of weightlessness and hypergravity by means of parabolic flight on the levels of the heart failure biomarkers H-FABP, sST2, IL-33, GDF-15, suPAR and Fetuin-A. Methods: 14 healthy volunteers (males: eight; mean age: 28.9) undergoing 31 short-term phases of weightlessness and hypergravity were included. At different time points (baseline, 1 h/24 h after parabolic flight), venous blood was drawn and analyzed by the use of ELISA. Results: sST2 evidenced a significant decrease 24 h after parabolic flight (baseline vs. 24, $p = 0.009$; 1 h vs. 24 h, $p = 0.004$). A similar finding was observed for GDF-15 (baseline vs. 24 h, $p = 0.002$; 1 h vs. 24 h, $p = 0.025$). The suPAR showed a significant decrease 24 h after parabolic flight (baseline vs. 24 h, $p = 0.1726$; 1 h vs. 24 h, $p = 0.009$). Fetuin-A showed a significant increase at 1 h and 24 h after parabolic flight (baseline vs. 24 h, $p = 0.007$; 1 h vs. 24 h, $p = 0.04$). H-FABP and IL-33 showed no significant differences at all time points. Conclusion: Our results suggest a reduction in cardiac stress induced by exposure to gravitational changes. Moreover, our findings indicate an influence of gravitational changes on proliferative processes and calcium homeostasis.

Keywords: space medicine; parabolic flight; microgravity; weightlessness; biomarkers; heart failure

1. Introduction

Human space missions have experienced a revival in recent years. While the National Aeronautics and Space Administration (NASA) aims for a manned mission to Mars in co-operation with other space agencies, suborbital commercial space flights are about to enter the private sector. Given the expected rise in manned space flights, space medicine is gaining major importance as a necessity for safe and successful missions in the future [1].

In the absence of gravity, the human body undergoes multiple adaptational processes, which have been analyzed in previous studies [2]. Above all, changes in the cardiovascular system have been reported [3]. Cardiovascular causes are involved in the majority of medical complications in human space missions and represent an important target in space medicine [3,4]. In this regard, the most

significant change is an increase in cardiac output of up to 40% in microgravity [3,5]. In consequence, a change in the baroreceptor reflex as well as in organ blood supply and a dysregulation of the cerebrovascular system can be observed in weightlessness [3,6]. However, it remains unclear if the increase in perfusion compensates for a higher metabolic demand in weightlessness or if the peripheral resistance is too low for the human heart in microgravity conditions [7]. Given the observed adaptational changes in the heart, recent studies also speculate about the possibility of a reduction in cardiac performance due to the deconditioning and restructuring of the heart, thus inducing heart failure and, in consequence, potential arrhythmias [8]. In addition to these changes, long-term exposure to weightlessness was reported to cause a dysregulation of the immune system and an alteration of the microbiome, leading to the increased virulence of pathogens in weightlessness [7]. Furthermore, atrophic processes in bones and muscles are frequent findings after long-term exposure to weightlessness [9]. A recent investigation of our study group also observed a decrease in hemoglobin and an increase in the glomerular filtration rate (GFR) [10]. However, while the changes mentioned above have been described and analyzed extensively by numerous studies, further investigations of the molecular background of these processes remain scarce.

Cardiac biomarkers have been studied extensively over recent years and represent novel and promising diagnostic tools in the assessment of cardiovascular disease entities. Especially in heart failure, biomarkers have been proven to have great potential regarding diagnosis and prognosis. In this context, a multimarker approach was reported as most effective due to the incorporation of different pathophysiological processes relevant to the cardiovascular system [11]. Among them, the heart-type fatty acid binding protein (H-FABP—myocardial ischemia), soluble suppression of tumorigenicity 2 (sST-2—myocardial strain/stress and inflammation) and its ligand interleukin-33 (IL-33—inflammation), growth differentiation factor-15 (GDF-15—inflammation, remodelling), soluble urokinase-type plasminogen activator receptor (suPAR—inflammation, remodelling) and Fetuin-A (vascular calcification) have shown promising results in prior studies and have also found clinical application in the treatment of heart failure and cardiovascular disease [12–16].

Accordingly, given the lack of information on the molecular background of physiologic changes in response to weightlessness, we sought to perform a head-to-head analysis of these six heart failure biomarkers in humans undergoing parabolic flight as a spaceflight analogue. Thereby, we aimed to better understand the molecular mechanisms and cardiac involvement in these adaptational processes and thus enlighten the topic of weightlessness-induced heart failure.

2. Results

In total, this study included 14 healthy volunteers (eight males) with a mean age of 28.9 years. The detailed baseline characteristics for all 14 volunteers are presented in Table 1.

Table 1. Baseline characteristics.

n	Sex	Age (y)	Height (m)	Weight (kg)	BMI (kg/m^2)	BSA (m^2)	BP Systolic (mmHg)	BP Mean (mmHg)	BP Diastolic (mmHg)	Heart Rate (bpm)
1	M	40	1.76	93	30	2.13	128	91	69	77
2	F	30	1.62	52	20	1.52	96	87	67	78
3	M	22	1.88	86	24	2.11	131	94	78	103
4	M	28	1.83	83	25	2.05	103	84	70	95
5	M	23	1.93	92	25	2.22	111	93	82	51
6	M	29	1.91	82	22	2.08	107	97	79	58
7	F	23	1.64	54	20	1.56	109	102	95	95
8	F	25	1.72	75	25	1.89	109	92	77	69
9	F	30	1.70	62	21	1.71	112	90	80	80
10	M	31	1.77	78	25	1.95	106	87	76	55
11	F	24	1.73	63	21	1.74	124	94	81	82
12	M	37	1.92	91	25	2.20	128	83	54	107

n	Sex	Age (y)	Height (m)	Weight (kg)	BMI (kg/m^2)	BSA (m^2)	BP Systolic (mmHg)	BP Mean (mmHg)	BP Diastolic (mmHg)	Heart Rate (bpm)
13	M	31	1.82	86	26	2.10	126	99	86	87
14	F	31	1.79	76	24	1.90	108	85	73	78
Mean	**m = 8**	**28.9**	**1.79**	**76.6**	**23.8**	**1.9**	**114.1**	**91.3**	**76.2**	**79.6**

2.1. Biomarker Levels

2.1.1. sST2

The serum levels of sST2 remained unchanged 1 h after parabolic flight (2672 pg/mL; SEM 276 pg/mL) compared to the baseline levels (2800 pg/mL; SEM 380 pg/mL, p = 0.760). By 24 h after parabolic flight (2050 pg/mL; SEM 199 pg/mL), a significant decrease in sST2 was found compared to the values at baseline and at 1 h after parabolic flight (p = 0.009 and p = 0.004, respectively; see Figure 1). This finding was consistent in the fold change analysis (baseline vs. 1 h, p = 1.0; baseline vs. 24 h, p = 0.0085; 1 h vs. 24 h, p = 0.006. See Figure 2).

2.1.2. IL-33

The serum levels of IL-33 were 545 pg/mL (SEM 392.0 pg/mL) at baseline, 521 pg/mL (SEM 396.0 pg/mL) after 1 h and 561 pg/mL (SEM 419.0 pg/mL) after 24 h. There were no significant differences between the respective timepoints (baseline vs. 1 h, p = 1.0; baseline vs. 24 h, p = 0.6875; 1 h vs. 24 h, p = 0.3750. See Figure 1). This finding was also consistent in the fold change analysis (baseline vs. 1 h, p = 1.0; baseline vs. 24 h, p = 0.3750; 1 h vs. 24 h, p = 0.1563. See Figure 2).

2.1.3. H-FABP

The H-FABP levels remained without any significant changes and were 23,000 pg/mL (SEM 7000 pg/mL) at baseline, 25,000 pg/mL (SEM 9000) at one hour and 15,000 ng/mL (SEM 8000 ng/mL) at 24 h after parabolic flight (baseline vs. 1 h, p = 0.625; baseline vs. 24 h, p = 0.3223; 1 h vs. 24 h, p = 0.0977. See Figure 1). This finding was also consistent in the fold change analysis (baseline vs. 1 h, p = 0.1094; baseline vs. 24 h, p = 0.2188; 1 h vs. 24 h, p = 0.0547. See Figure 2).

2.1.4. GDF-15

The GDF-15 levels were 385 pg/mL (SEM 51 pg/mL) at baseline and remained without significant changes 1 h after parabolic flight (389 pg/mL; SEM 45 pg/mL, p = 0.9515). At 24 h after parabolic flight (301 pg/mL; SEM 36 pg/mL), a significant decrease was evident (baseline vs. 24 h, p = 0.002; 1 h vs. 24 h, p = 0.025. See Figure 1). Similar findings were evident in the fold change analysis (baseline vs. 1 h, p= 0.8552; baseline vs. 24 h, p = 0.0085; 1 h vs. 24 h, p = 0.0031. See Figure 2).

2.1.5. suPAR

The suPAR levels did not evidence significant changes one hour after parabolic flight compared to the baseline values (1552 pg/mL; SEM 97 pg/mL and 1658 pg/mL; SEM 94 pg/mL, p = 0.1099). The levels at 24 h after parabolic flight were significantly decreased (1415 pg/mL; SEM 107 pg/mL, p = 0.009)) compared to the values at 1 h, while no significant changes were apparent compared to the baseline values (p = 0.1726; see Figure 1). This finding was also consistent in the fold change analysis (baseline vs. 1 h, p = 0.1272; baseline vs. 24 h, p = 0.1531; 1 h vs. 24 h, p = 0.004. See Figure 2).

2.1.6. Fetuin-A

The Fetuin-A levels were 173 µg/mL (SEM 18 µg/mL) at baseline without a significant change at one hour after parabolic flight (297 µg/mL; SEM 55 µg/mL, p = 0.3). By 24 h after parabolic flight,

a significant increase in Fetuin-A was evident compared to the levels at baseline (473 μg/mL; SEM 68 μg/mL, $p = 0.007$) and the levels at one hour after parabolic flight ($p = 0.04$; see Figure 1). Likewise, the fold change analysis evidenced a significant increase in Fetuin-A levels at 24 h after parabolic flight compared to the levels at baseline and 1 h (baseline vs. 1 h, $p = 0.1937$; baseline vs. 24 h, $p = 0.0052$; 1 h vs. 24 h, $p = 0.0419$. See Figure 2).
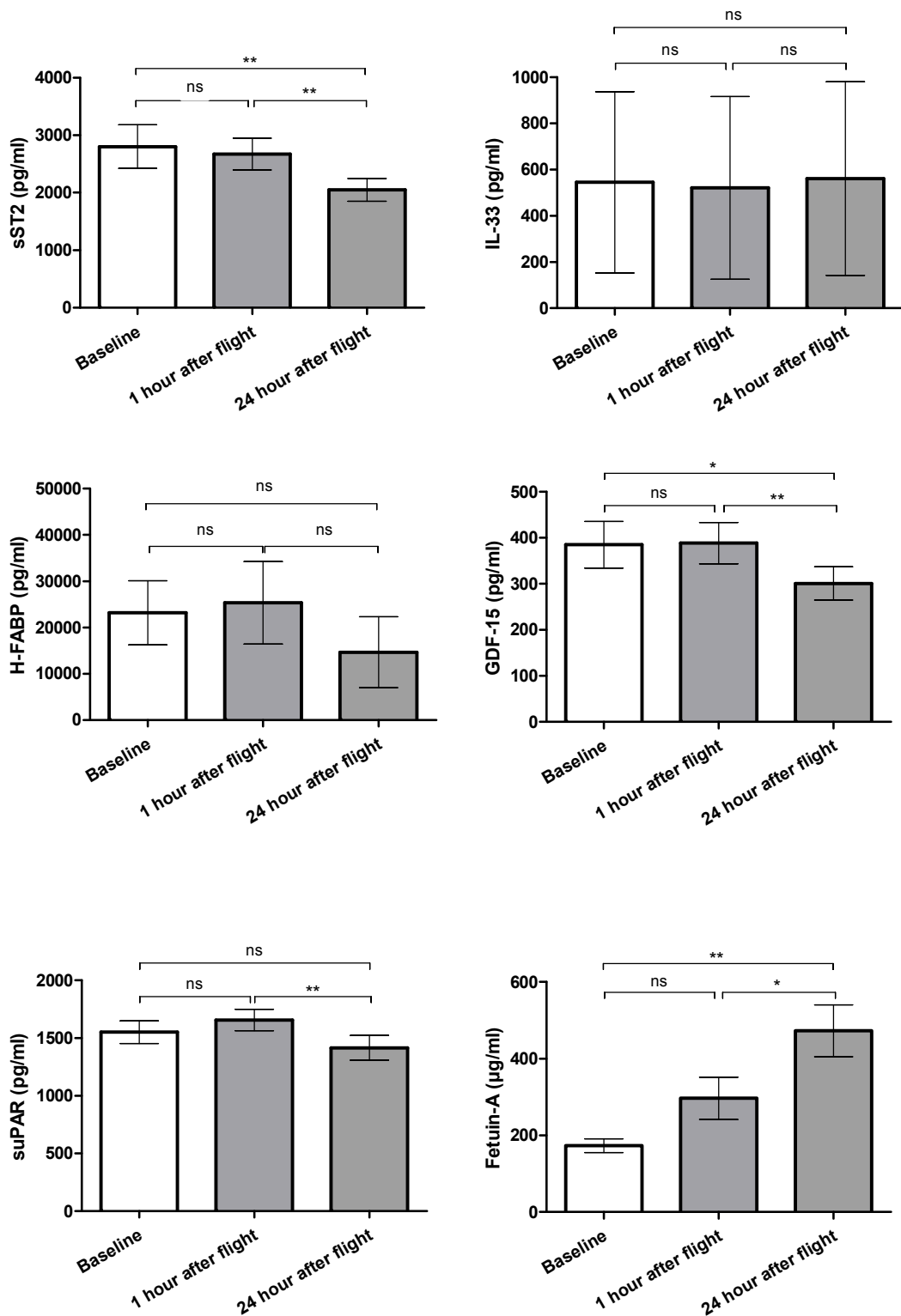
Figure 1. Comparison of biomarker levels at baseline/1 h after/24 h after parabolic flight (ns = not significant, * $p < 0.05$, ** $p < 0.01$).
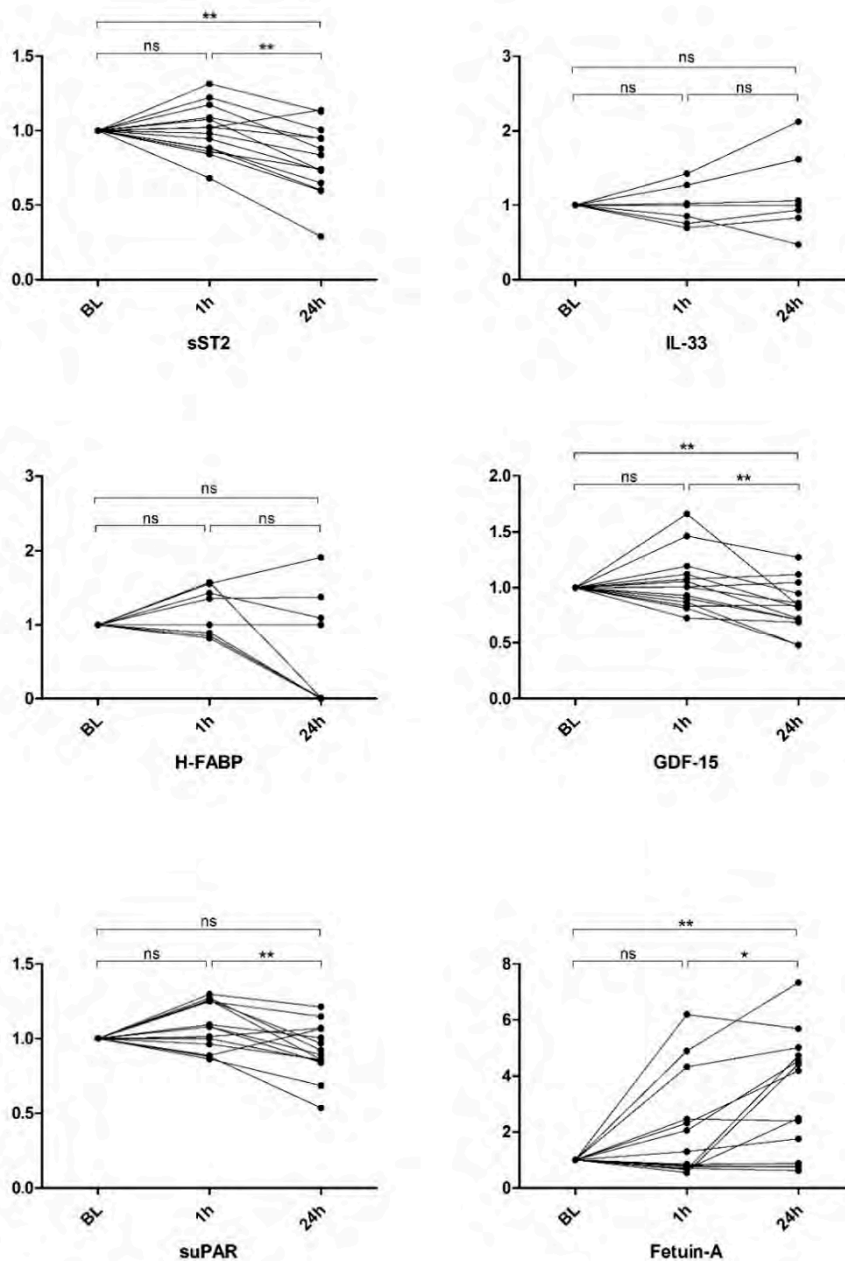
Figure 2. Fold change analysis of biomarkers at 1 h after/24 h after parabolic flight (ns = not significant, * *p* < 0.05, ** *p* <0.01).

2.2. Correlation Analysis

In a correlation analysis regarding the baseline characteristics, we found no relevant correlations between the biomarker expression and baseline characteristics. Likewise, the correlation of biomarker expression and laboratory parameters shown in the supplemental table showed no consistent correlations over all three time points. Of note, the GDF-15 levels (*p* = 0.03) and sST2 levels (*p* = 0.007) were associated with higher CRP levels at baseline. Additionally, myoglobin showed a significant correlation with the IL-33 levels (*p* = 0.025) and H-FABP levels (*p* = 0.01) at 24 h. A detailed correlation analysis is given in Table S1. There were no significant differences between male and female volunteers regarding the biomarker levels and laboratory parameters (Table S2).

3. Discussion

3. Discussion

Along with a growing focus on human space missions, space medicine as a prerequisite for safe and successful missions has gained significant awareness in recent years [3]. While different adaptational processes have been reported by numerous studies, cardiovascular complications still constitute the most important issues encountered during space travel [3,9]. The latest studies have also reported a potential deconditioning and restructuring of the heart, leading to heart failure [8]. However, the molecular mechanisms behind these findings remain largely unknown, thus giving rise to further investigations. Accordingly, to further analyze these adaptational processes and to address the topic of weightlessness-induced heart failure, we aimed for an analysis of heart failure biomarkers in response to parabolic flight as a spaceflight analogue.

Regarding the levels of sST2, we found a significant decrease 24 h after parabolic flight, while no changes were observed one hour after parabolic flight. While the membrane-bound ST2L receptor mediates cardioprotection by the binding of IL -33, sST2 acts as a decoy receptor for IL-33, thus preventing its (beneficial) effects [12]. Additionally, the correlation of the baseline levels of sST2 and CRP points out its suspected involvement in inflammatory processes [12]. sST2 is associated with increased cardiac strain and cardiac fibrosis and is elevated in clinical scenarios of heart failure and acute coronary syndrome [17]. Vice versa, the decrease in sST2 observed in our study could constitute an indicator of a reduction in cardiac stress and strain [12]. Our findings match at least in part former studies that speculate about an influence of microgravity on cardiac stress and cardiac strain. Among others, Iskovitz et al. reported a reduction in cardiac stress in microgravity, while the left ventricular strain distributions where not significantly different in different gravitational fields [8]. Additionally, an increase in left atrial and left ventricular volume was reported [18]. Together with an increase in cardiac output of up to 40% in zero gravity, as reported in former studies, a reduction in cardiac stress may seem contradictory [19]. However, cardioprotective effects, such as a reduction in heart rate as well as a decrease in peripheral vascular resistance, have been observed in weightlessness, similar to the therapeutic effects of heart failure treatment in the clinical setting [19]. Accordingly, these effects seem to surpass the cardiac stress induced by the increased pre-load volume in zero gravity. However, a recent study proposed a decrease in cardiac performance by means of the deconditioning and restructuring of the heart in response to the reduction in cardiac stress [8].

Interestingly, no significant changes were observed regarding the levels of IL-33 in our study. However, a trend towards higher levels was evident 24 h after parabolic flight. Considering that IL-33 represents the only known ligand for the ST2-receptor, an IL-33-independent effect induced by sST2 seems unlikely [20]. Accordingly, a delay in the increase in IL-33 in response to the decrease in its decoy receptor seems the most probable explanation for the lack of dynamic in IL-33. This is mainly attributed to the small time period in which the biomarker measurements were conducted.

Besides its cardioprotective effects, IL-33 is involved in numerous immunologic processes. It is responsible for immunomodulation, influencing the secretion and interaction of a range of immune defense cells, particularly T helper 2 (TH2) cells, mast cells, group 2 innate lymphoid cells, (ILC2s), regulatory T (Treg) cells, TH1 cells, CD8+ T cells and natural killer (NK) cells [21,22]. However, the interaction between these cell types and the role of IL-33 is not fully understood yet. Nevertheless, given the immunomodulatory role of IL-33, a decrease in sST2 might also be involved in the alterations of the immune system in weightlessness described in previous studies [23]. An essential role of IL-33 in allergic diseases, such as bronchial asthma and atopic dermatitis, further highlights the immunomodulatory effects of IL-33 and thus also of weightlessness [22]. Accordingly, the ST2/IL-33 interaction offers a promising target for space medicine in the future.

In contrast, the H-FABP levels did not show any significant changes at 1 h and 24 h after parabolic flight. H-FABP constitutes a highly sensitive marker of myocardial ischemia and myocardial damage, providing a sensitivity even superior to troponin [24]. Accordingly, these findings again indicate no increase in cardiac stress in response to gravity changes. Furthermore, based on these results, it seems that the myocardial oxygen demand is not critically elevated in response to gravitational changes.

Of note, considering the minimal secretion of H-FABP in non-ischemic cells together with our young and healthy study collective, a potential decrease in H-FABP levels in response to gravitational changes must be assumed as not detectable. This finding also suits a former study of our working group on the influence of parabolic flight on different blood parameters. Similar to H-FABP, we could not detect any significant changes in Troponin and BNP in response to parabolic flight [10]. This again emphasizes the assumption that no significant myocardial ischemia is induced by the gravitational changes encountered in parabolic flight. The levels of GDF-15 were significantly decreased at 1 h and showed a further decline at 24 h after parabolic flight. Accordingly, given its involvement in the response to cardiac stress and myocardial ischemia as well as coronary artery disease, the observed decrease in GDF-15 further supports the assumption of a reduction in cardiac stress and ischemia in response to microgravity [14]. However, as GDF-15 is also involved in inflammatory processes and the regulation of apoptosis and remodeling, it seems that the exposure to weightlessness could also have an additional influence on processes regarding the cell cycle and immune system, as was also proposed by recent studies [7,25]. Accordingly, the correlation of the GDF-15 levels at baseline with the CRP levels in our analyses matches former studies. In this regard, a recent study also reported an involvement of GDF-15 in the modulation of transcriptional regulation in the Smad pathway [25].

This theory is further confirmed by analyzing the levels of suPAR, which showed a significant decrease 24 h after parabolic flight, without any significant changes 1 h after parabolic flight. suPAR is a reliable indicator for the activity level of the immune and inflammatory system and correlates with organ damage in diverse organ systems, including the cardiovascular system [15,26]. Thus, the decrease in suPAR in response to zero gravity seems to indicate an anti-inflammatory effect accompanied by a decrease in the activity of the immune system. This finding matches the results of prior studies, describing an impairment of the immune system in zero gravity [7].

In contrast to the markers discussed above, Fetuin-A showed a significant increase 24 h after exposure to parabolic flight. Given the involvement of Fetuin-A in calcium homeostasis and vascular and tissue calcification, a decrease in free calcium levels resulting in a reduction in extraosseous calcification with a calcium shift towards the intraosseous departments could be suspected [16]. However, this finding represents a contradiction to the reports of osteoporotic processes in astronauts after long-term exposure to weightlessness in former studies [9]. Since our study proposes a possible reduction in extraosseous calcification processes at least in response to short-term gravitational changes, a change in calcium-homeostasis between short- and long-term exposures should be considered. Of note, metabolic diseases known to interfere with the secretion of Fetuin-A (e.g., diabetes, CKD) were ruled out in all study subjects.

Another important point with regard to our results is the biological variability of the tested biomarkers, since different timepoints were defined for the analysis of these markers. Of note, investigations into the circadian dynamics of GDF-15, suPAR, H-FABP and the sST2/IL-33 pathway were conducted in former studies [27–32]. Except for suPAR, which did not show a diurnal secretion pattern, a circadian dynamic was reported, with an interval of about 12 h between the peak and nadir in the majority of cases. Of note, the differences observed with regards to a circadian dynamic are lower than the changes observed in response to parabolic flight. While research on a potential circadian dynamic of Fetuin-A is still a matter for further investigation, recent studies have shown a stable expression pattern without significant changes over 72 h [33]. Accordingly, given the timepoints of blood-sampling with measurements at 5 h and 24 h after the baseline measurements, as well as the predominantly clockwise dynamic with comparably low circadian changes in biomarker levels, a difference in diurnal secretion patterns seems unlikely as a relevant confounder of our findings. Thus, with respect to the secretion profile of our tested heart failure biomarkers, we found molecular correlates for several weightlessness-dependent changes described in former studies. Above all, similar to former investigations, we suspect a decrease in cardiac stress, which might be most probably based on the decrease in peripheral vascular resistance and heart rate observed in zero-gravity. These findings are supported by studies that show a significant increase in cardiac biomarkers with long-term

physical activity [34]. Moreover, studies showing cardiac atrophy with an up-to-12% reduction in left ventricular mass in weightlessness underline the significant decrease in cardiac stress in zero gravity [3]. Additionally, further investigations in simulated microgravity and computer models observed a potential reduction in cardiac stress [8]. Accordingly, in synopsis with our findings and former studies, both indicating a decrease in cardiac stress, a potential reduction in cardiac performance by means of deconditioning and restructuring of the heart in response to weightlessness has to be taken into account. In this regard, the potential development of heart failure in long-term exposure to weightlessness represents an important target for future studies. Furthermore, our data emphasize the potential influence of weightlessness on the immune system through impairment and a decrease in inflammatory activation, reflected in the reduction in inflammatory biomarkers [7]. Additionally, our findings propose a potential difference in calcium homeostasis between short- and long-term space missions. While osteoporotic changes are observed in long-term missions, based on our findings, a short-time exposure to weightlessness may have an opposite effect [9,16].

However, given the novelty and the hypothesis-generating approach of the present study, the possible practical application of our findings will remain a topic for further investigation. Nevertheless, heart failure biomarkers could be of great benefit in the course of the timely identification of people at risk for complications in zero gravity, similar to risk stratification in clinical medicine [35]. In this regard, a multimarker measurement seems the most promising approach. By incorporating different pathophysiological processes present in the response to gravitational changes, heart failure biomarkers could be of value as monitoring and safety parameters, particularly in the course of preventive medical care for crews on long-term space missions.

4. Materials and Methods

4.1. Participants

The study was conducted in accordance with the Declaration of Helsinki (1975, revised in 2008) and the protocol was approved by the German Ethics Committee of the Medical Faculty of the University Hospital Duesseldorf, Germany (Date of approval: August 14th, 2017; Project Identification number: 2017054297) and by the French Ethics Committee (Comité de Protection des Personnes (CPP Nord-Ouest III) of the Medical Faculty of the University of Caen (Date of approval: 6 September 2017; Project Identification number: 2017-A01185-48). In total, we enrolled 14 healthy participants in this study. Recruitment was conducted at the University Hospital of Duesseldorf, Germany. All the participants signed a written informed consent form. The inclusion criteria were defined as: age >18 years, airworthiness, cardiorespiratory health, spontaneous circulation and signed informed consent. The exclusion criteria were defined as: a history of primary cardiovascular and respiratory diseases or the regular intake of medication, except for oral contraceptives; missing or withdrawal of informed consent; insufficient requirements for airworthiness; and a positive pregnancy test. Further details have been published in a study outline paper of our study group [36].

4.2. Parabolic Flight

A "Parabolic flight" represents a special aerial maneuver aimed at achieving a state of weightlessness (Figure 3). From a stabilized level-flight altitude (1 g), a steep ascent up to 47° is initiated by the pilots (1.8 g). After this climb, the so-called "injection" maneuver is performed. The power thrust is reduced, and the plane is directed into descent to follow the trajectory. During this phase, the vertical load factor shifts to zero gravity. With the plane tilting forward, the exit phase is initiated, leading to an up-to-45° descent and a second phase of hypergravity (1.8 g), before re-entering the steady flight (1 g) [37]. Each phase averages between 20 and 25 s, respectively [37].

Figure 3. Illustration of a parabolic flight maneuver (copyright by NoveSpace).

4.3. Experimental Set-Up

The study was conducted as part of the 31st Parabolic Flight Campaign (PFC) of the German space agency (Deutsches Zentrum für Luft- und Raumfahrt-DLR), which took place from February 26th to March 11th, 2018, in Bordeaux, France. All flights were performed by the company NoveSpace (France, Mérignac). In total, four flight days were conducted in the course of the PFC, with one flight day consisting of 31 parabolas. Each study subject participated in one flight day and repetitive participation was avoided. Blood samples were drawn at three different time-points: 1 h prior to parabolic flight (baseline 08:00 ± 0.75 h), one hour after the parabolic flight (13:00 ± 1.0 h) and 24 h after the parabolic flight (08:00 ± 0.75 h) Serum samples were collected with individual punctures at each time point, using the following materials: BD vacutainer tubes (Becton Dickinson, Mountain View, CA, USA), 3 serum-separating tubes (SST) (Reference # 367957; tube size: 75 × 13 mm; draw volume: 3.5 mL) and 1 SST tube (Reference # 367955; tube size: 100 × 13 mm; draw volume: 5 mL). The serum sample aliquots were frozen and stored at −80 °C for further analysis after blood withdrawal.

4.4. Statistical Analysis

A statistical analysis was performed using GraphPad Prism software (GraphPad Software, USA) and SPSS (IBM SPSS Statistics, USA). Correlation analyses were conducted using Spearman's Rank correlation. All data are given as mean ± standard error of the mean (SEM). The concentrations of biomarkers between time points were compared using the Wilcoxon matched-pairs test. To test the robustness of our findings, we also conducted a fold change analysis, again using the Wilcoxon matched-pairs test. p-values < 0.05 were considered statistically significant. A p-value of <0.05 was indicated as *, and a p of <0.01 as **.

5. Conclusions

In conclusion, our findings indicate a decrease in cardiac stress, matching former studies. On this regard, a potential reduction in cardiac performance by means of deconditioning and restructuring of the heart in weightlessness indicate a decrease in Cardiac stress, our data suggest an influence of weightlessness on the immune system through a decrease in inflammatory activity. Additionally, our findings propose a potential difference taken into account. Finally, our data suggest an influence of weightlessness on the immune system through a decrease in inflammatory activation. Additionally, our findings propose a potential difference in calcium-homeostasis between short- and long-term exposure to weightlessness. However, given the novelty and the hypothesis-generating approach of the present study, further investigations on the adaptational processes are warranted.

6. Limitations

6. Limitations

The biggest limitation of our study constitutes the small sample size, especially with regards to the biological and analytical variability of biomarkers. Nevertheless, the changes in biomarker levels were consistent in a fold change analysis, thus indicating robust results. When interpreting the findings of our study, one must keep in mind that the time frames of actual zero gravity were limited in the course of the parabolic flight maneuver. During an average flight day, the cumulative duration of weightlessness in total averaged 11 min and 20 s. Moreover, hypergravity must be considered as a potential confounder in parabolic flight. However, studies have shown a good comparability of short-time weightlessness by means of parabolic flight with space missions with regards to hemodynamic changes. Additionally, given the lack of previous analyses, no reference values are available in the literature. Thus, the hypothesis-generating character of this study must be emphasized.

Supplementary Materials: Supplementary materials can be found at http://www.mdpi.com/1422-0067/21/10/3467/s1. Table S1: Correlation analysis of biomarker expression and baseline characteristics/laboratory parameters. Table S2: Analysis on gender related differences in biomarker levels.

Author Contributions: Conceptualization, P.J., M.L., M.F., N.-Y.B.-B. and C.J.; data curation, P.J., B.W., M.L., T.K., T.A. and N.-Y.B.-B.; formal analysis, P.J., B.W., M.L., V.P. and C.J.; funding acquisition, N.-Y.B.-B. and C.J.; investigation, P.J., B.W., T.K., T.A., M.K., J.M.M. and C.J.; methodology, P.J., B.W., M.L., T.A., N.-Y.B.-B. and C.J.; project administration, P.J., N.-Y.B.-B. and C.J.; resources, M.L., M.F., T.K., M.K., N.-Y.B.-B., J.M.M and C.J.; software, B.W., V.P.; supervision, M.L., M.K. and C.J.; validation, P.J., V.P., M.F. and M.K.; visualization, P.J., B.W., V.P.; writing—original draft, P.J., M.F. and C.J.; writing—review and editing, B.W., M.L., V.P., M.F., T.K., T.A., M.K., J.M.M., N.-Y.B.-B. and C.J. All authors have read and agreed to the published version of the manuscript.

Conflicts of Interest: The funders had no role in the design of the study; in the collection, analysis, or interpretation of data; in the writing of the manuscript; or in the decision to publish the results.

Abbreviations

CKD	chronic kidney disease
DLR	Deutsches Zentrum für Luft- und Raumfahrt
ELISA	enzyme-linked immunosorbent assay
g	gravitational force
GDF-15	growth differentiation factor-15
H-FABP	heart-type fatty acid binding protein
IL-33	interleukin-33
NASA	National Aeronautics and Space Administration
PFC	parabolic flight campaign
sST2	soluble suppression of tumorigenicity 2
suPAR	soluble urokinase-type plasminogen activator receptor

References

1. Stepanek, J.; Blue, R.S.; Parazynski, S. Space Medicine in the Era of Civilian Spaceflight. *N. Engl. J. Med.* **2019**, *380*, 1053–1060. [CrossRef] [PubMed]
2. Hughson, R.L.; Shoemaker, J.K.; Blaber, A.P.; Arbeille, P.; Greaves, D.K.; Pereira-Junior, P.P.; Xu, D. Cardiovascular regulation during long-duration spaceflights to the International Space Station. *J. Appl. Physiol.* **1985**, *112*, 719–727. [CrossRef] [PubMed]
3. Shen, M.; Frishman, W.H. Effects of Spaceflight on Cardiovascular Physiology and Health. *Cardiol. Rev.* **2019**, *27*, 122–126. [CrossRef] [PubMed]

4. Lathers, C.M.; Charles, J.B.; Elton, K.F.; Holt, T.A.; Mukai, C.; Bennett, B.S.; Bungo, M.W. Acute hemodynamic responses to weightlessness in humans. *J. Clin. Pharmacol.* **1989**, *29*, 615–627. [CrossRef] [PubMed]

5. Convertino, V.A. Status of cardiovascular issues related to space flight: Implications for future research directions. *Respir. Physiol. Neurobiol.* **2009**, *169*, 19. [CrossRef]

6. Blaber, A.P.; Zuj, K.A.; Goswami, N. Cerebrovascular autoregulation: Lessons learned from spaceflight research. *Eur. J. Appl. Physiol.* **2013**, *113*, 1909–1917. [CrossRef]

7. Cervantes, J.L.; Hong, B.Y. Dysbiosis and Immune Dysregulation in Outer Space. *Int. Rev. Immunol.* **2016**, *35*, 67–82. [CrossRef]

8. Iskovitz, I.; Kassemi, M.; Thomas, J.D. Impact of weightlessness on cardiac shape and left ventricular stress/strain distributions. *J. Biomech. Eng.* **2013**, *135*, 4025464. [CrossRef]

9. Pietsch, J.; Bauer, J.; Egli, M.; Infanger, M.; Wise, P.; Ulbrich, C.; Grimm, D. The effects of weightlessness on the human organism and mammalian cells. *Curr. Mol. Med.* **2011**, *11*, 350–364. [CrossRef]

10. Bimpong-Buta, N.Y.; Jirak, P.; Wernly, B.; Lichtenauer, M.; Knost, T.; Abusamrah, T.; Kelm, M.; Jung, C. Blood parameter analysis after short term exposure to weightlessness in parabolic flight. *Clin. Hemorheol. Microcirc.* **2018**, *70*, 477–486. [CrossRef]

11. Savic-Radojevic, A.; Pljesa-Ercegovac, M.; Matic, M.; Simic, D.; Radovanovic, S.; Simic, T. Novel Biomarkers of Heart Failure. *Adv. Clin. Chem.* **2017**, *79*, 93–152. [PubMed]

12. Ciccone, M.M.; Cortese, F.; Gesualdo, M.; Riccardi, R.; Di Nunzio, D.; Moncelli, M.; Iacoviello, M.; Scicchitano, P. A novel cardiac bio-marker: ST2: A review. *Molecules* **2013**, *18*, 15314–15328. [CrossRef]

13. Ye, X.D.; He, Y.; Wang, S.; Wong, G.T.; Irwin, M.G.; Xia, Z. Heart-type fatty acid binding protein (H-FABP) as a biomarker for acute myocardial injury and long-term post-ischemic prognosis. *Acta Pharmacol. Sin.* **2018**, *39*, 1155–1163. [CrossRef] [PubMed]

14. Wollert, K.C.; Kempf, T.; Wallentin, L. Growth Differentiation Factor 15 as a Biomarker in Cardiovascular Disease. *Clin. Chem.* **2017**, *63*, 140–151. [CrossRef] [PubMed]

15. Eugen-Olsen, J.; Giamarellos-Bourboulis, E.J. suPAR: The unspecific marker for disease presence, severity and prognosis. *Int. J. Antimicrob. Agents* **2015**, *46*, 31. [CrossRef] [PubMed]

16. Jirak, P.; Stechemesser, L.; More, E.; Franzen, M.; Topf, A.; Mirna, M.; Paar, V.; Pistulli, R.; Kretzschmar, D.; Wernl, B.; et al. Clinical implications of fetuin-A. *Adv. Clin. Chem.* **2019**, *89*, 79–130. [PubMed]

17. Dieplinger, B.; Mueller, T. Soluble ST2 in heart failure. *Clin. Chim. Acta* **2015**, *443*, 57–70. [CrossRef]

18. Caiani, E.G.; Weinert, L.; Lang, R.M.; Vaida, P. The role of echocardiography in the assessment of cardiac function in weightlessness-Our experience during parabolic flights. *Respir. Physiol. Neurobiol.* **2009**, *169*, 16. [CrossRef]

19. Norsk, P.; Asmar, A.; Damgaard, M.; Christensen, N.J. Fluid shifts, vasodilatation and ambulatory blood pressure reduction during long duration spaceflight. *J. Physiol.* **2015**, *593*, 573–584. [CrossRef]

20. Kakkar, R.; Lee, R.T. The IL-33/ST2 pathway: Therapeutic target and novel biomarker. *Nat. Rev. Drug Discov.* **2008**, *7*, 827–840. [CrossRef]

21. Schmitz, J.; Owyang, A.; Oldham, E.; Song, Y.; Murphy, E.; McClanahan, T.K.; Zurawski, G.; Moshrefi, M.; Qin, J.; Li, X.; et al. IL-33, an interleukin-1-like cytokine that signals via the IL-1 receptor-related protein ST2 and induces T helper type 2-associated cytokines. *Immunity* **2005**, *23*, 479–490. [CrossRef] [PubMed]

22. Cayrol, C.; Girard, J.P. Interleukin-33 (IL-33): A nuclear cytokine from the IL-1 family. *Immunol. Rev.* **2018**, *281*, 154–168. [CrossRef] [PubMed]

23. Griesenauer, B.; Paczesny, S. The ST2/IL-33 Axis in Immune Cells during Inflammatory Diseases. *Front. Immunol.* **2017**, *8*. [CrossRef]

24. Otaki, Y.; Watanabe, T.; Kubota, I. Heart-type fatty acid-binding protein in cardiovascular disease: A systemic review. *Clin. Chim. Acta* **2017**, *474*, 44–53. [CrossRef]

25. Min, K.W.; Liggett, J.L.; Silva, G.; Wu, W.W.; Wang, R.; Shen, R.F.; Elin, T.E.; Baek, S.J. NAG-1/GDF15 accumulates in the nucleus and modulates transcriptional regulation of the Smad pathway. *Oncogene* **2016**, *35*, 377–388. [CrossRef] [PubMed]

26. Thuno, M.; Macho, B.; Eugen-Olsen, J. suPAR: The molecular crystal ball. *Dis. Markers* **2009**, *27*, 157–172. [CrossRef] [PubMed]

27. Kawauchi, T.; Ishimaru, K.; Nakamura, Y.; Nakano, N.; Hara, M.; Ogawa, H.; Okumura, K.; Shibata, S.; Nakao, A. Clock-dependent temporal regulation of IL-33/ST2-mediated mast cell response. *Allergol. Int.* **2017**, *66*, 472–478. [CrossRef]

28. Pelsers, M.M.; Chapelle, J.P.; Knapen, M.; Vermeer, C.; Muijtjens, A.M.; Hermens, W.T. Influence of age and sex and day-to-day and within-day biological variation on plasma concentrations of fatty acid-binding protein and myoglobin in healthy subjects. *Clin. Chem.* **1999**, *45*, 441–443.

29. Tsai, V.W.; Macia, L.; Feinle-Bisset, C.; Manandhar, R.; Astrup, A.; Raben, A.; Lorenze, J.K.; Schmidt, P.T.; Wiklund, F.; Pedersen, N.L.; et al. Serum Levels of Human MIC-1/GDF15 Vary in a Diurnal Pattern, Do Not Display a Profile Suggestive of a Satiety Factor and Are Related to BMI. *PLoS ONE* **2015**, *10*, e0133362. [CrossRef]

30. Andersen, O.; Eugen-Olsen, J.; Kofoed, K.; Iversen, J.; Haugaard, S.B. Soluble urokinase plasminogen activator receptor is a marker of dysmetabolism in HIV-infected patients receiving highly active antiretroviral therapy. *J. Med. Virol.* **2008**, *80*, 209–216. [CrossRef]

31. Chappuis, S.; Ripperger, J.A.; Schnell, A.; Rando, G.; Jud, C.; Wahli, W.; Albrecht, U. Role of the circadian clock gene Per2 in adaptation to cold temperature. *Mol. Metab.* **2013**, *2*, 184–193. [CrossRef]

32. Crnko, S.; Printezi, M.I.; Jansen, T.P.J.; Leiteris, L.; van der Meer, M.G.; Schutte, H.; van Faassen, M.; du Bre, B.C.; de Jonge, N.; Asselsberg, F.W.; et al. Prognostic biomarker soluble ST2 exhibits diurnal variation in chronic heart failure patients. *ESC Heart Fail.* **2020**, *31*, 12673. [CrossRef] [PubMed]

33. Hwang, J.J.; Thakkar, B.; Chamberland, J.P.; Mantzoros, C.S. Circulating fetuin-A levels are not affected by short and long-term energy deprivation and/or by leptin administration. *Metabolism* **2014**, *63*, 754–759. [CrossRef]

34. Sponder, M.; Lichtenauer, M.; Wernly, B.; Paar, V.; Hoppe, U.; Emich, M.; Fritzer-Szekeres, M.; Litschauer, B.; Strametz-Juranek, J. Serum heart-type fatty acid-binding protein decreases and soluble isoform of suppression of tumorigenicity 2 increases significantly by long-term physical activity. *J. Investig. Med.* **2019**, *67*, 833–840. [CrossRef] [PubMed]

35. Masyuk, M.; Wernly, B.; Lichtenauer, M.; Franz, M.; Kabisch, B.; Muessig, J.M.; Zimmermann, G.; Lauten, A.; Schulze, P.C.; Hoppe, U.C.; et al. Prognostic relevance of serum lactate kinetics in critically ill patients. *Intensive Care Med.* **2019**, *45*, 55–61. [CrossRef] [PubMed]

36. Bimpong-Buta, N.Y.; Jirak, P.; Wernly, B.; Lichtenauer, M.; Masyuk, M.; Muessig, J.M.; Braun, K.; Kaya, S.; Kelm, M.; Jung, C. Analysis of human microcirculation in weightlessness: Study protocol and pre-study experiments. *Clin. Hemorheol. Microcirc.* **2018**, *14*. [CrossRef]

37. Shelhamer, M. Parabolic flight as a spaceflight analog. *J. Appl. Physiol.* **1985**, *120*, 1442–1448. [CrossRef]
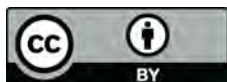
scientific reports

OPEN

Exposure to acute normobaric hypoxia results in adaptions of both the macro- and microcirculatory system

Moritz Mirna [1,9], Nana-Yaw Bimpong-Buta[2,9], Fabian Hoffmann[3,4], Thaer Abusamrah[2], Thorben Knost[2], Oliver Sander[5], Yayu Monica Hew[6], Michael Lichtenauer[1], Johanna M. Muessig[2], Raphael Romano Bruno[2], Malte Kelm[2], Jochen Zange[3], Jilada Wilhelm[3], Ulrich Limper[3,7], Jens Jordan[3,8], Jens Tank[3] & Christian Jung[2✉]

Although acute hypoxia is of utmost pathophysiologic relevance in health and disease, studies on its effects on both the macro- and microcirculation are scarce. Herein, we provide a comprehensive analysis of the effects of acute normobaric hypoxia on human macro- and microcirculation. 20 healthy participants were enrolled in this study. Hypoxia was induced in a normobaric hypoxia chamber by decreasing the partial pressure of oxygen in inhaled air stepwisely (pO$_2$; 21.25 kPa (0 k), 16.42 kPa (2 k), 12.63 kPa (4 k) and 9.64 kPa (6 k)). Macrocirculatory effects were assessed by cardiac output measurements, microcirculatory changes were investigated by sidestream dark-field imaging in the sublingual capillary bed and videocapillaroscopy at the nailfold. Exposure to hypoxia resulted in a decrease of systemic vascular resistance ($p < 0.0001$) and diastolic blood pressure ($p = 0.014$). Concomitantly, we observed an increase in heart rate ($p < 0.0001$) and an increase of cardiac output ($p < 0.0001$). In the sublingual microcirculation, exposure to hypoxia resulted in an increase of total vessel density, proportion of perfused vessels and perfused vessel density. Furthermore, we observed an increase in peripheral capillary density. Exposure to acute hypoxia results in vasodilatation of resistance arteries, as well as recruitment of microvessels of the central and peripheral microcirculation. The observed macro- and microcirculatory effects are most likely a result from compensatory mechanisms to ensure adequate tissue oxygenation.

Abbreviations

AMS	Acute mountain sickness
CaO$_2$	Arterial oxygen content
CD	Peripheral capillary diameter
CO	Cardiac output
CPI	Cardiac performance index
DBP	Diastolic blood pressure
DO$_2$	Oxygen delivery
FiO$_2$	Fraction of inspired oxygen
kPa	Kilopascal
HR	Heart rate

[1]Division of Cardiology, Department of Internal Medicine II, Paracelsus Medical University of Salzburg, Muellner Hauptstrasse 48, 5020 Salzburg, Austria. [2]Department of Cardiology, Pulmonology and Vascular Medicine, Medical Faculty, Heinrich-Heine-University, Duesseldorf, Germany. [3]German Aerospace Center (DLR), Institute of Aerospace Medicine, Cologne, Germany. [4]Department of Cardiology, University Hospital Cologne, Cologne, Germany. [5]Department of Rheumatology, Hiller Research Institute for Rheumatology, Medical Faculty, Heinrich-Heine-University, Duesseldorf, Germany. [6]Department of Aeronautics and Astronautics, Stanford University, Stanford, CA 94305, USA. [7]Department of Anesthesiology and Intensive Care Medicine, Merheim Medical Center, Hospitals of Cologne, University of Witten/Herdecke, Cologne, Germany. [8]Chair of Aerospace Medicine, Medical Faculty, University of Cologne, Cologne, Germany. [9]These authors contributed equally: Moritz Mirna and Nana-Yaw Bimpong-Buta. ✉email: christian.jung@med.uni-duesseldorf.de

LLS	Lake Louise Score
NC	Number of crossings
NIRS	Near-infrared spectroscopy
PCD	Peripheral capillary recruitment
pCO$_2$	Partial pressure of carbon dioxide
PNC	Perfused number of crossings
pO$_2$	Partial pressure of oxygen
PPV	Proportion of perfused vessels
PVD	Perfused vessel density
SBP	Systolic blood pressure
SV	Stroke volume
SVR	Systemic vascular resistance
THb	Total hemoglobin concentration
TSI	Tissue saturation index
TVD	Total vessel density

The microcirculatory system comprises a network of small blood vessels with a pivotal role in maintaining adequate tissue perfusion, oxygenation and nutrient supply at the cellular level. Anatomically, the network consists of arterioles, venules and capillaries, with diameters well below 100 μm[1]. Current evidence suggests that the microcirculation plays a paramount role in the pathophysiology of multi-organ failure in critically ill patients, which is why the evaluation of microcirculatory disorders is gaining increasing recognition in intensive care medicine[2]. In fact, reduced cardiac output, changes in peripheral vascular resistance or alterations of the volume status or pH-value can lead to microcirculatory disorders, which result in tissue edema[3,4], inadequate tissue perfusion and, subsequently, reduced cellular oxygen supply[2,5]. The resulting tissue hypoxia markedly aggravates tissue damage and thus promotes end-organ dysfunction in critically ill patients with sepsis or shock[6], which is why the restoration of tissue perfusion and oxygenation constitutes a paramount treatment goal in clinical practice[5].

Tissue hypoxia resulting from an inadequate uptake of ambient oxygen or an increase in cellular oxygen demand is one of the key features of the critically ill patient[7]. Since hypoxaemia, defined as a decrease in arterial oxygen tension[8], is also a predominant feature of the high-altitude environment, research on the pathophysiologic processes behind hypoxia was significantly facilitated with the advent of altitude simulation tests[9]. On the cellular level, hypoxic stress initiates a transcriptional response by hypoxia inducible factors (HIF; during intermittent hypoxia predominately HIF-1α[10–12]), which leads to a reduction of cellular energy consumption, a secretion of pro-angiogenic and survival factors[10], and qualitative changes in mitochondrial function[13], which in turn results in alterations of the cardiovascular, haematological and even urinary physiology[14,15]. Among the observed physiological alterations in response to hypoxia, the effects on the human macrocirculatory system have been subject to several extensive scientific investigations in the past. Hence, acute hypoxia is known to result in an initial increase in heart rate, blood pressure and cardiac output, whereas a decrease in stroke volume can be observed only after a few days of exposure[16–18]. In contrast, studies concerning the effects of hypoxia on the microcirculatory system are comparatively scarce. For example, previous studies reported an increase in sublingual microcirculatory blood flow and capillary density after ascent to high altitudes[19,20], which suggests microvascular recruitment after exposure to hypobaric hypoxia[21]. However, recent studies also reported that the physiological adaptions to hypobaric hypoxia can differ substantially from those to normobaric hypoxia[22,23], which is why the results of studies conducted in high altitude can not be fully applied to the normobaric environment.

Since the microcirculation constitutes one of the central components where hypoxia mediates its unfavourable effects in critically ill patients, a thorough investigation of the effects of normobaric hypoxia on the microcirculatory system, with regards to its interplay with larger vessels, is of interest. To further elucidate this matter, we conducted an altitude simulation test and investigated both the macro- and microcirculatory effects of acute normobaric hypoxia (Fig. 1 provides an overview of the conducted measurements).

Results

In total, we enrolled 20 healthy subjects in this study, who had no significant experience in climbing or competitive sports. Of the subjects enrolled, the majority was male (n = 11, 55%), the median age was 29 years (IQR 25–31) and the median body mass index (BMI) was 23 kg/m^2 (IQR 21–25.3). At baseline, the median systolic blood pressure (SBP) was 115 mmHg (IQR 106–128), the median diastolic blood pressure (DBP) was 70 mmHg (IQR 64.5–75), the median heart rate (HR) was 67 beats per minute (bpm; IQR 61.5–70), the median peripheral oxygen staturation (SpO$_2$) was 97% (IQR 96–98) and the median respiratory rate was 16 min^{-1} (IQR 14–17, see Table 1). Eighteen subjects completed the entire hypoxia protocol.

The atmospheric data of the two hypoxia runs are displayed in Supplementary Figure 1. Briefly, the partial pressure of oxygen (pO$_2$) in ambient air decreased significantly throughout the two hypoxia runs, whereas humidity, temperature, overall pressure and the partial pressure of carbon dioxide (pCO$_2$) remained relatively stable.

Regarding symptoms of acute mountain sickness (AMS), the median Lake Louise Score (LLS) at baseline was 0.2 points (IQR 0.0–0.6), with a gradual increase to the median LLS of 3.8 points (IQR 1.7–4.4) at 6 k.

Exposure to hypoxia resulted in a significant decrease of DBP, but it did not result in a change of SBP. Whereas HR increased significantly throughout the two tests, stroke volume remained unchanged. Systemic vascular resistance decreased, whereas cardiac output (CO) and cardiac performance index (CPI) increased significantly (see Fig. 2, Table 2 and Suppl. Figure 2). Furthermore, exposure to hypoxia resulted in a significant decrease of SpO$_2$ and a signficant increase in respiratory rate, as expected (see Table 2). Notably, there was no
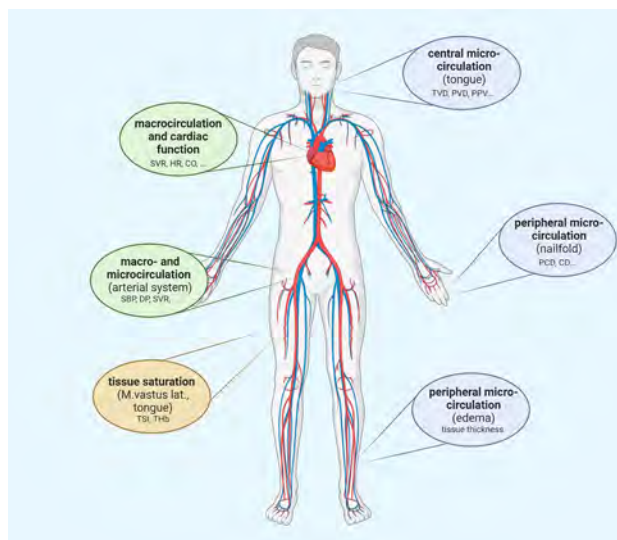
Figure 1. Schematic representation of the conducted measurements during the two hypoxia tests. *TVD* total vessel density, *PPV* proportion of perfused vessels, *PVD* perfused vessel density, *PCD* peripheral capillary recruitment, *CD* peripheral capillary diameter, *SV* stroke volume, *HR* heart rate, *CO* cardiac output, *SBP* systolic blood pressure, *DBP* diastolic blood pressure, *SVR* systemic vascular resistance, *TSI* tissue saturation index, *THb* total hemoglobin concentration.

	%	n (total = 20)
Sex (% male)	55	11
	Median	IQR
Age (years)	29	25–31
BMI (kg/m^2)	23	21–25.3
Height (cm)	176.5	169.5–181.3
Weight (kg)	71.5	63.8–78.5
Systolic blood pressure (mmHg)	115	106–128
Diastolic blood pressure (mmHg)	70	64.5–75
Heart rate (bpm)	67	61.5–70
Respiratory rate (min^{-1})	16	14–17
Peripheral oxygen saturation (%)	97	96–98

Table 1. Baseline characteristics of the subjects enrolled.

change in oxygen delivery (DO$_2$), although a trend towards an initial decrease, followed by an increase to 6 k, was observed (see Table 2).

In the sublingual microcirculation, acute hypoxia resulted in an increase in the number of crossings (NC), total vessel density (TVD), perfused number of crossings (PNC), proportion of perfused vessels (PPV) and perfused vessel density (PVD; see Fig. 3, Table 2 and Suppl. Figure 2).

In the capillary bed of the nailfold, we observed a signifiant increase in peripheral capillary recruitment (PCD) at 2 k and 4 k when compared to the baseline values (0 k mean: 78.33% vs. 2 k: 84.72% and 4 k: 83.01%, $p < 0.01$, see Fig. 3, Table 2 and Supplementary Figure 3). Correspondingly, the mean peripheral capillary diameter (CD) of arterial limb (11.6 μm at 0 k), apex (16.6 μm at 0 k) and venous limb (15.7 μm at 0 k) showed a significant increase of 4% at 2 k (all $p < 0.05$) and 2% at 4 k (apex signifiant at $p = 0.049$). As estimated by the law of Hagen-Poiseuille[24], which states that the flw rate is proportional to the radius of the vessel to the fourth power, the average flw increases corresponded to 17% (2 k) and 8% (4 k) and additionally 5% due to the increased capillary recruitment. Notably, the initial increase in PCD and CD was followed by a decrease in both variables at 6 k (see Table 2). A graphical overview of the findings concerning the macro- and microcirulatory system is provided in Supplementary Figure 2.

Changes in peripheral microcirculation did not result in clinical signs of increased microvascular permeability, since we observed no significant peripheral edema after hypoxia, as assessed by ultrasonographic tissue thickness of the lower leg or the forehead (see Table 2).

Concerning tissue oxygenation, we found only moderately diverging baseline values of the tissue saturation index (TSI) in both muscles at rest (see Table 2), but total hemoglobin concentration (THb) was almost three
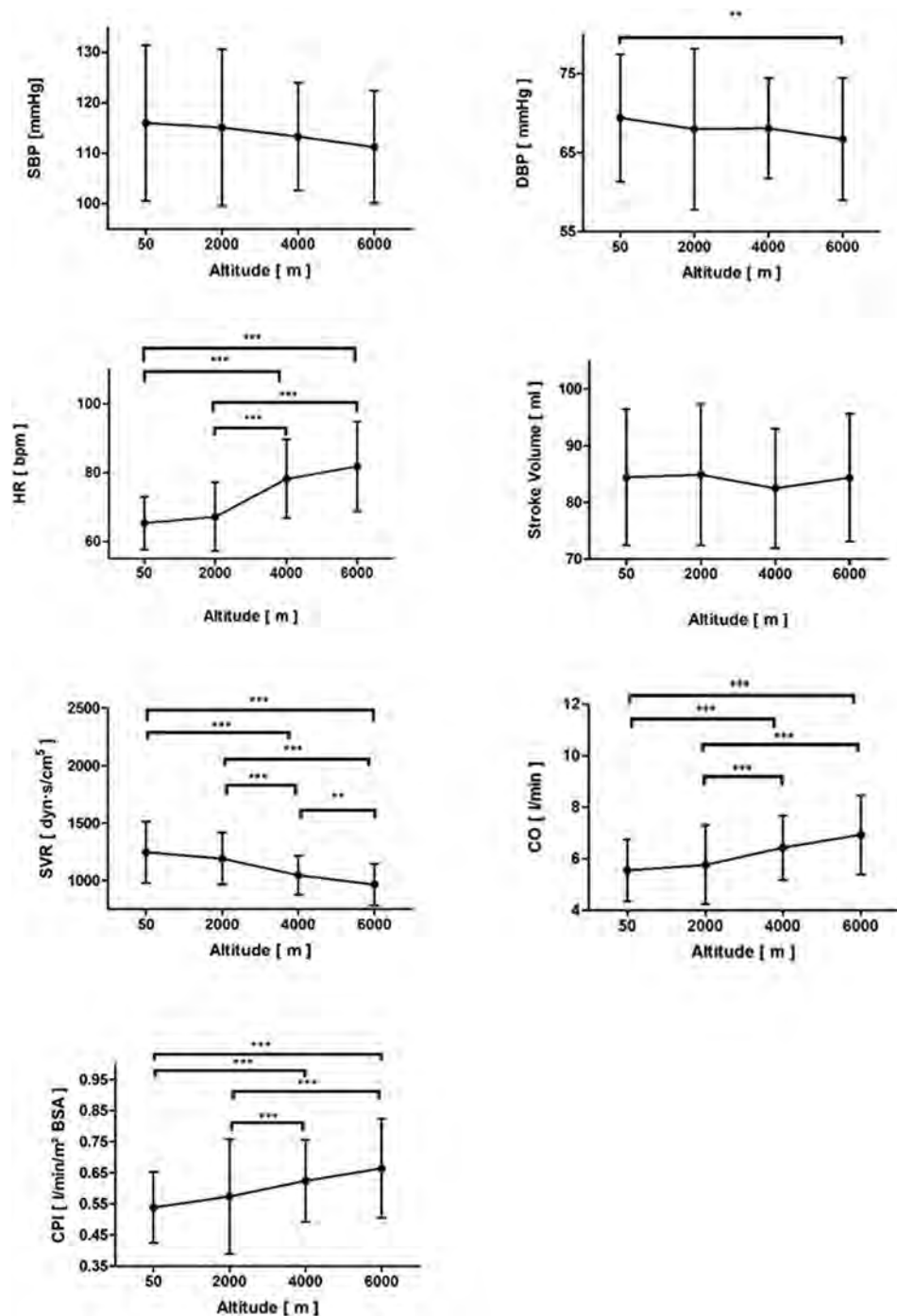
Figure 2. Systolic blood pressure (SBP), diastolic blood pressure (DBP), heart rate (HR), stroke volume (SV), systemic vascular resistance (SVR), cardiac output (CO) and cardiac performance index (CPI) throughout the altitude simulation test. $*p < 0.05$, $**p < 0.01$ and $***p < 0.001$.

times higher in the tongue than in the vastus lateralis muscle. Similar to the decrease in SpO_2, hypoxia resulted in a statistically signifiant, yet comparatively low change of the TSI of the tongue at 4 k and 6 k (baseline: mean 63.6% to 4 k: mean 58.3%, $p = 0.01$, and 6 k: mean 59.7%, $p = 0.009$) and of the vastus lateralis muscle at 6 k (baseline: mean 69.6% to 6 k: mean 66.4%, $p = 0.013$) when compared to the respective baseline values. In the tongue, however, the decrease in TSI in reponse to hypoxia reached statistical signifiance at more moderate levels of hypoxia and was in total more pronounced than in the vastus lateralis muscle. The THb was not signifiantly influenced by exposure to hypoxia (see Fig. 4 and Table 2). Also, the systemic red blood cell counts (RBC) and hemoglobin concentration remained unchangend (see Table 2).

	50 m (0 k)		2000 m (2 k)		4000 m (4 k)		6000 m (6 k)		
	Median	IQR	Median	IQR	Median	IQR	Median	IQR	p value
Hemorheological variables									
Red blood cell count (per pL)	4.9	4.3–5.5	4.9	4.2–5.4	4.9	4.3–5.4	4.9	4.3–5.3	0.984
Hemoglobin (g/dl)	14.8	12.9–15.7	14.4	13.0–15.7	14.5	12.8–15.5	14.6	12.7–15.5	0.944
Arterial oxygen content (ml/dl)	20.7	18.2–22.2	19.2	17.1–21.7	17.3	15.3–19.0	15.7	13.6–17.4	<0.0001
Oxygen delivery (ml/min)	1105	971.8–1189	1069	950.4–1209	1040	916.4–1139	1128	977.2–1255	0.455
Macrocirculation									
Peripheral oxygen saturation (%)	97	97–97.5	95	93–97	84	80–87	80	67–83.5	<0.0001
Respiratory rate (breaths per minute)	16	14–16	18	16–18	18	16–22	24	21–28	<0.0001
Systolic blood pressure (mmHg)	115	105–130	114	103–122	116	103–119	110	104–122	0.251
Diastolic blood pressure (mmHg)	70	63–76	68	58–75	66	64–70	65	63–74	0.014
Systemic vascular resistance (dynes*s/cm^5)	1206	1072–1421	1199	982–1352	1067	951–1152	940	814–1125	<0.0001
Heart rate (bpm)	65	60–70	66	61–72	76	69–86	80	73–92	<0.0001
Stroke volume (ml)	83	77–91	84	78–93	82	76–89	87	78–93	0.281
Cardiac output (l/min)	5.35	4.60–6.08	5.56	4.80–6.40	6.00	5.60–7.00	7.20	5.60–8.10	<0.0001
Cardiac performance index (l/min/m^2 BSA)	0.51	0.48–0.59	0.53	0.48–0.63	0.60	0.54–0.69	0.67	0.53–0.75	<0.0001
Sublingual microcirulation									
Perfused number of crossings	32	27–37	33	27–40	35	29–39	36	30–42	<0.0001
Perfused vessel density (mm/mm^2)	6.8	5.7–7.8	7.0	5.7–8.5	7.4	6.2–8.3	7.7	6.4–8.9	<0.0001
Proportion of perfused vessels (%)	94	89–97	94	89–98	95	90–98	95	91–100	0.017
Number of crossings	34	30–39	36	30–42	37	31–42	39	32–44	<0.0001
Total vessel density (mm/mm^2)	7.2	6.4–8.3	7.7	6.4–8.9	7.9	6.6–8.9	8.3	6.9–9.4	<0.0001
	Mean	**SEM**	**Mean**	**SEM**	**Mean**	**SEM**	**Mean**	**SEM**	**p value**
Peripheral microcirculation									
Vessel density (n/mm^2)	6.69	1.51	7.26	1.72	7.07	1.94	7.29	1.74	<0.01
Peripheral capillary recruitment (%)	78.33	0.15	84.72	0.15	83.01	0.17	83.45	0.14	<0.01
Peripheral capillary diameter, apex (μm)	16.58	7.77	17.32	8.09	16.99	8.26	17.14	8.12	0.01
	Baseline						**Post hypoxia**		**p value**
	Median	**IQR**					**Median**	**IQR**	
Peripheral edema (tissue thickness)									
Leg (mm)	5.14	4.4–7.0					5.54	4.7–6.4	0.936
Forehead (mm)	4.85	4.4–5.8					4.98	4.4–5.6	0.184
	Mean	**SEM**	**Mean**	**SEM**	**Mean**	**SEM**	**Mean**	**SEM**	**p value**
Tissue oxygen saturation									
Tissue saturation index tongue (%)	63.57	1.27	61.51	0.90	58.31	1.10	59.66	0.98	0.044
Tissue saturation index M.vastus lat. (%)	69.59	0.81	69.58	0.62	68.23	0.97	66.37	1.10	0.145
Total hemoglobin tongue (μmol/l)	129.5	4.14	136.3	5.56	123.1	6.91	123.8	7.24	0.356
Total hemoglobin M.vastus lat. (μmol/l)	48.27	3.94	46.83	3.56	49.57	4.48	48.43	4.20	0.997

Table 2. Investigated variables throughout the altitude simulation tests.

In the two hypoxia runs conducted, a total of 2 subjects had to exit the test prematurely because of severe symptoms of AMS. These two participants did not show any difference in the investigated macro- and microcirculatory variables when compared to participants who did not exit the tests prematurely.
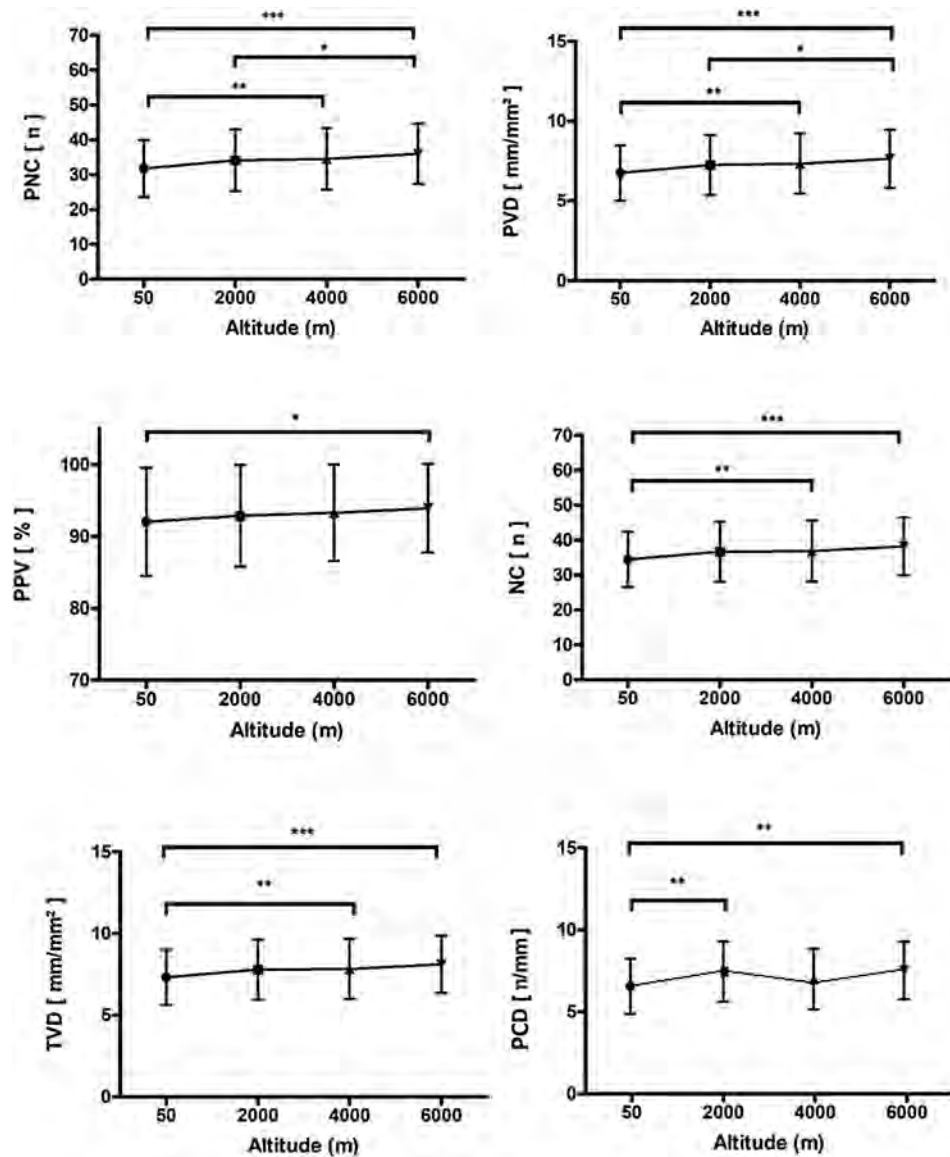
Figure 3. Perfused number of crossings (PNC), perfused vessel density (PVD), proportion of perfused vessels (PPV), number of crossings (NC), total vessel density (TVD), and peripheral capillary recruitment (PCD) throughout the altitude simulation test. *$p < 0.05$, **$p < 0.01$ and ***$p < 0.001$.

Participants who showed objective hypoxia, as portrayed by an $SpO_2 < 75\%$ at 6 k ($SpO_2 < 75\%$: n = 8) had a signifi antly higher LLS at 2 k (median 1.7 vs. 0.5, $p = 0.015$), but a signifi antly lower respiratory rate at 6 k (median 21.3 breathspm vs. 27.7 breathspm $p = 0.026$). Moreover, the increase in HR from baseline to 6 k was significantly higher in these patients (Delta HR at 6 k: 23.8 vs. 10.1, $p = 0.036$).

Supplementary Table 1 depicts an overview of the differences between female and male participants, while the rest of the investigated variables were not different between the two genders. Compared to male participants, we observed a significantly lower SBP, DBP and THb of the vastus lateralis muscle in female subjects.

Discussion

In the last decades, several studies have investigated the effects of hypoxia on the human macrocirculation. According to current evidence, chronic hypoxia leads to a signifi ant increase of systolic and diastolic blood pressure by an overstimulation of the adrenergic and renin-angiotensin system[25,26], as well as a downregulation of endothelial NO synthase (eNOS)[27]. Hence, long-term hypoxia is regarded a key precursor in the pathogenesis of arterial hypertension in patients with obstructive sleep apnea (OSA)[28]. In contrast, acute hypoxia is known to result in local or systemic vasodilatation via nitric oxide (NO), which is a direct result of enhanced secretion of adenosine, adenosine triphosphate (ATP), prostaglandins (PGs) and adrenaline[29], and constitutes a compensatory mechanism to ensure adequate tissue perfusion[30,31].
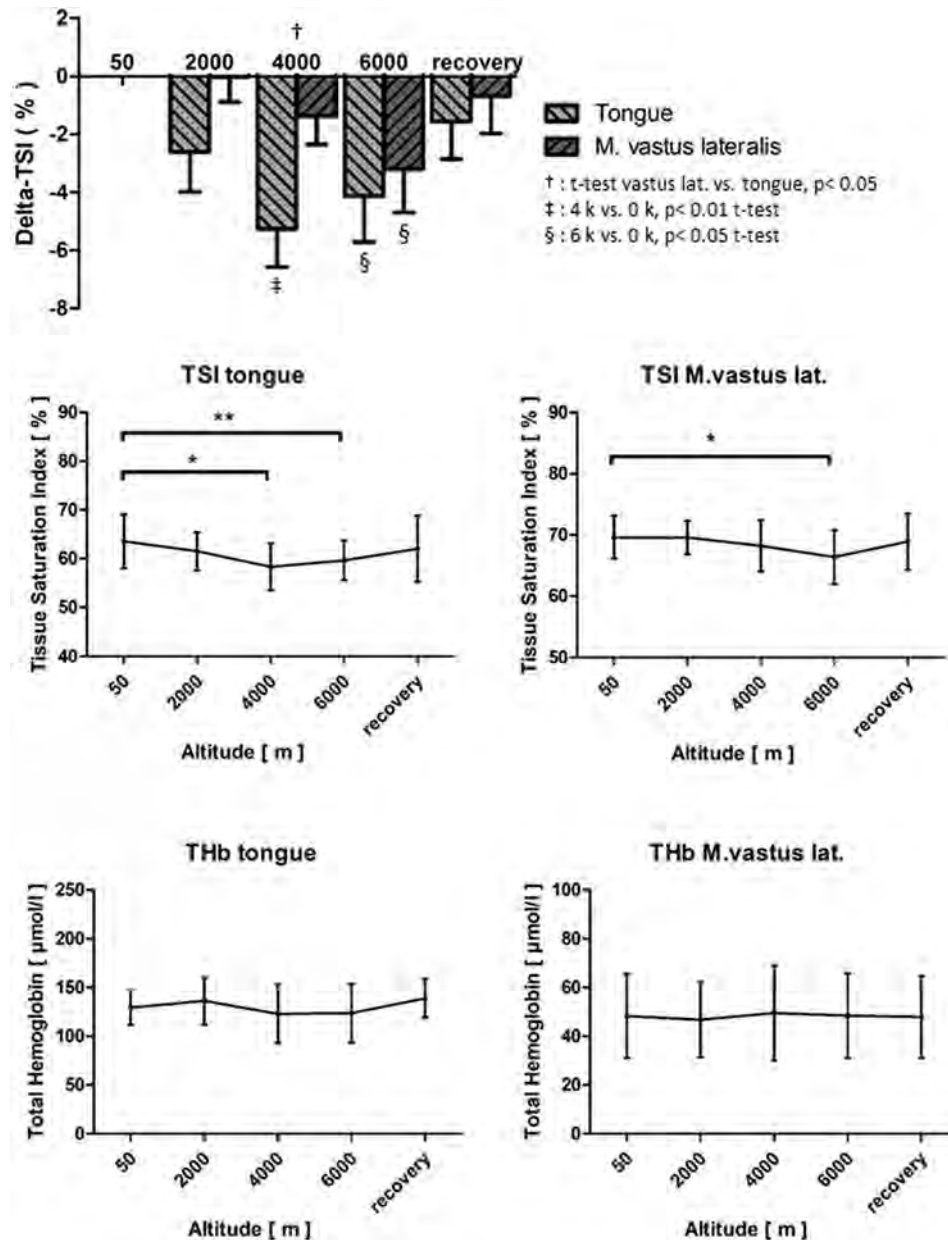
Figure 4. Tissue saturation index (TSI), Delta-TSI and total hemoglobin concentration (THb) of the tongue and the vastus lateralis muscle throughout the hypoxia test. † denotes the t-test of vastus lat. versus tongue at 4 k, where the p value was < 0.05; ‡ denotes the t-tests of the tongue and vastus lat. at 4 k versus 0 k, where the p value was < 0.01; § denotes the t-test of the tongue at 6 k versus 0 k, where the p value was < 0.05. *p < 0.05, **p < 0.01 and ***p < 0.001.

In our study, exposure to normobaric hypoxia resulted in profound systemic hypoxaemia, as portrayed by a significant decrease in SpO_2. In contrast, decreases in TSI of the tongue and of the vastus lateralis muscle were comparatively low and probably clinically irrelevant. However, the response of TSI to hypoxia was more sensitive and pronounced in the tongue than in the leg muscle (Delta-TSI tongue min. − 5.3% at 4 k, Delta-TSI vastus lateralis muscle min. − 3.2% at 6 k, see Fig. 4), which indicates that hypoxia was predominantly compensated by an increased perfusion in both muscles at rest, with a more effective compensation in the vastus lateralis muscle, which is also adapted to high increases in energy turn-over during work.

Similar to previous studies[30,31], we found that exposure to acute hypoxia resulted in a decrease of DBP. This finding was most likely a result from vasodilatation of the arterioles, as portrayed by a significant decrease in SVR. Concomitantly, we observed a compensatory increase in HR which, since there was no significant change in stroke volume, resulted in an increased CO (CO = HR × SV) and CPI.

The observed macrocirculatory effects of systemic hypoxaemia were accompanied by microcirculatory changes, which indicate an increase in organ perfusion. Hence, we found that exposure to normobaric hypoxia leads to a significant increase in TVD, PPV and PVD of the sublingual microcirculation, which can be interpreted

as a result of capillary recruitment. Capillary recruitment is known as an opening of previously closed capillaries by dilatation of the precapillary sphincters in response to unmet metabolic demands[32]. In fact, only 20–30% of the capillaries are actively participating in tissue perfusion under resting conditions[33]. Therefore, capillary recruitment constitutes an important compensatory mechanism to ensure adequate tissue perfusion and oxygenation in the capillary beds of several muscles[34] and the lungs[35]. Notably, our findings are in line with the results of a previous study by Hilty et al.[21], who found that exposure to high altitudes was associated with capillary recruitment of sublingual capillaries and thus an increase in microcirculatory oxygen extraction capacity.

Similar to the microcirulation of the sublingual capillary bed, we observed a significant increase in PCD and CD in the microcirculation of the nailfold. This indicates capillary recruitment in the peripheral microcirculation by exposure to acute hypoxia. Notably, Paparde et al. recently reported that acute hypoxia does not influence capillary recruitment in human nailfold capillaries, but rather leads to capillary vasodilatation[36]. Since capillary recruitment is a rapid adaptation, the short duration of hypoxia in this study is no plausible explanation for the discrepancy of the study's results to our current findings. In our study cohort, however, we were able to identify identical areas of the nailfold where we could demonstrate capillary recruitment directly (e.g. capillaries visible at 2 k that were not visible at 0 k, see Supplementary Figure 3) and could calculate recruitment rates fitting to the expected increase in circulation. Furthermore, in contrast to hypoxia, hyperoxia was recently found to reduce capillary recruitment[37]. Considering our current data and this previous finding, it seems plausible and credible that dysregulations of the pO_2 in blood affect the microcirculation of the nailfold.

In the last decades, clinicians have increasingly recognized the role of the microcirculatory system in the pathophysiology of different diseases. In fact, current evidence suggests, that microcirculatory disorders are a key component of the processes involved in the pathogenesis of multi-organ failure in critically ill patients[2]. Hence, microcirculatory dysfunctions can be found in a large proportion of patients admitted to intensive care units. For example, a reduction in PPV and PVD can be observed in patients with sepsis, and can be interpreted as a result of the impairment of the functional perfusion of the microcirculation[6,38,39]. Microcirculatory disorders themselves can result in tissue hypoxia, which markedly aggravates end-organ dysfunction in critically ill patients[6]. In fact, microcirculatory changes could even be associated with adverse outcomes in several previous studies[40], which is why the restoration of adequate tissue perfusion and oxygenation constitutes a paramount treatment goal in clinical practice.

The observed macro- and microcirculatory effects of acute hypoxia in healthy participants in our study are most likely a result from compensatory mechanisms which ensure adequate tissue perfusion in case of profound hypoxaemia. Hence, by recruiting microvessels of the central and peripheral microcirculation, the organism adapts to hypoxaemia to counteract the state of inadequate tissue oxygenation. In fact, tissue hypoxia resulting from inadequate uptake of ambient oxygen or an increase in cellular oxygen demand is one of the key features of the critically ill patient[7]. However, whether the observed compensatory mechanisms also occur in the hypoxaemic patient, and, if absent or reduced microcirculatory adaptions are associated with adverse outcomes, remains to be elucidated in clinical trials.

Materials and methods

The study protocol of this exploratory study was reviewed and approved by the ethics committee of the Heinrich-Heine-University, Düsseldorf, Germany (5925R) and conducted according to the principles of the Declaration of Helsinki and Good Clinical Practice. Informed consent was obtained from all subjects before enrollment.

The study was conducted at the 'DLR:envihab' of the German Aerospace Center (https://www.dlr.de/envihab/), Cologne, Germany. In total, 20 healthy subjects without significant experience in climbing or competitive sports were enrolled by an announcement at the University of Düsseldorf. The anthropometric data and baseline characteristics of the study participants are depicted in Table 1.

Induction of hypoxia, measurement of oxygen delivery and Lake Louise Score (LLS).
Baseline measurements of 20 healthy participants were acquired under normoxic conditions and compared to measurements under normobaric hypoxic conditions. Hypoxia tests were performed in a normobaric hypoxia chamber, which comprises a laboratory space of about 120 m² including examination rooms, sanitary facilities and a big common room where subjects could move freely and where they waited for individual examinations. Hypoxia was achieved by nitrogen dilution through the air conditioning system in the atmoshperic self-sufficient hypoxia chamber. Nitrogen was supplied by an external tank. Hence, four different altitudes above sea level were simulated (50 m (0 k), 2000 m (2 k), 4000 m (4 k) and 6000 m (6 k) above sea level). Throughout the test, the partial pressure of nitrogen in ambient air was gradually increased, which led to a reduction of the partial pressure of oxygen (pO_2; 21.25 kPa (0 k), 16.42 kPa (2 k), 12.63 kPa (4 k) and 9.64 kPa (6 k), FiO2: median 0.21 (0 k), 0.16 (2 k), 0.12 (4 k), 0.10 (6 k), see Supplementary Figure 1). The partial pressure of carbon dioxide remained relatively stable throughout the two hypoxia runs (pCO_2 median 0.046 kPa (0 k), 0.060 kPa (2 k), 0.72 kPa (4 k) and 0.059 kPa (6 k)). The subjects were exposed to an 'altitude' for two hours before proceeding to the next level. Measurements were performed at each oxygen level to investigate the effects of hypoxia on the micro- and macrocirculation (Fig. 1 provides an overview).

Oxygen delivery (DO_2) was calculated as previously published (DO_2 = cardiac output (CO) × CaO_2 × 10; where CaO_2 was the arterial O_2-content defined as: (1.34 × hemoglobin concentration × SpO_2) + (0.003 × PaO_2) and the amount of dissolved oxygen in blood was estimated by 0.003 × pO_2)[41]. Hemoglobin concentration and red blood cell count (RBC) were measured at each of the four different altitudes using an ABL800 FLEX blood gas analyzer (Radiometer Medical, Copenhagen, Denmark).

Symptoms of hypoxia and severity of acute mountain sickness (AMS) were assessed by the Lake Louise Score (LLS), as previously published. Mild AMS was defi ed as LLS 3–5 points, moderate AMS as 6–9 points, and severe AMS as 10–12 points[42].

Macrocirculation and cardiac function. Systolic and diastolic blood pressure (SBP and DBP) were assessed using a ProBP 3400 (Welch Allyn, Skaneateles Falls, New York, USA) blood pressure monitor, peripheral oxygen saturation was assessed using a PULOX PO-300 (Novidion, Cologne, Germany) pulse oximeter. Systemic vascular resistance (SVR), heart rate (HR), cardiac output (CO), cardiac performance index (CPI) and stroke volume (SV) were measured using transthoracic impedance cardiography (ICON, OSYPKA Medical, Berlin, Germany) and non-invasive Electrical Cardiometry (EC, OSYPKA Medical, Berlin, Germany).

Central and peripheral microcirculation. A sidestream darkfi ld microscope (MicroScan device, Micro-Vision Medical, Amsterdam, The Netherlands) was used to assess the sublingual microcirculation as described previously[43]. Only suffici tly trained researchers performed measurements. In brief, on the tip of this device, a highly sensitive camera digitally recorded the sublingual capillary network. Different regions under the tongue were used for all videos and at least four videos were taken per area. In the next step, a tablet computer was used (Microsoft Surface Pro 4, (Redmond, Washington, USA)) for video analysis. After recording videos with suffici-ent quality, a validated automatic algorithm-software (AVA, Version 4.3 C, MicroVision Medical, Amsterdam, The Netherlands) was used to perform the offl e analysis. Agreeing to the second consensus on the assessment of sublingual microcirculation in critically ill patients (European Society of Intensive Care Medicine), the following variables were assessed[44]:

Microvascular values can offer information about both convexity and diffusion. The proportion of perfused vessels (PPV = 100 * (Total number of perfused vessels / total number of vessels) gives information both about convexity and perfusion. Diffusion can be assessed by the total vessel density (TVD) and the number of crossings (NC). Density was evaluated by the total vessel density and the number of crossings. With both information, the perfused vessel density (PVD = total length of perfused vessels divided by the analyzed area) and perfused number of crossings (PNC = number of vessel crossings with continuous fl w) can be calculated. Vessels with diameters of less than 20 mm correspond mostly to capillaries and are primarily responsible for the microcircula-tion. These small vessel values are signed with the prefix "s" (e.g. sPPV = PPV of small vessels). The values for all vessels can be considered as a quality check to exclude for example pressure artifacts. Before AVA 4.3C analysis, all videos were evaluated according to the microcirculation image quality score (MIQS), that were originally introduced by Massey et al.[45]. In brief, MIQS rates the acquired videos into three categories: "good", "accept-able", and "non-acceptable". Overall, six different criteria are evaluated: illumination, focus, content, stability, pressure, and the duration was not rated. A video without signifi ant impairment in all criteria gets zero points. Mild impairment results in 1 point for each impaired criterion. Severe impairment in one criterion is defined to be rated with 10 points, which results in the category "non-acceptable".

Peripheral microcirculation at the nailfold was assessed at two areas of fingers III-V of both hands, images of the nailfold of 1 mm were obtained using videocapillaroscopy (Di-Li 2100, Distelkamp-Electronic, Kaiser-slautern, Germany). The acquired images were assigned to each other and identical capillaries were compared in density (PCD), visibility (visible 1, scanty 0.5, not visible 0, not shown x), shape (hairpin 1, tortuous 2, abnormal 3), distance (to the right capillary 50 μm before apex in μm), diameter (CD) of the arterial limb (50 μm before apex in μm), apical (in the middle in μm), venous limb (50 μm behind apex in μm) and tail (diameter between arterial and venous limb 50 μm from apex in μm).

Assessment of the microcirculation was conducted according to the current recommendations of the European Society of Intensive Care Medicine[44].

Peripheral microcirculation and edema. To investigate whether microcirculatory disorders resulting from generalized hypoxia cause peripheral edema, we performed ultrasonographic measurements of the tissue thickness of the leg and the forehead in supine position. Measurements were conducted in the evening before the hypoxia tests and immediately after the subject left the hypoxic atmosphere. Tissue thickness was measured repeatedly by ultrasound (10–18 MHz linear-probe) at both the anterior tibia and the midline forehead locations (MyLab25, Esaote, Genova, Italy). In more detail, a self-made mechanical fix ure device was used to avoid meas-urement bias due to hand-held measurements and different surface pressure of the ultrasound probe on tissue. In addition an automatic, Matlab (Matlab 2017b, The MathWorks Inc., Natick, USA) based tissue identifi ation software was used to reliably estimate tissue thickness. The software enables automatic and robust tissue thick-ness estimation from the ultrasound images to minimize analysis biases and improves analysis effici cy dur-ing tissue thickness identifi ation and evaluation. The average tissue thickness was calculated from the central section of the ultrasound image (only 50% of the image at the center) to reduce calculation bias caused by the imaging technique. Tissue thickness was defi ed as the distance between the surfaces of the skin and the tibia and frontal bone, respectively.

Tissue oxygenation. We investigated the effects of hypoxia on oxygen saturation and blood content of the muscles by assessing the tissue saturation index (TSI = $100*(O_2Hb)/(O_2Hb + (HHb)$; O_2Hb = oxygenated hemo-globin, HHb = desoxygenated hemoglobin) and the content of total hemoglobin (THb = $O_2Hb + HHb$) in the vastus lateralis muscle and the tongue by near-infrared spectroscopy (NIRS) at each of the different altitude levels and after the end of the hypoxia tests. For the examination of vastus lateralis muscle we placed a PortaMon device (Artinis Medical Systems, Elst, The Netherlands) over the belly of the muscle. For measuring the tongue

we used the PortaLite device (Artinis Medical Systems, Elst, The Netherlands) placing the sensor part on the tongue after shielding it from saliva fluid using a thin plastic foil.

Statistical analysis.   Statistical analysis was conducted using GraphPad Prism software (GraphPad Software, USA) and SPSS (Version 24.0, SPSSS Inc., USA). Normally distributed data were expressed as mean and standard error of the mean (SEM), whereas not normally distributed data were shown as median and interquartile range (IQR). A Kolmogorov–Smirnov test was used to test the distribution of data for normality. Medians of the data on micro- and macrocirculation were analyzed using a Kruskal–Wallis test with Dunn's post-hoc test, data on the tissue thickness were analyzed using a Wilcoxon signed-rank test, and data on the TSI and THb of the muscles were interpreted by applying a Student's t-test and a Linear Mixed Effects (LME)-analysis. A p value < 0.05 was considered statistically significant.

Ethics approval.   The study was reviewed and approved by the ethics committee of the Heinrich-Heine-University, Düsseldorf, Germany (5925R) and conducted according to the principles of the Declaration of Helsinki and Good Clinical Practice. Informed consent was obtained from all subjects before enrollment.

Conclusions

Exposure to acute normobaric hypoxia results in enhanced perfusion of the central and peripheral microcirculation, as well as an increase in cardiac output. The observed macro- and microcirculatory effects are most likely a result from compensatory mechanisms to ensure adequate tissue perfusion in case of profound hypoxaemia.

Limitations

Since this study was an exploratory study, we did not conduct a statistical power calculation prior to enrollment. Hence, a type one error can not certainly be excluded. Another limitation is that SVR, CO, CPI and SV were investigated using transthoracic impedance cardiography, which is less accurate than invasive methods. Due to the technique of impedance cardiography, which is based on calculations derived from the basic laws of electricity, several limitations and possibilities for bias arise[46,47], which have to be taken into consideration when interpreting the findings of our study. However, invasive methods, such as thermodilution, are labor- and time-intensive and unsuitable for the narrow setting of a hypoxia chamber. Hence, we chose transthoracic impedance cardiography over invasive methods in our study.

Perspectives

Herein, we provide a comprehensive analysis of the effects of acute normobaric hypoxia on the macro- and microcirculation in healthy subjects. Our findings can contribute to the understanding of health and disease, since hypoxia and the following systemic reactions are of utmost relevance in the pathophysiology of various diseases.

Data availability

The datasets generated during and analyzed during the current study are available from the corresponding author on reasonable request.

References

1. Thi le, H. *et al.* Intraaortic balloon support for myocardial infarction with cardiogenic shock. *N. Engl. J. Med.* **367**, 1287–1296 (2012).
2. Jung, C. & Kelm, M. Evaluation of the microcirculation in critically ill patients. *Clin. Hemorheol. Microcirc.* **61**, 213–224 (2015).
3. Fuchs, C., Ertmer, C. & Rehberg, S. Effects of vasodilators on haemodynamic coherence. *Best Pract. Res. Clin. Anaesthesiol.* **30**, 479–489 (2016).
4. Senra Barros, B., Kakkos, S. K., De Maeseneer, M. & Nicolaides, A. N. Chronic venous disease: from symptoms to microcirculation. *Int. Angiol.* **38**, 211–218 (2019).
5. Jung, C., Jung, F. & Kelm, M. The microcirculation in hypoxia: the center of the battlefield for oxygen. *Clin. Hemorheol. Microcirc.* **63**, 169–172 (2016).
6. De Backer, D., Creteur, J., Preiser, J.-C., Dubois, M.-J. & Vincent, J.-L. Microvascular blood flow is altered in patients with sepsis. *Am. J. Respir. Crit. Care Med.* **166**, 98–104 (2002).
7. Damiani, E., Donati, A. & Girardis, M. Oxygen in the critically ill. *Curr. Opin. Anaesthesiol.* **31**, 129–135 (2018).
8. Samuel, J. & Franklin, C. Hypoxemia and Hypoxia. In *Common Surgical Diseases* 391–394 (Springer New York, 2008). https://doi.org/10.1007/978-0-387-75246-4_97.
9. Grocott, M., Montgomery, H. & Vercueil, A. High-altitude physiology and pathophysiology: implications and relevance for intensive care medicine. *Crit. Care* **11**, 203 (2007).
10. Majmundar, A. J., Wong, W. J. & Simon, M. C. Hypoxia-inducible factors and the response to hypoxic stress. *Mol. Cell* **40**, 294–309 (2010).
11. Lee, J. W., Bae, S. H., Jeong, J. W., Kim, S. H. & Kim, K. W. Hypoxia-inducible factor (HIF-1)α: its protein stability and biological functions. *Exp. Mol. Med.* **36**, 1–12 (2004).
12. Dengler, V. L., Galbraith, M. D. & Espinosa, J. M. Transcriptional regulation by hypoxia inducible factors. *Crit. Rev. Biochem. Mol. Biol.* **49**, 1–15 (2014).
13. Balestra, G. M., Legrand, M. & Ince, C. Microcirculation and mitochondria in sepsis: getting out of breath. *Curr. Opin. Anaesthesiol.* **22**, 184–190 (2009).
14. Verratti, V. *et al.* Urinary physiology and hypoxia: a pilot study of moderate-altitude trekking effects on urodynamic indices. *Am. J. Physiol. Physiol.* https://doi.org/10.1152/ajprenal.00333.2019 (2019).
15. Wheatley, K., Creed, M. & Mellor, A. Haematological changes at altitude. *J. R. Army Med. Corps* **157**, 38–42 (2011).

16. Hoon, R. S. *et al.* Effect of high-altitude exposure for 10 days on stroke volume and cardiac output. *J. Appl. Physiol.* **42**, 722–727 (1977).
17. Naeije, R. Physiological adaptation of the cardiovascular system to high altitude. *Prog. Cardiovasc. Dis.* **52**, 456–466 (2010).
18. Savla, J. J., Levine, B. D. & Sadek, H. A. The effect of hypoxia on cardiovascular disease: friend or foe?. *High Alt. Med. Biol.* **19**, 124–130 (2018).
19. Gilbert-Kawai, E. *et al.* Sublingual microcirculatory blood fl w and vessel density in Sherpas at high altitude. *J. Appl. Physiol.* **122**, 1011–1018 (2017).
20. Gilbert-Kawai, E. *et al.* Changes in labial capillary density on ascent to and descent from high altitude [version 1; referees: 2 approved]. *F1000Research* **5**, (2016).
21. Hilty, M. P. *et al.* Recruitment of non-perfused sublingual capillaries increases microcirculatory oxygen extraction capacity throughout ascent to 7126 m. *J. Physiol.* **597**, 2623–2638 (2019).
22. Millet, G. P., Faiss, R. & Pialoux, V. Point: hypobaric hypoxia induces/does not induce different responses from normobaric hypoxia. *J. Appl. Physiol.* **112**, 1783–1784 (2012).
23. Millet, G. P. & Debevec, T. CrossTalk proposal: barometric pressure, independent of, is the forgotten parameter in altitude physiology and mountain medicine. *J. Physiol.* **598**, 893–896 (2020).
24. Zhang, B., Sun, Y., Xia, L. & Gu, J. Time-dependent fl w velocity measurement using two-dimensional color Doppler fl w imaging and evaluation by Hagen–Poiseuille equation. *Australas. Phys. Eng. Sci. Med.* **38**, 755–766 (2015).
25. Calbet, J. A. L. Chronic hypoxia increases blood pressure and noradrenaline spillover in healthy humans. *J. Physiol.* **551**, 379–386 (2003).
26. Calbet, J. A. L. *et al.* Chronic hypoxia increases arterial blood pressure and reduces adenosine and ATP induced vasodilatation in skeletal muscle in healthy humans. *Acta Physiol.* **211**, 574–584 (2014).
27. Barton, C., Ni, Z. & Vaziri, N. D. Blood pressure response to hypoxia: role of nitric oxide synthase. *Am. J. Hypertens.* **16**, 1043–1048 (2003).
28. Dopp, J. M., Reichmuth, K. J. & Morgan, B. J. Obstructive sleep apnea and hypertension: mechanisms, evaluation, and management. *Curr. Hypertens. Rep.* **9**, 529–534 (2007).
29. Casey, D. P. & Joyner, M. J. Compensatory vasodilatation during hypoxic exercise: Mechanisms responsible for matching oxygen supply to demand. *J. Physiol.* **590**, 6321–6326 (2012).
30. Kulandavelu, S., Balkan, W. & Hare, J. M. Regulation of oxygen delivery to the body via hypoxic vasodilation. *Proc. Natl. Acad. Sci. USA* **112**, 6254–6255 (2015).
31. Dinenno, F. A. Skeletal muscle vasodilation during systemic hypoxia in humans. *J. Appl. Physiol.* **120**, 216–225 (2016).
32. Lamah, M., Mortimer, P. S. & Dormandy, J. A. Study of temporal and perfusion physiology of skin capillaries in the dorsum of the foot. *J. Vasc. Res.* **38**, 59–63 (2001).
33. do Amaral Tafner, P. F. *et al.* Recent advances in bedside microcirculation assessment in critically ill patients. *Rev. Bras. Ter. intensive* **29**, 238–247 (2017).
34. Bourdillon, N., Mollard, P., Letournel, M., Beaudry, M. & Richalet, J.-P. Non-invasive evaluation of the capillary recruitment in the human muscle during exercise in hypoxia. *Respir. Physiol. Neurobiol.* **165**, 237–244 (2009).
35. Hanson, W. L. *et al.* Site of recruitment in the pulmonary microcirculation. *J. Appl. Physiol.* **66**, 2079–2083 (1989).
36. Paparde, A., Nēringa-Martinsone, K., Plakane, L. & Aivars, J. I. Nail fold capillary diameter changes in acute systemic hypoxia. *Microvasc. Res.* **93**, 30–33 (2014).
37. Orbegozo -Cortés, D. *et al.* Normobaric hyperoxia alters the microcirculation in healthy volunteers. *Microvasc. Res.* **98**, 23–8 (2015).
38. Kanoore Edul, V. S. *et al.* Quantitative assessment of the microcirculation in healthy volunteers and in patients with septic shock*. *Crit. Care Med.* **40**, 1443–1448 (2012).
39. Edul, V. S. K. *et al.* Dissociation between sublingual and gut microcirculation in the response to a fluid challenge in postoperative patients with abdominal sepsis. *Ann. Intensive Care* **4**, 39 (2014).
40. Koh, I. H. J. *et al.* Microcirculatory evaluation in sepsis. *Shock* **34**, 27–33 (2010).
41. Roberson, R. S. & Bennett-Guerrero, E. Impact of red blood cell transfusion on global and regional measures of oxygenation. *Mt. Sinai J. Med.* **79**, 66–74 (2012).
42. Roach, R. C. *et al.* The 2018 Lake Louise acute mountain sickness score. *High Alt. Med. Biol.* **19**, 4–6 (2018).
43. Massey, M. J. *et al.* Microcirculatory perfusion disturbances in septic shock: results from the ProCESS trial. *Crit. Care* **22**, 308 (2018).
44. Ince, C. *et al.* Second consensus on the assessment of sublingual microcirculation in critically ill patients: results from a task force of the European Society of Intensive Care Medicine. *Intensive Care Med.* **44**, 281–299 (2018).
45. Massey, M. J. *et al.* The microcirculation image quality score: development and preliminary evaluation of a proposed approach to grading quality of image acquisition for bedside videomicroscopy. *J. Crit. Care* **28**, 913–917 (2013).
46. Bernstein, D. P., Lemmens, H. J. M. & Brodsky, J. B. Limitations of impedance cardiography. *Obes. Surg.* **15**, 659–660 (2005).
47. Cotter, G., Schachner, A., Sasson, L., Dekel, H. & Moshkovitz, Y. Impedance cardiography revisited. *Physiol. Meas.* **9**, 817–827 (2006).

Acknowledgments

Author contributions

O.S., Y.H., J.M., M.K., J.Z., J.W., U.L., J.J., J.T. and C.J. conceived and designed the study. N.B., F.H., T.A., T.K., R.B., U.L. and C.J. conducted the experiments, O.S., U.L., M.L. and M.M. analyzed data. M.M., F.H., C.J., O.S., U.L., R.B., J.W. and J.T. wrote the manuscript. All authors read and approved the manuscript.

Funding

Competing interests

Additional information

Reprints and permissions information is available at www.nature.com/reprints.

Publisher's note Springer Nature remains neutral with regard to jurisdictional claims in published maps and institutional affiliations.

ARTICLE   OPEN

Check for updates

Next-generation sequencing analysis of circulating micro-RNA expression in response to parabolic flight as a spaceflight analogue

Peter Jirak[1], Bernhard Wernly[1], Michael Lichtenauer [1], Marcus Franz[2], Thorben Knost[3], Thaer Abusamrah[3], Malte Kelm[3], Nana-Yaw Bimpong-Buta[3] and Christian Jung [3] ✉

Understanding physiologic reactions to weightlessness is an indispensable requirement for safe human space missions. This study aims to analyse changes in the expression of circulating miRNAs following exposure to gravitational changes. Eight healthy volunteers (age: 24.5 years, male: 4, female: 4) were included. Each subject underwent 31 short-term phases of weightlessness and hypergravity induced by parabolic flight as a spaceflight analogue. At baseline, 1 and 24 h after parabolic flight, venous blood was withdrawn. Analysis of circulating miRNAs in serum was conducted by means of next generation sequencing. In total, 213 miRNAs were robustly detected (TPM > 5) by small RNA sequencing in all 24 samples. Four miRNAs evidenced a significant change in expression after adjusting for multiple testing. Only miR-223-3p showed a consistent significant decrease 24 h after parabolic flight compared to baseline values and values at 1 h after parabolic flight. miR-941 and miR-24-3p showed a significant decrease 24 h after parabolic flight compared to 1 h after parabolic flight but not to baseline values. miR-486-5p showed a significant increase 24 h after parabolic flight compared to 1 h after parabolic flight but not to baseline values. A target network analysis identified genes of the p53 signaling pathway and the cell cycle highly enriched among the targets of the four microRNAs. Our findings suggest cellular adaption to gravitational changes at the post-transcriptional level. Based on our results, we suggest a change in cell cycle regulation as potential explanation for adaptational changes observed in space missions.

npj Microgravity (2020)6:31 ; https://doi.org/10.1038/s41526-020-00121-9

INTRODUCTION

Human space missions regained international focus in the last years. Besides an established Mars program by the National Aeronautics and Space Administration (NASA) and a manned mission to the moon planned by both the Chinese space agency and NASA, space flights are also entering the private sector. Therefore space medicine, representing an indispensable requirement for save and successful missions, gained major awareness[1,2].

The adaptation of human organ systems following exposure to microgravity has been investigated in former studies. The most important changes comprise an increase in cardiac output and pulmonary flow as well as changes of the baroreceptor reflex and the cerebrovascular autoregulatory system[3–7]. Long term changes commonly affect bones and muscles atrophy. Additionally, an impairment of lung function and liver function as well as a dysregulation of the immune system have been described[8–11]. A decrease in hemoglobin and an increase in glomerular filtration rate (GFR) and levels of myoglobin were reported by our study group[12]. While adaptive responses have been described recently, the molecular background of these adaptations, necessary to understand the changes in physiology, remains topic to ongoing investigations. First studies showing an alteration of miRNA expression in T-cell activation as well as a change in miRNA signature potentially influencing TGF-Beta response, and fibroblast growth suggest a weightlessness induced change in microRNA (miRNA) expression patterns as a potential explanation[13–15].

miRNAs are small, single stranded noncoding RNAs, usually between 19 and 24 nucleotides long[16]. They are found in both, plants and animals and probably represent a well-preserved system of gene regulation[17]. miRNAs originate from precursor molecules known as primary miRNAs (pri-miRNAs), which can span up to several hundred bases and undergo sequential processing via the ribonuclease III complexes "Drosha" and "Dicer" in the nucleus and cytoplasm, respectively[16,17]. After the processing, mature miRNAs bind to the RNA-induced silencing complex (RISC)[16,17]. Via a complementary sequence also known as the seed region (6–8 nucleotides long), the miRNA can guide the RISC to a target messenger RNA (mRNA), leading to translational repression[16,17], a mechanism referred to as RNA interference[18]. Accordingly, miRNA expression levels represent a key factor in the regulation of gene expression on the posttranscriptional level, influencing cell function and differentiation as well as autoregulation of protein formation[18]. Of note, individual miRNAs can target a huge number of different genes and thus regulate the whole gene expression patterns instead of only one specific gene. Apart from their intracellular role, miRNAs are also present in a cell-free and circulating form[19]. While cell-free miRNAs can be found in different body fluids (e.g., saliva, spine fluid) circulating miRNAs are only found in the blood. Besides a passive leakage following apoptosis, necrosis, and inflammatory processes, the majority of circulating miRNAs depends on different carriers for active secretion to avoid degradation[19,20]. Such carriers comprise protein complexes, lipoproteins as well as extracellular vesicles such as exosomes and microvesicles[19,20]. However, the exact distribution

[1]Clinic of Internal Medicine II, Department of Cardiology, Paracelsus Medical University of Salzburg, Salzburg, Austria. [2]Department of Internal Medicine I, Jena University Hospital, Friedrich Schiller University Jena, Jena, Germany. [3]Division of Cardiology, Pulmonology, and Vascular Medicine, Medical Faculty, University Duesseldorf, Duesseldorf, Germany. ✉email: christian.jung@med.uni-duesseldorf.de

npj nature partner journals

across the carriers mentioned above and their potential influence on the mode of action of the respective miRNAs is still topic to investigation. Circulating miRNAs can be disseminated as autocrine, paracrine, and endocrine signaling molecules within the body[19,21]. Studies have shown that circulating miRNAs are fully functional at their recipient cells, with a similar effect on gene silencing as observed for cellular miRNAs[19,21]. Accordingly, circulating miRNAs represent an important mode of intercellular communication, with the possibility of donor cells being able to influence the gene expression and the microenvironment of distant recipient cells[16]. Several studies have shown that miRNA transcription is cell-type specific and highly dynamic, with transcriptional changes occurring within minutes following a stimulus[22]. However, while the mode of action of circulating miRNAs appears similar to that of cellular miRNAs, their secretion patterns can differ considerably. This fact must be considered when interpreting findings made for circulating miRNAs.

Considering the different physical requirements in microgravity, an involvement of miRNAs in weightlessness-induced changes is assumed and was already described in small studies[13–15]. However, further analysis on the influence of space travel on miRNA regulation is needed to better understand the involved adaptational processes on a post-transcriptional level. In the present study, we hypothesized that exposure to gravitational changes might lead to rapid changes in intracellular miRNA profiles in various cell types, which would alter miRNA release from cells. Accordingly, we aimed for an analysis of circulating miRNA expression following exposure to gravitational changes induced by parabolic flight as a spaceflight analog.

RESULTS

Baseline characteristics

In total, eight study participants were included in the study, four male and four females. The median age was 24.5 years. Baseline characteristics are depicted in Tables 1 and 2.

Table 1. Baseline characteristics + laboratory parameters and miRNA levels at baseline/1 h after parabolic flight/24 h after parabolic flight.			
Parameter	Timepoint	Median	IQR
Male/female sex n (%)	Baseline	4 (50)/4 (50)	
Age (years)	Baseline	24.5	12.5
Weight (kg)	Baseline	80.5	27
Height (cm)	Baseline	177.5	17
Creatinine (µmol/l)	Baseline	72.93	7.52
	1 h after parabolic flight	66.3	8.18
	24 h after parabolic flight	67.63	13.26
GFR (ml/min/1,73 m²)	Baseline	93.95	26.4
	1 h after parabolic flight	106.3	34.45
	24 h after parabolic flight	106.15	16.35
CRP (mg/l)	Baseline	2	1.75
	1 h after parabolic flight	1.5	1.75
	24 h after parabolic flight	1.5	1.75
BNP (pg/ml)	Baseline	9.5	2.75
	1 h after parabolic flight	10	3
	24 h after parabolic flight	9	9
CK (U/l)	Baseline	113	130.75
	1 h after parabolic flight	120	121.5
	24 h after parabolic flight	141	125.5
Myoglobin (µg/l)	Baseline	33.5	24.6
	1 h after parabolic flight	40.35	43.7
	24 h after parabolic flight	30.3	47.2
mir-486-3p (TPM)	Baseline	807.113.74	600.797.18
	1 h after parabolic flight	503.349.41	331.243.28
	24 h after parabolic flight	1.067.561.35	629.299.14
mir-24-3p (TPM)	Baseline	414.17	180.57
	1 h after parabolic flight	554.23	211.55
	24 h after parabolic flight	318.63	99.47
mir-223-3p (TPM)	Baseline	705.58	972.14
	1 h after parabolic flight	665.82	1082.92
	24 h after parabolic flight	182.72	170.26
mir-941 (TPM)	Baseline	953.54	447.29
	1 h after parabolic flight	884.13	702.23
	24 h after parabolic flight	546.08	350.6

µmol/l micromole/liter, *ml/min/1.73 m²*: milliliter/minute/1.73 square meters, *mg/l* milligram/liter, *pg/ml* picogram/milliliter, *U/l* units/litre, *µg/l* microgram/liter, *TPM* tags per million.

Table 2. Baseline characteristics + baseline laboratory parameters of each individual study subject.

Study subject	sex (m/f)	age (years)	weight (kg)	height (cm)	Creatinine (µmol/l)	GFR (ml/min/ 1.73 m²)	CRP (mg/l)	BNP (pg/ml)	CK (U/l)	Myoglobin (µg/l)
P1	m	40	93	176	70.7	108	1	9	65	24.8
P3	m	22	86	188	78.7	107.8	1	9	96	38.7
P5	m	23	95	193	73.4	116	2	9	209	26.7
P7	f	23	54	164	65.4	98.3	1	12	91	24.8
P8	f	25	75	172	69.8	89.6	3	16	182	53.6
P12	f	24	64	174	72.5	86.5	2	11	130	38.3
P14	f	31	69	179	74.3	79.9	5.2	10	56	28.7
P15	m	37	90	190	98.1	75.3	2	9	304	86.7

µmol/l micromole/liter, *ml/min/1.73 m²* milliliter/minute/1.73 square meters, *mg/l* milligram/liter, *pg/ml* picogram/milliliter, *U/l* units/litre, *µg/l* microgram/liter.

Assessment of hemolysis

The degree of hemolysis in serum samples was determined using two different methods: spectrophotometric analysis of free hemoglobin (414 nm) and quantification of the level of miR-451a relative to the level of miR-23a (hemolysis ratio (ΔCq = CqmiR-23a – CqmiR-451a), as reported by Blondal et al.[23]. In our studies both methods were applied. Supplement Fig. 1a presents levels for RNA spike-in and cDNA spike-in determined by RT-qPCR. The data indicate homogenous RNA extraction efficiency across all 24 samples and absence of enzyme inhibition. Next the hemolysis miRNA ratio was determined (Supplement Fig. 1b). None of the 24 samples showed a ratio above the report threshold of ΔCq > 7. Next, OD 414 was determined in all samples. Only one sample exceeded an absorbance of 0.3 but did not show a noticeable increase in the hemolysis miRNA ratio (Supplement Fig. 1c). As potential explanation, lipid contaminants but not hemolysis might have increased the OD414 in this sample. Finally, we compared the levels of miR-23a-3p, miR-451a, the hemolysis ratio and OD414 across the three groups (Supplement Fig. 1d). We did not observe a significant difference in the levels of these biomarker and indicators of hemolysis between the respective groups. Interestingly, a trend towards an increase in miR-23a-3p (not responsive to hemolysis) after 24 h was observed. Together, these results demonstrate that the quality of all 24 serum samples was not impaired by hemolysis and adequate for miRNA profiling by next-generation sequencing.

Expression-analysis

Regarding miRNA analysis, 213 miRNAs were robustly (tags per million (TPM) > 5) detected in all eight subjects for each time point. RNA spike-in recovery was assessed by NGS to confirm homogenous RNA extraction efficiency (Supplement Fig. 2a). A summary of sequencing quality data and RNA classification tables are provided in Supplement Fig. 3a–g.

As depicted in Fig. 1a (principal component analysis, PCA), a change in the distribution of miRNA expression patterns for each respective timepoint was observed following exposure to gravitational changes. Besides, also donor-dependent differences between individuals were observed, as shown in the expression heatmap (Fig. 1b), where samples collected at baseline and 1 h cluster for several subjects (P3, P5, P7, P15, and P8). Figure 1c depicts the same heatmap ordered according to the donor number and time point to better illustrate donor-specific changes in miRNA patterns at 1 and 24 h compared to baseline.

Using the EdgeR GLM model, a significant alteration in miRNA expression (false discovery rate (FDR) < 0.05) was observed for 4 of the 213 miRNAs screened in our analysis 24 h after exposure to gravitational changes compared to baseline values and/or to levels 1 h after parabolic flight (miR-941, miR-24-3p, miR-486-5p,

and miR-223-3p; Figs. 2 and 3). However, no significant differences in miRNA expression were observed between baseline values and levels 1 h after parabolic flight after adjusting for multiple testing (Fig. 4).

As depicted in Fig. 5, after adjusting for multiple testing, miR-223-3p was the only miRNA to show a consistent significant change by means of a decrease 24 h after parabolic flight compared to levels at baseline and 1 h after parabolic flight. miR-24-3p and miR-941 showed a significant decrease at 24 h after parabolic flight compared to levels at 1 h after parabolic flight but not to baseline values. Inversely, miR-486-5p evidenced a significant increase at 24 h after parabolic flight compared to levels at 1 h after parabolic flight but again not to baseline levels. The detailed results of the EdgeR GLM method together with Benjamini–Hochberg adjustment for multiple testing are depicted in Table 3 and Fig. 5. A list of all miRNAs with TPM > 5 that were identified at each time point for each sample is depicted in Supplement Table 1.

In order to provide further evidence for the robustness of the NGS data, we have repeated the analysis of four miRNAs with significant (FDR < 0.05) change by RT-qPCR (Fig. 6). Again, miR223-3p was the only miRNA to show a consistent significant change with a decrease at 24 h after parabolic flight compared to levels at baseline and 1 h after parabolic flight. miR-941 evidenced a significant decrease at 24 h after parabolic flight compared to levels at 1 h after parabolic flight but not to baseline values. miR-486-5p evidenced a significant increase 24 h after parabolic flight compared to levels at 1 h after parabolic flight but not to baseline levels. In contrast, no significant change but only a trend towards a decrease was observed for miR-24-3p at 24 h after parabolic flight compared to levels at 1 h after parabolic flight.

Correlation analysis

In a correlation analysis on baseline characteristics, we found no relevant correlations between miRNA expression and gender, age, or body mass index (BMI). Additionally, no relevant correlations were observed regarding miRNA expression and laboratory parameters. The detailed correlation analysis is given in the supplement Table 2 (miR-486-5p), 3 (miR-24-3p), 4 (miR-223-3p), and 5 (miR-941).

Target network analysis

We performed a target network analysis for the four differentially regulated miRNAs using miRNet. We identified that genes from two KEGG pathways, the p53 signaling pathway ($p < 0.0001$) and the cell cycle ($p < 0.0001$) were highly enriched (hypergeometric test and empirical sampling) among the targets of the four microRNAs (Fig. 7 and Supplement table 6). We observed that TP53 and E2F1 (miR-223-3p and miR-24-3p), and CDK4 (miR-24-3p
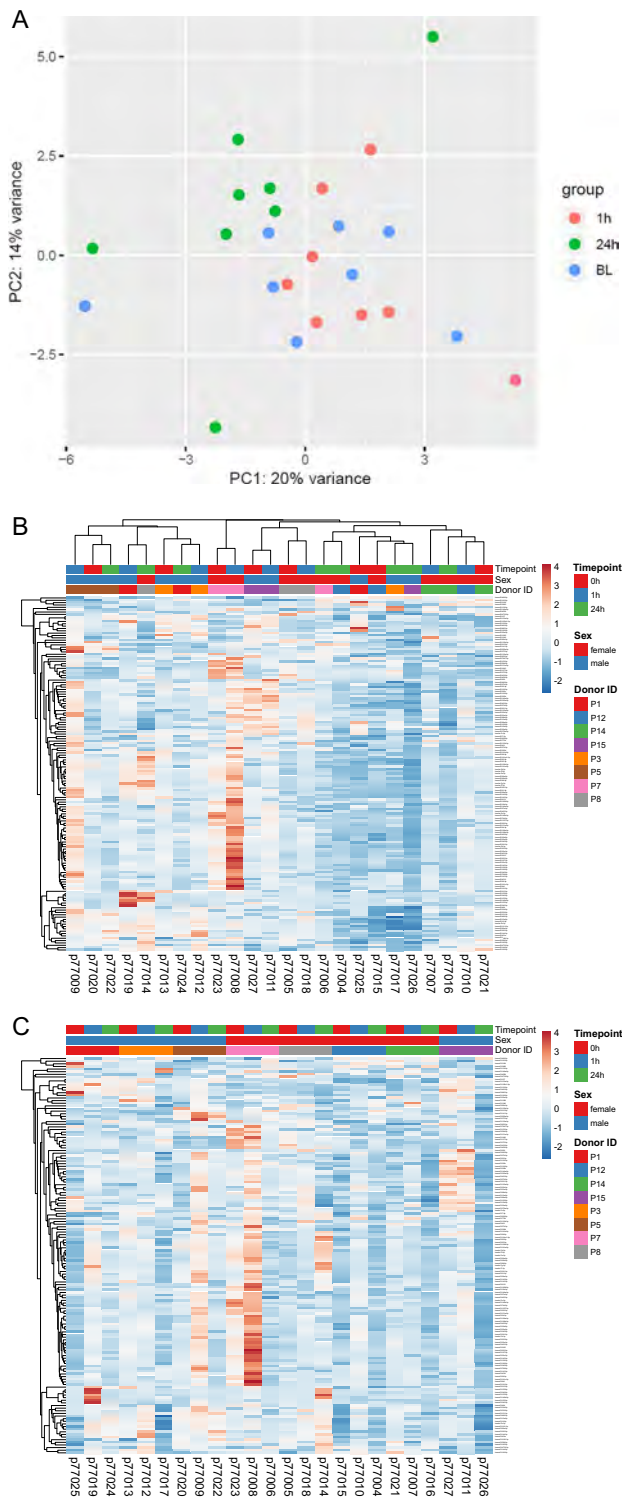
Fig. 1 **Unsupervised data analysis. a** Principal component analysis (PCA) highlights microRNA patterns observed in subjects at baseline (BL), 1 and 24 h after parabolic flight. Data from 213 circulating microRNAs detected in all 24 samples by small RNAseq was used (regularized log tags per million data). The first and second principal component explain 20 and 14% of the variance, respectively. **b** Expression heatmap with unit variance scaling applied to rows (microRNAs). Both rows and columns are clustered using correlation distance and average linkage. Pearson correlation was used as correlation distance. **c** Expression heatmap with unit variance scaling applied to rows (microRNAs). Only rows are clustered using Pearson correlation as measure of distance and average linkage.

and miR-486-5p) were targeted by two of the four miRNAs. All other genes were only targeted by one miRNA. miR-24-3p was found to be the most important regulator of both pathways. A detailed list of genes regulated by at least one of the four miRNAs is given in the Supplement Tables 7a (p53) and 7b (cell cycle).

DISCUSSION

In this study, we present an analysis of the expression profile of circulating miRNAs following exposure to gravitational changes induced by parabolic flight as a space-flight analog. Exposure to weightlessness induces adaptations in autoregulatory mechanisms and functions of virtually all organs, with the cardiovascular system being responsible for most severe complications[3,5,24]. Adaptations to microgravity have been reported in previous studies especially in the cardiovascular field. First studies showing an alteration of miRNA expression in T-cell activation as well as a change in miRNA signature potentially influencing TGF-Beta response and fibroblast growth suggest a weightlessness induced change in micro-RNA expression patterns as a potential explanation[13,14].

In contrast to recent research targeting miRNA expression following spaceflight and exposure to gravitational changes, our study aimed for the analysis of circulating miRNAs from serum. Accordingly, our results reflect the secretion of circulating miRNAs following exposure to gravitational changes but limited conclusion can be drawn with regards to definite intracellular processes[19]. Thus, also direct comparability of our results with former projects is limited[16,19,21].

In our study, four miRNAs, miR-941, miR-24-3p, miR-486-5p, and miR-223-3p evidenced a significant change following exposure to gravitational changes after adjusting for multiple testing. Of note, only miR-223-3p showed a consistent significant decrease 24 h after parabolic flight compared to both baseline levels and levels 1 h after parabolic flight. For the rest of the miRNAs, significant changes were only observed between 1 and 24 h. Accordingly, the effect of these changes is assumed to be lower compared to miR-223-3p. However, the results of the RT-qPCR analyses in our study point emphasize the consistency of our results. Of note, hemolysis was ruled out as a potential confounder by spectrophotometric analysis of free hemoglobin (414 nm) as well as by quantification of the level of miR-451a relative to the level of miR-23a in our samples. Hence, the possibility of our findings being not a directional biological effect, but the product of noise variability is highly unlikely. Thus, given the hypothesis generating design, the miRNAs identified in our analysis might provide important hints towards adaptational processes despite their low dynamic.

Since different timepoints were defined for miRNA analysis, an influence by means of a circadian dynamic of miRNA expression must be considered. For two of the biomarkers mentioned above, a diurnal secretion pattern has been reported, miR-223-3p and miR-24-3p. For miR-223-3p peak-levels were observed at 11:38 a. m., for miR-24-3p peak levels were observed at 12:23 according to Heegaard et al.[25]. However, with regards to a diurnal secretion, it is important to note that the reported circadian changes in miRNA expression are low, and are by far surpassed by the changes observed following exposure to parabolic flight[25]. Thus, changes in miRNA expression during 24 h in normal conditions are unlikely as a relevant confounder[25]. Accordingly, the influence on the other two miRNAs miR-941 and miR-486-5p, which were not included in previous studies on diurnal expression changes is assumed to be negligible.

With regards to previous studies, miR-223-3p is known to be involved in myocardial injury and positively correlates with cardiac apoptosis and oxidative stress through interaction with krüppel-like factor 15 (KLF-15). Furthermore, an inverse correlation of miR-223-3p with an improved cell viability, prevention of cardiomyocyte apoptosis as well as with inhibition of reactive oxygen species
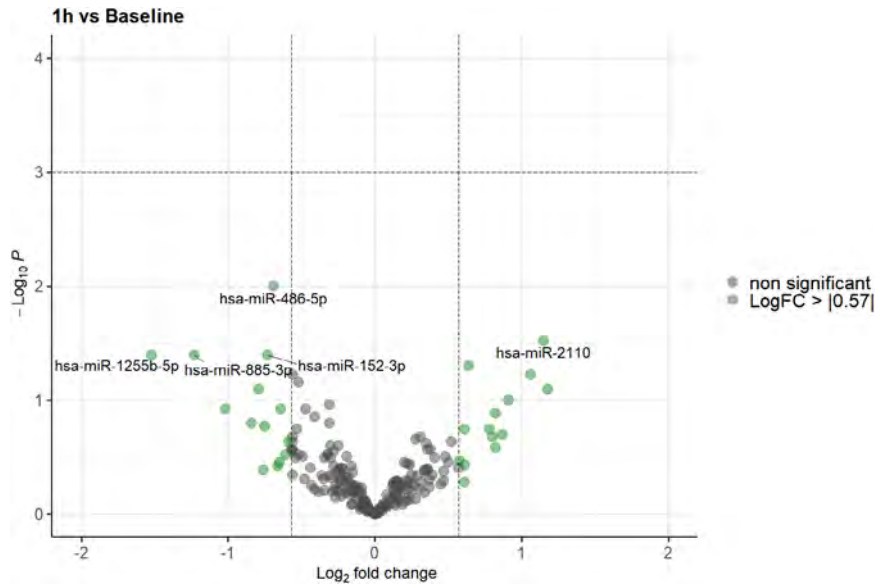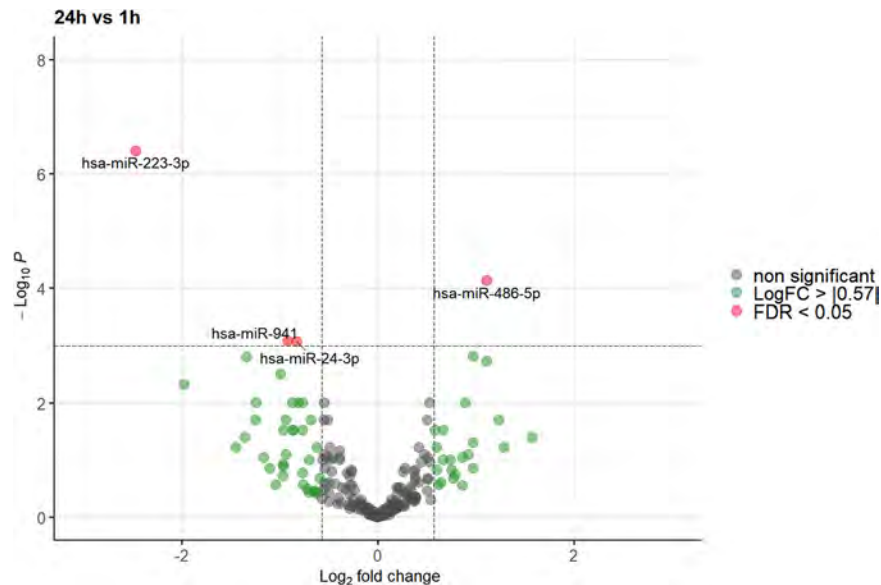
Fig. 2 Volcano plot illustrating the effect of gravitational changes on serum levels of 213 miRNAs detected and quantified by next-generation sequencing. Plot depicts the relation between unadjusted *p*-value (*y*-axis, −log10 transformed) and effect size (*x*-axis, $\log_2$ transformed fold change) for serum microRNA of subjects at 1 h compared to baseline. MicroRNAs with a $\log_2$ fold change > 0.57 (1.5 fold linear change) are indicated in green. MicroRNAs with an adjusted *p*-value (FDR) of < 0.05 are highlighted in red. FDR false discovery rate.
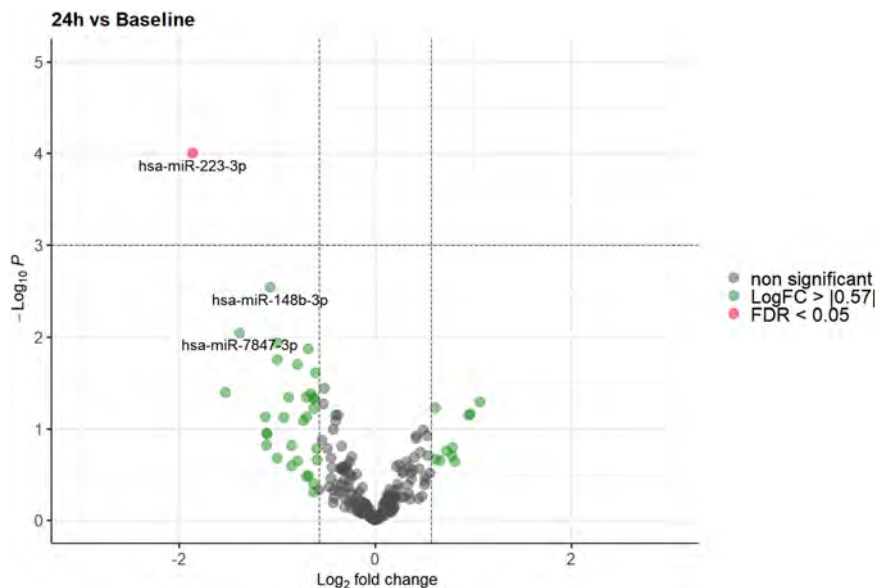
Fig. 3 Volcano plot illustrating the effect of gravitational changes on serum levels of 213 miRNAs detected and quantified by next-generation sequencing. Plot depicts the relation between unadjusted *p*-value (*y*-axis, −log10 transformed) and effect size (*x*-axis, $\log_2$ transformed fold change) for serum microRNA of subjects at 24 h compared to baseline. MicroRNAs with a $\log_2$ fold change > 0.57 (1.5 fold linear change) are indicated in green. MicroRNAs with an adjusted *p*-value (FDR) of < 0.05 are highlighted in red. FDR false discovery rate.

and lipid peroxidation was shown in a former study[26]. Similar, elevated levels of miR-223-3p were reported under simulated microgravity in rats with an inhibitory effect on hepatocyte proliferation trough a cyclin dependent kinase 2/Cullin1 (CDK2/CUL1) signaling pathway[11].

For miR-941, a significant upregulation in acute coronary syndrome was reported[27]. As miR-941 is associated with metabolic processes, inflammation and cell proliferation through its role in insulin-activated, mitogen-activated protein kinase (MAPK)—and T-cell receptor signaling, a connection with atherosclerosis was suggested as a potential explanation[27]. Additionally an involvement in proliferative processes and cell migration was reported in

recent studies[28,29]. miR-941 expression levels have been shown to be elevated in cancer-derived cell lines and human embryonic stem cells and might also be involved in neuronal development[28,29]. A balancing effect of tumor suppressing P73 antisense RNA 1 T (TP73-AS1) by means of a miR-941 sponge was observed, emphasizing its proliferative aspect[28,29].

miR-24-3p is known to be involved in cell proliferation and migration as well as inhibition of apoptosis in several malignancies such as lung cancer, hepatocellular carcinoma, and colon cancer[30–32]. Accordingly, miR-24-3p acts as a regulator of cell proliferation and apoptosis. Another study investigated the role of miR-24-3p in a murine cardiac ischemia-reperfusion model. A

Fig. 4 Volcano plot illustrating the effect of gravitational changes on serum levels of 213 miRNAs detected and quantified by next-generation sequencing. Plot depicts the relation between unadjusted p-value (y-axis, $-\log 10$ transformed) and effect size (x-axis, $\log_2$ transformed fold change) for serum microRNA of subjects at 24 h compared to 1h. MicroRNAs with a $\log_2$ fold change > 0.57 (1.5 fold linear change) are indicated in green. MicroRNAs with an adjusted p-value (FDR) of < 0.05 are highlighted in red. FDR false discovery rate.
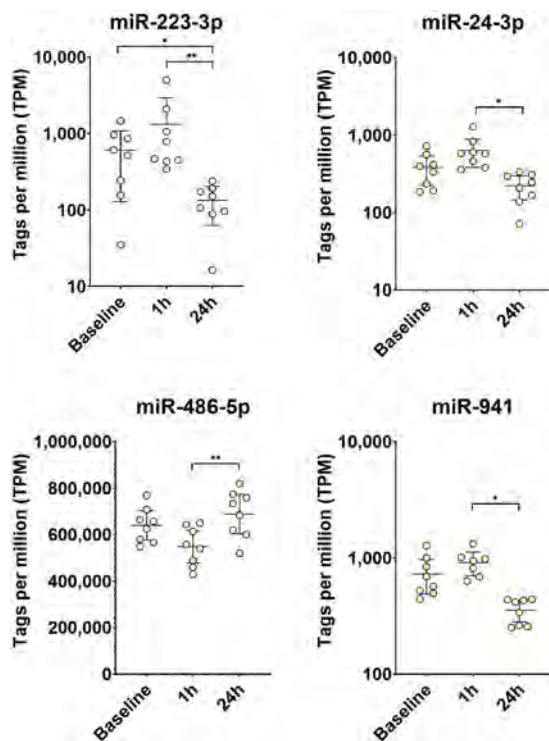
Fig. 5 Levels of miRNAs with significant changes after 24 h compared to baseline or 1 h. EdgeR GLM method together with Benjamini–Hochberg adjustment for multiple testing. *adj-p value < 0.05, **adj-p value < 0.01.

cardioprotective effect of miR-24-3p through an inhibition of receptor-interacting serine/threonine-protein kinase 1 (RIPK1) is suspected, correlating with a significant reduction in infarct size[33]. Furthermore, the same study showed an inverse correlation of miR-24-3p with the rate of apoptosis and the levels of Fas and tumor necrosis factor alpha (TNF-α)[33].

miR-486-5p was investigated in various malignant diseases and mostly acts as a regulator of tumor-suppressor-genes. Negative regulations of NIMA-related kinase 2 (NEK2) in hepatocellular carcinoma and a repression of GRB2-associated-binding protein 2 (GAB2) in nonsmall cell lung cancer have been reported[34,35]. Besides its role in malignant processes, miR-486-5p was investigated in ischemic kidney injury and seems to attenuate ischemic effects in the kidney by targeting the phosphatase and tensin homolog (PTEN) and the Akt pathway[36].

Regarding potential pathways involved in our findings discussed above, a target network analysis identified that genes from two KEGG pathways, the p53 signaling pathway and the cell cycle were highly enriched among the targets of the four microRNAs[37]. We observed that TP53 and E2F1 (miR-223-3p and miR-24-3p), and CDK4 (miR-24-3p and miR-486-5p) were targeted by two miRNAs. All other genes were targeted by only one miRNA. Accordingly, the interaction between the four miRNAs in the regulation of the p53 signaling pathway and the cell cycle are considered to be low. However, despite the high enrichment it must be pointed out that both pathways mentioned above are highly studied and annotated. Thus, they have a high likelihood of being linked with a selected group of miRNAs.

Interestingly, the findings of our study are in part consistent with former findings of a reduction in cell proliferation and a higher rate of apoptosis of in vitro and in vivo studies on changes in miRNA expression following exposure to microgravity. In vitro an altered expression pattern of miRNAs in human peripheral blood lymphocytes was shown to increase apoptosis and decrease cell proliferation following exposure to microgravity[38]. A recent study reported a decrease in TGF-Beta response and a change in miRNA signature as potential regulators of weightlessness induced changes in rodents. Above all, a reduction in cell proliferation and a higher rate of apoptosis was reported, matching prior in vitro studies[13]. Furthermore, an upregulation of miR-21 was reported to limit immune-response through a regulation of T-cell activation in microgravity[14]. A change in the expression pattern of immune-related miRNAs was also reported as a potential link to skeletal muscle atrophy in another investigation[39]. Of note, all studies mentioned above were conducted in cellular miRNAs.

Table 3. miRNA expression analysis.

	Abundance	1 h vs. Baseline			24 h vs. Baseline			24 h vs. 1 h		
microRNA ID	Avg TPM	logFC	p value	FDR	logFC	p value	FDR	logFC	p value	FDR
hsa-miR-223-3p	563	0,61	0.18	0.98	−1.86	<0.01	0.02	−2.47	<0.01	<0.01
hsa-miR-24-3p	364	0.31	0.21	0.98	−0.52	0.04	0.62	−0.83	<0.01	0.04
hsa-miR-486-5p	698.389	−0.69	0.01	0.98	0.42	0.13	0.78	1.11	<0.01	0.01
hsa-miR-941	686	0.24	0.37	0.98	−0.68	0.01	0.58	−0.92	<0.01	0.04

Avg TPM average tags per million, logFC log fold change, FDR false discovery rate.
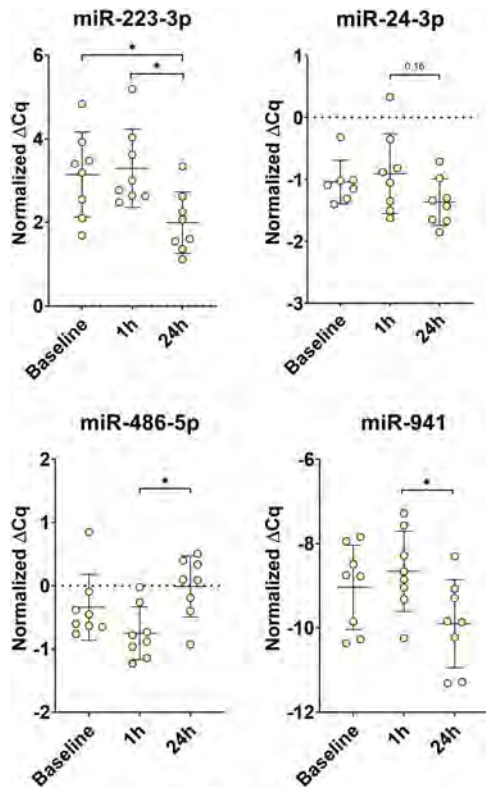
Fig. 6 Technical verification of NGS results by RT-qPCR. Three miRNAs were selected for RT-qPCR analysis. Normalized delta Cq-values (ΔCq) values to the RNA spike-in as internal standard are shown. *adj-p value < 0.05, **adj-p value < 0.01.

Considering the novelty but also the hypothesis generating character of our study, we can only speculate about the potential adaptational processes following exposure to gravitational changes due to the hypothesis generating design of our study. Despite limited comparability with former studies, our results suggest an involvement in cardioprotective mechanisms as well as myocardial strain and the susceptibility for ischemic damage. Furthermore, cell-proliferation and apoptosis and possibly also the immune-system might be influenced by gravitational changes. As a rationale, a change in activation of DNA-repair mechanisms, a change in apoptotic processes and in the regulation of cell cycle progression and cell fate decision can be taken into consideration[40,41]. Potential implications of our findings are to be further validated and elucidated. However, analysis of the expression of circulating miRNAs might prove of further relevance for space medicine in the future, similar to the application of miRNA

expression patterns in other extreme situations as for example in intensive care patients[42].

With regards to the limitations of the present study, the hypothesis generating character must be emphasized. While parabolic flight was reported as a suitable space flight analog, the respective effects of microgravity and hypergravity cannot be distinguished properly in this study. Additionally, as we focused on circulating miRNAs, comparability with former studies conducted on cellular miRNAs is limited. Therefore, the results obtained must be interpreted with care. Additionally, a large part of research on miRNAs focuses on malignancies, thus complicating the interpretation of our results. On the other hand, the strength of the study is its novelty in a unique setting.

In conclusion, the present data indicate an alteration of expression patterns of circulating miRNAs following exposure to gravitational changes. We identified that genes from two KEGG pathways, the p53 signaling pathway and the cell cycle were highly enriched among the targets of the four microRNAs. This might suggest a change in cell cycle regulation as a potential explanation for weightlessness induced changes observed in former studies. Together, these findings point towards an adaption to gravitational changes already at the post-transcriptional level even after short term exposure, providing an important framework for future studies in this area.

METHODS

Participants

Eight healthy participants were enrolled in this study. All voluntary participants were recruited and included at the University Clinic Düsseldorf after written informed consent. The study was conducted in accordance with the Declaration of Helsinki. The study protocol was approved by the German Ethics Committee (Medical Faculty of the University Hospital Duesseldorf, Germany) and by the French Ethics Committee (Medical Faculty of the University of Caen). The inclusion criteria were defined as: age >18 years; airworthiness; cardiorespiratory health; spontaneous circulation; signed informed consent. The exclusion criteria were defined as: history of primary cardiovascular and respiratory diseases or regular intake of medication except for oral contraceptives, missing or withdrawal of informed consent, insufficient requirements for airworthiness and pregnancy. Further details have been published in a study-outline paper[43].

Parabolic flight

The term "Parabolic flight" denominates a special aerial manoeuvre, in which the aircraft follows the trajectory of a parabola. By means of this manoeuvre, short phases of weightlessness and hypergravity can be induced. After starting at steady flight (1 g), an up to 47° ascent initiates a phase of hypergravity (1.8 g). After the climb, the plane is decelerated and directed into descent to follow the trajectory. In this state, a phase of weightlessness is achieved (0 g). With the plane tilting forward, an up to 45° descent is initiated, again inducing a phase of hypergravity (1.8 g), before re-entering the steady flight (1 g)[44]. Each of these phases averages 20–25 s, respectively.
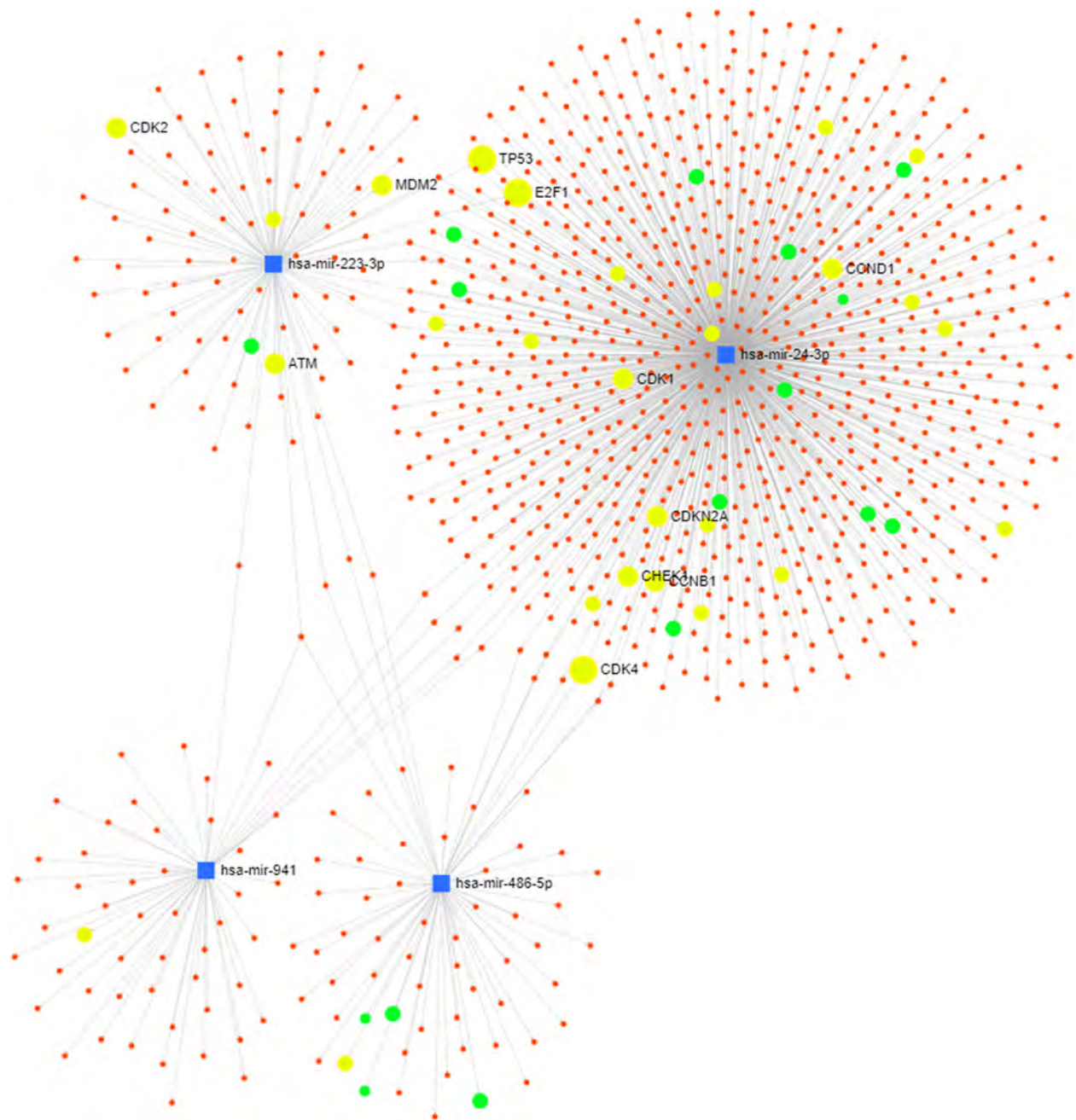
Fig. 7 Target network analysis. Target network analysis for the four differentially regulated miRNAs—p53 signaling pathway (blue), cell cycle (green).

Set-up
The present study was performed in the course of the 31st Parabolic Flight Campaign (PFC) of the German space agency (Deutsches Zentrum für Luft- und Raumfahrt - DLR) conducted by the company NoveSpace, which took place from February 26th to March 11th 2018, in Bordeaux, France. The aircraft used in this campaign was a modified Airbus A-310. The PFC consisted of four flight days, with 31 parabolic flight manoeuvres per flight day. Each study subject participated in one complete flight day. In all participants serum samples were withdrawn before entering the plane 1 h prior parabolic flight (baseline 08:00 ± 0.75 h), 1 h after parabolic flight (13:00 ± 1.0 h) and 24 h after parabolic flight 08:00 ± 0.75 h). At each of the time points, serum samples were collected with individual punctures. For each blood withdraw, the following materials were used: BD vacutainer tubes (Becton Dickinson, Mountain View, CA), 3 SST tubes (Reference # 367957, Tube size: 75 × 13 mm, draw volume: 3.5 ml), 1 SST tube (Reference # 367955, Tube size: 100 × 13 mm, Draw volume: 5 ml. After

completion of each blood-draw, blood was stored at room-temperature for 3 min. Afterwards, centrifugation at 2000×g for 7 min was conducted. Following centrifugation, serum samples aliquots were frozen and stored at −80 °C until further analysis.

Total RNA extraction
Serum samples were thawed at room temperature followed by centrifugation at 12,000×g for 5 min at 4 °C to remove any cellular debris. Extraction was conducted by use of the miRNA easy QIAgen kit. For homogenization, 200 µl of serum were mixed with 1000 µl Qiazol and 1 µl of a mix of three synthetic spike-in controls (Qiagen, Germany). After a 10-min incubation at room temperature, 200 µl chloroform were added to the lysates followed by cooled centrifugation at 12,000×g for 15 min at 4 °C. Precisely 650 µl of the upper aqueous phase were mixed with 7 µl glycogen (50 mg/ml) to enhance precipitation. Samples were transferred to a miRNeasy mini

column, and RNA was precipitated with 750 μl ethanol followed by automated washing with RPE and RWT buffer in a QiaCube liquid handling robot. Finally, total RNA was eluted in 30 μl nuclease free water and stored at −80 °C until further analysis.

Small RNA sequencing

Equal volumes of total RNA (2 μl) were used for small RNA library preparation using the CleanTag smallRNA library preparation kit (TriLink Biotechnologies, US). Homogeneity of RNA extraction efficiencies across all samples was confirmed by RT-qPCR (Supplement Fig. 2B). Adapter-ligated libraries were amplified using barcoded Illumina reverse primers in combination with the Illumina forward primer. Twenty-four PCR cycles were used for library preparation according to the manufacturers recommendation for low RNA input samples. A pool consisting of all 24 sequencing libraries was prepared by mixing samples at equimolar rates on the basis of a DNA-1000 high-sensitivity bioanalyzer results (Agilent, CA). The DNA library pool was gel-purified to enrich for microRNAs with an insert size of 18–24 nt, corresponding to a library size of approximately 145 bp (Supplement Fig. 2B).

Sequencing was performed on an Illumina HiSeq 2500 with 50 bp single-end runs. Overall quality of the next-generation sequencing data was evaluated automatically and manually with fastQC v0.11.8[45] and multiQC v1.7[46]. Reads from all passing samples were adapter trimmed and quality filtered using cutadapt v2.3[47] and filtered for a minimum length of 17 nt. Mapping steps were performed with bowtie v1.2.2[48] and miRDeep2 v2.0.1.2[49], whereas reads were mapped first against the genomic reference GRCh38.p12 provided by Ensembl[50] allowing for two mismatches. Those reads showing a genome alignment were subsequently mapped against miRbase v22.1[51], filtered for miRNAs of hsa only, allowing for one mismatch. For a general RNA composition overview, nonmiRNA mapped reads were mapped against RNAcentral[52] and then assigned to various RNA species of interest.

Raw and normalized data were uploaded to NCBI Gene Expression Omnibus[53] and are accessible through GEO Series accession number GSE147380.

Assessment of hemolysis

As lysis of red blood cells (hemolysis) could confound the analysis of circulating microRNAs due to the release of miRNAs from red blood cells, an assessment of hemolysis was conducted[54]. In order to determine the degree of hemolysis two methods were applied: First, 2 μl of serum were loaded on a NanoDrop spectrophotometer to determine absorbance at 414 nm (free hemoglobin). Secondly, miR-23a-3p and miR-451a were analyzed by RT-qPCR and the hemolysis miRNA ratio according to Blondal et al.[23] was calculated: $\Delta Cq = CqmiR\text{-}23a\text{-}3p - CqmiR\text{-}451a$.

Reverse transcription and qPCR (RT-qPCR)

The identical RNA samples that were used for NGS analysis, were used for results verification by RT-qPCR. Starting from total RNA samples, cDNA was synthesized using the miRCURY RT Kit (Qiagen, Germany). Reaction conditions were set according to recommendations by the manufacturer. In total, 2 μl of total RNA were used per 10 μl reverse transcription (RT) reaction. To monitor RT efficiency and presence of impurities with inhibitory activity, a synthetic RNA spike-in (cel-miR-39-3p) was added to the RT reaction. Validated LNA-enhanced forward and reverse miRCURY primer assays for all targets, including spike-in controls, were obtained from Qiagen. PCR amplification was performed in a 96-well plate format in a Roche LC480 II instrument (Roche, Germany) using miRCURY SYBR® Green mix (Qiagen, Germany) with the following settings: 95 °C for 10 min, 45 cycles of 95 °C for 10 s, and 60 °C for 60 s, followed by melting curve analysis. To calculate the cycle of quantification values (Cq-values), the second derivative method was used. Cq-values were normalized to the RNA spike-in control level, by subtracting the individual miRNA Cq-value from the RNA Spike-In Cq, thus obtaining delta-Cq (ΔCq) values that were used for the analysis.

Target network analysis

Target network analysis was conducted using miRNet (www.mirnet.ca), a public and web-based tool that allows to visualize the intersections between individual miRNA regulatory functions based on miRNA-target interaction data from 11 databases[55]. miRbase miRNA IDs for the differentially regulated miRNAs were uploaded. Since cell-free circulating miRNAs were analyzed no tissue background was selected ("exosomes" were not selected since most miRNAs in serum are in protein complexes). A "hypergeometric test" and "empirical sampling" were performed to identify gene pathways enriched among the identified targets.

Statistics

Statistical analysis of preprocessed NGS data was done with R v3.6 and the packages pheatmap v1.0.12, pcaMethods v1.78 and genefilter v1.68. Differential expression analysis with edgeR v3.28[56] used the quasi-likelihood negative binomial generalized log-linear model (GLM) functions provided by the package. FDR correction was performed to adjust for multiple testing, and a cut-off of FDR < 5% was applied[57]. No paired testing model in EdgeR was applied. Significance of differentially regulated miRNAs (according to EdgeR) was determined by using EdgeR GLM method together with Benjamini–Hochberg adjustment for multiple testing. An FDR of <5% was considered statistically significant. Repeated measures ANOVA analysis combined with Tukey's multiple comparison test was used to assess RT-qPCR data. Regarding baseline characteristics and laboratory parameters, analysis was conducted using SPSS 25 (IBM SPSS Statistics, USA). Non-normally distributed data are given as median + interquartile range (IQR). Categorical data are given in number (%). Correlation analysis were performed using Spearman's rank correlation coefficient. A p-value < 0.05 was considered statistically significant for comparison of baseline characteristics and correlation analysis. All tests were two-sided.

Reporting summary

Further information on research design is available in the Nature Research Reporting Summary linked to this article.

DATA AVAILABILITY

The datasets of raw and normalized generated and analysed during the current study are were uploaded to NCBI Gene Expression Omnibus[53] and are accessible through GEO Series accession number GSE147380.

REFERENCES

1. Yaqub, F. Space travel: medicine in extremes. *Lancet Respir. Med.* **3**, 20–21 (2015).
2. Hughes-Fulford, M. To infinity… and beyond! Human spaceflight and life science. *Faseb J.* **25**, 2858–2864 (2011).
3. Convertino, V. A. Status of cardiovascular issues related to space flight: Implications for future research directions. *Respir. Physiol. Neurobiol.* **169**, 19 (2009).
4. Hughson, R. L. et al. Cardiovascular regulation during long-duration spaceflights to the International Space Station. *J. Appl. Physiol.* **112**, 719–727 (1985).
5. Lathers, C. M. et al. Acute hemodynamic responses to weightlessness in humans. *J. Clin. Pharm.* **29**, 615–627 (1989).
6. Norsk, P., Asmar, A., Damgaard, M. & Christensen, N. J. Fluid shifts, vasodilatation and ambulatory blood pressure reduction during long duration spaceflight. *J. Physiol.* **593**, 573–584 (2015).
7. Blaber, A. P., Zuj, K. A. & Goswami, N. Cerebrovascular autoregulation: lessons learned from spaceflight research. *Eur. J. Appl. Physiol.* **113**, 1909–1917 (2013).
8. Pietsch, J. et al. The effects of weightlessness on the human organism and mammalian cells. *Curr. Mol. Med.* **11**, 350–364 (2011).
9. Crawford-Young, S. J. Effects of microgravity on cell cytoskeleton and embryogenesis. *Int. J. Dev. Biol.* **50**, 183–191 (2006).
10. Zuj, K. A. et al. Impaired cerebrovascular autoregulation and reduced CO(2) reactivity after long duration spaceflight. *Am. J. Physiol. Heart Circ. Physiol.* **302**, 6 (2012).
11. Chen, Y. et al. Upregulation of miR-223 in the rat liver inhibits proliferation of hepatocytes under simulated microgravity. *Exp. Mol. Med.* **49**, 80 (2017).
12. Bimpong-Buta, N. Y. et al. Blood parameter analysis after short term exposure to weightlessness in parabolic flight. *Clin. Hemorheol. Microcirc.* **17**, CH-189314 (2018).
13. Beheshti, A., Ray, S., Fogle, H., Berrios, D. & Costes, S. V. A microRNA signature and TGF-beta1 response were identified as the key master regulators for spaceflight response. *PLoS ONE* **13**, e0199621 (2018).

14. Hughes-Fulford, M., Chang, T. T., Martinez, E. M. & Li, C. F. Spaceflight alters expression of microRNA during T-cell activation. *Faseb J.* **29**, 4893–4900 (2015).

15. Zhang, Y. et al. Transient gene and microRNA expression profile changes of confluent human fibroblast cells in spaceflight. *Faseb J.* **30**, 2211–2224 (2016).

16. Armand-Labit, V. & Pradines, A. Circulating cell-free microRNAs as clinical cancer biomarkers. *Biomol. Concepts* **8**, 61–81 (2017).

17. Mirna, M. et al. MicroRNAs in inflammatory heart diseases and sepsis-induced cardiac dysfunction: a potential scope for the future? *Cells* **8**, 1352 (2019).

18. Zeng, Y. Principles of micro-RNA production and maturation. *Oncogene* **25**, 6156–6162 (2006).

19. Cortez, M. A. et al. MicroRNAs in body fluids–the mix of hormones and bio-markers. *Nat. Rev. Clin. Oncol.* **8**, 467–477 (2011).

20. Cui, M. et al. Circulating microRNAs in cancer: potential and challenge. *Front. Genet.* **10**, 626 (2019).

21. Bell, E. & Taylor, M. A. Functional roles for exosomal microRNAs in the tumour microenvironment. *Comput. Struct. Biotechnol. J.* **15**, 8–13 (2016).

22. Reichholf, B. et al. Time-resolved small RNA sequencing unravels the molecular principles of MicroRNA homeostasis. *Mol. Cell* **75**, 756–768 (2019).

23. Blondal, T. et al. Assessing sample and miRNA profile quality in serum and plasma or other biofluids. *Methods* **59**, 2 (2013).

24. Limper, U. et al. Interactions of the human cardiopulmonary, hormonal and body fluid systems in parabolic flight. *Eur. J. Appl. Physiol.* **114**, 1281–1295 (2014).

25. Heegaard, N. H. et al. Diurnal variations of human circulating cell-free Micro-RNA. *PLoS ONE* **11**, e0160577 (2016).

26. Tang, Q. et al. Absence of miR-223-3p ameliorates hypoxia-induced injury through repressing cardiomyocyte apoptosis and oxidative stress by targeting KLF15. *Eur. J. Pharm.* **841**, 67–74 (2018).

27. Bai, R. et al. miR-941 as a promising biomarker for acute coronary syndrome. *BMC Cardiovasc. Disord.* **17**, 017–0653 (2017).

28. Hu, H. et al. Recently evolved tumor suppressor transcript TP73-AS1 functions as sponge of human-specific miR-941. *Mol. Biol. Evol.* **35**, 1063–1077 (2018).

29. Hu, H. Y. et al. Evolution of the human-specific microRNA miR-941. *Nat. Commun.* **3**, 1–10 (2012).

30. Yan, L. et al. miR-24-3p promotes cell migration and proliferation in lung cancer by targeting SOX7. *J. Cell Biochem.* **119**, 3989–3998 (2018).

31. Fan, J. C., Zeng, F., Le, Y. G. & Xin, L. LncRNA CASC2 inhibited the viability and induced the apoptosis of hepatocellular carcinoma cells through regulating miR-24-3p. *J. Cell Biochem.* **119**, 6391–6397 (2018).

32. Dong, X. et al. MiR-24-3p enhances cell growth in hepatocellular carcinoma by targeting metallothionein 1M. *Cell Biochem. Funct.* **34**, 491–496 (2016).

33. Tan, H. et al. MicroRNA-24-3p attenuates myocardial ischemia/reperfusion injury by suppressing RIPK1 expression in mice. *Cell Physiol. Biochem.* **51**, 46–62 (2018).

34. Fu, S. J. et al. MiR-486-5p negatively regulates oncogenic NEK2 in hepatocellular carcinoma. *Oncotarget* **8**, 52948–52959 (2017).

35. Yu, S., Geng, S. & Hu, Y. miR-486-5p inhibits cell proliferation and invasion through repressing GAB2 in non-small cell lung cancer. *Oncol. Lett.* **16**, 3525–3530 (2018).

36. Vinas, J. L. et al. Transfer of microRNA-486-5p from human endothelial colony forming cell-derived exosomes reduces ischemic kidney injury. *Kidney Int.* **90**, 1238–1250 (2016).

37. Kanehisa, M. & Goto, S. KEGG: kyoto encyclopedia of genes and genomes. *Nucleic Acids Res.* **28**, 27–30 (2000).

38. Girardi, C. et al. Integration analysis of microRNA and mRNA expression profiles in human peripheral blood lymphocytes cultured in modeled microgravity. *Biomed. Res. Int.* **296747**, 23 (2014).

39. Teodori, L., Costa, A., Campanella, L. & Albertini, M. C. Skeletal muscle atrophy in simulated microgravity might be triggered by immune-related microRNAs. *Front. Physiol.* **9**, 1926 (2019).

40. Engeland, K. Cell cycle arrest through indirect transcriptional repression by p53: I have a DREAM. *Cell Death Differ.* **25**, 114–132 (2018).

41. Barnum, K. J. & O'Connell, M. J. Cell cycle regulation by checkpoints. *Methods Mol. Biol.* 0888-0882_0882 (2014).

42. Masyuk, M. et al. Prognostic relevance of serum lactate kinetics in critically ill patients. *Intensive Care Med.* **45**, 55–61 (2019).

43. Bimpong-Buta, N. Y. et al. Analysis of human microcirculation in weightlessness: Study protocol and pre-study experiments. *Clin. Hemorheol. Microcirc.* **70**, 119–127 (2018).

44. Shelhamer, M. Parabolic flight as a spaceflight analog. *J. Appl Physiol.* **120**, 1442–1448 (1985).

45. Andrews, S. FastQC: a quality control tool for high throughput sequence data http://www.bioinformatics.babraham.ac.uk/projects/fastqc/ (2010).

46. Ewels, P., Magnusson, M., Lundin, S. & Kaller, M. MultiQC: summarize analysis results for multiple tools and samples in a single report. *Bioinformatics* **32**, 3047–3048 (2016).

47. Martin, M. Cutadapt removes adapter sequences from high-throughput sequencing reads. *EMBnet* https://doi.org/10.14806/ej.17.1.200 (2011).

48. Langmead, B., Trapnell, C., Pop, M. & Salzberg, S. L. Ultrafast and memory-efficient alignment of short DNA sequences to the human genome. *Genome Biol.* **10**, 2009–2010 (2009).

49. Friedlander, M. R., Mackowiak, S. D., Li, N., Chen, W. & Rajewsky, N. miRDeep2 accurately identifies known and hundreds of novel microRNA genes in seven animal clades. *Nucleic Acids Res.* **40**, 37–52 (2012).

50. Zerbino, D. R. et al. Ensembl 2018. *Nucleic Acids Res.* **46**, D754–D761 (2018).

51. Griffiths-Jones, S. The microRNA registry. *Nucleic Acids Res.* **32**, D109–D111 (2004).

52. The RNAcentral Consortium. RNAcentral: a hub of information for non-coding RNA sequences. *Nucleic Acids Res.* **47**, D221–D229 (2018).

53. Barrett, T. et al. NCBI GEO: archive for functional genomics data sets—update. *Nucleic Acids Res.* **41**, D991–D995 (2012).

54. Kirschner, M. B. et al. Haemolysis during sample preparation alters microRNA content of plasma. *PLoS ONE* **6**, 1 (2011).

55. Fan, Y. et al. miRNet—dissecting miRNA-target interactions and functional associations through network-based visual analysis. *Nucleic Acids Res.* **44**, 21 (2016).

56. Robinson, M. D., McCarthy, D. J. & Smyth, G. K. edgeR: a Bioconductor package for differential expression analysis of digital gene expression data. *Bioinformatics* **26**, 139–140 (2010).

57. Benjamini, Y. & Hochberg, Y. Controlling the false discovery rate: a practical and powerful approach to multiple testing. *J. R. Stat. Soc. Ser. B* **57**, 289–300 (1995).

AUTHOR CONTRIBUTIONS

P.J.: Conceptualization, data curation, formal analysis, investigation, methodology, project administration, resources, software, validation, visualization, writing—original draft, writing—review and editing; M.L.: Conceptualization, data curation, formal analysis, resources, software, writing—review and editing; B.W.: data curation, formal analysis, investigation, methodology, resources, software, statistics, visualization, writing—original draft, writing—review and editing; M.F.: Conceptualization, resources, validation, visualization, writing—original draft, writing—review and editing; T.K.: Data curation, investigation, project administration, resources, software, writing—original draft, writing—review and editing; T.A.: Data curation, investigation, project administration, resources, software, writing—original draft, writing—review and editing; M.K.: Conceptualization, methodology, resources, writing—review and editing; N.-Y.B.-B.: Conceptualization, data curation, funding acquisition, investigation, methodology, project administration, writing—original draft, writing—review and editing; C.J.: Conceptualization, data curation, funding acquisition, formal analysis, investigation, methodology, project administration, resources, validation, visualization, writing—original draft, writing—review and editing.

COMPETING INTERESTS

The authors declare no competing interests.

ADDITIONAL INFORMATION

Supplementary information is available for this paper at https://doi.org/10.1038/s41526-020-00121-9.

Correspondence and requests for materials should be addressed to C.J.

Reprints and permission information is available at http://www.nature.com/reprints

Publisher's note Springer Nature remains neutral with regard to jurisdictional claims in published maps and institutional affiliations.

Premature ventricular contractions with inferior axis: how can the electrocardiogram help?

Konstantinos Iliodromitis, Sebastian Robl, Nana-Yaw Bimpong-Buta & Harilaos Bogossian

ONLINE
FIRST

Springer

Springer

EP-Quiz

Premature ventricular contractions with inferior axis: how can the electrocardiogram help?

Konstantinos Iliodromitis[1] · Sebastian Robl[1] · Nana-Yaw Bimpong-Buta[1] · Harilaos Bogossian[1,2]

[1] Klinik für Kardiologie und Rhythmologie, Evangelisches Krankenhaus Hagen-Haspe, Hagen, Germany

[2] Universität Witten/Herdecke, Witten, Germany

Case presentation

A 65-year-old patient was referred to the authors' department for symptomatic palpitations and exertional dyspnea NYHA III. His electrocardiogram (ECG) revealed a left bundle branch block and monomorphic premature ventricular contractions (PVC) (◘ Fig. 1). The 24-h Holter revealed a high degree of PVC burden of 40%.

An electrophysiological study for PVC ablation was scheduled, after exclusion of relevant structural heart disease. Based on the acquired morphology of the PVC in the ECG (◘ Fig. 1), which is the most probable site of origin of the PVC?

1. Lateral right ventricular outflow tract (RVOT)
2. Septal RVOT
3. Aortic coronary cusp
4. Aortomitral continuity (AMC)
5. Left ventricular (LV) free wall

Fig. 1 ▲ A 12-lead electrocardiogram with bigeminus: (**a**) paper speed 25 mm/s, (**b**) paper speed 50 mm/s
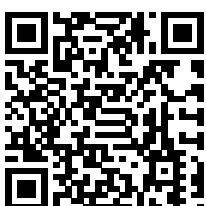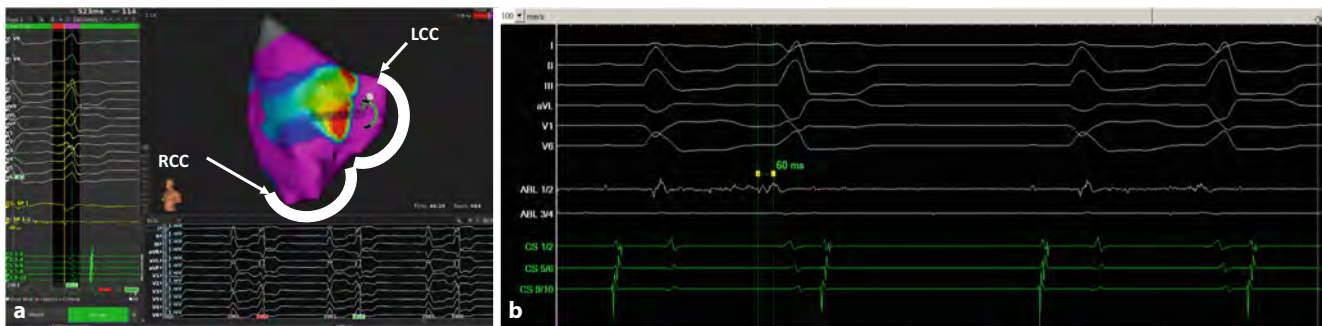
Fig. 2 ▲ **a** Three-dimensional mapping of the artic root with right coronary cusp (*RCC*) and left coronary cusp (*LCC*), (**b**) earliest ventricular signal on the ablation catheter at 60 ms
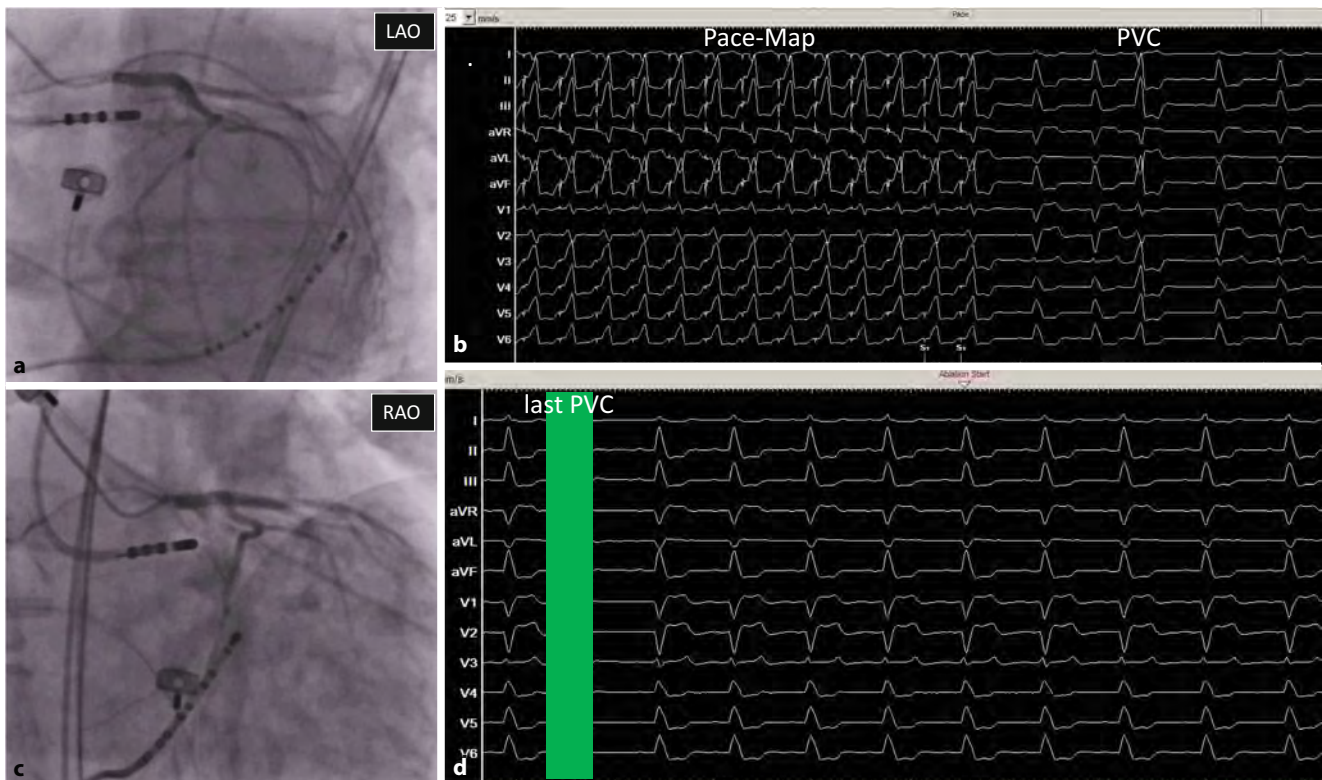
Fig. 3 ▲ (**a, c**) Coronary angiography of the left coronary artery and relation to the ablation catheter at the successful ablation site, (**b**) perfect pace map with 98% congruence to the clinical ventricular extrasystole, (**d**) ablation effect of the first irrigated ablation with immediate abolishment of the extrasystole. *LAO* left anterior oblique, *RAO* right anterior oblique, *PVC* premature ventricular contraction

Correct answer: 3

Answer

The correct answer is (3): the aortic coronary cusp. Three-dimensional (3D) electroanatomic mapping was implemented in this case. Local activation time (LAT) and pace mapping were used. The LAT mapping revealed a site of earliest activation at the left coronary cusp (LCC) of the aorta, with earliest activation 60 ms before beginning of the QRS complex in the surface ECG (☐ Fig. 2). Additionally, the unipolar signal at the site of the LCC exhibited a deep QS wave (☐ Fig. 2). Pace mapping at this site had a 98% correlation with the clinical PVC, thus confirming its origin (☐ Fig. 3b). Due to the proximity of the site of origin of the PVC to the ostium of the left main stem (LMS) coronary artery and prior to irrigated radiofrequency (RF) ablation, a coronary angiogram was performed to assess the distance between the tip of the ablation catheter and the LMS ostium for safety reasons (☐ Fig. 3a, c). Adequate space was confirmed, and 5 s after the application of RF energy the PVC disappeared (☐ Fig. 3d). A waiting period of 30 min followed, without recording any further activity of the PVC. Drug provocation with intravenous isoprenaline and external stimulation followed, without induction of the PVCs. The procedure was successfully completed.

Discussion

In patients without structural heart disease, PVCs are in general benign and may arise from multiple anatomical sites of the right or left ventricle. Nevertheless, this dysrhythmia may be severely symptomatic and result in impairment of the left ventricular ejection fraction if left untreated. RF ablation is a therapeutic option with high efficacy and safety when performed in experienced centers. Prior to invasive therapy, an in-depth evaluation of the 12-lead ECG is important for an initial assessment of the origin of the PCV and ablation strategy [1].

The morphology of the clinical PVC from the obtained ECG shows an inferior axis (positive QRS in leads II, III and aVF). This is suggestive of a site in proximity to an outflow tract of a heart chamber, but also from the upper portion of the left ventricular inflow tract [2]. The next step is to evaluate the R/S transition in the precordial leads. For a first estimation, the use of the Yoshida Index is very helpful ($SV_2:RV_3 \leq 1.5$ is predictive for a left-sided origin) [3]. In the present case, the $SV_2:RV_3$ is 0.5, making a right-sided origin comparatively unlikely. Localization of the PVC from the anterior RVOT should have been accompanied with a much later transition of the ECG in the precordial leads.

Here one can see an r/s wave in leads V_1 and V_2 and an R wave from V_{3-6}. Additionally, at 148 ms, the width of the QRS complex of the PVC is relatively narrow, and a slight notching at its peak can be observed (◻ Fig. 1b.). On the basis of the current findings, one can exclude the LV free wall and the AMC as the origin, since a right bundle branch block (RBBB) morphology or a positive concordance over the precordial leads, respectively, would be expected. The third step is to evaluate lead I. This is very helpful for differentiating between right and left outflow tract, but can be misleading if the precordial transition is not taken into account. A negative lead I is almost always suggestive for an origin from the left heart chamber, whereas a positive lead I is almost always suggestive for an origin from the right heart chamber. Exceptions can be a more cranial origin, where RVOT PVCs may present a more negative lead I, whereas PVC from the septal LVOT at the level of the right coronary cusps commonly present a positive lead I. This can be explained from "overlapping" of the two anatomical structures from the midline of the chest. In contrast, the LCC is located on the left side of the midline, generating a negative QRS in lead I when PVCs arise from this cusp.

Corresponding address

PD Dr. Harilaos Bogossian
Klinik für Kardiologie und Rhythmologie,
Evangelisches Krankenhaus Hagen-Haspe
Brusebrinkstraße 20, 58135 Hagen, Germany
bogossian@evk-haspe.de

Declarations

References

1. Fries B, Johnson V, Rutsatz W, Schmitt J, Bogossian H (2021) Localization of ventricular premature contractions by 12-lead ECG. Herzschrittmachertherapie Elektrophysiol 32(1):21–26
2. Bogossian H, Frommeyer G, Ninios I, Hasan F, Nguyen QS, Karosiene Z et al (2016) Spot diagnosis of inferior axis and concordant R-pattern predicts left ventricular inflow tract tachycardia: ablation from the great cardiac vein of an underdiagnosed entity. Int J Cardiol 214:175–179
3. Yoshida N, Yamada T, McElderry HT, Inden Y, Shimano M, Murohara T et al (2014) A novel electrocardiographic criterion for differentiating a left from right ventricular outflow tract tachycardia origin: the V2S/V3R index. J Cardiovasc Electrophysiol 25(7):747–753

Contents lists available at ScienceDirect

IJC Heart & Vasculature

journal homepage: www.journals.elsevier.com/ijc-heart-and-vasculature
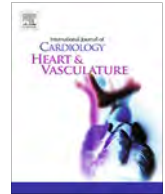
QTc evaluation in patients with bundle branch block

Harilaos Bogossian [a,b,c,*], Dominik Linz [c], Jordi Heijman [c], Nana-Yaw Bimpong-Buta [a],
Dirk Bandorski [d], Gerrit Frommeyer [e], Damir Erkapic [f], Melchior Seyfarth [b,g], Markus Zarse [b], Harry J. Crijns [c]

[a] Department of Cardiology and Rhythmology, Ev. Krankenhaus Hagen, Hagen, Germany
[b] Department of Cardiology, University Witten/Herdecke, Witten, Germany
[c] Department of Cardiology, Maastricht University Medical Center (MUMC+) and Cardiovascular Research Institute Maastricht (CARIM), Maastricht, the Netherlands
[d] Faculty of Medicine, Semmelweis University Campus Hamburg, Hamburg, Germany
[e] Division of Electrophysiology, Department of Cardiovascular Medicine, University of Münster, Münster, Germany
[f] Diakonie Klinikum Siegen, Department of Cardiology and Electrophysiology, Siegen, Germany
[g] Department of Cardiology, Helios Klinikum Wuppertal, Germany

ARTICLE INFO

ABSTRACT

Proper measurement of the QT interval on the 12-lead body-surface ECG is challenging in daily practice. Even more difficult is its correct estimation in the presence of repolarization abnormalities, arrhythmias or bundle-branch blocks (BBB). The QT interval results from two parts of the ECG: (1) the QRS complex, describing the excitation of the ventricles and (2) the JT interval, describing the repolarisation of the ventricles. Prolongation of the QRS width – like in the presence of BBB – entails prolongation of the QT interval, making the estimation of the true repolarisation time challenging. The US recommendations for the standardization and interpretation of the ECG suggest focusing on the JT interval in presence of BBB. However, in clinical practice physicians have become more familiar with the interpretation of QT-interval measurements than with the interpretation of the JT Interval.

In the last decade, a simple formula for the estimation of the "modified QT interval" in the presence of left or right BBB has been developed and evaluated. In this formula, the modified QT interval is calculated by subtracting 50% of the length of the BBB-QRS from the measured QT interval ($QT_m = QT_{BBB} - 50\% QRS_{BBB}$). Subsequently, rate-correction formula should be applied as usual. In this review, we discuss the determination of the QT-interval in the presence of BBB and summarize the origin and application of the modified QT-interval formula.

© 2020 The Author(s). Published by Elsevier B.V. This is an open access article under the CC BY-NC-ND license (http://creativecommons.org/licenses/by-nc-nd/4.0/).

Contents

---

* Corresponding author at: Chefarzt der Klinik für, Kardiologie und Rhythmologie, Ev. Krankenhaus Hagen, Brusebrinkstr. 20, 58135 Hagen, Germany.
  E-mail address: bogossianh@esv.de (H. Bogossian).

1. Introduction

From 2007 to 2009, the American Heart Association (AHA), the American College of Cardiology Foundation (ACCF) and the Heart Rhythm Society (HRS) published a series of recommendations for the standardization and interpretation of the ECG [1–5]. The fourth section of this series deals with the ST segment, the T wave, the U wave and the QT interval [1]. The QT interval describes the depolarization and repolarization of the ventricles (normal values in women <460 ms, in men <450 ms) [1]. QT-interval prolongation can result from alterations in both components: Depolarization disorders lead to the broadening of the QRS complex, whereas repolarization disorders lead to the prolongation of the JT time. The importance of QT prolongation due to repolarization disorders has been shown in several large studies [6,7].

2. Arrhythmogenic risk in the setting of QT-interval prolongation

During the last two decades different mechanisms of arrhythmogenesis have been investigated. In the setting of prolonged repolarization inheritable arrhythmogenic disorders due to gene mutations were identified as an important cause of arrhythmogenesis. In these disorders, loss-of-function mutations in repolarizing K^+ channels, e.g., long-QT syndrome type 2 (LQT2) due to the rapid delayed rectifier (IKr) channel malfunction, or gain-of-function mutations in depolarizing sodium (Na^+) or calcium (Ca^{2+}) channels lead to excessive repolarization prolongation. This repolarization prolongation can result in triggered activity by promoting the genesis of early afterdepolarizations and is often spatially heterogeneous, providing a substrate for conduction block and reentrant arrhythmias. Various cardiovascular and non-cardiovascular drugs can also cause relevant QT prolongation, also [8]. This increase in QT time, in turn, is associated with an increased risk of arrhythmia. In this context, Torsade de pointes tachycardia in particular can occur, particularly in the presence of additional risk factors such as bradycardia or hypokalemia [9].

Although many alternative measures have been suggested (e.g., T-peak-Tend; T-wave right slope; beat-to-beat variability of QT intervals) and the correlation between QT-interval and arrhythmogenesis is imperfect, the QT interval remains the most commonly used indicator of arrhythmogenic risk [10].

Besides the arrhythmogenic aspects, QT interval serves also as a predictor for cardiovascular events. In the multi-ethnic study of Atherosclerosis (MESA-Study), Beinart et al. analyzed the prognostic association between the baseline QT interval and the incidence of cardiovascular events in participants without known cardiac diseases. An increase in the baseline QT interval (for every 10 ms) was associated with increased incidence for heart failure, cardiovascular disease events and stroke [11]. Compared to patients with QT intervals below 500 ms, patients with QT intervals above 500 ms are exposed to a higher short-term mortality risk, independent from the underlying comorbidities, [12]. Additionally, QT-prolongation has been described as a prognostic parameter in Non-ST-Elevation Myocardial Infarction (NSTEMI) patients. Rajvanshi et al. defined the corrected QT Interval above 468 ms as a cut-off value to predict poor prognosis for the occurrence of major adverse cardiac events (MACE) with a sensitivity of 72% and a specificity of 61% [13].

3. Assessing QT-interval in the presence of bundle-branch block

Widening of the QRS complex – in the setting of left bundle-branch block (LBBB) or right bundle-branch block (RBBB) – leads to QT-interval prolongation without significant alterations to the

repolarization duration [14]. Therefore, the AHA / ACCF / HRS recommendations for standardized ECG interpretation recommend the use of the JT time to assess the repolarization. However, in daily clinical practice, the measurement of the JT time is not yet common. Moreover, tables for rate adjustment of the JT interval are lacking. However, given the strong dependence of repolarization duration on heart rates, an adequate rate correction seems essential for correct interpretation of potential pathological alterations, especially in the presence of right or left BBB [1].

A bundle brunch block is commonly associated with extended prolonged QTc interval. However, in this setting, the QT interval, which is easily overestimated, is the result of a prolongation of depolarisation and not primarily caused by repolarisation. Interpretation in chronic LBBB with consecutive electrical remodelling is more challenging: unloading of LV areas results in shortening of repolarisation, whilst increased loading in late activated regions may cause lengthening of repolarisation due to downregulation of the slow delayed rectifier channel (IKs).

Besides the suggestion to evaluate the JT interval in patients with LBBB as an alternative risk-stratification method in the presence of LBBB [1], several formulas were developed the last years for avertable estimation of the QT interval [14–20] (Table 1). A different approach in pacemaker recipients is the subtraction of 50 ms of the QTc$_{LBBB}$ as a rule of thumb. However this application may lead to a relevant overestimation of up to 80 ms [21].

For easier QT time assessment in the presence of BBB, recent studies have proposed a formula that corrects for prolongations of QT intervals due to QRS widening (due to pacing, LBBB or RBBB) (Figs. 1 and 2) [16].

3.1. Development of different formulas for modified QT estimation in the presence of LBBB

The correct judgment of the QT interval in the presence of LBBB was focus of several research activities in the past. In 1973, Tablot et al. suggested subtraction of a fixed time interval: QT minus 60 ms in LBBB and minus 30 ms in RBBB or QTc minus 70 ms and minus 40 ms, respectively. As the QRS duration in patients with a BBB varies from 120 ms to more than 200 ms, this formula runs the risk to overestimate or underestimate the modified QT interval in accordance to the QRS width. A more precise formula was developed and described by Rautaharju et al. and covers all kinds of ventricular conduction defects (LBBB, RBBB and intraventricular delay) and the complete heart-rate spectrum (Table 1). However, the complexity of the formula, does not offer a good solution for daily clinical practice. In 2014, a further formula was developed for estimation of the QT interval in presence of LBBB [16] (Fig. 2). In a proof-of-concept study, the alterations of the QRS complex and QT intervals were analyzed during right ventricular (RV) pacing in patients with inherent normal – not widened – QRS complex, who presented for an electrophysiological study and ablation. Thus, the documented LBBB in these patients was due to RV pacing, providing an opportunity to compare QT times and JT times in the presence or absence of simulated LBBB. The results of these comparisons were subsequently translated into a formula for the modified QT interval (QT_m). This formula suggested subtracting a particular QRS amount from the measured QT interval (in detail: QT_m = QT_{LBBB} – 48.5% of QRS_{LBBB}). Subsequently, this formula was simplified for easier applicability in daily practice (to: QT_m = QT_{LBBB}- 50% of QRS_{LBBB}) [16].

In a second step, the formula was analyzed in patients with intrinsic LBBB by comparing ECGs of patients presenting with both a narrow QRS complex and an LBBB [22]. For this purpose, two patient collectives were examined. First, patients with inherent intermittent LBBB and second, patients with peri- or postprocedural LBBB after a trans-venous percutaneous aortic valve

Table 1

Overview of the different QT-Formulas. *applicability of this formula in RBBB was shown in a following publication [26].**further assessment performed in four following publications [22,23,25,26]. ***further assessment performed in the same publication [20].

Year	Author	Journal	fixed Formula	additional HR-correction	Applicable in LBBB and RBBB	primary assessment patients [n]	further assessment patients [n]
1973	Talbot S.	BHJ	LBBB: QTm = QT − 60 ms; QTmc = QT − 70 ms;	Yes/No	No	95	–
1973	Talbot S.	BHJ	RBBB: QTm = QT − 30 ms; QTmc = QT − 40 ms	Yes/No	No	93	–
2004	Rautaharju PM. et al.	Am J Cardiol	$QT_{RR,QRS} = QT − 155 \times (60/heart\ rate − 1) − 0.93 \times (QRS − 139) + k$; [k = −22 ms for men and − 34 ms for women]	No	Yes	1251	–
2014	Bogossian H. et al.	Heart Rhythm	QTm = QT − 48.5%QRS; simplified: QTm = QT − 50% QRS	Yes	Yes*	60	480**
2016	Tabatabaei P. et al.	Res Cardiovasc Med	$QTmc = (0.786 \times QT) + (0.305 \times CL) − 188.733$	No	No	101	–
2017	Wang B. et al.	JCE	$QTm = QT – (0.86 \times QRS – 71)$	Yes	No	62	–
2018	Yankelson L. et al.	J of Electrocardiol	male: QTmc = QTc-QRS + 95 ms; female: QTmc = QTc-QRS + 88 ms	No	No	48	–
2019	Tang JKK. Et al.	Canad J Cardiol	$QTmc = 0.945 \times QTc(RBK) − 26$	No	No	17	2610***
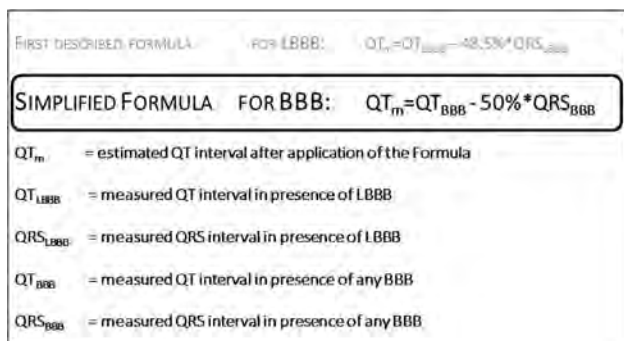
Fig. 1. Formula for easy correction of QT interval in presence of LBBB and the simplified formula for BBB.
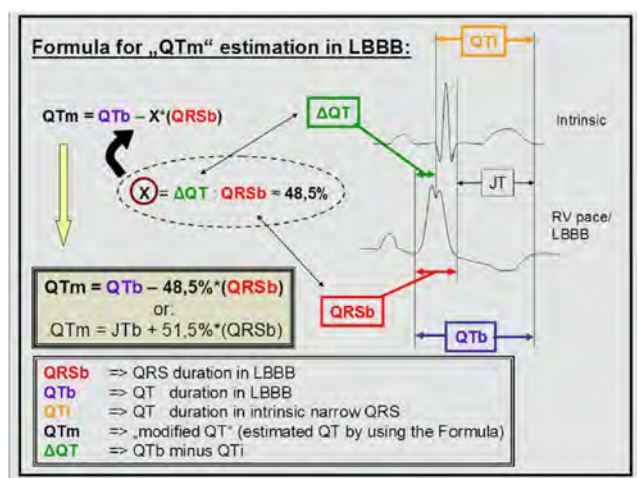
Fig. 2. Figure from the first Publication in patients with artificial LBBB. (Reprinted from Publication: New formula for evaluation of the QT interval in patients with left bundle branch block. Heart Rhythm, 2014. 11(12): p. 2273–2277; Bogossian, H., et al., with permission from Elsevier.)

implantation (TAVI) [22]. These patients served as their own control groups, since they had both ECGs with a narrow QRS and ECGs with LBBB. In both groups (15 patients each), the acquired mean native QTc intervals and those calculated by the formula during LBBB were not significantly different.

Another patient population with intermittent artificial LBBB are patients with implanted pacemakers. A further step in the analysis of the formula was therefore to check the applicability of the formula in these patients [23]. In total, 163 patients with a cardiac one- or two-chamber pacemaker were included in this prospective, multicentre observational study. Although there was a slight systematic overestimation of the true QT interval by the BBB correction formula, the overall agreement was high [23]. Subsequently, several additional formulas followed and were used in a similar way to the prior assessment methods. Like for the development of the Bogossian-formula in 2014, Tabatabaei et al. (2016) and Wang et al. (2017) used also the method of artificial LBBB during right ventricular pacing in patients who underwent electrophysiological studies [17,18]. Finally, Yankelson et al. (2018) and Tang et al. (2019) used the second assessment-method of the Bogossian-formula and analyzed patients with intermittent LBBB or with LBBB after *trans*-aortic valve replacement (TAVR) [19,20,22].

3.2. Applicability of the LBBB formula in heart failure patients

LBBB is a common ECG feature in patients with heart failure due to impaired left-ventricular (LV) function. Hence, the applicability
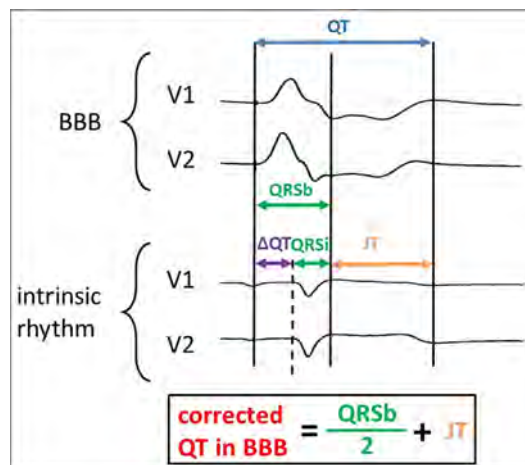

Fig. 3. Figure from the last Publication in patients with artificial RBBB. (Reprinted from Publication "How to measure QT-interval in right bundle branch block and bifascicular block". Clin Cardiol, 2020; Erkapic D et al.)

of the formula was also verified for these patients. As patients with severe LV dysfunction typically have extensive structural and electrical remodeling leading to an increased risk of sudden cardiac death [24], this observation has great implications for daily medical practice. LV dysfunction might persist despite optimal drug therapy. In these cases, the implantation of a cardioverter defibrillator (ICD) is recommended. The adequate functioning of the defibrillator lead (placed in the right ventricle) is checked telemetrically during regular follow-ups. Part of the routine examination is the measurement of the lead threshold. During this maneuver, the right ventricle is stimulated, resulting in a typical change of the ECG with artificial LBBB. Again, taking advantage of this setting, the modified QT formula could be assessed for measurement of QT times in the presence and absence of provoked LBBB, for this patient cohort [25].

3.3. Applicability of the LBBB formula in RBBB

As presented in Table 1, just the formulas by Rautaharju and Bogossian were studied regarding the applicability in the presence of RBBB. In the study by Ratauharju, 593 out of 1251 patients presented a RBBB pattern. Erkapic et al. investigated the applicability of the Bogossian-formula to assess the QT interval in patients with RBBB. Based on a similar method of design as for the development of the LBBB-formula, the appropriate use during RBBB was further investigated [26]. In particular, during left-sided EP procedures an artificial RBBB (with left anterior or left posterior hemiblock) was induced by left ventricular pacing. Again, the same patient collective could serve as control group by comparing their initial ECGs (with narrow QRS complexes) to the generated ECGs during LV pacing (with broadened QRS-complexes in the course of artificial RBBB) (Fig. 3). In this prospective multicenter observational study, 71 patients were included. The mean difference between intrinsic QTc and corrected QTc during RBBB was -3 ± 24 ms and -6 ± 25 ms for RBBB with left posterior and left anterior hemiblock, respectively [26], thus demonstrating the applicability of the LBBB formula in patients with RBBB.

3.4. Combination of BBB formula and heart rate correction formula

The estimation of the QT interval in the presence of BBB is significantly more complex at extreme heart rates (i.e., heart-rates other than 60 bpm and especially in bradycardia or tachycardia). This was a relevant aspect in the Publications of Rautaharju, Tang and Erkapic [14,20,26]. In the Study of Rautahrju et al., rate- and gender-adjusted JT interval was in focus during the formula investigation. Tang et al. focuses for the rate correction on the spline QT formula (QTcRBK) [27], which was earlier described by the same working group.

During the first description of the Bogossian-formula a rate-correction was not necessary, as the paced QRS complexes were generated just a few beats faster than the intrinsic heart rate [16]. In the subsequent publications, the paced rhythm was significantly higher than the intrinsic heart rate [22,23,25], making heart-rate correction indispensable in these cohorts. Initially, the Bazett formula was applied, resulting in a substantial deviation in corrected intervals whenever the heart-rate deviation was high. A regression analysis revealed a linear relationship between the deviation of the intrinsic QTc from the modified QTc and the difference between the intrinsic heart rate and paced heart rate [23]. A fast heart rate resulted in an increasing difference between intrinsic and modified QTc. Recently, in the manuscript evaluating the LBBB-formula in RBBB-QRS-complexes, the authors applied three different heart rate correction formulas (Bazett, Fridericia, and Hodges) after QT-correction (due to QRS width) [26]. This comparison revealed that the smallest deviation was achieved by the Hodges-formula, intermediate deviation by the Fridericia-formula and the greatest deviation by Bazett's formula.

4. Conclusions and clinical implications

Different QRS-QT-formulas have recently been introduced in order to identify easier patients with LBBB or RBBB at high risk for ventricular arrhythmias due to true prolonged QT duration. None of the formulas has the power to unmask the real QT time behind the BBBs. Incorporating more complex formulas (like that by Rautaharju) in automated ECG analysis programs may help to keep deviations as small as possible and increase comparability in the assessment of QT intervals during BBB. Furthermore, better heart rate corrections (as described by Rabkin and Tang) could lead to further reduce heart rate related deviations.

However, in routine clinical practice, easy formulas (as described by Bogossian) for the estimation of the modified QTc in the presence of LBBB, RBBB or in pacemaker patients with LBBB-like ECG patterns remain reliable tools for a quick appraisal. Additional rate correction should in this case preferably be performed by Hodges' formula (or alternatively using the Fridericia formula). Bazett's formula seems to lead to the greatest deviation of the expected values.

5. Limitation

In the presence of BBB, the estimation of the real repolarization time from the ECG remains very challenging. The JT interval seems to be the best representative value for this evaluation. However, in clinical practice the experience with the JT interval is limited. The estimation of the exact and real QT interval in the presence of BBB needs further experimental and clinical investigations.

Declaration of Competing Interest

The authors declare that they have no known competing financial interests or personal relationships that could have appeared to influence the work reported in this paper.

Acknowledgement

References

[1] P.M. Rautaharju et al., AHA/ACCF/HRS recommendations for the standardization and interpretation of the electrocardiogram: part IV: the ST segment, T and U waves, and the QT interval: a scientific statement from the American Heart Association Electrocardiography and Arrhythmias Committee, Council on Clinical Cardiology; the American College of Cardiology Foundation; and the Heart Rhythm Society: endorsed by the International Society for Computerized Electrocardiology, Circulation 119 (10) (2009) e241–e250.

[2] P. Kligfield et al., Recommendations for the standardization and interpretation of the electrocardiogram: part I: The electrocardiogram and its technology: a scientific statement from the American Heart Association Electrocardiography and Arrhythmias Committee, Council on Clinical Cardiology; the American College of Cardiology Foundation; and the Heart Rhythm Society: endorsed by the International Society for Computerized Electrocardiology, Circulation 115 (10) (2007) 1306–1324.

[3] J.W. Mason et al., Recommendations for the standardization and interpretation of the electrocardiogram: part II: electrocardiography diagnostic statement list a scientific statement from the American Heart Association Electrocardiography and Arrhythmias Committee, Council on Clinical Cardiology; the American College of Cardiology Foundation; and the Heart Rhythm Society Endorsed by the International Society for Computerized Electrocardiology, J. Am. Coll Cardiol. 49 (10) (2007) 1128–1135.

[4] E.W. Hancock et al., AHA/ACCF/HRS recommendations for the standardization and interpretation of the electrocardiogram: part V: electrocardiogram changes associated with cardiac chamber hypertrophy: a scientific statement from the American Heart Association Electrocardiography and Arrhythmias Committee, Council on Clinical Cardiology; the American College of Cardiology Foundation; and the Heart Rhythm Society. Endorsed by the International Society for Computerized Electrocardiology, J. Am. Coll. Cardiol. 53 (11) (2009) 992–1002.

[5] G.S. Wagner et al., AHA/ACCF/HRS recommendations for the standardization and interpretation of the electrocardiogram: part VI: acute ischemia/infarction: a scientific statement from the American Heart Association Electrocardiography and Arrhythmias Committee, Council on Clinical Cardiology; the American College of Cardiology Foundation; and the Heart Rhythm Society. Endorsed by the International Society for Computerized Electrocardiology, J. Am. Coll. Cardiol. 53 (11) (2009) 1003–1011.

[6] J.B. Nielsen et al., Risk prediction of cardiovascular death based on the QTc interval: evaluating age and gender differences in a large primary care population, Eur. Heart J. 35 (20) (2014) 1335–1344.

[7] S.G. Priori et al., Risk stratification in the long-QT syndrome, N Engl. J. Med. 348 (19) (2003) 1866–1874.

[8] P. Indraratna et al., Measurement and management of QT interval prolongation for general physicians, J. Gen Int. Med. 35 (3) (2020) 865–873.

[9] W. Shimizu et al., Bradycardia-dependent early afterdepolarizations in a patient with QTU prolongation and torsade de pointes in association with marked bradycardia and hypokalemia, Pacing Clin. Electrophysiol. 14 (7) (1991) 1105–1111.

[10] J. Heijman, H.J. Crijns, T-wave right slope provides a new angle in the prediction of drug-induced ventricular arrhythmias: editorial to: "Electrocardiographic Predictors of Torsadogenic Risk During Dofetilide or Sotalol Initiation: Utility of a Novel T Wave Analysis Program" by Sugrue A. et al. Cardiovasc Drugs Ther 29(5) (2015) 411–3.

[11] R. Beinart et al., The QT interval is associated with incident cardiovascular events: the MESA study, J Am Coll Cardiol 64 (20) (2014) 2111–2119.

[12] C. Gibbs et al., QT prolongation predicts short-term mortality independent of comorbidity, Europace 21 (8) (2019) 1254–1260.

[13] S. Rajvanshi et al., Correlation of corrected QT interval with quantitative cardiac troponin-I levels and its prognostic role in Non-ST-elevation myocardial infarction, Int. J. Cardiol. 240 (2017) 55–59.

[14] P.M. Rautaharju et al., Assessment of prolonged QT and JT intervals in ventricular conduction defects, Am. J. Cardiol. 93 (8) (2004) 1017–1021.

[15] S. Talbot, QT interval in right and left bundle-branch block, Br. Heart J. 35 (3) (1973) 288–291.

[16] H. Bogossian et al., New formula for evaluation of the QT interval in patients with left bundle branch block, Heart Rhythm 11 (12) (2014) 2273–2277.

[17] P. Tabatabaei et al., Assessment of QT and JT intervals in patients with left bundle branch block, Res. Cardiovasc. Med. 5 (2) (2016) e31528.

[18] B. Wang et al., A new formula for estimating the true QT interval in left bundle branch block, J. Cardiovasc. Electrophysiol. 28 (6) (2017) 684–689.

[19] L. Yankelson et al., New formula for defining "normal" and "prolonged" QT in patients with bundle branch block, J. Electrocardiol. 51 (3) (2018) 481–486.

[20] J.K.K. Tang, S.W. Rabkin, Determination of the QT interval in left bundle branch block: development of a novel formula, Can. J. Cardiol. 35 (7) (2019) 855–865.

[21] S. Chakravarty et al., Corrected QT in ventricular paced rhythms: what is the validation for commonly practiced assumptions?, Cardiology 130 (4) (2015) 207–210.

[22] H. Bogossian et al., A new experimentally validated formula to calculate the QT interval in the presence of left bundle branch block holds true in the clinical setting, Ann. Noninvasive Electrocardiol. 22 (2) (2017).

[23] K.F. Weipert et al., Application of the Bogossian formula for evaluation of the QT interval in pacemaker patients with stimulated left bundle branch block, Clin. Res. Cardiol. 107 (11) (2018) 1033–1039.

[24] S.G. Priori et al., 2015 ESC Guidelines for the management of patients with ventricular arrhythmias and the prevention of sudden cardiac death: The Task Force for the Management of Patients with Ventricular Arrhythmias and the Prevention of Sudden Cardiac Death of the European Society of Cardiology (ESC)Endorsed by: Association for European Paediatric and Congenital Cardiology (AEPC), Europace 17 (11) (2015) 1601–1687.

[25] G. Frommeyer et al., Applicability of a Novel Formula (Bogossian formula) for Evaluation of the QT-Interval in Heart Failure and Left Bundle Branch Block Due to Right Ventricular Pacing, Pacing. Clin. Electrophysiol. 40 (4) (2017) 409–416.

[26] D. Erkapic et al., QTc interval evaluation in patients with right bundle branch block or bifascicular blocks, Clin. Cardiol. (2020).

[27] S.W. Rabkin, E. Szefer, D.J.S. Thompson, A new QT interval correction formulae to adjust for increases in heart rate, JACC Clin. Electrophysiol. 3 (7) (2017) 756–766.

EP-Quiz

Check for
updates

Schnelle und unregelmäßige Breitkomplextachykardie

Harilaos Bogossian[1,2] · Konstantinos Iliodromitis[1,2] · Nikolaos Tsianakas[1] ·
Nana-Yaw Bimpong-Buta[1,2]

[1] Klinik für Kardiologie und Rhythmologie, Evangelisches Krankenhaus Hagen-Haspe, Hagen, Deutschland

[2] Universität Witten/Herdecke, Witten, Deutschland

Fallpräsentation

Ein 28-jähriger Patient wurde unserer Klinik mit symptomatischen Palpitationen und retrosternalem Druckgefühl zugewiesen. Er beschreibt, dass er aus dem Schlaf heraus mit Schweißausbruch wach geworden sei. Das aufgezeichnete EKG in der Notaufnahme ist in ◨ **Abb. 1** zu sehen. Es besteht eine variable Herzfrequenz zwischen 150/min und 300/min. Die QRS-Komplexe präsentieren sich polymorph. Nach initialer Gabe von 5 mg Metoprolol intravenös terminierte die Tachykardie.

Bei der im Verlauf durchgeführten elektrophysiologischen Untersuchung kam es beim Platzieren der Katheter zur spontanen Initiierung und Terminierung der Tachykardie (◨ **Abb. 2**). Bei der Überprüfung des antegraden Wenckebach-Punkts – unter Stimulation im hohen rechten Vorhof (HRA) – veränderten sich die QRS-Komplexe, wie in ◨ **Abb. 2b** dargestellt.

Folgende Aussagen zu den ◨ **Abb. 1 und 2** sind zutreffend:

A. Es liegt eine FBI-Tachykardie bei rechtsseitiger akzessorischer Leitungsbahn vor.

B. Bei der Tachykardie handelt es sich um Vorhofflattern mit aberranter Überleitung.

C. Bei der Tachykardie handelt es sich um Vorhofflimmern mit frequenzabhängigem LSB.

D. Bei der Tachykardie handelt es sich um Vorhofflimmern und eine linksseitige akzessorische Bahn.

E. Es handelt sich um eine Bundle-Branch-Reentry-Tachykardie bei breitem QRS-Komplex auch im Sinusrhythmus.

QR-Code scannen & Beitrag online lesen
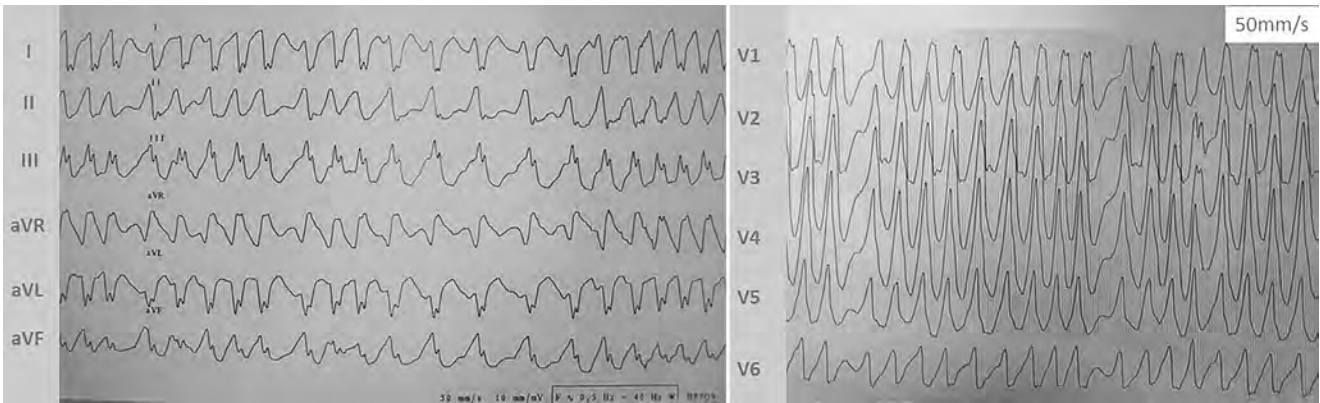
Abb. 1 ▲ Ruhe-EKG in der Notaufnahme

Abb. 2 ▲ Elektrophysiologische Untersuchung. **a** Tachykardie und spontane Terminierung während der Katheterplatzierung. **b** Zunahme der QRS-Breite während inkrementaler Stimulation vom HRA-Katheter (*HRA* „high right atrium")
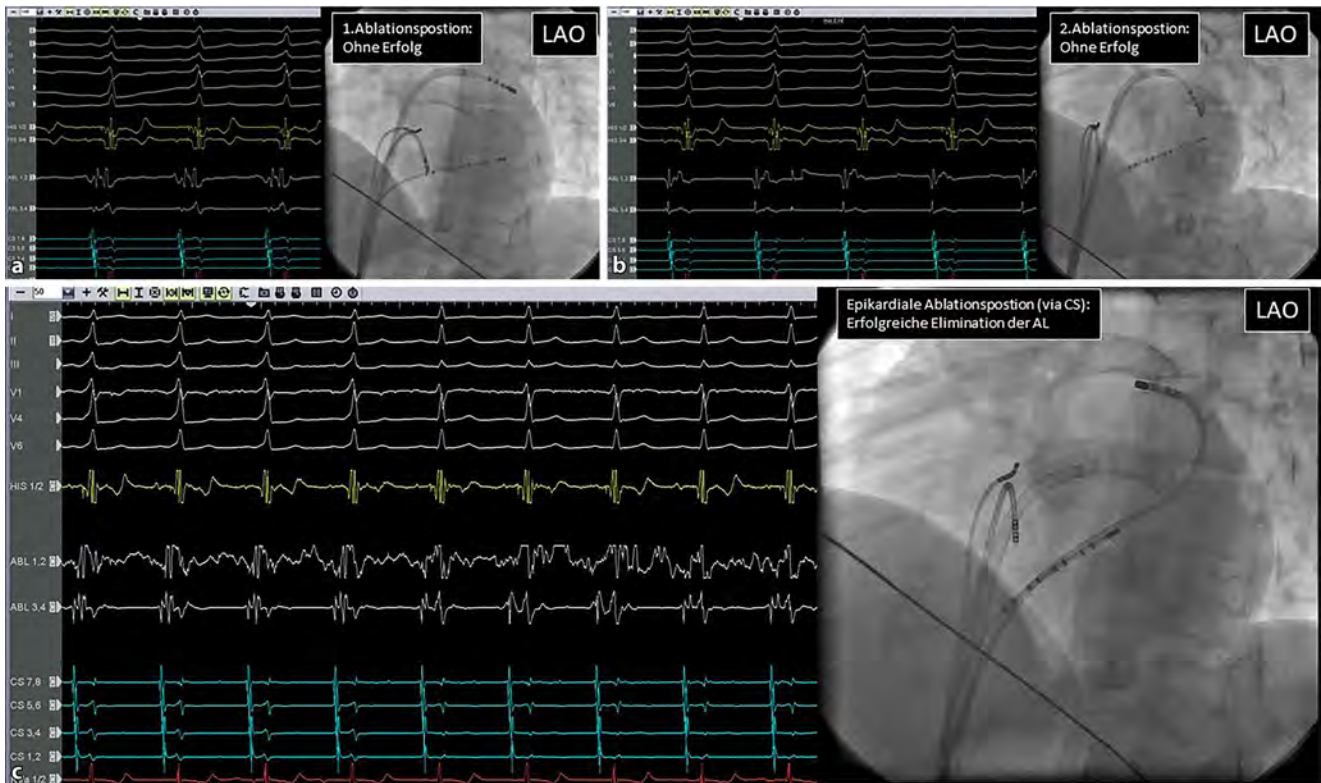
Abb. 3 ▲ Ablationspositionen. **a, b** Endokardiale Ablationspositionen (**a** anterolateral, **b** lateral) ohne Erfolg. **c** Erfolgreiche Ablation über den CS. In den EKG-Ableitungen zeigt sich während Ablation das Verschwinden der Delta-Welle und auf dem Ablationskatheter (ABL) die Separation von Vorhof- und Ventrikelsignal. *AL* akzessorische Leitungsbahn, *CS* Koronarsinus, *HRA* „high right atrium", *LAO* „left anterior oblique"

Die richtige Antwort ist D

Antwort

Im Ruhe-EKG sieht man eine schnelle unregelmäßige Breitkomplextachykardie (**Abb. 1**). Diese ist bekannt unter der Abkürzung FBI-Tachykardie („fast, broad, irregular tachycardia") und kann während Vorhofflimmern (VHF) auftreten, wenn gleichzeitig eine antegrad leitende akzessorische Leitungsbahn (AL) vorliegt [1]. Trotzdem ist die Antwort A falsch, da der Arrhythmie-Mechanismus im vorliegenden Fall auf das Vorhandensein einer linksseitigen AL beruht (Antwort D korrekt). Durch die unregelmäßige Überleitung von Vorhof zu Ventrikel – teilweise über den AV-Knoten und teilweise über die AL – kommt es zu polymorphen QRS-Komplexen, die weder einer typischen Aberranz noch einem frequenzabhängigen Linksschenkelblock (LSB) entsprechen (Antwort B und C falsch). Auch eine Bundle-Branch-Reentry-Tachykardie präsentiert sich mit typischer Schenkelblock-Morphologie und ist re-gelmäßig und monomorph (Antwort E falsch). Für die Vorhersage der Lokalisation einer antegrad leitenden AL ist die korrekte Beurteilung der Delta-Welle im EKG essenziell. Hierfür bieten die „2019 ESC Guidelines for the management of patients with supraventricular tachycardia" [2] zwei alternative Algorithmen. Wenn man diese auf das EKG mit der maximalen Präexzitation anwendet (**Abb. 2b**), so ist von einer links-anterolateralen AL auszugehen (Antwort D korrekt).

Beurteilung

Die FBI-Tachykardie stellt meist eine Blickdiagnose dar. Sie beschreibt schnell übergeleitetes Vorhofflimmern mit gemischter Überleitung auf den Ventrikel, teilweise über das spezifische Reizleitungssystem, teilweise über die vorliegende antegrad leitende AL. Da es sich um eine lebensbedrohliche Rhythmusstörung handelt, ist eine dauerhafte Behandlung zu empfehlen [2, 3]. Die Katheterablation stellt eine Klasse-IB-Indikation dar, während die me-dikamentöse Therapie mit Betablockern oder Kalziumkanalblockern eine Klasse-IIa-B-Indikation darstellt.

Auch im vorliegenden Fall erfolgte die Ablation der AL. Über einen transseptalen Zugang ließ sich die AL trotz fusionierter Vorhof- und Kammersignale auf dem Ablationskatheter nicht eliminieren (in endokardialer anterolateraler und lateraler Position; **Abb. 3a,b**), erst eine epikardiale Ablation via Koronarsinus war erfolgreich (**Abb. 3**). Unter Ablation trennen sich einerseits Vorhof- und Ventrikelsignale auf dem Ablationskatheter; anderseits ist im Oberflächen-EKG (nach den ersten 4 QRS-Komplexen auf **Abb. 3c**) das Verschwinden der Delta-Welle als Zeichen der erfolgreichen Ablation erkennbar.

Korrespondenzadresse

PD Dr. Harilaos Bogossian
Klinik für Kardiologie und Rhythmologie,
Evangelisches Krankenhaus Hagen-Haspe
Brusebrinkstraße 20, 58135 Hagen,
Deutschland
bogossian@evk-haspe.de

Einhaltung ethischer Richtlinien

Literatur

1. Kofflard M, van Mechelen R (2006) FBI: fast broad and irregular tachycardia. Neth Heart J 14:68–74
2. Brugada J, Katritsis DG, Arbelo E, Arribas F, Bax JJ, Blomström-Lundqvist C, Calkins H, Corrado D, Deftereos SG, Diller GP, Gomez-Doblas JJ, Gorenek B, Grace A, Ho SY, Kaski JC, Kuck KH, Lambiase PD, Sacher F, Sarquella-Brugada G, Suwalski P, Zaza A (2020) 2019 ESC Guidelines for the management of patients with supraventricular tachycardiaThe Task Force for the management of patients with supraventricular tachycardia of the European Society of Cardiology (ESC). Eur Heart J 41:655–720
3. Etheridge SP, Escudero CA, Blaufox AD, Law IH, Dechert-Crooks BE, Stephenson EA, Dubin AM, Ceresnak SR, Motonaga KS, Skinner JR, Marcondes LD, Perry JC, Collins KK, Seslar SP, Cabrera M, Uzun O, Cannon BC, Aziz PF, Kubuš P, Tanel RE, Valdes SO, Sami S, Kertesz NJ, Maldonado J, Erickson C, Moore JP, Asakai H, Mill L, Abcede M, Spector ZZ, Menon S, Shwayder M, Bradley DJ, Cohen MI, Sanatani S (2018) Life-threatening event risk in children with Wolff-Parkinson-white syndrome: a multicenter international study. JACC Clin Electrophysiol 4:433–444

Spotlight: Wie bestimmt man das QTc-Intervall richtig?

Thieme

Spotlight: Wie bestimmt man das QTc-Intervall richtig?

Spotlight: How to Measure QTc Interval?

Autoren

Harilaos Bogossian[1], Nana-Yaw Bimpong-Buta[1], Bernd Lemke[2]

Institute

1 Klinik für Kardiologie und Rhythmologie, Evangelisches Krankenhaus Hagen Haspe, Hagen, Deutschland
2 Kardiologie, Angiologie und Elektrophysiologie, Klinikum Lüdenscheid, Deutschland

Korrespondenzadresse

Dr. Harilaos Bogossian
Klinik für Kardiologie und Rhythmologie, Evangelisches Krankenhaus Hagen Haspe
Brusebrinkstraße 20, 58135 Hagen, Deutschland
Tel.: 0 23 31/4 76 24 51, Fax: 0 23 31/4 76 24 52
bogossian@evk-haspe.de

ZUSAMMENFASSUNG

Das EKG stellt eine der wichtigsten nicht invasiven Untersuchungsmethoden dar. Im klinischen Alltag bietet es einen hohen Informationsgehalt bei sehr geringen Kosten. Nichts-destotrotz ist die EKG-Interpretation für viele Ärzte herausfordernd. Selbst bei einem normalen EKG bedarf es ausreichender Sorgfalt, um die einzelnen Zeitintervalle ordentlich zu vermessen. Deutlich schwieriger wird die Interpretation beim Auftreten von Herzrhythmusstörungen. Hier müssen dann (wie z. B. beim Vorhofflimmern) mehrere Messungen durchgeführt und berücksichtigt werden, um das QT-Intervall korrekt zu beurteilen. Weitere EKG-Veränderungen können die Messung und Interpretation der QT-Zeit weiter beeinflussen. So kommt insbesondere bei Frequenzvariabilität (Tachykardien/Bradykardien) und beim Auftreten von Schenkelblockierungen die Anwendung diverser Formeln zum Tragen. Erst nach Berücksichtigung all dieser Aspekte kann eine ordentliche Messung und Interpretation der QTc-Zeit erfolgen.

ABSTRACT

The 12-lead ECG continues to be one of the most important noninvasive diagnostic tools in daily clinical practice, since it offers high level of clinincal information at low costs. However, accurate interpretation of the ECG remains a challenge for many physicians. Correct assessment of the different time intervals may be time-consuming even in a normal ECG, particularly since automated ECG softwares have proven to be rather unprecise. Measuring ECG intervals needs even more diligence in the presence of arrhythmias (e.g. atrial fibrillation) where accurate determination of the QT interval has to be based on averaging several measurements. Interpretation of the QT interval may be further hampered by the presence of tachycardia or severe bradycardia. Thus, the influence of heart rate as well as of bundle branch blocks on repolarization measures need to be corrected (QTc). For this purpose, several correction formulas have been developed and validated for use in clinical practice. Considering these aspects is the base for correct measurement and interpretation of cardiac repolarization.

Hintergrund

Das EKG ist eine der häufigsten nicht invasiven Untersuchungen, die im klinischen Alltag erhoben werden. Die Interpretation des EKGs bedarf einer hohen Sorgfalt – nicht nur in Notfallsituationen, sondern auch bei vermeintlichen Routineuntersuchungen. Insbesondere die Beurteilung der QT-Zeit ist dabei essenziell, um das potenzielle Risiko für lebensbedrohliche Rhythmusstörungen zeitnah zu erkennen.

Ursächlich für eine QT-Zeit-Verlängerung sind zum einen angeborene Gendefekte, zum anderen können externe Faktoren (wie Medikamente, Elektrolytentgleisungen, Ischämien, Herzinsuffizienz) zu einer erworbenen Verlängerung der QT-Zeit führen [1].

Das QT-Intervall stellt die Dauer der Depolarisation und der Repolarisation der Ventrikel dar. Dabei repräsentieren insbesondere der QRS-Komplex die Depolarisation und die JT-Zeit überwiegend die Repolarisation. Abnormale Verlängerung der QT-Zeit kann zu Torsade-de-pointes-Tachykardien (TdP) führen. Daher ist es wich-

ABKÜRZUNGEN

|	
LSB	Linksschenkelblock
RSB	Rechtsschenkelblock
TdP	Torsade de pointes
VHF	Vorhofflimmern

tig, die QT-Zeit immer individuell zu vermessen und sich nicht alleine auf die automatische EKG-Interpretation der EKG-Schreiber zu verlassen (obwohl neue Geräte inzwischen deutlich verbesserte Messungen liefern) (▶ **Abb. 1**).

Für die korrekte QT-Zeit-Beurteilung ist im Vorfeld eine korrekte Erkennung des Herzrhythmus unerlässlich. So ist die Beurteilung bei Patienten mit Vorhofflimmern komplexer als bei Patienten, die einen Sinusrhythmus vorweisen. Neben dem Herzrhythmus hat auch die Herzfrequenz wesentliche Auswirkungen auf die QT-Zeit. Zur besseren Interpretation wird nach Frequenzkorrektur die QTc-Zeit ermittelt. Beim Vorliegen eines Schenkelblocks muss vor Anwendung der Frequenzkorrekturformeln die QT-Verlängerung durch den verlängerten QRS-Komplex modifiziert werden. Dies führt zur QTm- bzw. QTmc-Zeit [2].
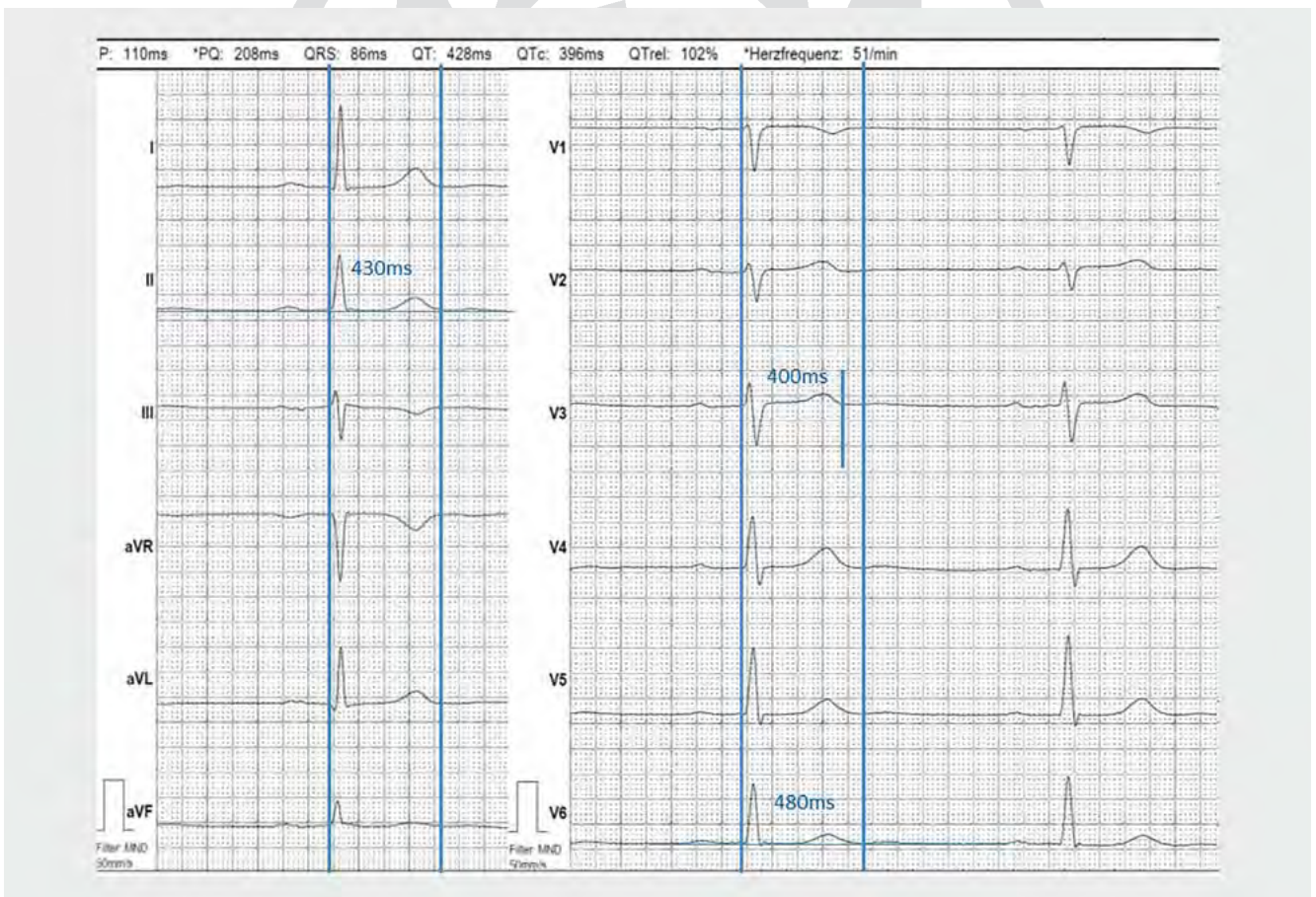
▶ **Abb. 1** Variabilität der QT-Zeit bei einem vermeintlich „normalen" EKG. Die Messung des QT-Intervalls durch den EKG-Schreiber beträgt 428 ms. Dies entspricht unserer Messung (nach Zählung der kleinen Kästchen) in Ableitung II mit ca. 430 ms. Das Ende der T-Welle und somit die längste QT-Zeit in den Brustwandableitung ist allerdings in Ableitung V6 und führt zu einer QT-Zeit von nahezu 480 ms, während die Ableitung V3 eine scharf abgrenzbare QT-Zeit mit nur 400 ms vorweist.
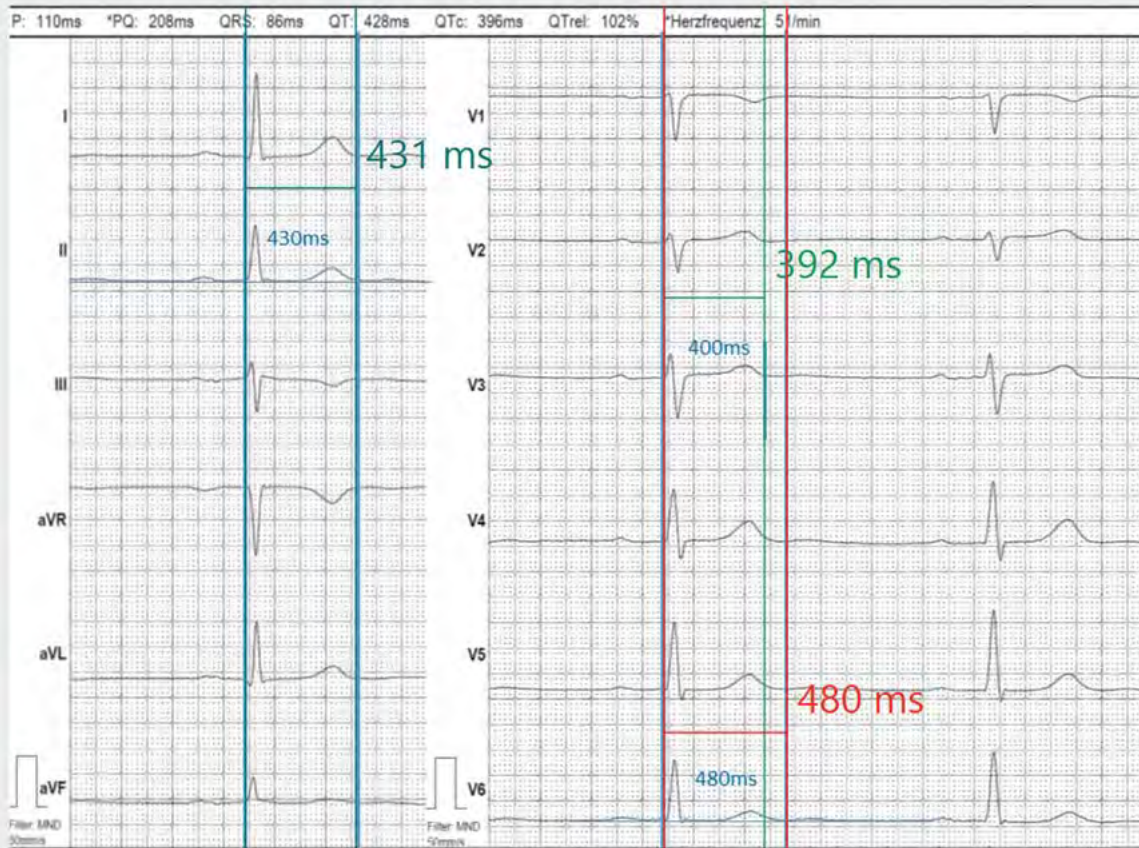
► **Abb. 2** Die ► **Abb. 1** wurde mit der Software EP Calipers bearbeitet. Nach Eichung (50 kleine Kästchen wurden dem Wert 1000 ms gleichgesetzt) ist eine genauere Messung möglich.

Die korrekte Messung der QTc-Zeit

Die amerikanische Gesellschaft für Kardiologie hat Empfehlungen zur standardisierten EKG-Interpretation publiziert (AHA/ACC/HRS Recommendations) [3]. In diesem Rahmen wurden auch Normwerte definiert. Hiernach ist die normale QT-Zeit – bei Abwesenheit eines Linksschenkelblocks oder eines stimulierten Rhythmus – bis zu 450 ms für Männer und bis zu 460 ms für Frauen beschrieben [3]. Eine Verlängerung über 500 ms zeichnet ein hohes Risiko für TdP-Tachykardien aus.

Bei der Messung der QTc-Zeit sind dabei 3 Punkte zu beachten:
- korrekte Definition des Beginns und des Endes der QT Zeit,
- Definition der Ableitung, in der man die QT-Zeit am besten messen kann,
- Anwendung von entsprechenden Formeln bei QRS-Verbreiterung (durch Schenkelblockierungen oder Schrittmacherstimulation) und zur Frequenzkorrektur.

Bei nicht eindeutigen Befunden ist es empfehlenswert, den Beginn des QRS und das Ende der QT-Zeit über alle Ableitungen zu vergleichen und mit einer senkrechten Linie im EKG zu definieren.

Während der QRS-Beginn meist sehr eindeutig erkennbar ist, ist bei dem Ende der QT-Zeit eine große Variabilität in den einzelnen Ableitungen möglich (teilweise bis zu 60 ms) (► **Abb. 1**). Diese als QT-Dispersion bezeichnete Schwankung der QT-Zeit gilt als grobes Maß für die Abnormalität der Repolarisation und damit für eine gesteigerte Vulnerabilität des Herzens. Da sich die Werte zwischen Herzkranken und Gesunden sehr stark überlappen, weisen nur stark variierende Werte (über 100 ms) auf ein gesteigertes Risiko hin [4].

Alternativ zur manuellen Markierung von Beginn und Ende ist heutzutage bei digital erhobenen EKGs (oder bei gescannten EKGs) die Anwendung von elektronischen Applikationen (z. B. EP Calipers) möglich (► **Abb. 2**).

Die Empfehlungen, welche Ableitungen für die Messung benutzt werden sollten, variieren extrem: Einige Autoren empfehlen Ableitung II oder V5, andere empfehlen Ableitungen V2 oder V3 und wieder andere aVR und aVF [3, 5, 6]. Dabei schützt die Messung in Ableitung II vor Fehlmessung, da es hier selten zum Auftreten von U-Wellen kommt (gleiches gilt auch für aVR und aVF) – während die linkspräkordialen Ableitungen häufiger eine U-Welle vorweisen. Nichtsdestotrotz ist die längste QT-Zeit meist in den Ableitung V2 und V3 zu finden [3].

Praktikabel ist die Empfehlung „Ableitungen mit sehr flacher QT-Zeit nur mit Vorsicht zu interpretieren", und solche, wo „die
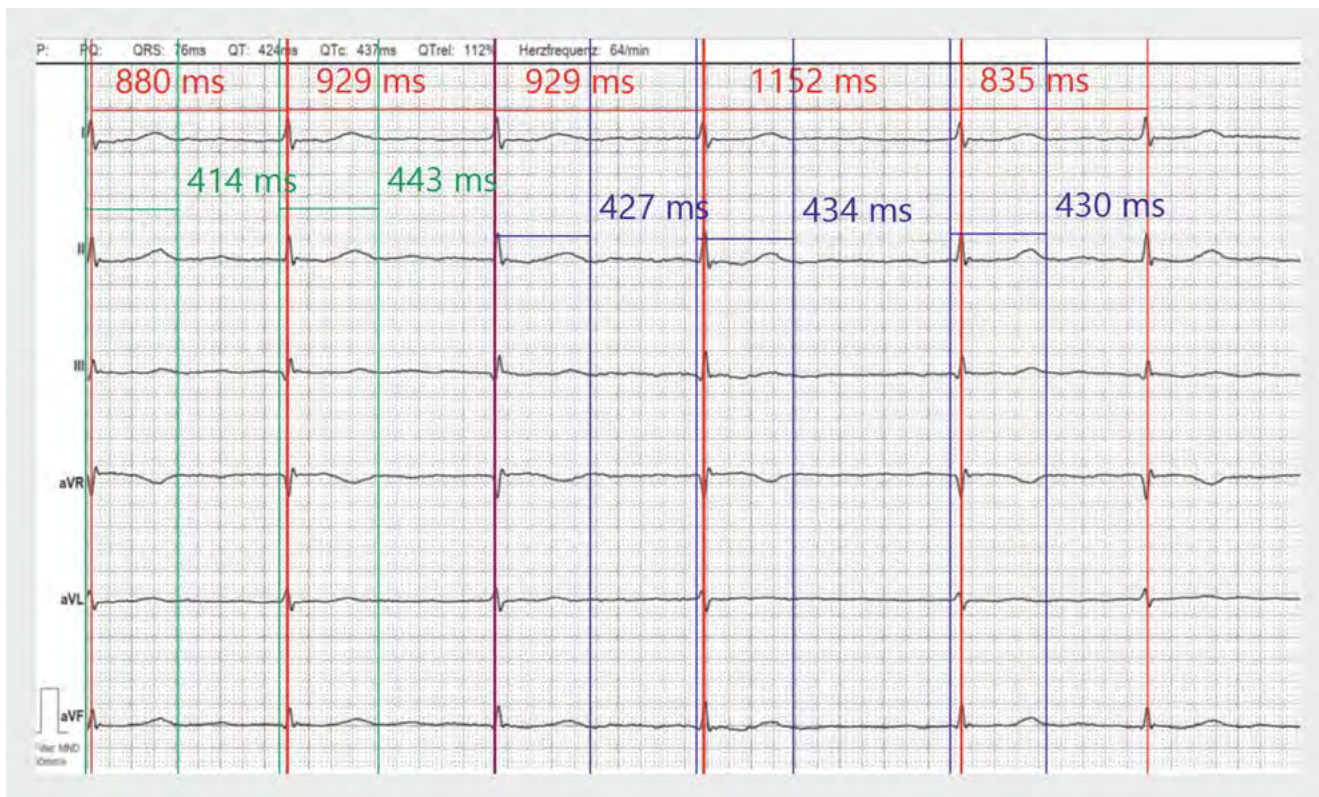
▶ **Abb. 3** EKG mit VHF. Sowohl die „half-RR"-Formel als auch die detaillierte Messung von 5 konsekutiven Komplexen bieten keine Hinweise für das Vorliegen eines Long-QT in den Extremitätenableitungen. Die RR-Intervalle sind rot markiert. Die längste und kürzeste QT-Zeit sind jeweils grün markiert; weitere 3 QT-Intervalle sind blau markiert. Manuelle Messung in Ableitung II: RR_{mean} = 945 ms (→ HF = 63 bpm), QT_{mean} = 430 ms; Messung des EKG-Schreibers: HF = 64 bpm, QT = 424 ms.

T-Welle klar definiert ist", zu bevorzugen. Nichtsdestotrotz gilt es, die längste QT-Zeit zu identifizieren [7].

Bei der Messung kann man sich neben dem EKG-Lineal und den elektronischen Applikationen auch die Kästchen auf dem Millimeterpapier zur Hilfe nehmen. Dabei entspricht jedes kleine Quadrat – bei der in Deutschland üblichen Schreibweise (50 mm/s) – einem Zeitintervall von 20 ms. Bei der 25-mm/s-Schreibweise (üblich in nicht deutschsprachigen Ländern) entspricht ein kleines Quadrat 40 ms. Bei der schnelleren Papiergeschwindigkeit ist die Länge/Dauer der QT-Zeit durch die „gestreckte Zeit" etwas genauer zu messen. Bei der langsameren Papiergeschwindigkeit generiert die „gestauchte Zeit" etwas höhere Ausschläge und etwas spitzere Winkel, sodass das Ende der T-Welle etwas besser zu definieren ist.

Erschwert wird die Bestimmung der QT-Zeit beim Vorliegen einer U-Welle. Dabei wird die Anwendung der Tangententechnik empfohlen, bei der im absteigenden Schenkel der T-Welle eine Tangente gesetzt wird. Dabei wird das Ende des QT-Intervalls an diesem Punkt definiert, an dem sich die Tangente mit der Basislinie (PQ-Strecke und TP-Strecke) schneidet [8].

KURZGEFASST
Für die korrekte Messung der QTc-Zeit muss zunächst das QT-Intervall in allen Ableitungen bewertet werden. Im zweiten Schritt gilt es, Einflüsse durch Herzrhythmus, Herzfrequenz und durch QRS-Veränderungen zu berücksichtigen.
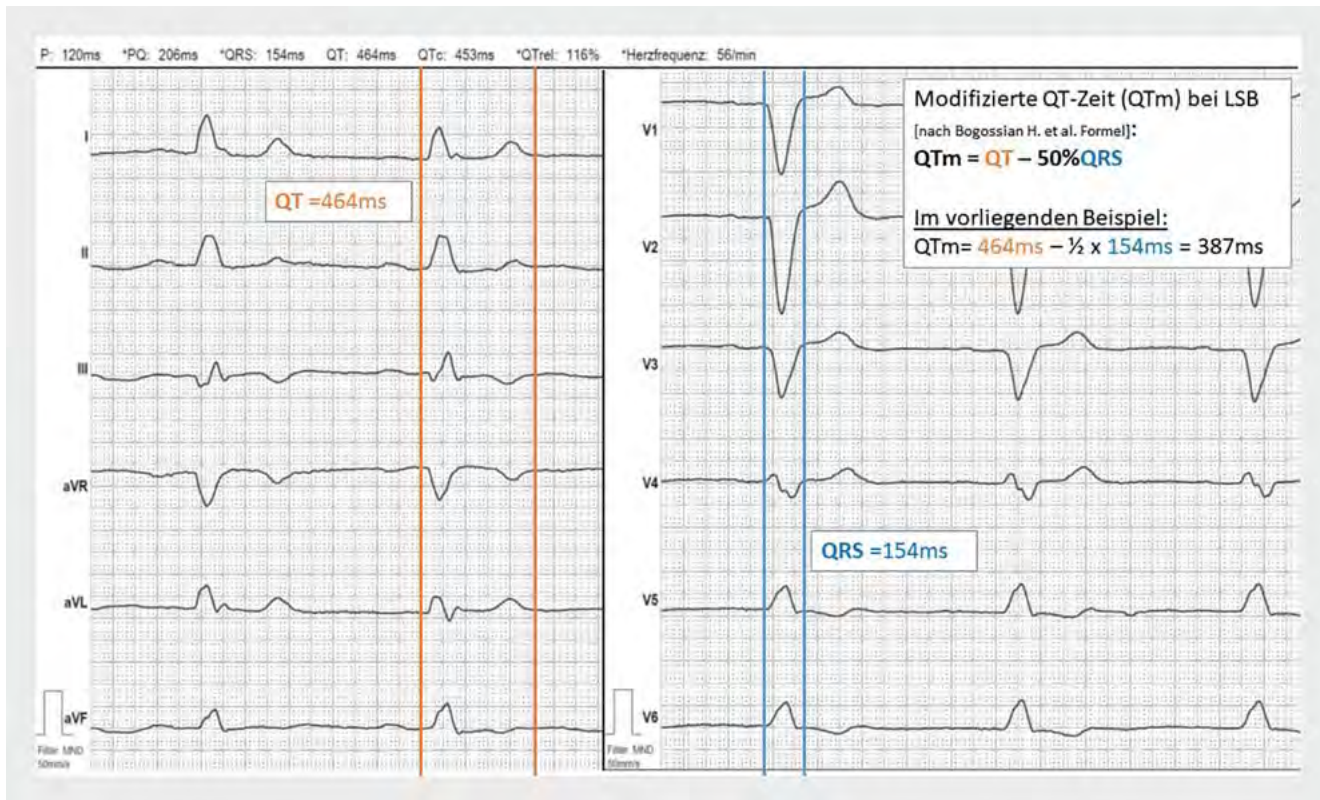
Einfluss der Herzfrequenz auf die QTc-Zeit

Es existieren verschiedene Formeln für die Frequenzkorrektur [7]. Dabei gilt für alle Formeln, dass bei extremer Bradykardie oder Tachykardie die Zuverlässigkeit abnimmt. Die am häufigsten benutzte „Bazett"-Formel hat sich als ausreichend zuverlässig im Frequenzspektrum zwischen 50 und 70 bpm erwiesen:

$$QTc = QT\ (ms)/\sqrt{RR}\ (s);\ RR = 60/Herzfrequenz\ (HF)$$

Kommt es jedoch zu relevanten Bradykardien, so ist die Formel nach „Fridericia" akkurater:

$$QTc = QT/\sqrt[3]{RR}$$

P: 120ms *PQ: 206ms *QRS: 154ms QT: 464ms QTc: 453ms *QTrel: 116% *Herzfrequenz: 56/min

QT = 464ms

Modifizierte QT-Zeit (QTm) bei LSB
[nach Bogossian H. et al. Formel]:
QTm = QT − 50%QRS

Im vorliegenden Beispiel:
QTm= 464ms − ½ x 154ms = 387ms

QRS = 154ms

▶ **Abb. 4** EKG mit Linksschenkelbock (LSB). Die gemessene QT-Zeit mit 464 ms ist bei männlichem Geschlecht oberhalb der Norm. Die Verlänge-rung ist jedoch führend durch die verlängerte Depolarisation verursacht. Die JT-Zeit entspricht der zu erwartenden JT-Zeit bei schmalem QRS-Komplex. Nach Anwendung unserer QRS-QT-Formel für LSB entspricht die modifizierte QT-Zeit 387 ms [2].

Kommt es zu Tachykardien, so sind die komplexeren Formeln „Framingham" und „Hodges" zu bevorzugen [7]:

Framingham: QTc = QT + 0,154 (1 − RR)

Hodges: QTc = QT + 1,75 (HF − 60)

Insbesondere beim Vorliegen von QRS-Verbreiterungen im Sinne von Schenkelblockierungen hat sich bei höheren Frequenzen die Hodges-Formel als zuverlässiger erwiesen [9]. Wegen der Kom-plexität der Formeln ist die Kalkulation durch einen QTc-Rechner zu empfehlen.

KURZGEFASST
Bei niedrigen Herzfrequenzen Anwendung der Fridericia-For-mel; bei mittleren Herzfrequenzen Anwendung der Bazett-Formel; bei hohen Herzfrequenzen Anwendung der Hodges- oder Framingham-Formel.

Einfluss von Rhythmusstörungen auf die QTc-Zeit

Die häufigste Rhythmusveränderung, durch welche die Bestim-mung der QT-Zeit erschwert wird, ist das Vorhofflimmern (VHF). Insbesondere im Rahmen einer Tachyarrhythmia absoluta oder Bradyarrhythmia absoluta wird der Schwierigkeitsgrad für die kor-rekte Beurteilung potenziert.

Ist wiederum die Herzfrequenz (trotz VHF) bei ca. 60 Schlägen pro Minute, so empfiehlt sich eine erste Abschätzung der QT-Zeit durch die Anwendung der „half-RR"-Formel [10]. Hierbei gilt eine QT-Zeit, die weniger als die Hälfte des R-R-Intervalls beträgt, als nicht pathologisch. Dauert die QT-Zeit jedoch länger als die Hälfte des R-R-Intervalls an, so empfiehlt sich eine weitere, detailliertere Messung des QT-Intervalls (▶ **Abb. 3**). Wie bei den meisten For-meln ist leider auch bei dieser leicht anwendbaren Formel die Sen-sitivität und die Spezifität limitiert.

Moderne EKG-Schreiber sind inzwischen in der Lage, über meh-rere Komplexe die Messwerte gut zu mitteln [11]. Nichtsdesto-trotz sollten diese Werte gegengeprüft werden. Dabei sollte die QT-Zeit an 5 aufeinanderfolgenden Komplexen gemessen und ge-mittelt werden, um eine bessere Abschätzung des QT-Intervalls zu erzielen [12].

KURZGEFASST

Drei Optionen für die Abschätzung der QT-Zeit beim Vorliegen von VHF:

- moderner EKG-Schreiber mit weiterentwickelter Software,
- „half-RR"-Formel,
- Messung von 5 konsekutiven Intervallen und Ermitteln des Mittelwerts.

Einfluss der QRS-Verbreiterung auf die QTc-Zeit

Die QT-Zeit wird durch das Auftreten von QRS-Verbreiterungen direkt beeinflusst. Eine Verbreiterung des QRS entsteht durch Schenkelblockierungen, durch intraventrikuläre Leitungsstörungen sowie durch Schrittmacherstimulation. Die langsame Depolarisation des Myokards führt konsekutiv auch zu einer verspäteten Repolarisation. Hier gibt es nur eine kurze Überschneidung der verschiedenen elektrischen Phasen. Daher befürworten die amerikanischen Empfehlungen der EKG-Interpretation idealerweise die Verwendung der JT-Zeit. Bedauerlicherweise ist die Erfahrung in der Beurteilung der JT-Zeit im klinischen Alltag sehr eingeschränkt.

Neben diversen komplexeren Formeln wurde 2014 eine leicht anwendbare Formel zur Korrektur der QT-Zeit beim Vorliegen eines Linksschenkelblocks (LSB) beschrieben [2]. Diese wurde in weiteren Arbeiten evaluiert und ihre Anwendbarkeit bei Schrittmacherstimulation, Herzinsuffizienz und Rechtsschenkelblöcken weiter überprüft [9, 13–15]. Vereinfacht empfiehlt die Formel, von der gemessenen QT-Zeit 50 % des QRS abzuziehen (▶ **Abb. 4**). Anschließend kann die Frequenzkorrektur nach favorisierter Formel durchgeführt werden. Bei der Arbeit zur Überprüfung der Anwendbarkeit der neuen QT-Formel beim Vorliegen von Rechtsschenkelblöcken (RSB) wurden zusätzlich verschiedene Frequenzkorrekturformeln überprüft (Bazett, Fridericia, Hodges). Dabei scheint die Formel nach Hodges den geringsten Fehler vorzuweisen, während die Bazett-Formel die größte Abweichung aufweist [9].

KURZGEFASST

Beim Vorliegen eines RSB, LSB oder stimulierten QRS-Komplexes bietet die Formel nach Bogossian u. Mitarb. ($QT_m = QT - 50\,\%\;QRS$ [2]) eine Möglichkeit zur zügigen Abschätzung der modifizierten QT-Zeit. Nach Anwendung dieser Formel sollte die Frequenzkorrektur idealerweise mit der Hodges-Formel erfolgen.

Fazit

Die Messung der QT-Zeit ist ein wesentlicher Bestandteil der EKG-Beurteilung. Insbesondere beim Vorliegen von Arrhythmien, Frequenzschwankungen und Schenkelblockierungen ist die Beurteilung erschwert. Auch bei Patienten, die diese komplexen EKGs

bieten, ist unter Anwendung diverser Formeln eine ordentliche Beurteilung möglich.

Interessenkonflikt

Die Autorinnen/Autoren geben an, dass kein Interessenkonflikt besteht.

Literatur

[1] Mazzanti A, Maragna R, Vacanti G et al. Interplay between genetic substrate, QTc duration, and arrhythmia risk in patients with long QT syndrome. J Am Coll Cardiol 2018; 71: 1663–1671

[2] Bogossian H, Frommeyer G, Ninios I et al. New formula for evaluation of the QT interval in patients with left bundle branch block. Heart Rhythm 2014; 11: 2273–2277

[3] Rautaharju PM, Surawicz B, Gettes LS et al. AHA/ACCF/HRS recommendations for the standardization and interpretation of the electrocardiogram: part IV: the ST segment, T and U waves, and the QT interval: a scientific statement from the American Heart Association Electrocardiography and Arrhythmias Committee, Council on Clinical Cardiology; the American College of Cardiology Foundation; and the Heart Rhythm Society: endorsed by the International Society for Computerized Electrocardiology. Circulation 2009; 119: e241

[4] Malik M, Batchvarov VN. Measurement, interpretation and clinical potential of QT dispersion. J Am Coll Cardiol 2000; 36: 1749–1766

[5] Garson A jr. How to measure the QT interval–what is normal? Am J Cardiol 1993; 72: 14B–16B

[6] Salvi V, Karnad DR, Kerkar V et al. Choice of an alternative lead for QT interval measurement in serial ECGs when Lead II is not suitable for analysis. Indian Heart J 2012; 64: 535–540

[7] Indraratna P, Tardo D, Delves M et al. Measurement and Management of QT Interval Prolongation for General Physicians. J Gen Intern Med 2020; 35: 865–873

[8] Postema PG, De Jong JS, van der Bilt IA et al. Accurate electrocardiographic assessment of the QT interval: teach the tangent. Heart Rhythm 2008; 5: 1015–1018

[9] Erkapic D, Frommeyer G, Brettner N et al. QTc interval evaluation in patients with right bundle branch block or bifascicular blocks. Clin Cardiol 2020; 43: 957–962

[10] Phoon CK. Mathematic validation of a shorthand rule for calculating QTc. Am J Cardiol 1998; 82: 400–402

[11] Dash A, Torado C, Paw N et al. QT correction in atrial fibrillation – Measurement revisited. J Electrocardiol 2019; 56: 70–76

[12] Tooley J, Ouyang D, Hadley D et al. Comparison of QT interval measurement methods and correction formulas in atrial fibrillation. Am J Cardiol 2019; 123: 1822–1827

[13] Frommeyer G, Bogossian H, Pechlivanidou E et al. Applicability of a novel formula (Bogossian formula) for evaluation of the QT-interval in heart failure and left bundle branch block due to right ventricular pacing. Pacing Clin Electrophysiol 2017; 40: 409–416

[14] Bogossian H, Frommeyer G, Ninios I et al. A new experimentally validated formula to calculate the QT interval in the presence of left bundle branch block holds true in the clinical setting. Ann Noninvasive Electrocardiol 2017; 22: e12393

[15] Weipert KF, Bogossian H, Conzen P et al. Application of the Bogossian formula for evaluation of the QT interval in pacemaker patients with stimulated left bundle branch block. Clin Res Cardiol 2018; 107: 1033–1039

DR. RAPHAEL ROMANO BRUNO (Orcid ID : 0000-0003-3776-3530)

Sublingual microcirculation in Prehospital Critical Care Medicine – a Proof of Concept Study

Raphael Romano Bruno[1], Markus Reed[1], Nana-Yaw Bimpong-Buta[2], Johanna M. Muessig[1], Maryna Masyuk[1], Stephan Binneboessel[1], Marcus Franz[3], Malte Kelm[1], Christian Jung[1*]

[1]Division of Cardiology, Pulmonology, and Vascular Medicine, Medical Faculty, University Hospital Düsseldorf, Germany; [2]Clinic for Cardiology, Electrophysiology and Internal Intensive Care Medicine, EVK Hagen-Haspe, Germany; [3] Clinic for Cardiology, Internal Intensive Care Medicine, Angiology, Pneumology/Allergology, University Hospital Jena, Germany

*Corresponding author: Christian Jung, MD, PhD, University Hospital Düsseldorf, email: Christian.Jung@med.uni-duesseldorf.de, Fax: +49 (0)211-81-18812

ABSTRACT

Objective:

Diagnostic and risk stratification are limited in emergencies. The measurement of microcirculation might identify patients with poor perfusion but compensated macrocirculation such as in beginning shock. This proof-of-concept study examines whether sublingual prehospital sidestream dark field microscopy is feasible.

Methods:

This prospective observational study included patients receiving medical aid by an emergency ambulance who had a spontaneous circulation and offered access to the sublingual mucosa. Sublingual measurement of microcirculation was performed using a sidestream dark field camera. Video-quality was evaluated with MIQS (microcirculation image quality score). AVA 4.3C software calculated microcirculatory parameters.

Results:

Thirty patients (47% male) were included. The average age was 63 years (± 20 years SD), the severity of the disease (quantified by NACA) was 3.4 (± 0.7 SD). Macrocirculation presented within the normal range. The most frequent cause preventing the measurement was a time-critical disease (64%). In 17 patients (57%), the videos could be analyzed immediately. The average quality of the video was 2.2 ± 0.45 points ("acceptable"). There were minor restrictions of microcirculation. Microcirculation correlated with NACA, but not with the macrocirculation. No complications occurred.

Conclusion:

The prehospital sublingual measurement is safe and valid. Despite normal macrocirculation, microcirculation was impaired and correlated with NACA.

List of Abbreviations

SDF	Sidestream Darkfield microscopy
NACA	National Advisory Committee on Aeronautics
MIQS	microcirculation image quality score
IDF	Incident darkfield illumination
ECG	electrocardiogram
PPV	Percentage of perfused vessels
TVD	Total vessel density
NC	Number of crossings
PVD	Perfused vessel density
PNC	Perfused number of crossings

<center>**MANUSCRIPT**</center>

Introduction

Risk stratification is a key element in emergency medicine and might serve to improve preclinical and clinical patient management. Thus, there is great interest to identify and validate novel tools and parameters, which are easy to handle even in the emergency setting by emergency physicians and paramedics. The changes in hospital coverage have resulted in longer transport distances. Dwindling clinical resources and an increasing number of emergency calls require the meticulous selection of a suitable target hospital [1, 2]. The main challenge is to identify critically ill patients. Unfortunately, prehospital diagnostic options are very limited and time-critical. Usually, an ambulance disposes on clinical examination and basic hemodynamic values such as non-invasive blood pressure, pulse quality, heart rate, oxygen saturation, electrocardiogram, and capnometry. Very few emergency crews use hand-held ultrasound devices. Hence, diagnostic tools are limited to the assessment of the macrocirculation. However, macrocirculatory parameters are not very reliable and might not necessarily reflect factual organ perfusion. Despite intact macro-hemodynamic parameters, severe diseases such as shock may endanger patients [3]. Focusing only on macrocirculation masks the following issue: Tissue hypoxia is crucial and microcirculatory collapse or at least dysregulation occurs very early [4]. Reduced microcirculation results in attenuated cellular nutrient and oxygen supply, which can result in severe cell damage. Microcirculatory flow can independently alter from global circulatory parameters. Impaired microcirculation is ubiquitous in shock and can be found even in the setting of hemodynamic compensation. Furthermore, an acute microcirculatory impairment is a stronger predictor of outcome than global hemodynamic variables [5]. An impaired microcirculation is often the very first sign of alarm for deteriorating critically ill patients.

Taking all these considerations into account, the following question occurs: How should microcirculation be assessed *in vivo*? There are several non-invasive methods. A promising attempt is the use of sublingual IDF- and SDF-measurement (IDF: incident dark-field; SDF: sidestream dark field) devices. Sublingual microcirculation is a suitable target because it reliably reflects organ perfusion [6]. Measuring sublingual microcirculation has already been used to identify high-risk patients both in septic and

cardiogenic shock [7, 8], chronic heart failure [9], in coronary artery disease, [10] and to predict outcome after cardiac arrest [11-14].

The assessment tools are easy to use hand-held devices. The newest generation of SDF offers the great advantage of automatic software which independently calculates various microcirculatory parameters. Thus, there is no need for the treating physician to interpret the videos. Taking these considerations into account, microcirculation has become a directly detectable physiological compartment with quantifiable measurement parameters.

Until now, the described hand-held devices were mainly used in the intensive care unit or in healthy volunteers. To our knowledge, there have never been attempts to use direct sublingual microcirculatory assessment in out-of-hospital critical care medicine.

Materials and Methods

Ethics

The study was approved by the German Ethics Committee of the Medical Faculty of the University Hospital Duesseldorf, Germany (Date of approval: July 11th, 2017; (Study No.: 5805R; Registry No.: 2016085397). Written informed consent was mandatorily provided by all participating patients of the study. The principles of the Declaration of Helsinki and the national rules and regulations on personal data protection were applied. The study has been registered in clinicaltrials.gov with the registration number NCT04265066.

Inclusion and Exclusion

This investigation took place in the ambulance emergency service of the metropolitan area around Düsseldorf, Germany. To participate in the study, patients had to meet the following criteria: 1) the call for an acute emergency outside the hospital with the indication for sending out an emergency doctor, 2) a spontaneous circulation without previous resuscitation, 3) informed consent, 4) the sublingual mucosa had to be accessible. The following data was collected: age, sex, cause for emergency alarm (cardiac reason, respiratory reason, gastroenterological, oncological, general internal medicine, renal, neurological, psychiatric, paediatric, traumatic), and the National Advisory Committee on Aeronautics' (NACA), that ranges from 0 = no injury, 7 = lethal injury severity score (see Supplement 1).

Macrocirculation

Vital parameters (heart rate, non-invasive blood pressure, peripheral oxygen saturation) were assessed using a standard out-of-hospital monitoring device (Corpuls3 (GS Elektromedizinische Geräte G. Stemple GmbH, Kaufering, Germany)). Mean arterial pressure (MAP) was calculated as follows: (2 * diastolic pressure + systolic pressure) /3. The capillary refill was evaluated in a standardized manner as described previously [15].

SDF-measurement and Video-analysis

Only sufficiently trained investigators performed measurements. The microcirculation was assessed by the implementation of the sidestream darkfield microscope (MicroScan® device, Microvision Medical, Amsterdam, The Netherlands) as described before [16]. At

the tip of the device, a highly sensitive camera digitally records the sublingual capillary network (see Figure 1, left). The software analysis can directly be performed and visualized on a tablet screen. Additionally, the videos are saved for later analysis. For this purpose, a suitable tablet computer was used (Microsoft Surface Pro 4, (Redmond, Washington, USA). After acquisition of the videos, the video-quality was assessed using the microcirculation image quality score (MIQS) established by Massey et al. [17]. Only videos with a good or at least acceptable result score qualified for further analysis A validated automatic algorithm-software (AVA, Version 4.3 C) performed the analyses (see Figure 1, right). According to the second consensus on the assessment of sublingual microcirculation in critically ill patients (European Society of Intensive Care Medicine), the following parameters of microcirculation were assessed [18]:

Microvascular values can offer information about both convexity and diffusion capacities [19]. Information about convexity and perfusion can be gained by measuring the proportion of perfused vessels (PPV = 100 * (Total number of perfused vessels / total number of vessels) [20]. Information about diffusion can be estimated by the total vessel density (TVD) and the number of crossings (NC). Density was assessed by the total vessel density and the number of crossings. Both information can be combined for perfused vessel density (PVD = total length of perfused vessels divided by the analyzed area) and perfused number of crossings (PNC = number of vessel crossings with continuous flow). Vessels with diameters less than 20 mm are mostly capillaries that are primarily responsible for the microcirculation. The small vessel values are marked by the prefix "s" (e.g. sPPV = PPV of small vessels). The values for all vessels can be considered as a quality check to exclude for example pressure artifacts [21].

Statistics

Analyses were performed with Microsoft® Excel 2010 for Windows, the IBM Statistical Package for the Social Sciences (SPSS) 23.0 for Windows and Graph Pad Prism (Graph Pad Prism Software, Version 5, Graph Pad Software, San Diego, California, USA). The data were checked for normal distribution by the Shapiro-Wilk test and are presented as mean ± standard deviation. Categorical data are expressed as numbers (percentage). In this regard, the statistical tests applied were the Mann Whitney U and t-test, respectively. Data with a skewed distribution are reported as the median (25th–75th percentiles). Changes were evaluated using the Wilcoxon´s matched-pair test. A 2-tailed p-value < 0.05 was considered statistically significant.

Results

Patients' characteristics

Thirty patients were included. In 17 patients (57%), the video quality was directly judged sufficient for direct evaluation. The average age of patients that could immediately be analyzed was 60 years (± 21 years SD), the severity of the disease – measured by NACA - was 3 (± 1). Vital parameters were within the normal range (heart rate 89 ± 20 beats per minute; respiratory rate 14 ± 5 / minute; SpO_2 95 ± 5%; systolic blood pressure 141 ± 20 mmHg / diastolic 86 ± 14 mmHg, calculated mean arterial pressure 104 ± 12 mmHg). The most frequent causes for an emergency call were cardiac reasons (47%), generally internal (24%) and respiratory reasons (18%; see also Table 1).

Recruitment under "field-conditions"

Several factors limit the suitability of SDF-measurement in the ambulance car. All comatose or confused patients could not be included due to their inability for informed consent. Patients with advanced dementia or psychiatric disorders had to be excluded. Furthermore, in case of time-crucial emergencies such as myocardial infarction, acute stroke or polytrauma, "time-on-scene" naturally had to be as short as possible. The most frequent reasons preventing SDF-measurement in patients without a lack of consent were a time-critical disease (64%) or technical problems with the devices (14%). No patient refused to give informed consent No complications regarding the SDF measurements occurred.

Duration of the SDF-measurement under "field-conditions"

Lack of time was one of the most important problems measuring microcirculation. On average, it took 02:24±01:08 minutes for the SDF camera and software to be ready for use, when the camera was connected and the tablet was on "standby". 05:32±02:22 minutes were necessary for the recording of sufficient video quality, and 01:15±00:23 minutes for software to automatically evaluate one video.

Quality scores

The videos of 17 patients (57%) could be analyzed directly. The average quality of the video (MIQS) was 2.2 ± 0.45 points ("acceptable"). The most frequent points that

prevented a direct analysis were awarded for lack of focus (23%) and image stability (27%).

Microcirculation

There were no higher degree restrictions of circulation in all vessels with regard to vessel density (NC 41±6.1 /mm², TVD 8.8±1.4 cpll/mm²) and perfusion (PVD 8.2±1.0 mm/mm², PPV 93.1±4.7 %, Figure 2). In the small vessels, that are responsible for the microcirculation, there was an impaired vessel density (sNC 14.8±8.5 /mm², sTVD 3.1±1.8 cpll/mm²) and blood flow (sPVD 2.8±2.1 mm/mm², sPPV 86.1±1.3%; sPNC 12.3±7.3 /mm²; Figure 3). A Spearman's rank-order correlation was run to determine the relationship between NACA scores and the microcirculatory values. There was a statistically significant strong, negative correlation between NACA scores and the microcirculatory values with the exception for sPVV (see Table 2). Furthermore, with exception for sPVV, all microcirculatory parameters positively correlated in a moderate manner with each other. Vital signs did not correlate with the microcirculation.

Follow up

The follow up asked for the length of stay, intra-hospital mortality and 30 days mortality. Neither macro- nor microcirculatory parameters showed a significant correlation with the length of stay, intra-hospital mortality or 30 days mortality (see Table 3).

Discussion

This proof-of-concept study investigates the feasibility and safety of sublingual intravital sidestream darkfield microscopy in the acute emergency setting of an ambulance car outside the hospital. The main finding of this study is that this technology offers reliable results and acceptable image quality in the prehospital setting.

Early risk stratification is very important for several reasons: The number of emergency calls is continuously rising [22]. Demographic and social reasons lead to more patients with multiple morbidities, but also to significantly more "unnecessary" calls for the ambulance [2]. In general, prehospital resources to recognize severely ill patients are limited. To plan further treatment for patients, it is important to assess the severity of the acute illness of the patient as soon as possible. In particular, in rural areas, there are significantly fewer hospitals and ambulance units in charge. Furthermore, distances between the place of action and the hospitals increase, thus resulting in longer transport times. In brief, the ambulance-team must rapidly decide, which type of transport and which hospital is appropriate. The wrong choice might result in a negative outcome and – a growing threat - legal complaints.

The gold standard, the serum lactate and its kinetics [23], is very rarely available in ambulances. In addition, this parameter requires an existing microcirculation disorder to increase. The direct real-time assessment of microcirculation using intravital sidestream darkfield microscopy can offer several important advantages: There is growing evidence that sublingual SDF-measurement helps in recognizing acute circulatory failure at the early stages, in which both systemic compensatory mechanisms and metabolic adaptations at the microcirculatory level still maintain "stable blood pressure" [3, 5, 24]. Several clinical tests exist to estimate the microcirculation such as capillary refill time [15], mottling score [25] and skin temperature. However, in practice there is a great inter-observer-difference in not trained persons, as these tests remain highly subjective [26].

In contrast, calculated microcirculatory parameters are user-independent, if specially trained medical personnel have recorded the videos in sufficient quality. This study clearly demonstrates that the precise point-of-care evaluation of sublingual microcirculation is both feasible and safe in emergency patients outside the hospital. Calculated microcirculatory values are better prognostic indicators for the development of multiple organ dysfunction syndromes than more traditional indices such as the "shock-

index" [27]. Another important field for intravital sidestream darkfield microscopy might be the prehospital fluid therapy. The correct identification of patients needing fluids and patients suffering from hypervolemia is often challenging [28]. For these purposes, it is important to get the measurements readily available and interpretable without the need for extensive calculations or manual interpretation. The administration of fluids can lead to shear stress to the endothelial glycocalyx and its accumulation often results in haemodilution, venous congestion and interstitial edema [24, 29]. Finally, all these effects contribute to inhibition of oxygen diffusion between capillaries and the end organ tissues. The sublingual microcirculatory assessment might help to avoid these harmful effects. In the future, SDF-based microcirculation values could help to guide adequate fluid therapy. SDF-measurement is not restricted to physicians and can be learned by nurses in a safe and reliable way (MICRONURSE) [30]. An important difference of the current study and MICRONURSE is the evaluation of the sublingual microcirculation. MICRONURSE used manually collected parameters such as the MFI (microvascular flow index) that demonstrated an excellent agreement with the conventional offline analysis by physicians. In contrast, the present study lacks a corresponding manual offline control. Future studies will be necessary to verify the reliability of the automated systems by medical personnel that is untrained for microvascular analysis.

In this study, the whole acquirement and analysis of one video could be done in less than 10 minutes. Every additional video acquirement and analysis needed more time. Therefore, two parameters of the device should be optimized for routine use: First, there is an urgent need for acceleration of performing the analysis. Second, the device should be "all-in-one" without the need for an additional tablet computer. Intravital sidestream darkfield microscopy should need less or equal time than a 10 lead ECG. With such improvements, this technology might save time in recognizing critically ill patients. Thus, treatment might start earlier and the right destination hospital might be chosen more accurately. Further studies are needed to explore the value of intravital sidestream darkfield microscopy for immediate risk stratification in a prehospital emergency setting.

This study has several limitations. The method used by AVA 4.3C to assess vessel density is not yet sufficiently validated at this time. The patients that gave informed

consent had relatively low NACA-scores. The NACA score usually offers a good out-of-hospital prediction for mortality [31]. Due to ethical restrictions, all patients that were not fully orientated or suffered from a time-critical disease had to be excluded because of lacking informed consent. However, the microcirculatory values for small vessels were impaired and had a good correlation with NACA scores, which might reflect the acute emergency that leads to the ambulance call.

Conclusion

Sublingual intravital sidestream darkfield microscopy is a promising, feasible and safe tool for point-of-care risk-stratification outside the hospital. The main reason that obstructed the use of this technology was the amount of time required. Microcirculation correlated with NACA scores and was slightly impaired despite normal macrocirculatory values.

Perspectives

This technology has the potential to make valid statements about the microcirculation of emergency patients in real time and non-invasively at the patient's bedside. Technical improvements of the device and the software are to be expected, so that the time required for the examination will be reduced. Thus, the direct intravital sidestream darkfield microscopy has the potential to make an essential contribution to the individual risk stratification of critically ill patients.

References

1. Gries, A., et al., *Realistic assessment of the physician-staffed emergency services in Germany.* Anaesthesist, 2006. **55**(10): p. 1080-6.

2. Bader, K., et al., *[Development of ground-based physician-staffed emergency missions in the city of Leipzig from 2003 to 2013].* Anaesthesist, 2018. **67**(3): p. 177-187.

3. Jung, C., *Assessment of microcirculation in cardiogenic shock.* Curr Opin Crit Care, 2019. **25**(4): p. 410-416.

4. Dubin, A., et al., *Increasing arterial blood pressure with norepinephrine does not improve microcirculatory blood flow: a prospective study.* Crit Care, 2009. **13**(3): p. R92.

5. De Backer, D., et al., *Microcirculatory alterations in patients with severe sepsis: impact of time of assessment and relationship with outcome.* Crit Care Med, 2013. **41**(3): p. 791-9.

6. Qian, J., et al., *Post-resuscitation intestinal microcirculation: its relationship with sublingual microcirculation and the severity of post-resuscitation syndrome.* Resuscitation, 2014. **85**(6): p. 833-9.

7. Pan, P., et al., *Role of Combining Peripheral with Sublingual Perfusion on Evaluating Microcirculation and Predicting Prognosis in Patients with Septic Shock.* Chin Med J (Engl), 2018. **131**(10): p. 1158-1166.

8. den Uil, C.A., et al., *Impaired microcirculation predicts poor outcome of patients with acute myocardial infarction complicated by cardiogenic shock.* Eur Heart J, 2010. **31**(24): p. 3032-9.

9. Wadowski, P.P., et al., *Sublingual functional capillary rarefaction in chronic heart failure.* Eur J Clin Invest, 2018. **48**(2).

10. Mulders, T.A., et al., *Non-invasive assessment of microvascular dysfunction in families with premature coronary artery disease.* Int J Cardiol, 2013. **168**(5): p. 5026-8.

11. Omar, Y.G., et al., *Sublingual microcirculation is impaired in post-cardiac arrest patients.* Resuscitation, 2013. **84**(12): p. 1717-22.

12. Donadello, K., et al., *Sublingual and muscular microcirculatory alterations after cardiac arrest: a pilot study.* Resuscitation, 2011. **82**(6): p. 690-5.

13. van Genderen, M.E., et al., *Persistent peripheral and microcirculatory perfusion alterations after out-of-hospital cardiac arrest are associated with poor survival.* Crit Care Med, 2012. **40**(8): p. 2287-94.

14. Buijs, E.A., et al., *Early microcirculatory impairment during therapeutic hypothermia is associated with poor outcome in post-cardiac arrest children: a prospective observational cohort study.* Resuscitation, 2014. **85**(3): p. 397-404.

15. Hernandez, G., et al., *Effect of a Resuscitation Strategy Targeting Peripheral Perfusion Status vs Serum Lactate Levels on 28-Day Mortality Among Patients With Septic Shock: The ANDROMEDA-SHOCK Randomized Clinical Trial.* JAMA, 2019. **321**(7): p. 654-664.

16. Bimpong-Buta, N.Y., et al., *Analysis of human microcirculation in weightlessness: Study protocol and pre-study experiments.* Clin Hemorheol Microcirc, 2018. **70**(1): p. 119-127.

17. Massey, M.J., et al., *The microcirculation image quality score: development and preliminary evaluation of a proposed approach to grading quality of image acquisition for bedside videomicroscopy.* J Crit Care, 2013. **28**(6): p. 913-7.

18. Ince, C., et al., *Second consensus on the assessment of sublingual microcirculation in critically ill patients: results from a task force of the European Society of Intensive Care Medicine.* Intensive Care Med, 2018. **44**(3): p. 281-299.

19. Massey, M.J. and N.I. Shapiro, *A guide to human in vivo microcirculatory flow image analysis.* Crit Care, 2016. **20**: p. 35.

20. Vellinga, N.A., et al., *International study on microcirculatory shock occurrence in acutely ill patients.* Crit Care Med, 2015. **43**(1): p. 48-56.

21. Rorije, N.M.G., et al., *High-salt intake affects sublingual microcirculation and is linked to body weight change in healthy volunteers: a randomized cross-over trial.* J Hypertens, 2019. **37**(6): p. 1254-1261.

22. Scherer, M., et al., *Patients Attending Emergency Departments A Cross-sectional Study of Subjectively Perceived Treatment Urgency and Motivation for Attending.* Deutsches Arzteblatt International, 2017. **114**(39): p. 645-I.

23. Masyuk, M., et al., *Prognostic relevance of serum lactate kinetics in critically ill patients.* Intensive Care Med, 2019. **45**(1): p. 55-61.

24. Ince, C., *Hemodynamic coherence and the rationale for monitoring the microcirculation.* Crit Care, 2015. **19 Suppl 3**: p. S8.

25. Jouffroy, R., et al., *Skin mottling score and capillary refill time to assess mortality of septic shock since pre-hospital setting.* Am J Emerg Med, 2019. **37**(4): p. 664-671.

26. Hanson, J., et al., *The reliability of the physical examination to guide fluid therapy in adults with severe falciparum malaria: an observational study.* Malar J, 2013. **12**: p. 348.

27. Hutchings, S.D., et al., *Microcirculatory Impairment Is Associated With Multiple Organ Dysfunction Following Traumatic Hemorrhagic Shock: The MICROSHOCK Study.* Crit Care Med, 2018. **46**(9): p. e889-e896.

28. Cecconi, M., et al., *Fluid administration for acute circulatory dysfunction using basic monitoring: narrative review and expert panel recommendations from an ESICM task force (vol 45, pg 21, 2019).* Intensive Care Medicine, 2019. **45**(1): p. 136-136.

29.   Monge Garcia, M.I., et al., *Effects of fluid administration on arterial load in septic shock patients.* Intensive Care Med, 2015. **41**(7): p. 1247-55.

30.   Tanaka, S., et al., *Qualitative real-time analysis by nurses of sublingual microcirculation in intensive care unit: the MICRONURSE study.* Crit Care, 2015. **19**: p. 388.

31.   Raatiniemi, L., et al., *Do pre-hospital anaesthesiologists reliably predict mortality using the NACA severity score? A retrospective cohort study.* Acta Anaesthesiol Scand, 2013. **57**(10): p. 1253-9.

	Mean	SD	Minimum	Maximum
Age [years]	60	21	25	91
Male sex [%]	47			
NACA	3	1	2	5
Heart rate [Beats per minute]	88.9	20.1	37.8	120.2
Respiratory rate per Minute	14.3	5.3	10.0	33.0
SPO_2 [%]	95.7	5.7	75.8	101.2
RR syst. [mmHg]	140.5	20.1	116.0	191.0
RR diast. [mmHg]	85.6	13.6	60.4	106.2
MAP [mmHg]	103.9	11.9	78.93	120.33
Capillary refill time > 3 seconds [%]	12,00			

Table 1: *Patients' characteristics*

		sPNC	sPVD	sPPV	sNC	sTVD	NACA
sPNC	r_s	1.000	.999**	-0.300	.980**	.987**	-.508*
	p		0.000	0.241	0.000	0.000	0.037
sPVD	r_s	.999**	1.000	-0.301	.983**	.990**	-.518*
	p	0.000		0.240	0.000	0.000	0.033
sPPV	r_s	-0.300	-0.301	1.000	-0.396	-0.355	0.074
	p	0.241	0.240		0.116	0.162	0.778
sNC	r_s	.980**	.983**	-0.396	1.000	.990**	-.525*
	p	0.000	0.000	0.116		0.000	0.030
sTVD	r_s	.987**	.990**	-0.355	.990**	1.000	-.531*
	p	0.000	0.000	0.162	0.000		0.028
NACA	r_s	-.508*	-.518*	0.074	-.525*	-.531*	1.000
	p	0.037	0.033	0.778	0.030	0.028	

*Table 2: Correlation of microcirculatory parameters (small vessels) with the NACA scores (r_s, Spearman-Rho-correlation; significance two-tailed: * = p<0.05, ** = p<0.001; n=17)*

	LOS [days]	intra-hospital mortality n, [%]	30d mortality n, [%]
Mean	5.4	1 (7%)	1 (9%)
SD	13.6		
Minimum	1		
Maximum	56		
Patients[1]	15 (100%)	15 (100%)	11 (73%)
LOS = Length of stay; (Mortality, no. (% of total)); [1]Patients who were reached for a follow-up; Data are presented as n (%)			

Table 3: Follow up

Total vessel density

TVD [cpll/mm²]

Percentage of perfused vessels

[%]

Perfused vessel density

PVD [/mm²]

Perfused number of crossings

PNC [/mm²]
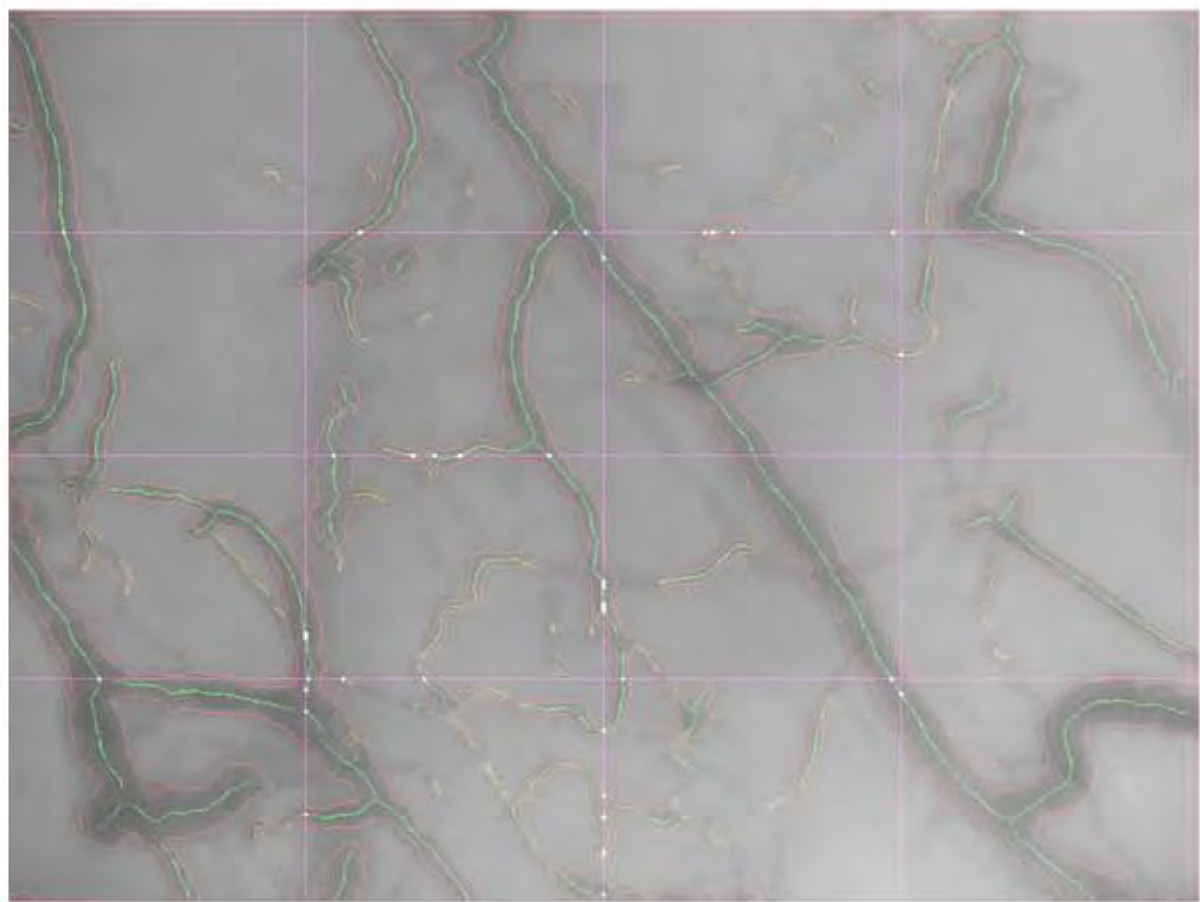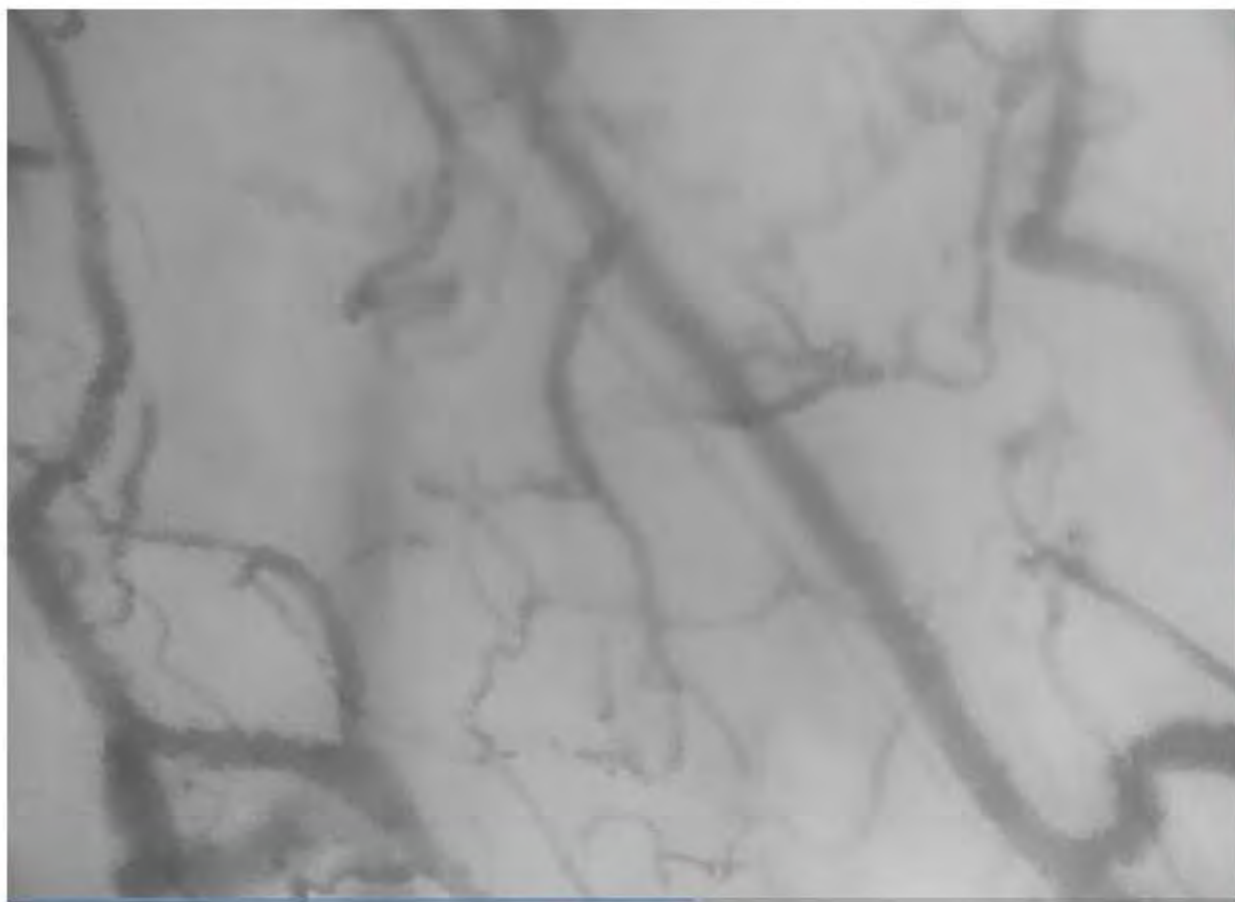
Total small vessel density

Percentage of perfused small vessels
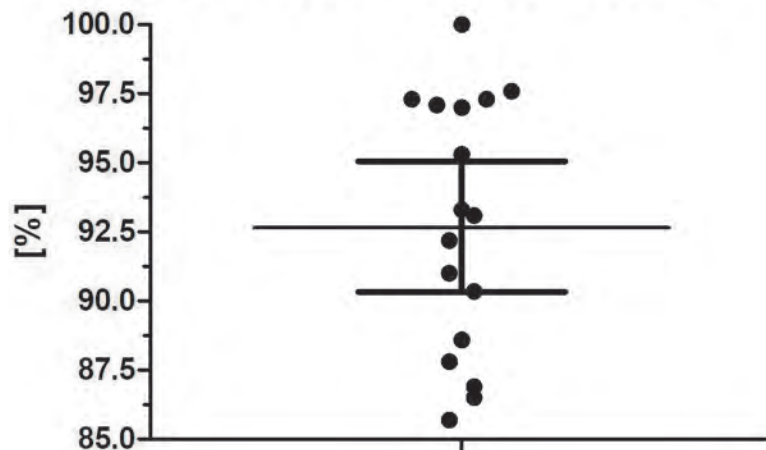
Perfused small vessel density

Perfused Number of Crossings (small)
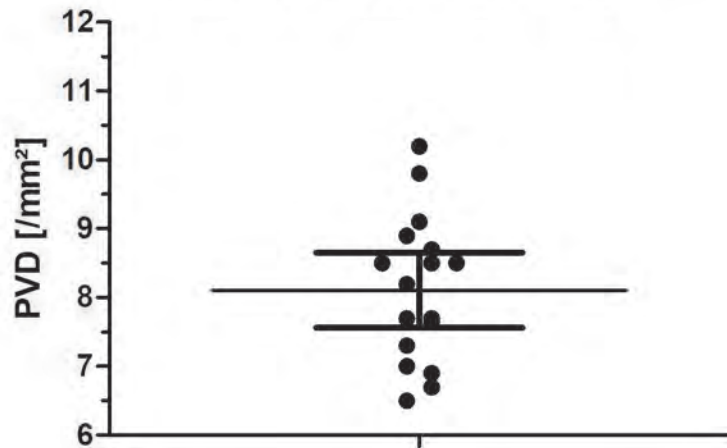
Taylor & Francis
healthsciences
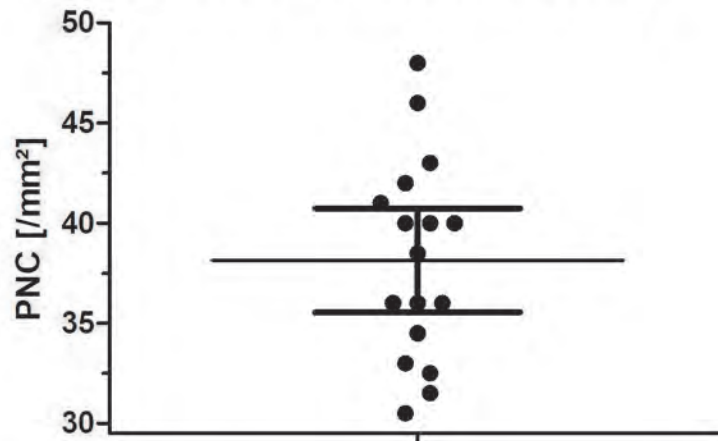
The Role of Mitochondria in Epilepsy: Implications for Neurodegenerative Diseases

Wolfram S. Kunz, Nana Yaw-B. Bimpong-Buta, Alexei P. Kudin, and Christian E. Elger

Department of Epileptology, University of Bonn Medical Center, Bonn, Germany

The epileptic seizures observed in a broad variety of diseases involving mitochondrial DNA (mtDNA) and central nervous system pathology strongly suggest the possible role of mitochondria in the pathomechanism of various forms of epilepsy. The mtDNA mutations in these diseases affect the functions of complexes of oxidative phosphorylation that have mitochondria-encoded subunits. Similar deficiencies of oxidative phosphorylation, in particular of Complexes I and IV, have been detected in the epileptogenic brain regions of therapy-resistant focal epilepsies, such as the hippocampal subfield CA3 in temporal lobe epilepsy with Ammon's horn sclerosis. This suggests that impaired mitochondrial function can affect the viability and excitability of hippocampal neurons because of (1) decreased production of adenosine 5′-triphosphate; (2) increased generation of reactive oxygen species; and (3) alteration of calcium homeostasis.

DYSFUNCTION OF THE MITOCHONDRIAL RESPIRATORY CHAIN IN EPILEPSY

The major source of adenosine 5′-triphosphate (ATP) in neurons is mitochondrial oxidative phosphorylation. Therefore, defects in oxidative phosphorylation in the central nervous system (CNS) have deleterious effects causing so-called mitochondrial encephalopathies. In a broad variety of these diseases, epileptic seizures have been observed. An overview of mitochondrial disorders that present with an epileptic phenotype is given in Table 1. Most of them are associated with mutations in the autonomous mitochondrial DNA, which consists of 13 polypeptide genes, a 16S and a 12S ribosomal RNA (rRNA) gene, and 22 transfer RNA (tRNA) genes. A well-known mitochondrial

disorder with an epileptic phenotype is myoclonus epilepsy with ragged red fibers (MERRF) syndrome, which has been associated with mutations in the mitochondrial tRNA[Lys] gene (Silvestri et al. 1992). However, as shown in Table 1, other mitochondrial DNA mutations, localized predominantly in the mitochondrial tRNA genes for lysin, serin, leucin, isoleucin, or cystein, have also been associated with epileptic phenotypes.

These mutations affect the protein biosynthesis of all mitochondria-encoded subunits of the following complexes of the mitochondrial oxidative phosphorylation pathway: Complex I (NADH: CoQ oxidoreductase, containing seven mitochondria-encoded subunits); Complex III (CoQH$_2$: cytochrome *c* oxidoreductase, containing one mitochondria-encoded subunit); Complex IV (cytochrome *c* oxidase, containing three mitochondria-encoded subunits); and Complex V (F$_0$F$_1$-ATPase, containing two mitochondria-encoded subunits). Quite rarely, mutations in polypeptide-coding mitochondrial genes have been reported in patients with epilepsy: in the ATPase 6 gene (Canafoglia et al. 2001; de Vries et al. 1993); in the CO III gene (Manfredi et al. 1995); and in the ND 1 gene (Brown et al. 2001). We have recently identified a novel mutation in the CO I gene associated with epilepsia partialis continua (Varlamov et al. 2002). This mutation leads to an exchange of a highly conserved leucine in helix V of COX subunit I to isoleucine which destabilizes this α helix.

The large variation in the clinical phenotype, even for a given mutation, is a well-known feature of mitochondrial diseases. It is therefore very likely that the distribution of the mitochondrial defect within the CNS is the factor responsible for determining the association of a certain mutation with epilepsy. Thus, mitochondrial encephalopathy with lactic acidosis and stroke-like episodes (MELAS) is characterized by foci of necrosis that are localized predominantly in the cerebral cortex and also in the hippocampus, a highly epileptogenic area, whereas MERRF preferentially involves the inferior olivary nucleus, the cerebellar dentate nucleus, the red necleus, and the pontine tegmentum, structures that are implicated in the genesis of myoclonus.

In contrast to the relatively rare mitochondrial encephalopathies associated with mtDNA mutations, epilepsy is a common neurological disorder that is usually well controlled by

RIGHTSLINK

TABLE 1
Mitochondrial disorders associated with epileptic phenotypes

Clinical diagnosis	Detected mtDNA mutations	Reference
MERRF ($n = 3$)	A8344G in tRNA Lys	Canafoglia et al. 2001
Atypical MERRF ($n = 4$)	A8344G in tRNA Lys	Canafoglia et al. 2001; Silvestri et al. 1992;
	T8356C in tRNA Lys	Zeviani et al. 1993
MELAS ($n = 7$)	A3243G in tRNA Leu in 3 patients	Canafoglia et al. 2001; Manfredi et al. 1995,
	A5814G in tRNA Cys in 1 patients	1996
	T9957C in COX III in 1 patients	
Other ME ($n = 4$)	A3243G in tRNA Leu in 2 patients	Canafoglia et al. 2001
ME with cardiomyopathy ($n = 2$)	A4269G or C4320T in tRNA Ile	Santorelli et al. 1995; Taniike et al. 1992
ME with recurrent episodes of epilepsia partialis continua ($n = 3$)	T7512C in tRNA Ser(UCN)	Jaksch et al. 1998; Schülke et al. 1998
ME with recurrent episodes of epilepsia partialis continua ($n = 1$)	C6489A mutation in COX I	Varlamov et al. 2002
LHON ($n = 2$)	G3460A in ND1	Brown et al. 2001
LHON ($n = 1$)	C4640A in ND2	W. S. Kunz, unpublished data
Leigh syndrome ($n = 6$)	T8993G in ATPase6 1 patients	Canafoglia et al. 2001; de Vries et al. 1993
	T8993C in ATPase6 1 patients	
ME with PDH deficiency ($n = 6$)	nd	Canafoglia et al. 2001
ME with various RC defects ($n = 6$)	nd	Canafoglia et al. 2001

LHON, Leber's hereditary optical neuropathy; ME, mitochondrial encephalopathy; MELAS, mitochondrial encephalopathy with lactic acidosis and stroke-like episodes; MERRF, myoclonus epilepsy with ragged red fibers; n, Number of different patients; nd, not detected; RC, respiratory chain; PDH, pyruvate dehydrogenase.

currently available drugs. However, 20% to 30% of patients do not experience seizure control with the available medication. The majority of these patients suffer from focal epilepsies that can develop subsequent to brain trauma, complicated febrile convulsions, status epilepticus, ischemic lesions, or brain tumors. The areas of epileptogenesis in these cases are usually characterized by cell loss. It is well documented that during seizures, both nerve cells and glia undergo necrotic and apoptotic cell death. Neuropathological investigations have repeatedly pointed to a similarity between ischemia-related and seizure-related alterations of neurons that are characterized by swollen and disrupted mitochondria. In patients with Ammon's horn sclerosis, mitochondrial ultrastructural pathology has been described as a characteristic feature of hilar neurons (Blümcke et al. 1999). In this context, it is noteworthy to mention that in addition to the pathological abnormalities, functional defects have also been reported in mitochondria in the areas of epileptogenesis. Thus, we observed a severe impairment of respiratory-chain Complex I activity in CA3 neurons in the hippocampus in patients with Ammon's horn sclerosis and in the parahippocampal gyrus of patients with parahippocampal lesions (Kunz et al. 2000). In these reports the mitochondrial abnormalities have been observed only close to or directly in the epileptic focus, whereas the surrounding brain tissue examined (e.g., the parahippocampal gyrus in patients with clearly pronounced hippocampal pathology and hippocampal seizure focus) showed no mitochondrial pathology.

MITOCHONDRIA AND EPILEPSY-RELATED NEURONAL CELL DEATH

It has been reported that prolonged seizures (status epilepticus) induced by kainic acid or pilocarpine in experimental models activate programmed cell-death mechanisms (Bengzon et al. 1997; Meldrum 1993). This cell death is also characteristic of human epilepsy and is one of the most important aspects of epileptogenesis. In the hippocampus, the loss of CA1, CA3, and CA4 pyramidal neurons, with relative sparing of the granular neurons of the dentate gyrus and some types of interneurones, is the histopathological hallmark of Ammon's horn sclerosis. The mechanism that underlies this regional selectivity remains to be elucidated, although some data point to differential expression of proaportotic and antiapoptotic genes. Probably the most important factor preceding neuronal cell death after status epilepticus is the increased level of reactive oxygen species observed in various models of experimentally induced epileptiform activity in brain slices and slice cultures such as kainate-induced hippocampal damage, pilocarpine treatment, and low levels of magnesium cations (Kovacs et al. 2001; Kubova et al. 2001; Liang et al. 2000; Schuchmann et al. 1999). The mitochondrial respiratory chain is known to be the most important source of production of reactive oxygen species. The direct reaction product is the superoxide anion, which is readily converted by manganese superoxide dismutase into hydrogen peroxide. To illustrate this feature, we measured the generation of hydrogen peroxide by isolated rat brain mitochondria (Fig. 1). Mitochondria
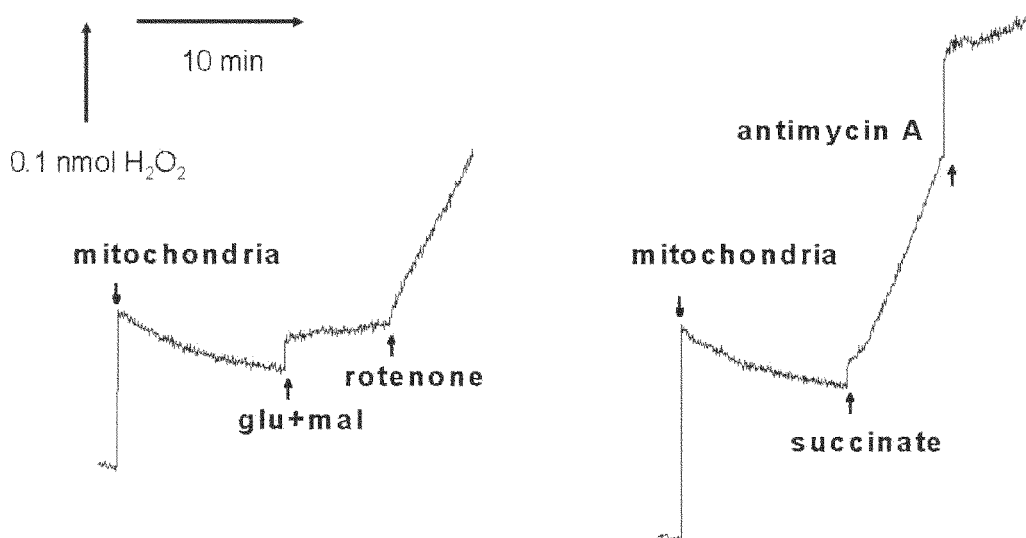
FIG. 1. The generation of hydrogen peroxide (H_2O_2) by isolated rat brain mitochondria was measured by monitoring the change in fluorescence of para-hydroxyphenylacetic acid ($\lambda_{ex} = 317$ nm, $\lambda_{em} = 414$ nm) catalyzed by horseradish peroxidase. Additions: 10 mM glutamate + 5 mM malate (glu + mal); 5 μM rotenone; 10 mM succinate; 1 μM antimycin A. (Excitation wavelength-$\lambda_{ex} = 317$ nm, emission wavelength-$\lambda_{em} = 414$ nm)

in the presence of glutamate and malate alone generate only small amounts of hydrogen peroxide, whereas abundant production is observed after the addition of the Complex I inhibitor rotenone or in the presence of the respiratory substrate succinate alone. This is an indication that most of the superoxide radicals are produced at Complex I and that strong production of reactive oxygen species is a feature of respiratory-chain–inhibited mitochondria or of reversed electron flow. It is important to note that the rate of hydrogen peroxide generation by respiratory-chain Complex III, which can be observed in the presence of the Complex III inhibitor antimycin A, is substantially lower (see Fig. 1).

It is noteworthy in this context that decreased activity in respiratory-chain Complex I can be detected in the areas of epileptogenesis, that is, in the CA3 neurons of the hippocampus in patients with Ammon's horn sclerosis and in the parahippocampal gyrus in patients with parahippocampal lesions (Kunz et al. 2000). Similar observations were made in the vulner-

able CA1 and CA3 hippocampal subfields of pilocarpine-treated, chronic-epileptic rats (Kudin et al. 2002). These data are summarized in Figure 2. In the context of the results found in isolated brain mitochondria (see Fig. 1) this would strongly imply increased rates of generation of oxygen radicals by respiratory-chain Complex I in the epileptogenic brain areas.

As potential cause of the detected respiratory-chain impairment, we could delineate a decrease in the mitochondrial DNA (mtDNA) copy number. This finding indicates a possible substantial role of oxygen radicals in causing neuronal mtDNA damage that occurs selectively in the areas of epileptogenesis (Kudin et al. 2002). To explain these findings we would like to suggest the following scheme (Fig. 3) to explain the self-accelerating mitochondrial dysfunction and neuronal cell death in the epileptogenic foci of patients with temporal lobe epilepsy and in the hippocampi of pilocarpine-treated chronic-epileptic rats.
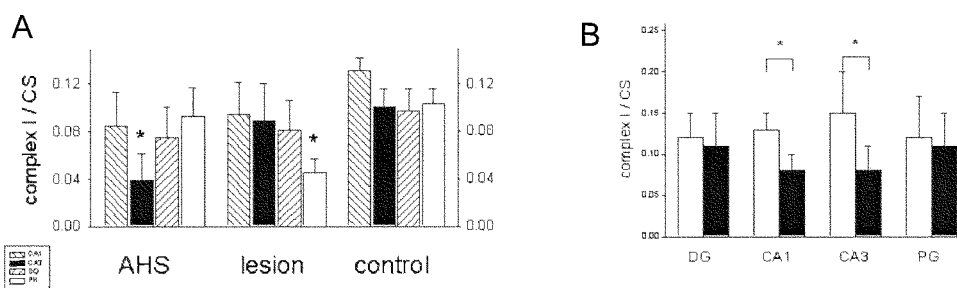

FIG. 2. The activities of Complex I (rotenone-sensitive NADH:CoQ1 oxidoreductase) and citrate syntase in dissected hippocampal subfields, determined as described by Kunz et al. (2000) and Kudin et al. (2001). (A) Human hippocampi. AHS (Ammon's horn sclerosis), $n = 15$; parahippocampal lesions, $n = 5$; nonepileptic control patients, $n = 2$. Up/down hatched bars, CA1 subfield; black bars, CA3 subfield; down/up hatched bars, dentate gyrus; white bars, parahippocampal gyrus. (B) Rat hippocampi. White bars, control rats; black bars, pilocarpine-treated chronic-epileptic rats; *, significant difference from controls ($p < .05$). *Note:* For details of the experiment, see Kunz et al. (2000) and Kudin et al. (2002).
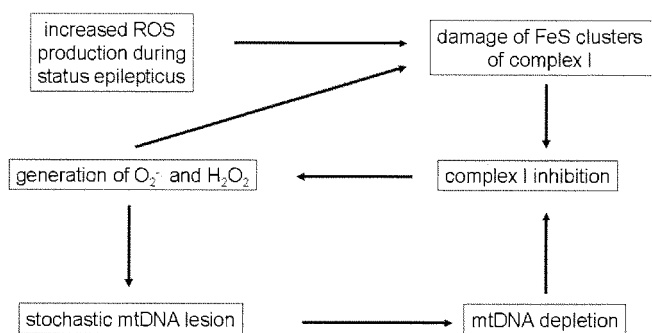
FIG. 3. Possible self-accelerating mechanism leading to mitochondrial dysfunction and neuronal cell death in the epileptogenic focus. FeS cluster, iron-sulphur cluster; H_2O_2, hydrogenperoxide; ROS, reactive oxygen species.

CAN MITOCHONDRIAL DYSFUNCTION ALTER NEURONAL EXCITABILITY?

It has been reported that the direct partial inhibition of enzymes in the mitochondrial respiratory chain (cytochrome c oxidase by cyanide, and succinate dehydrogenase by 3-nitropropionic acid) evokes seizures. The potential direct links between the observed impairment of mitochondrial function and the increased neuronal excitability causing epileptiform activity are (1) decreased intracellular ATP levels and (2) alterations in neuronal calcium homeostasis. A relatively high impact of neuronal ATP levels can be postulated because epileptic seizures are observed in patients with Leigh syndrome who harbor the mutations T8993G and T8993C in the ATPase 6 gene. Under these conditions, mitochondria still have a high membrane potential, which enables normal ion transport. Therefore, for cybrids with the T8993G NARP mutation, normal mitochondrial calcium-handling properties at decreased cellular ATP levels were observed (Brini et al. 1999). It has to be mentioned that mitochondrial oxidative phosphorylation provides the major source of ATP in neurons, and adequate ATP levels are essential to maintain the neuronal plasma membrane potential via the sodium-potassium ATPase, which consumes about 40% of the energy. Therefore, the decreased neuronal plasma membrane potential is most likely responsible for epileptic seizures observed in Leigh syndrome patients harboring ATPase 6 gene mutations.

On the other hand, it is well established that mitochondria are an important intracellular sequestration system for calcium cations (Ca^{++}). Especially because of this feature, mitochondria are believed to modulate neuronal excitability and synaptic transmission, which are altered in epilepsy. In agreement with this concept is our own demonstration that in kainate-treated chronic-epileptic rats, impaired oxidative phosphorylation occurs because of Ca^{++} cycling at the inner membrane of hippocampal mitochondria (Kunz et al. 1999). Similarly, impaired cellular Ca^{++} homeostasis resulting from substantial alterations in mitochondrial handling of Ca^{++} seems to be a feature of cybrid cells harboring the mitochondrial T8356C mutation that is associated with MERRF (Brini et al. 1999).

CONCLUSIONS

We have presented evidence that impaired mitochondrial function can affect the viability and excitability of hippocampal neurons as a result of (1) decreased production of ATP; (2) increased generation of reactive oxygen species; and (3) an alteration in calcium homeostasis. Therefore, mitochondrial oxidative phosphorylation has to be considered an important target for future therapeutic strategies in epilepsy and other neurodegenerative disorders.

REFERENCES

Bengzon, J., Kokaia, Z., Elmer, E., Nanobashvili, A., Kokaia, M., and Lindvall, O. 1997. Apoptosis and proliferation of dentate gyrus neurons after single and intermittent limbic seizures. *Proc. Natl. Acad. Sci. USA* 94:10432–10437.

Blümcke, I., Zuschratter, W., Schewe, J. C., Suter, B., Lie, A. A., Riederer, B. M., Meier, B., Schramm, J., Elger, C. E., and Wiestler, O. D. 1999. Cellular pathology of hilar neurons in Ammon's horn sclerosis. *J. Comp. Neurol.* 414:437–453.

Brini, M., Pinton, P., King, M. P., Davidson, M., Schon, E. A., and Rizutto, R. 1999. A calcium signalling defect in the pathogenesis of a mitochondrial DNA inherited oxidative phosphorylation deficiency. *Nat. Med.* 5:951–954.

Brown, M. D., Zhadanov, S., Allen, J. C., Hosseini, S., Newman, N. J., Atamonov, V. V., Mikhailovskaya, I. E., Sukernik, R. I., and Wallace, D. C. 2001. Novel mtDNA mutations and oxidative phosphorylation dysfunction in Russian LHON families. *Hum. Genet.* 109:33–39.

Canfoglia, L., Franceschetti, S., Antozzi, C., Carrara, C., Farina, L., Granata, T., Lamantea, E., Savoiardo, M., Uziel, G., Villani, F., Zeviani, M., and Avanzini, G. 2001. Epileptic phenotypes associated with mitochondrial disorders. *Neurology* 56:1340–1346.

deVries, D. D., van Engelen, B. G., Gabreels, F. J., Ruitenbeek, W., and van Oost, B. A. 1993. A second missense mutation in the mitochondrial ATPase 6 gene in Leigh's syndrome. *Ann. Neurol.* 34:410–412.

Jaksch, M., Klopstock, T., Kurlemann, G., Dorner, M., Hofmann, S., Kleinle, S., Hegemann, S., Weissert, M., Muller-Hocker, J., Pongratz, D., and Gerbitz, K. D. 1998. Progressive myoclonus epilepsy associated with mutations in the tRNA (Ser(UCN)) gene. *Ann. Neurol.* 44:635–640.

Kovacs, R., Schuchmann, S., Gabriel, S., Kardos, J., and Heinemann, U. 2001. Ca^{2+} signalling and changes of mitochondrial function during low-Mg^{++}–induced epileptoform activity in organotypic hippocampal slice cultures. *Eur. J. Neurosci.* 13:1311–1319.

Kubova, H., Druga, R., Lukasiuk, K., Suchomelova, L., Haugvicova, R., Jirmanova, I., and Pitkanen, A. 2001. Status epilepticus causes necrotic damage in the mediodorsal nucleus of the thalamus in immature rats. *J. Neurosci.* 21:3593–3599.

Kudin, A. P., Kudina, T. A., Seyfried, J., Vielhaber, S., Beck, H., Elger, C. E., and Kunz, W. S. 2002. Seizure-dependent modulation of mitochondrial oxidative phosphorylation in rat hippocampus. *Eur. J. Neurosci.* 15:1105–1114.

Kunz, W. S., Goussakov, I. V., Beck, H., and Elger, C. E. 1999. Altered mitochondrial oxidative phosphorylation in hippocampal slices of kainate-treated rats. *Brain Res.* 826:236–242.

Kunz, W. S., Kudin, A. P., Vielhaber, S., Blümcke, I., Zuschratter, W., Schramm, J., Beck, H., and Elger, C. E. 2000. Mitochondrial complex I deficiency in the epileptic focus of patients with temporal lobe epilepsy. *Ann. Neurol.* 48:766–773.

Liang, L. P., Ho, Y. S., and Patel, M. 2000. Mitochondrial superoxide production in kainate-induced hippocampal damage. *Neuroscience* 101:563–570.

Manfredi, G., Schon, E. A., Bonilla, E., Moraes, C. T., Shauske, S., and DiMauro, S. 1996. Identification of a mutation in the mitochondrial tRNACys gene associated with mitochondrial encephalopathy. *Hum. Mutat.* 7:158–163.

Manfredi, G., Schon, E. A., Moreas, C. T., Bonilla, E., Berry, G. T., Sladky, J. T., and DiMauro, S. 1995. A new mutation associated with MELAS is located in a mitochondrial polypeptide-coding gene. *Neuromuscul. Disord.* 5:391–398.

Meldrum, B. S. 1993. Excitotoxicity and selective neuronal loss in epilepsy. *Brain Pathol.* 3:405–412.

Nakamura, M., Nakano, S., Goto, Y., Ozawa, M., Nagahama, Y., Fukuyama, H., Akiguchi, I., Kaji, R., Kimura, J. 1995. A novel point mutation in the mitochondrial tRNASer(UCN) gene detected in a family with MERRF/MELAS overlap syndrome. *Biochem. Biophys. Res. Commun.* 214:86–93.

Santorelli, F. M., Vazques-Acevedo, M., Gonzalez-Astiarazan, A., Ridaura-Sauz, C., Gonzalez-Halphen, D., and DiMauro, S. 1995. A novel mitochondrial DNA point mutation associated with mitochondrial encephalocardiomyopathy. *Biochem. Biophys. Res. Commun*. 216:835–840.

Schuchmann, S., Buchheim, K., Meierkord, H., and Heinemann, U. 1999. A relative energy failure is associated with low Mg^{++} but not with 4-aminopyridine–induced seizure-like events in entorhinal cortex. *J. Neurophysiol.* 81:399–403.

Schuelke, M., Bakker, M., Stoltenburg, G., Sperner, J., and von Moers, A. 1998. Epilepsia partialis continua associated with a homoplasmic mitochondrial tRNA (Ser(UCN)) mutation. *Ann. Neurol.* 44:700–704.

Silvestri, G., Moreas, C. T., Shanske, S., Oh, S. J., and DiMauro, S. 1992. A new mtDNA mutation in the tRNALys gene associated with myoclonic epilepsy and ragged red fibers (MERRF). *Am. J. Hum. Genet.* 51:1213–1217.

Taniike, M., Kukushima, H., Yanagihara, I., Tsukamoto, H., Tanaka, J., Fujimura, H., Nagai, T., Sano, T., Yamaoka, K., and Inui, K. 1992. Mitochondrial tRNA^{Ile} mutation in fatal cardiomyopathy. *Biochem. Biophys. Res. Commun.* 186:47–53.

Varlamov, D. A., Kudin, A. P., Vielhaber, S., Schröder, R., Sassen, R., Becker, A., Kunz, D., Haug, K., Rebstock, J., Heils, A., Elger, C. E., and Kunz, W. S. 2002. Metabolic consequences of a novel missense mutation of the mtDNA *COI* gene. *Hum. Mol. Genet*. 11:1797–1805.

Zeviani, M., Muntoni, F., Savarese, N., Serra, G., Tiranti, V., Carrara, F., Mariotti, C., and DiDonato, S. 1993. A MERRF/MELAS overlap syndrome with a new point mutation in the mitochondrial DNA tRNALys gene. *Eur. J. Hum. Genet.* 1:80–87.

Touching the Membranous Septum: A Thin Line between Treating and Threatening?

Harilaos Bogossian[a, b]   Nana-Yaw Bimpong-Buta[a]   Patrick Müller[c]

[a]Department of Cardiology and Rhythmology, Evangelisches Krankenhaus Hagen, Hagen, Germany; [b]Department of Cardiology, Witten/Herdecke University, Witten, Germany; [c]Department of Cardiology II – Electrophysiology, Universitätsklinikum Münster, Münster, Germany

The article by Stachon et al. [1] is an important contribution because it highlights the impact of diverse calcification patterns on the conduction system of the heart after transcatheter aortic valve replacement (TAVR). In this regard, the cardiologists of the University of Freiburg performed focused multi-sliced computed tomography for the preprocedural assessment of valve morphology and the valve calcification status on the one hand, and the possible effects on an occasional – yet clinically critical – complication: "postprocedural AV block."

The impact of aortic valve calcification (in particular, its volume, distribution and localization) has been investigated regarding the occurrence of high-degree AV conduction block and the consecutive need for postprocedural pacemaker (PM) implantation. Prior anatomical and electrophysiological studies showed the close topographic relation of the membranous septum to the atrioventricular node and the bundle of His, respectively [2, 3]. Likewise, the topographies of fundamental anatomical structures in the right-sided heart chambers, particularly within the triangle of Koch, have been very well described, the knowledge of which is the framework for established electrophysiological procedures such as slow-pathway ablations in patients with atrioventricular node re-entrant tachycardia. For instance, in the era of His bundle and left bundle pacing, this knowledge has proven useful [4–7].

In prior investigations pertaining the affection of the conduction system in the course of ablation and pacing procedures, alternative procedural access routes, such as left-sided access, have become popular [8, 9]. In these scenarios, the intraprocedural anatomical adjacencies to the right coronary and noncoronary cusps of the aortic valve have been of concern. Due to the anatomical proximity of the abovementioned anatomical structures, notably in TAVR, inherent procedural maneuvers entailing overstretching of the left ventricular outflow tract may cause accidental affection of the conduction system, as is commonly seen during balloon dilatation in TAVR.

This effect might become even more prominent with deeper implantation levels and oversizing of the implemented valve prosthesis, respectively [10]. Alas, in patients with relevant annular calcification, the risk of this effect is even tripled [11].

Commentary on Stachon et al. "Impact of Preprocedural Aortic Valve Calcification on Conduction Disturbances after Transfemoral Aortic Valve Replacement."

Harilaos Bogossian
Department of Cardiology and Rhythmology
Evangelisches Krankenhaus Hagen, Brusebrinkstrasse 20
DE–58135 Hagen (Germany)
bogossianh @ esv.de

In the setting of TAVR, in the light of procedural planning, calcification of the aortic valve is a boon and a bane: on the one hand, it can aid in adequate fixation of the prosthesis, whereas, on the other hand, conduction disturbances may lie in wait.

Bearing this in mind, the present study by Stachon et al. [1] focused on two substantial characteristics of annular valve calcifications: their shape and their orientation. Here, the main finding is that an evaluation of the orientation of calcification has more weight than an evaluation of its shape.

The rate of necessity of PM implantation due to AV block was increased when calcifications crossed the aortic annulus. In patients with this formation, AV block occurred within the first 2 days after TAVR. Even more interesting is the observation that the intensity of the effect on the conduction system seemed to correlate with the orientation of the annular calcification of the valve; in this regard, an orthogonal orientation of the annular calcification, as compared to its tangential orientation, was linked to an even fivefold higher probability of necessity of postprocedural PM implantation. In these cases of "jeopardizing" orthogonal annular valve calcifications, these were located on the contralateral side with respect to the conduction system (particularly below the left coronary cusp). As a hard tissue, the calcification remains in place even after TAVR. In fact, this calcific immobility, with its location in the region of the left coronary cusp, rather acts as a slider towards the region of the conduction system (located between the right coronary and the noncoronary cusp). Thus, one of the potential mechanisms of severe AV conduction disturbances with consecutive necessity of PM implantation in patients with orthogonal annular calcifications could be an inferoseptal shift of TAVR, causing stress on the membranous septum with consecutive injury to the His bundle and/or the left bundle branch.

Although it is a small retrospective study, Stachon et al. [1] describe a novel mechanism of development of post-TAVR AV conduction disturbances. Without any doubt, for interventional cardiologists and physician teams in this context, a profound knowledge about these anatomical correlations of structures in the heart chambers is crucial for any procedural TAVR planning.

Conflict of Interest Statement

The authors have no conflicts of interest to declare.

Funding Sources

Author Contributions

H. Bogossian: substantial contributions to the design of the manuscript; final approval of the version to be published; and agreement to be accountable for all aspects of the work. N.-Y. Bimpong-Buta: substantial contributions to the design of the manuscript, and final approval of the version to be published. P. Müller: substantial contributions to the design of the manuscript, and final approval of the version to be published.

References

1 Stachon P, Steinfurt J, van de Loo T, Trolese L, Faber T, Kaier K, et al. Impact of preprocedural aortic valve calcification on conduction disturbances after transfemoral aortic valve replacement. Cardiology. DOI: 10.1159/000509389.

2 Auffret V, Puri R, Urena M, Chamandi C, Rodriguez-Gabella T, Philippon F, et al. Conduction Disturbances after Transcatheter Aortic Valve Replacement: Current Status and Future Perspectives. Circulation. 2017 Sep;136(11):1049–69.

3 Upadhyay GA. The Variable Arrangement of the Atrioventricular Conduction Axis within the Triangle of Koch: Millimeters Matter. JACC Clin Electrophysiol. 2020 Apr;6(4):378–81.

4 Upadhyay GA, Cherian T, Shatz DY, Beaser AD, Aziz Z, Ozcan C, et al. Intracardiac Delineation of Septal Conduction in Left Bundle-Branch Block Patterns. Circulation. 2019 Apr;139(16):1876–88.

5 Teng AE, Lustgarten DL, Vijayaraman P, Tung R, Shivkumar K, Wagner GS, et al. Usefulness of His Bundle Pacing to Achieve Electrical Resynchronization in Patients with Complete Left Bundle Branch Block and the Relation Between Native QRS Axis, Duration, and Normalization. Am J Cardiol. 2016 Aug; 118(4):527–34.

6 Israel CW. [His bundle stimulation: is it time for routine use?]. Herzschrittmacherther Elektrophysiol. 2020 Jun;31(2):101–3.

7 Israel CW, Tribunyan S, Kalyani M. [His bundle pacing: troubleshooting at implantation]. Herzschrittmacherther Elektrophysiol. 2020 Jun;31(2):160–76.

8 Kaneko Y, Naito S, Okishige K, Morishima I, Tobiume T, Nakajima T, et al. Atypical Fast-Slow Atrioventricular Nodal Reentrant Tachycardia Incorporating a "Superior" Slow Pathway: A Distinct Supraventricular Tachyarrhythmia. Circulation. 2016 Jan;133(2):114–23.

9 Salden FC, Luermans JG, Westra SW, Weijs B, Engels EB, Heckman LI, et al. Short-Term Hemodynamic and Electrophysiological Effects of Cardiac Resynchronization by Left Ventricular Septal Pacing. J Am Coll Cardiol. 2020 Feb;75(4):347–59.

10 Franzoni I, Latib A, Maisano F, Costopoulos C, Testa L, Figini F, et al. Comparison of incidence and predictors of left bundle branch block after transcatheter aortic valve implantation using the CoreValve versus the Edwards valve. Am J Cardiol. 2013 Aug;112(4): 554–9.

11 Hein-Rothweiler R, Jochheim D, Rizas K, Egger A, Theiss H, Bauer A, et al. Aortic annulus to left coronary distance as a predictor for persistent left bundle branch block after TAVI. Catheter Cardiovasc Interv. 2017 Mar; 89(4):E162–8.
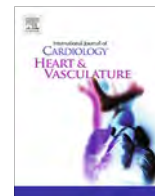
Correspondence

Transaortic pulmonary vein isolation in the presence of situs inversus and total venous anomaly; technical capabilities for 3D reconstruction and considerations of adequate choice of ablation catheters

1. Introduction

Dextrocardia and situs inversus is a very rare anatomical variant. Even more seldom is the co-occurrence with total venous anomaly and absence of a usual Inferior Vena Cava (IVC) draining into the right atrium cranially. [1,2]

The Trans-Septal Puncture (TSP) through the femoral vein in patients with situs inversus has been reported for PVI. Likewise, the retrograde PVI using the magnetic navigation system in the cases of venous anomaly has been described.

A patient with the above mentioned complete anatomical anomaly presented in our hospital for PVI due to highly symptomatic atrial fibrillation (AF). We performed the procedure via the retrograde approach by a 3D mapping system (Ensite NavX precision), 20 polar diagnostic catheter and two different ablation catheters.

2. Patient history

A 51-year-old female with dextrocardia and situs inversus presented with highly symptomatic paroxysmal atrial fibrillation episodes lasting for hours for the past few months under Metoprolol 47,5 mg, bid and Flecainide 100 mg bid.

The patient also underwent DDD-Pacemaker implantation due to Sick Sinus Syndrome in 2012 at an external hospital. Transthoracic echocardiography revealed a normal left ventricular function with concentric left ventricular hypertrophy, normal left atrial diameter and a left ventricular ejection fraction of 60%.

She was referred for catheter ablation. However, the usual TSP approach for the left atrium through femoral vein was not available because the computed tomography (and 3D-CT-reconstruction) revealed that the inferior vena cava was connected to the left brachiocephalic vein and drained cranially into the right atrium through the superior vena cava.

3. Alternative approaches for PVI

Kato et al. reported the technic for trans-septal puncture and catheter ablation via the superior vena cava for atrial fibrillation in a patient with poly-splenia syndrome and interruption of the inferior vena cava.[3] They performed the trans-septal puncture through the right jugular vein using a manually curved Brockenbrough needle and intracardiac echocardiographic guidance accomplishing pulmonary vein isolation using the deflectable guiding sheath and a contact force-sensing ablation catheter. Their method has a few advantages compared to trans-aortic pulmonary vein isolation. For example, they could confirm the complete pulmonary vein isolation using a ring catheter which was introduced through the trans-septal sheath. However, this technique has not been reported for patients with the dextrocardia. Additionally, the superior vena cava approach was rather difficult in our patient. From the left side, the jugular approach was limited due to the presence of two implanted pacemaker electrodes. From the right side the venous anomaly with persistent right superior vena cava draining into the right atrium caudally would have required bending of the transseptal needle with more than 180° to perform the TSP, which would have been beyond the elasticity of the vessels and the needle material.

Also a surgical epicardial approach as possible alternative for PVI had to be considered, specially taking into consideration epicardial cryoablation with predesigned forms. However, in this young patient the situs inversus and the total venous anomaly were also combined with an atypical origin of the pulmonary veins which would have made a surgical ablation even more challenging.

In patients with congenital heart disease an alternative access to the right atrium via the trans-hepatic vein was described for both pacemaker implantation and electrophysiology procedures. After co-consideration of the CT of our patient with our radiologists, this approach was esteemed risky with regard to the narrow caliber of the hepatic vessels. Hence, our interventional radiologists discouraged this approach.

Recently Okajima et al. reported the technique of trans-aortic pulmonary vein isolation using the magnetic navigation system in a patient with dextrocardia, situs inversus and inferior vena cava continuity with the azygous vein.[4] Considering our case, with the presence of the pacemaker (which was not MRI compatible) and also looking at the lack of a magnetic navigation system in our hospital this approach was ruled out much earlier.

Taking into consideration these thoughts and discussions, we esteemed the retrograde approach the optimal procedural way for curative therapy of this patient.

4. Retrograde PVI

After the informed consent of the patient was obtained, we attempted pulmonary vein isolation through the retrograde trans-aortic approach using NavX precision® for the guidance in addition to the 3D Model of the left atrium and pulmonary veins anatomy obtained from the pre-interventional CT-Imaging (Fig. 1A–G).

The CS catheter was introduced via the left femoral vein and was positioned in the coronary sinus through the inferior vena cava which (with a big arch) drained cranially into the right atrium.
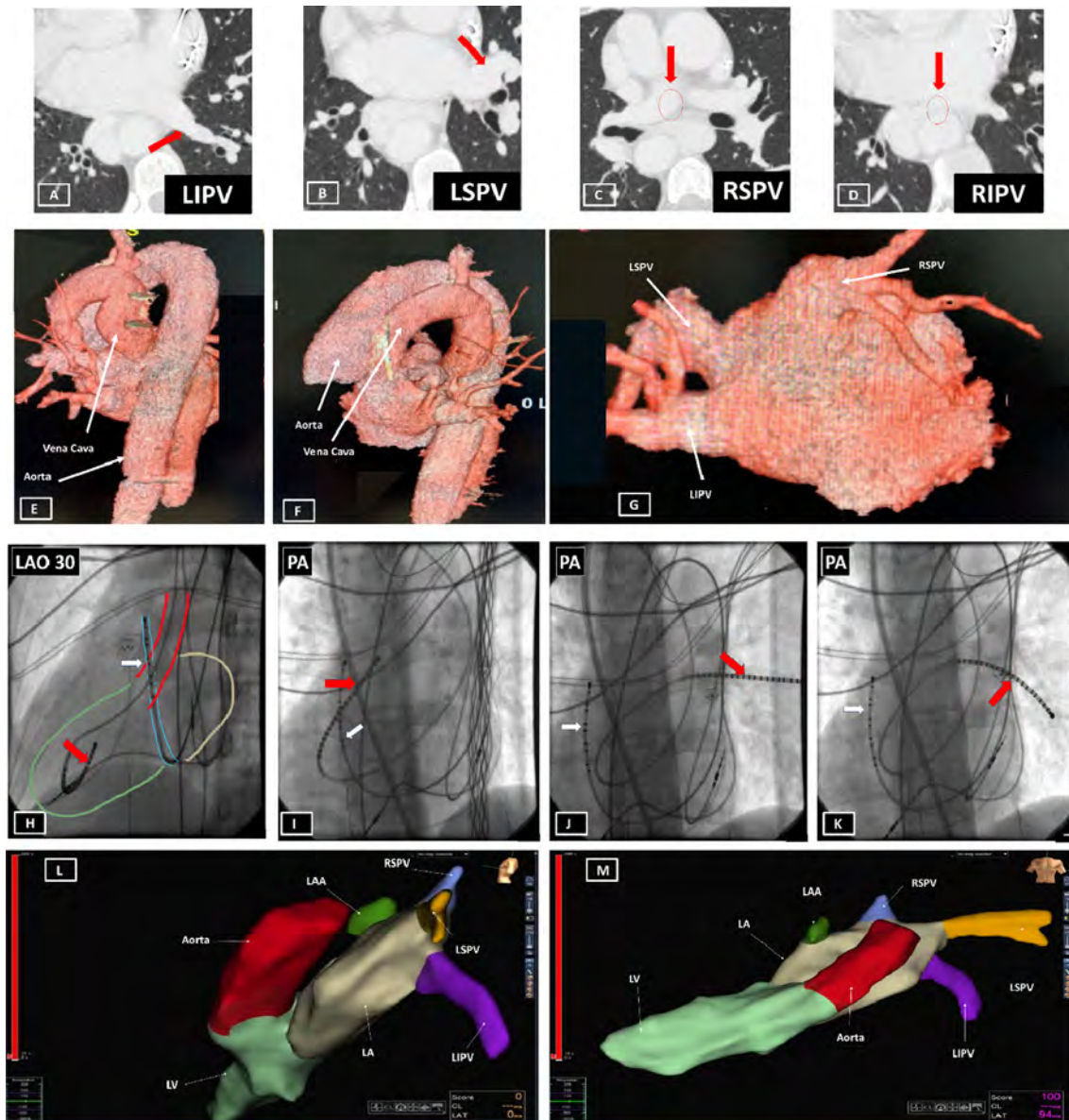
Fig. 1. Computed tomography image of the (A) left inferior pulmonary vein, (B) left superior pulmonary vein, (C) very small and posterior right inferior pulmonary vein, (D) big right superior pulmonary vein with cranially entrance in the left atrium. 3D reconstruction of the aorta, inferior vena cava (E, F), left atrium and pulmonary veins anatomy (G) obtained from the pre-interventional CT-Imaging. (H–K) Fluoroscopic anteroposterior images showed mapping catheter in the left ventricle (H), right superior pulmonary vein (I), left superior pulmonary vein (J) and left inferior pulmonary vein (K). (L) and (M) present the 3D reconstruction of the aortic root, the left ventricle, the left atrium and the pulmonary veins.

The arterial access was gained through the right femoral artery using an 8.5F SL 1 sheath to manually introduce the catheters: initially a mapping catheter which was later exchanged with an ablation catheter. In the course of the last decade the quality of mapping catheters has remarkably improved. However, the use in such a complex anatomy requires critical preliminary choices. [5] In this regard, choosing the most optimal mapping catheter for this case, we took different options into consideration:

1. A circular mapping catheter was ruled out initially due to the risk of papillary muscle entrapment when passing through the Left Ventricle (LV).
2. The high-density catheters, for example, Abbott HD Grid and Boston Scientific Orion, were also not considered optimal due to their stiffness and small distal curve.

3. After further careful deliberation, we esteemed the smooth Abbott Lifewire 20 polar catheter (with narrow spacing 2–2–2; usually used for VT mapping) the best choice.

After passing the aortic valve, the LV and the mitral valve with this catheter, mapping of the geometry and the signals of the left atrium and the PV became feasible (Fig. 1H–M).

For the planed wide antral circumferential ablation (WACA) we decided to start with the FlexAbility D/F (Abbott), hoping that the two different curves of the bidirectional catheter would help us reach all required areas. However, with this catheter it was only possible to very accurately isolate the left inferior PV (LIPV) (Fig. 2A). Respecting the stiffness of the catheter, we consciously refrained from forcefully advancing it to the superior veins. Consequently, we decided to implement a second ablation catheter,
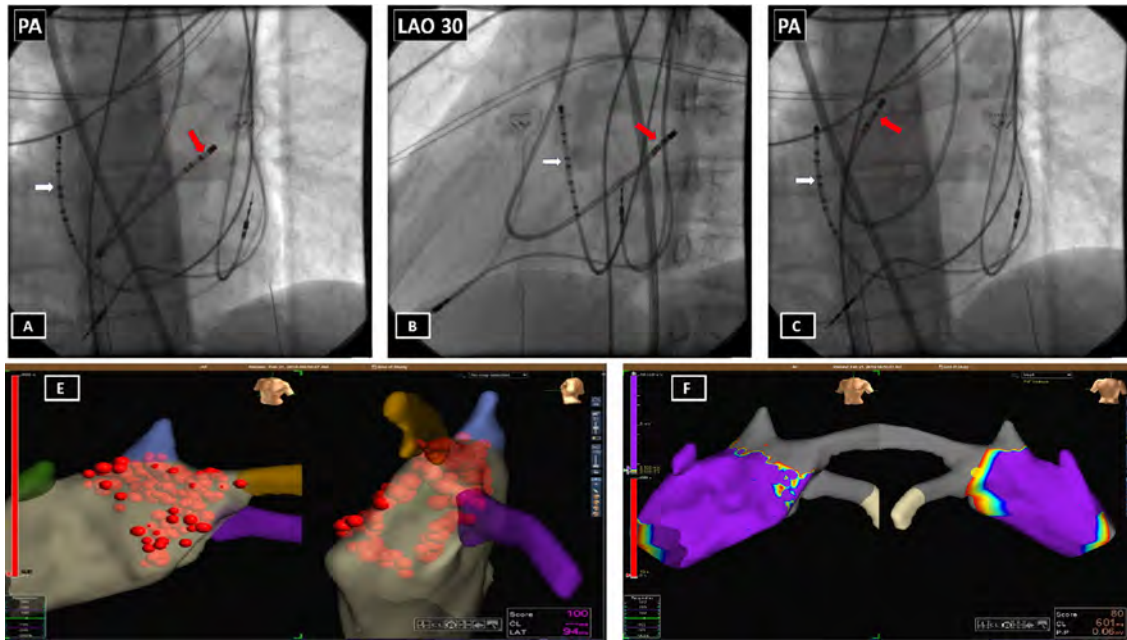
Fig. 2. (A–C) Fluoroscopic anteroposterior images showed ablation catheter in the (A) left inferior pulmonary vein using FlexAbility catheter with D/F dual curves and (B) left superior and (C) right pulmonary veins using Thermocool J-Curve ablation catheter. Red dots (E) indicate the ablation points during WACA. Successful isolation of the pulmonary veins from left atrium was confirmed after remap with the 20-polar lifewire catheter (F). (For interpretation of the references to colour in this figure legend, the reader is referred to the web version of this article.)

which is smoother and offers a bigger curve (Biosense Webster, Thermocool J-Curve). With this catheter, the PVI could be successfully completed (Fig. 2B, C).

Finally, complete antral isolation was confirmed by a voltage remap so that all catheters could be withdrawn (Fig. 2D, E). Total procedure and ablation time were about 180 and 90 min respectively.

5. Conclusion

To the best of our knowledge, this is the first case report of *trans*-aortic pulmonary vein isolation in a patient with dextrocardia, situs inversus and total venous anomaly without magnetic navigation. It clearly states that with a team of experienced operators and with proper procedural planning and a broad catheter portfolio, the retrograde *trans*-aortic mapping of the LA and the PVs and WACA are feasible.

Declaration of Competing Interest

The authors declare that they have no known competing financial interests or personal relationships that could have appeared to influence the work reported in this paper.

References

[1] Y. Yoshiga, A. Shimizu, T. Ueyama, M. Ono, T. Fumimoto, H. Ishiguchi, M. Yano, Successful cryoballoon pulmonary vein isolation in a patient with situs inversus and dextrocardia, J. Arrhythmia. 32 (2016) 493–495.

[2] T. Yamada, H.T. McElderry, H. Doppalapudi, M. Platonov, A.E. Epstein, V.J. Plumb, G.N. Kay, Successful catheter ablation of atrial fibrillation in a patient with dextrocardia, Europace: Eur. Pac. Arrhythmia. Cardiac Electrophysiol.: J. Work. Groups Cardiac Pac. Arrhythmia. Cardiac Cellular Electrophysiol. Eur. Soc. Cardiol. 10 (2008) 1120–1122.

[3] H. Kato, S. Kubota, T. Goto, K. Inoue, N. Oku, T. Haba, M. Yamamoto, Transseptal puncture and catheter ablation via the superior vena cava approach for persistent atrial fibrillation in a patient with polysplenia syndrome and interruption of the inferior vena cava: contact force-guided pulmonary vein isolation, Europace: Eur. Pac. Arrhythmia. Cardiac Electrophysiol.: J. Work. Groups Cardiac Pac. Arrhythmia. Cardiac Cellular Electrophysiol. Eur. Soc. Cardiol. 19 (2017) 1227–1232.

[4] K. Okajima, T. Nakanishi, H. Ichibori, T. Shirai, M. Kadotani, H. Shimizu, Y. Onishi, K. Yamashiro, Trans-aortic pulmonary vein isolation using magnetic navigation system for paroxysmal atrial fibrillation in a patient with dextrocardia, situs inversus, and inferior vena cava continuity with azygos vein, J. Arrhythmia. 34 (2018) 583–585.

[5] F. Bourier, F. Sacher, Modern mapping technologies: technical background and clinical use, Herzschrittmachertherapie Elektrophysiologie. 29 (2018) 271–277.

Atisha Khan [a]
Fuad Hasan [a]
Dirk Bandorski [b]
Bernd Lemke [a]
Dominik Linz [c,d]
Markus Zarse [a,e]
Nana-Yaw Bimpong-Buta [f]
Harilaos Bogossian [c,e,f,*]
[a] *Märkische Kliniken GmbH, Department of Cardiology, Electrophysiology and Angiology, Klinikum Lüdenscheid, Lüdenscheid, Germany*
[b] *Faculty of Medicine, Semmelweis University Campus Hamburg, Hamburg, Germany*
[c] *Department of Cardiology, Maastricht University Medical Centre and Cardiovascular Research Institute Maastricht, the Netherlands*
[d] *Department of Cardiology, Radboud University Medical Centre, Nijmegen, the Netherlands*
[e] *Department of Cardiology, Witten/Herdecke University, Witten, Germany*
[f] *Department of Cardiology and Rhythmology, Ev. Krankenhaus Hagen, Hagen, Germany*
⁎ Corresponding author at: Chefarzt der Klinik für, Kardiologie und Rhythmologie, Ev. Krankenhaus Hagen, Brusebrinkstr. 20, 58135 Hagen, Germany.
E-mail address: bogossianh@esv.de (H. Bogossian)
Received 25 June 2020
Accepted 26 June 2020

**Harilaos Bogossian[1,2] · Sebastian Robl[1] · Nana-Yaw Bimpong-Buta[1] ·
Konstantinos Iliodromitis[1]**

[1] Klinik für Kardiologie und Rhythmologie, Evangelisches Krankenhaus Hagen-Haspe, Hagen, Deutschland

[2] Universität Witten/Herdecke, Witten, Deutschland

Ventrikuloatrialer Block während Tachykardie

Ein klar definiertes elektrophysiologisches Kriterium für eine unklare Tachykardie

Fallvorstellung

Eine 52-jährige Patientin berichtet seit Jahren über Herzrasen und Palpitationen. Zur weiteren Abklärung wurde eine elektrophysiologische Untersuchung in Ablationsbereitschaft durchgeführt.

Die Basisintervalle (AH und HV Zeit) wurden ausgemessen und waren normwertig. Es wurde ein 4-poliger Katheter im rechten Vorhofohr (HRA), ein 10-poliger Katheter im Sinus coronarius (CS), ein 4-poliger Katheter in His-Bündel Position (His) und ein 4-poliger Katheter im rechtsventrikulären Apex (RVA) platziert. Bei der ventrikulären Stimulation aus dem RV-Apex zeigte sich eine dekrementale VA-Leitung mit konzentrischer Aktivierungssequenz am 10-poligen Katheter.

Durch programmierte atriale Stimulation wurde die klinische Tachykardie in den ◘ **Abb. 1 und 2** ausgelöst.

Anschließend erfolgte ein ventrikuläres Overdrive-Pacing. Die Beendigung der ventrikulären Überstimulation ist in ◘ **Abb. 3** dargestellt:

Frage

Was ist der Mechanismus der klinischen Tachykardie?

1. AV-Knoten-Reentry-Tachykardie (AVNRT)
2. AV-Reentry-Tachykardie (AVRT) bei einer links gelegenen posterolateralen akzessorischen Leitungsbahn
3. AV-Reentry-Tachykardie (AVRT) bei einer rechts gelegenen posteroseptalen akzessorischen Leitungsbahn mit dekrementalen Leitungseigenschaften (PJRT)
4. Faszikuläre Tachykardie
5. Ventrikuläre Tachykardie (VT)

Abb. 1 ▲ Programmierte atriale Stimulation und Induktion einiger tachykarder Aktionen bei atrialer Stimulation mit einer Zykluslänge von 400 ms und einem gekoppelten Extrastimulus von 320 ms. EKG bei 100 mm/s
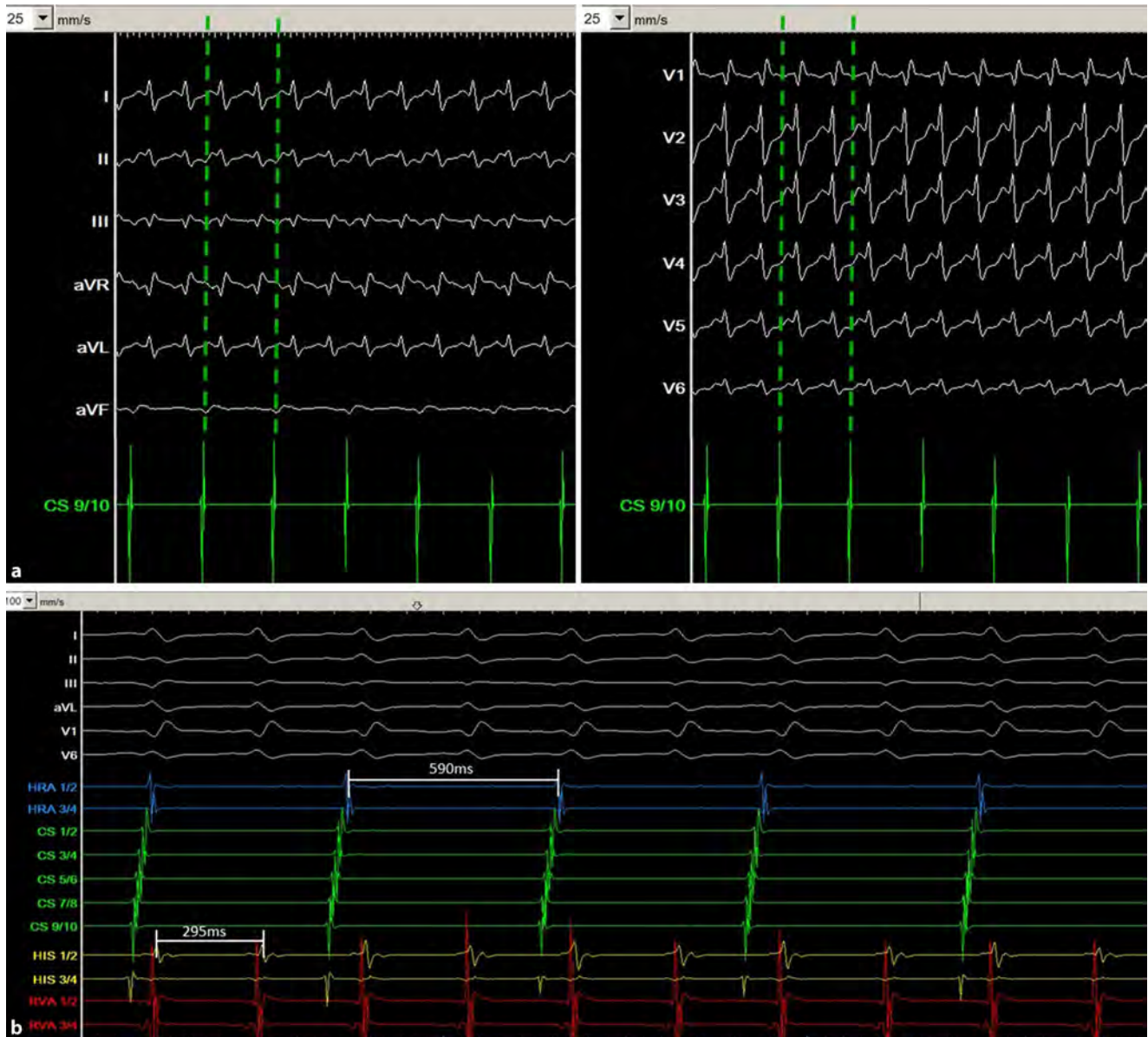
Abb. 2 ▲ Induzierte Tachykardie. **a** 12-Kanal-EKG der laufenden Tachykardie mit Aufzeichnung der intrakardialen Signale auf Sinus coronarius (CS) 9/10 (25 mm/s). **b** Die intrakardiale Aufzeichnung zeigt eine atriale Zykluslänge von 590 ms und eine ventrikuläre Zykluslänge von 295 ms. **a** 12-Kanal-EKG bei 25 mm/s. **b** EKG bei 100 mm/s
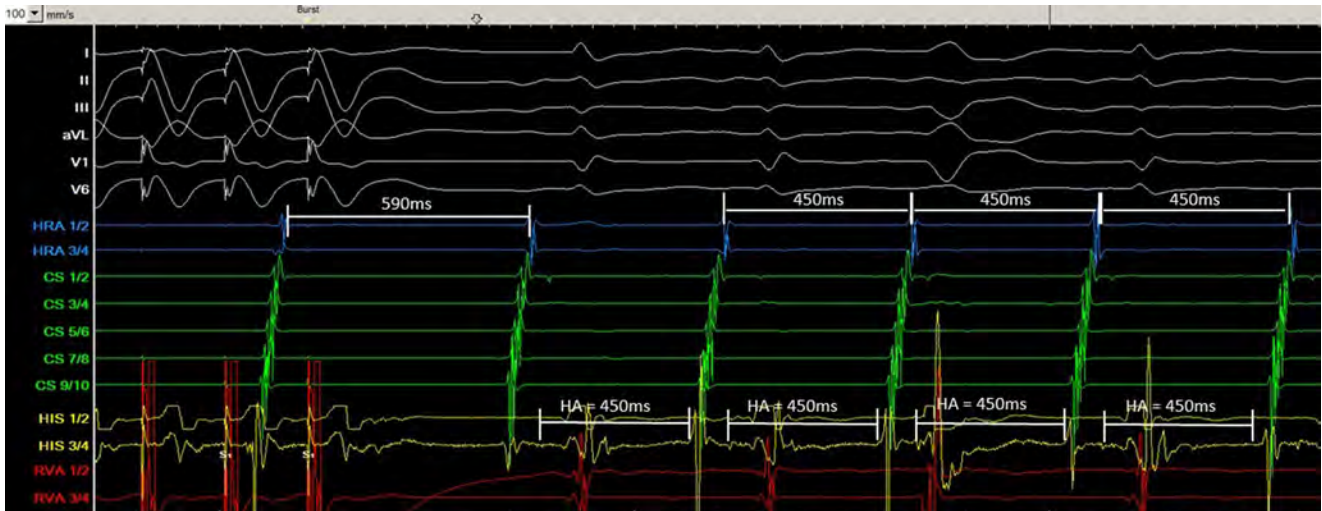
Abb. 3 ▲ EKG und intrakardiale Elektrogramme nach Beendigung der ventrikulären Überstimulation. EKG bei 100 mm/s

Tab. 1 Elektrophysiologische Charakteristika der verschiedenen AVNRT-Formen

Tachykardie-Parameter	Slow-fast-AVNRT	Slow-slow-AVNRT	Fast-slow-AVNRT
Zykluslänge (ms)	361 ± 59 (235–660)	411 ± 62 (320–565)	342 ± 61 (250–440)
AH-Intervall (ms)	312 ± 61 (190–545)	282 ± 71 (185–470)	90 ± 39 (35–160)
HA-Intervall (ms)	45 ± 11 (25–145)	141 ± 32 (90–210)	245 ± 62 (125–405)

Richtige Antwort: 1

Antwort

Die Antworten 2 und 3 sind elektrophysiologisch nicht möglich. In ◻ **Abb. 2** ist erkennbar, dass keine dauerhafte VA- oder AV-Leitung besteht. Jede Art von AV-Reentry-Tachykardie (AVRT) setzt eine 1:1 ventrikuläre und atriale Korrelation voraus.

Die ventrikuläre Extrasystole in ◻ **Abb. 3** (vorletzter Schlag, deutlich verbreiterter QRS-Komplex) tritt während der refraktären His-Periode auf, ohne Veränderung der atrialen Zykluslänge. Das heißt, dass durch eine exakt berechnet einfallende frühere ventrikuläre Erregung, die nicht über den AV-Knoten retrograd geleitet werden kann, die atriale Erregung nicht in gleicher Weise *vorgezogen* wird. Dies hätte für das Vorliegen einer akzessorischen Bahn mit VA-Leitung gesprochen, ist im vorliegenden Fall (kein Einfluss auf die nachfolgende atriale Erregung) jedoch nicht zu sehen, somit „negative atriale Vorziehbarkeit" als weiteres Kriterium gegen das Vorhandensein einer akzessorischen Leitungsbahn.

Schließlich verbleibt die Aktivierungssequenz am CS-Katheter konzentrisch: In CS9/10 (proximaler CS) ist die Erregung früher zu sehen als in CS1/2 (distal) während der gesamten Tachykardiedauer, ohne Zeichen eines *Bracketing* und spätester atrialer Erregung am HRA.

Eine faszikuläre Tachykardie könnte durch eine programmierte atriale Stimulation ausgelöst werden und zu einer VA-Dissoziation führen. Allerdings liegt im vorliegenden Fall die QRS-Breite bei 115 ms, und die QRS-Morphologie ist mit dem intrinsischen QRS vor Auslösen der Tachykardie identisch. Die QRS-Komplexe bei einer faszikulären Tachykardie weisen meist eine rechtsschenkelblockartige Morphologie mit begleitendem links-anteriorem oder links-poste-riorem Hemiblock auf (somit scheidet auch Antwort 4 aus).

Obwohl eine 2:1 VA-Leitung während einer VT durchaus möglich ist (z. B. bei einer retrograden zweitgradigen VA-Blockierung), ist es sehr unwahrscheinlich, dass eine VT mit programmierter atrialer Stimulation und Jump-Phänomen ausgelöst werden kann. Ebenso ist der relativ schmale QRS-Komplex (115 ms), der dem intrinsischen QRS gleicht, ein Ausschlusskriterium für Antwort 5.

In ◻ **Abb. 1** zeigt sich bei der atrialen programmierten Stimulation ein AH-Jump von 64 ms, dem 3 Echo-Beats mit einer verlängerten HA-Zeit von 150 ms folgen.

Dieser Befund macht die Diagnose einer AVNRT vom Slow-slow-Typ sehr wahrscheinlich.

Die ◻ **Abb. 2** zeigt ein konstantes 1:2-AV-Verhältnis mit einer ventrikulären Tachykardie-Zykluslänge von 295 ms und einer atrialen Zykluslänge von 590 ms. Dies passiert aufgrund eines retrograden 2:1-Blocks vom AV-Knoten (AVN) zu den Vorhöfen. In ◻ **Abb. 2a** sind die retrograden P-Wellen in Ableitung III sehr klar erkennbar (die gleichzeitig dargestellte CS-Sequenz unter dem 12-Kanal-EKG zeigt den Zeitpunkt der erwarteten P-Wellen).

In ◻ **Abb. 3** führt die ventrikuläre Überstimulation zur passageren Blockierung der VA-Leitung, und die AVNRT perpetuiert im AVN mit 2:1 retrograder Leitung in den Vorhof. Hiernach ändert sich der Tachykardiemechanismus von Slow-slow-AVNRT mit VA-Block zu Fast-slow-AVNRT („uncommon type") mit 1:1-Leitung und Tachykardie-Zykluslänge von 450 ms und sehr langem HA-Intervall (350 ms).

Eine ventrikuläre Extrasystole trat während der refraktären His-Periode ohne Veränderung der AA-Sequenz auf. Dies bestätigt den AVNRT-Mechanismus und schließt die Existenz einer paraseptalen akzessorischen Bahn

aus. Im Unterschied zur AVRT ist die AVNRT nicht auf ein 1:1-Verhältnis zwischen Ventrikel und Atrium angewiesen. Während die AVRT durch eine ventrikuläre Extrasystole terminiert oder die folgende atriale Aktion vorgezogen wird, läuft die AVNRT davon unbeeindruckt unverändert weiter, solange die ventrikuläre Extrasystole nicht retrograd in den Reentry zwischen den langsamen und schnellen Bahnen eindringt.

Die langsame Leitungsbahn konnte erfolgreich an loco typico abladiert werden. Hiernach war weder die langsame Leitungsbahn nachweisbar noch eine Tachykardie-Induktion möglich.

Diskussion

Die AV-Knoten-Reentry-Tachykardie (AVNRT) ist die häufigste regelmäßige supraventrikuläre Tachykardie bei Erwachsenen. Der AV-Knoten ist keine wahre rechtskardiale Struktur, wie es sich häufig in Abbildungen darstellt, sondern eine septal gelegene Struktur, mit kompaktem AVN und schneller Leitungsbahn sowie mit rechts- und linksseitigen Ausläufern (verschiedene langsame Leitungsbahnen).

Die AVNRT kann – je nachdem, welche Leitungsbahnen beteiligt sind – in drei verschiedenen Formen auf eten: slow-fast („common type"), fast-slow („uncommon type") und slow-slow.

Elektrophysiologische Charakteristika der verschiedenen AVNRT-Formen sind in ◻ **Tab. 1** zusammengefasst [1].

Das Auftreten verschiedener VA-Blockierungen während einer laufenden AVNRT ist in der Literatur häufig beschrieben [2–5]. Die Elimination der langsamen AV-Leitungsbahn im Bereich des CS-Ostiums resultierte in der erfolgreichen Behandlung der Herzrhythmusstörung. Unterschiedliche retrograde atriale Aktivierungszeiten und Zykluslängen könnten Ausdruck der Präsenz mehrerer langsamer Leitungsbahnen sein.

Fazit

VA-Blockierungen können während einer AVNRT auftreten. Die Analyse der HA-Intervalle während der Tachykardie

helfen, die unterschiedlichen Formen der AVNRT zu unterscheiden. Bei Bestätigung der Diagnose ist die Ablation der langsamen Leitungsbahn in loco typico die Therapie der Wahl.

Korrespondenzadresse

PD Dr. Harilaos Bogossian
Klinik für Kardiologie und Rhythmologie, Evangelisches Krankenhaus Hagen-Haspe
Brusebrinkstraße 20,
58135 Hagen, Deutschland
bogossian@evk-haspe.de

Literatur

1. Shoei K, Huang S, Miller JM (2014) Catheter ablation of cardiac arrhythmias, 3. Aufl. Saunders,
2. Miles WM, Hubbard JE, Zipes DP, Klein LS (1994) Elimination of AV nodal reentrant tachycardia with 2:1 VA block by posteroseptal ablation. J Cardiovasc Electrophsiol 5:510–516
3. Figa F, Chiu C, Gow RM (1995) Unusual electrophysiological findings in atrioventricular node reentrant tachycardia. Pacing Clin Electrophysiol 18:1324–1326
4. Hamdan MH, Page RL, Scheinman MM (1997) Diagnostic approach to narrow complex tachycardia with VA block. Pacing Clin Electrophysiol 20:2984–2988
5. Hamdan MH, Kalman JM, Lesh MD, Lee RJ, Saxon LA, Dorostkar P, Scheinman MM (1998) Narrow complex tachycardia with VA block: Diagnostic and therapeutic implications. Pacing Clin Electrophysiol 21:1196–1206

Ventrikuloatrialer Block während Tachykardie

Harilaos Bogossian, Sebastian Robl, Nana-Yaw Bimpong-Buta & Konstantinos Iliodromitis

Springer

Check for
updates

Harilaos Bogossian[1,2] · **Sebastian Robl**[1] · **Nana-Yaw Bimpong-Buta**[1] ·
Konstantinos Iliodromitis[1]

[1] Klinik für Kardiologie und Rhythmologie, Evangelisches Krankenhaus Hagen-Haspe, Hagen, Deutschland

[2] Universität Witten/Herdecke, Witten, Deutschland

Ventrikuloatrialer Block während Tachykardie

Ein klar definiertes elektrophysiologisches Kriterium für eine unklare Tachykardie

Fallvorstellung

Eine 52-jährige Patientin berichtet seit Jahren über Herzrasen und Palpitationen. Zur weiteren Abklärung wurde eine elektrophysiologische Untersuchung in Ablationsbereitschaft durchgeführt.

Die Basisintervalle (AH und HV Zeit) wurden ausgemessen und waren normwertig. Es wurde ein 4-poliger Katheter im rechten Vorhofohr (HRA), ein 10-poliger Katheter im Sinus coronarius (CS), ein 4-poliger Katheter in His-Bündel Position (His) und ein 4-poliger Katheter im rechtsventrikulären Apex (RVA) platziert. Bei der ventrikulären Stimulation aus dem RV-Apex zeigte sich eine dekrementale VA-Leitung mit konzentrischer

Aktivierungssequenz am 10-poligen Katheter.

Durch programmierte atriale Stimulation wurde die klinische Tachykardie in den ◘ **Abb. 1 und 2** ausgelöst.

Anschließend erfolgte ein ventrikuläres Overdrive-Pacing. Die Beendigung der ventrikulären Überstimulation ist in ◘ **Abb. 3** dargestellt:

Frage

Was ist der Mechanismus der klinischen Tachykardie?

1. AV-Knoten-Reentry-Tachykardie (AVNRT)
2. AV-Reentry-Tachykardie (AVRT) bei einer links gelegenen posterolateralen akzessorischen Leitungsbahn
3. AV-Reentry-Tachykardie (AVRT) bei einer rechts gelegenen posteroseptalen akzessorischen Leitungsbahn mit dekrementalen Leitungseigenschaften (PJRT)
4. Faszikuläre Tachykardie
5. Ventrikuläre Tachykardie (VT)

Abb. 1 ▲ Programmierte atriale Stimulation und Induktion einiger tachykarder Aktionen bei atrialer Stimulation mit einer Zykluslänge von 400 ms und einem gekoppelten Extrastimulus von 320 ms. EKG bei 100 mm/s
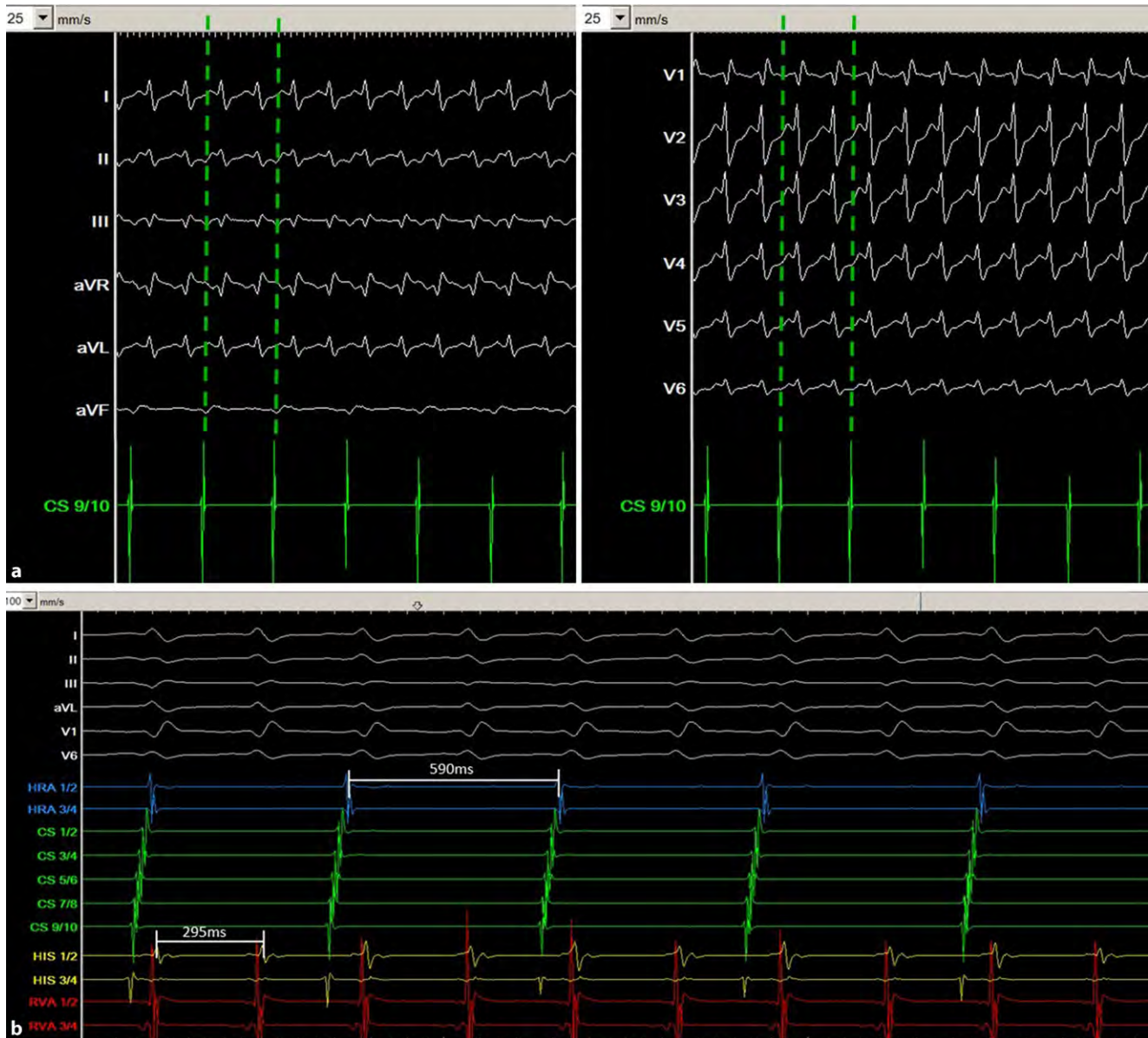
Abb. 2 ▲ Induzierte Tachykardie. **a** 12-Kanal-EKG der laufenden Tachykardie mit Aufzeichnung der intrakardialen Signale auf Sinus coronarius (CS) 9/10 (25 mm/s). **b** Die intrakardiale Aufzeichnung zeigt eine atriale Zykluslänge von 590 ms und eine ventrikuläre Zykluslänge von 295 ms. **a** 12-Kanal-EKG bei 25 mm/s. **b** EKG bei 100 mm/s
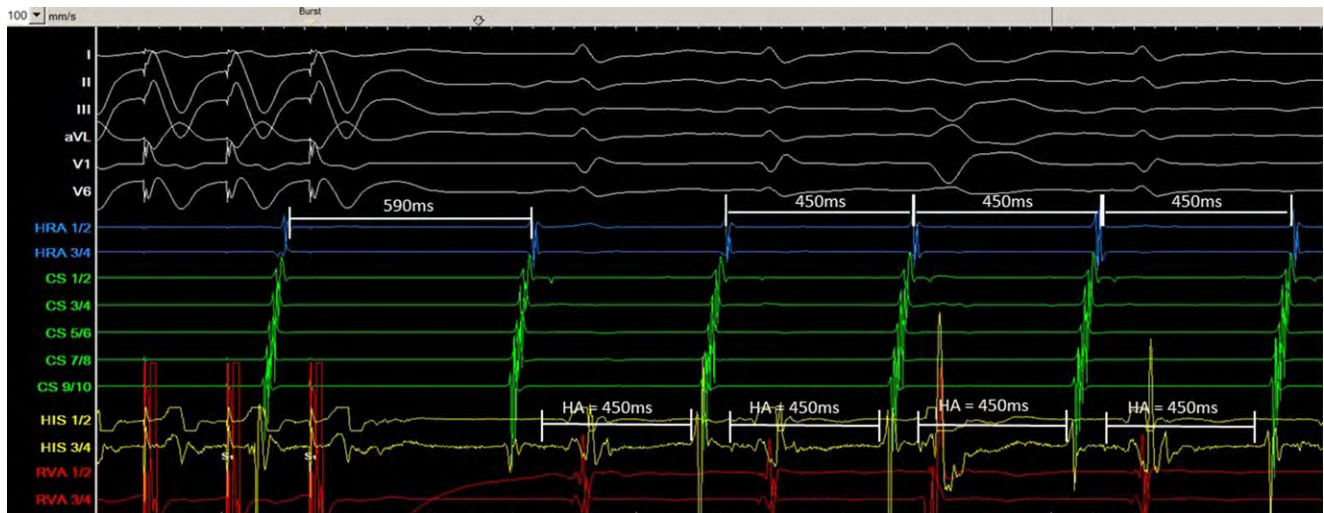
Abb. 3 ▲ EKG und intrakardiale Elektrogramme nach Beendigung der ventrikulären Überstimulation. EKG bei 100 mm/s

Tab. 1	Elektrophysiologische Charakteristika der verschiedenen AVNRT-Formen		
Tachykardie-Parameter	**Slow-fast-AVNRT**	**Slow-slow-AVNRT**	**Fast-slow-AVNRT**
Zykluslänge (ms)	361 ± 59 (235–660)	411 ± 62 (320–565)	342 ± 61 (250–440)
AH-Intervall (ms)	312 ± 61 (190–545)	282 ± 71 (185–470)	90 ± 39 (35–160)
HA-Intervall (ms)	45 ± 11 (25–145)	141 ± 32 (90–210)	245 ± 62 (125–405)

Richtige Antwort: 1

Antwort

Die Antworten 2 und 3 sind elektrophysiologisch nicht möglich. In ◘ **Abb. 2** ist erkennbar, dass keine dauerhafte VA- oder AV-Leitung besteht. Jede Art von AV-Reentry-Tachykardie (AVRT) setzt eine 1:1 ventrikuläre und atriale Korrelation voraus.

Die ventrikuläre Extrasystole in ◘ **Abb. 3** (vorletzter Schlag, deutlich verbreiterter QRS-Komplex) tritt während der refraktären His-Periode auf, ohne Veränderung der atrialen Zykluslänge. Das heißt, dass durch eine exakt berechnet einfallende frühere ventrikuläre Erregung, die nicht über den AV-Knoten retrograd geleitet werden kann, die atriale Erregung nicht in gleicher Weise *vorgezogen* wird. Dies hätte für das Vorliegen einer akzessorischen Bahn mit VA-Leitung gesprochen, ist im vorliegenden Fall (kein Einfluss auf die nachfolgende atriale Erregung) jedoch nicht zu sehen, somit „negative atriale Vorziehbarkeit" als weiteres Kriterium gegen das Vorhandensein einer akzessorischen Leitungsbahn.

Schließlich verbleibt die Aktivierungssequenz am CS-Katheter konzentrisch: In CS9/10 (proximaler CS) ist die Erregung früher zu sehen als in CS1/2 (distal) während der gesamten Tachykardiedauer, ohne Zeichen eines *Bracketing* und spätester atrialer Erregung am HRA.

Eine faszikuläre Tachykardie könnte durch eine programmierte atriale Stimulation ausgelöst werden und zu einer VA-Dissoziation führen. Allerdings liegt im vorliegenden Fall die QRS-Breite bei 115 ms, und die QRS-Morphologie ist mit dem intrinsischen QRS vor Auslösen der Tachykardie identisch. Die QRS-Komplexe bei einer faszikulären Tachykardie weisen meist eine rechtsschenkelblockartige Morphologie mit begleitendem links-anteriorem oder links-poste- riorem Hemiblock auf (somit scheidet auch Antwort 4 aus).

Obwohl eine 2:1 VA-Leitung während einer VT durchaus möglich ist (z. B. bei einer retrograden zweitgradigen VA-Blockierung), ist es sehr unwahrscheinlich, dass eine VT mit programmierter atrialer Stimulation und Jump-Phänomen ausgelöst werden kann. Ebenso ist der relativ schmale QRS-Komplex (115 ms), der dem intrinsischen QRS gleicht, ein Ausschlusskriterium für Antwort 5.

In ◘ **Abb. 1** zeigt sich bei der atrialen programmierten Stimulation ein AH-Jump von 64 ms, dem 3 Echo-Beats mit einer verlängerten HA-Zeit von 150 ms folgen.

Dieser Befund macht die Diagnose einer AVNRT vom Slow-slow-Typ sehr wahrscheinlich.

Die ◘ **Abb. 2** zeigt ein konstantes 1:2-AV-Verhältnis mit einer ventrikulären Tachykardie-Zykluslänge von 295 ms und einer atrialen Zykluslänge von 590 ms. Dies passiert aufgrund eines retrograden 2:1-Blocks vom AV-Knoten (AVN) zu den Vorhöfen. In ◘ **Abb. 2a** sind die retrograden P-Wellen in Ableitung III sehr klar erkennbar (die gleichzeitig dargestellte CS-Sequenz unter dem 12-Kanal-EKG zeigt den Zeitpunkt der erwarteten P-Wellen).

In ◘ **Abb. 3** führt die ventrikuläre Überstimulation zur passageren Blockierung der VA-Leitung, und die AVNRT perpetuiert im AVN mit 2:1 retrograder Leitung in den Vorhof. Hiernach ändert sich der Tachykardiemechanismus von Slow-slow-AVNRT mit VA-Block zu Fast-slow-AVNRT („uncommon type") mit 1:1-Leitung und Tachykardie-Zykluslänge von 450 ms und sehr langem HA-Intervall (350 ms).

Eine ventrikuläre Extrasystole trat während der refraktären His-Periode ohne Veränderung der AA-Sequenz auf. Dies bestätigt den AVNRT-Mechanismus und schließt die Existenz einer paraseptalen akzessorischen Bahn aus. Im Unterschied zur AVRT ist die AVNRT nicht auf ein 1:1-Verhältnis zwischen Ventrikel und Atrium angewiesen. Während die AVRT durch eine ventrikuläre Extrasystole terminiert oder die folgende atriale Aktion vorgezogen wird, läuft die AVNRT davon unbeeindruckt unverändert weiter, solange die ventrikuläre Extrasystole nicht retrograd in den Reentry zwischen den langsamen und schnellen Bahnen eindringt.

Die langsame Leitungsbahn konnte erfolgreich an loco typico abladiert werden. Hiernach war weder die langsame Leitungsbahn nachweisbar noch eine Tachykardie-Induktion möglich.

Diskussion

Die AV-Knoten-Reentry-Tachykardie (AVNRT) ist die häufigste regelmäßige supraventrikuläre Tachykardie bei Erwachsenen. Der AV-Knoten ist keine wahre rechtskardiale Struktur, wie es sich häufig in Abbildungen darstellt, sondern eine septal gelegene Struktur, mit kompaktem AVN und schneller Leitungsbahn sowie mit rechts- und linksseitigen Ausläufern (verschiedene langsame Leitungsbahnen).

Die AVNRT kann – je nachdem, welche Leitungsbahnen beteiligt sind – in drei verschiedenen Formen auf eten: slow-fast („common type"), fast-slow („uncommon type") und slow-slow.

Elektrophysiologische Charakteristika der verschiedenen AVNRT-Formen sind in ◘ **Tab. 1** zusammengefasst [1].

Das Auftreten verschiedener VA-Blockierungen während einer laufenden AVNRT ist in der Literatur häufig beschrieben [2–5]. Die Elimination der langsamen AV-Leitungsbahn im Bereich des CS-Ostiums resultierte in der erfolgreichen Behandlung der Herzrhythmusstörung. Unterschiedliche retrograde atriale Aktivierungszeiten und Zykluslängen könnten Ausdruck der Präsenz mehrerer langsamer Leitungsbahnen sein.

Fazit

VA-Blockierungen können während einer AVNRT auftreten. Die Analyse der HA-Intervalle während der Tachykardie

helfen, die unterschiedlichen Formen der AVNRT zu unterscheiden. Bei Bestätigung der Diagnose ist die Ablation der langsamen Leitungsbahn in loco typico die Therapie der Wahl.

Korrespondenzadresse

PD Dr. Harilaos Bogossian
Klinik für Kardiologie und Rhythmologie, Evangelisches Krankenhaus Hagen-Haspe
Brusebrinkstraße 20,
58135 Hagen, Deutschland
bogossian@evk-haspe.de

Einhaltung ethischer Richtlinien

Literatur

1. Shoei K, Huang S, Miller JM (2014) Catheter ablation of cardiac arrhythmias, 3. Aufl. Saunders,
2. Miles WM, Hubbard JE, Zipes DP, Klein LS (1994) Elimination of AV nodal reentrant tachycardia with 2:1 VA block by posteroseptal ablation. J Cardiovasc Electrophsiol 5:510–516
3. Figa F, Chiu C, Gow RM (1995) Unusual electrophysiological findings in atrioventricular node reentrant tachycardia. Pacing Clin Electrophysiol 18:1324–1326
4. Hamdan MH, Page RL, Scheinman MM (1997) Diagnostic approach to narrow complex tachycardia with VA block. Pacing Clin Electrophysiol 20:2984–2988
5. Hamdan MH, Kalman JM, Lesh MD, Lee RJ, Saxon LA, Dorostkar P, Scheinman MM (1998) Narrow complex tachycardia with VA block: Diagnostic and therapeutic implications. Pacing Clin Electrophysiol 21:1196–1206